

1. Report No. FHWA/TX-86/40+316-2	2. Government Accession No.	3. Recipient's Catalog No.	
4. Title and Subtitle STRUCTURAL EFFECTS OF TRANSVERSE PRESTRESSING IN BRIDGE DECKS		5. Report Date July 1985	6. Performing Organization Code
7. Author(s) A. R. Phipps, R. A. Almustafa, M. L. Ralls, R. W. Poston, J. E. Breen, and R. L. Carrasquillo		8. Performing Organization Report No. Research Report 316-2	
9. Performing Organization Name and Address Center for Transportation Research The University of Texas at Austin Austin, Texas 78712-1075		10. Work Unit No.	11. Contract or Grant No. Research Study 3-5-82-316
12. Sponsoring Agency Name and Address Texas State Department of Highways and Public Transportation; Transportation Planning Division P. O. Box 5051 Austin, Texas 78763		13. Type of Report and Period Covered Interim	
15. Supplementary Notes Study conducted in cooperation with the U. S. Department of Transportation, Federal Highway Administration Research Study Title: "Application of Transverse Prestressing to Bridge Decks"		14. Sponsoring Agency Code	
16. Abstract <p>Transverse prestressing of bridge decks is an attractive concept with substantial benefits in both economy and improved durability. This report summarizes a series of inter-related physical tests and computer analyses which were conducted to provide necessary information for development of design criteria for transverse prestressing of bridge decks. It addresses such important design areas as the effective distribution of edge prestressing force across a bridge slab as affected by both diaphragm and girder restraints, realistic friction losses in transverse prestressing systems, and the behavior of transversely prestressed decks under typical wheel loadings. The principal attention is focused on slab and girder bridges but analytical results are extended to box girder bridges. Experimental verification of the analysis programs allowed substantial parameter studies to be carried out with reasonable confidence. The results of the major experimental and analytical studies are summarized in this report.</p>			
17. Key Words bridge decks, transverse prestressing, structural effects, physical tests, computer analysis, design criteria		18. Distribution Statement No restrictions. This document is available to the public through the National Technical Information Service, Springfield, Virginia 22161.	
19. Security Classif. (of this report) Unclassified	20. Security Classif. (of this page) Unclassified	21. No. of Pages 246	22. Price

STRUCTURAL EFFECTS OF TRANSVERSE PRESTRESSING
IN BRIDGE DECKS

by

A. R. Phipps
R. A. Almustafa
M. L. Ralls
R. W. Poston
J. E. Breen
and
R. L. Carrasquillo

Research Report 316-2
Research Project No. 3-5-82-316

"Application of Transverse Prestressing to Bridge Decks"

Conducted for

Texas

State Department of Highways and Public Transportation

In cooperation with the
U.S. Department of Transportation
Federal Highway Administration

by

CENTER FOR TRANSPORTATION RESEARCH
BUREAU OF ENGINEERING RESEARCH
THE UNIVERSITY OF TEXAS AT AUSTIN

July 1985

The contents of this report reflect the views of the authors who are responsible for the facts and accuracy of the data presented herein. The contents do not necessarily reflect the views or policies of the Federal Highway Administration. This report does not constitute a standard, specification, or regulation.

P R E F A C E

This report is the second in a series which summarizes a detailed investigation assessing the use of deck prestressing as a method of improving durability of bridge decks. The first report summarized an extensive experimental corrosion study which was conducted to assess the use of deck prestressing as a method of improving bridge deck durability. This report summarizes an extensive analytical and experimental program which was performed to document the structural behavior of bridge decks utilizing transverse prestressing. The third and final report in the series draws on the findings from the durability and structural studies. The final report develops design recommendations and suggested AASHTO Specification provisions to use combined longitudinal and transverse prestressing for economical and durable bridge decks. The third report also contains several design examples to illustrate the application of the design recommendations and procedures.

This work is part of Research Project 3-5-82-316, entitled "Application of Transverse Prestressing to Bridge Decks." The study was conducted at the Phil M. Ferguson Structural Engineering Laboratory as part of the overall research program of the Center for Transportation Research, Bureau of Engineering Research, of The University of Texas at Austin. The work was sponsored jointly by the Texas State Department of Highways and Public Transportation and the Federal Highway Administration.

Liaison with the TSDHPT was maintained through the contact representative, Mr. James C. Wall; the Area IV Committee Chairman, Mr. Robert L. Reed; and the State Bridge Engineer, Mr. Wayne Henneberger. Mr. Jerry W. Bowman was the contact representative for the Federal Highway Administration.

The overall study was directed by Dr. Ramon L. Carrasquillo, Associate Professor of Civil Engineering, and Dr. John E. Breen, who holds the Nasser I. Al-Rashid Chair in Civil Engineering. The detailed work was carried out under the immediate supervision of Dr. Randall W. Poston, Research Engineer, Center for Transportation Research.

S U M M A R Y

Transverse prestressing of bridge decks is an attractive concept with substantial benefits in both economy and improved durability. This report summarizes a series of inter-related physical tests and computer analyses which were conducted to provide necessary information for development of design criteria for transverse prestressing of bridge decks. It addresses such important design areas as the effective distribution of edge prestressing force across a bridge slab as affected by both diaphragm and girder restraints, realistic friction losses in transverse prestressing systems, and the behavior of transversely prestressed decks under typical wheel loadings. The principal attention is focused on slab and girder bridges but analytical results are extended to box girder bridges. Experimental verification of the analysis programs allowed substantial parameter studies to be carried out with reasonable confidence. The results of the major experimental and analytical studies are summarized in this report.

I M P L E M E N T A T I O N

This report is the second in a series which summarizes a major experimental and analytical study aimed at developing specific recommendations for design of posttensioned bridge decks. The recommendations should be considered by the Texas State Department of Highways and Public Transportation and by AASHTO for inclusion in design specifications and codes. It contains documentation of the structural analysis and behavior study on which many of the design recommendations are based. In addition, it contains specific information regarding the structural effects of transverse prestressing for a wide range of bridge variables. Many of the illustrations presented could be used as design aids in developing transverse prestressed deck standards. The use of transversely prestressed bridge decks should lead to more durable bridge decks and should result in important savings in both maintenance and replacement funds.

TABLE OF CONTENTS

Chapter		Page
1	INTRODUCTION	1
	1.1 Problems with Bridge Deck Durability	1
	1.2 Design Needs for Transverse Prestressing.....	3
	1.3 Objectives of this Research	3
	1.4 Report Contents	4
2	BACKGROUND OF SLAB DESIGN	7
	2.1 Review of Concrete Slab Behavior and Analysis...	7
	2.1.1 Elastic	7
	2.1.2 Inelastic	8
	2.2 Previous Applications of Prestressed Concrete Slabs	11
	2.2.1 Bridges	13
	2.2.2 Buildings	15
	2.2.3 Pavements	15
	2.3 Related Research	18
	2.3.1 The University of Illinois	18
	2.3.2 Ontario	19
	2.3.3 Other Research	19
	2.4 Current Design Practice	20
	2.4.1 AASHTO Specifications	20
	2.4.2 OHBDC Provisions	23
	2.4.3 Other Design Requirements	24
3	TRANSVERSE PRESTRESSING	25
	3.1 Introduction	25
	3.2 Previous Applications of Transverse Prestressing	25
	3.3 Prestressing Systems for Bridge Decks	27
	3.4 Current Applicable Code Provisions and Practice	28
	3.4.1 Design Bending Moments	28
	3.4.2 Stress Distributions	31
	3.4.3 Use of Diaphragms	31
	3.4.4 Anchorage Zone Design	32
	3.4.5 Tendon and Anchor Protection	32
	3.4.6 Transverse Prestressing Specifications...	36

TABLE OF CONTENTS (continued)

Chapter		Page
4	STRUCTURAL BRIDGE MODEL	39
4.1	Introduction	39
4.2	General Description	39
4.3	Model Prototype Design	40
4.4	Deck Design	42
	4.4.1 Two-Dimensional Finite Element Analysis of Structural Effects	42
	4.4.2 Design Philosophy	54
	4.4.3 Other Design Considerations	58
	4.4.4 Design Calculations	61
4.5	Method of Analysis	68
	4.5.1 General	68
	4.5.2 Finite Element Method	68
	4.5.3 Finite Element Modeling of Bridge Structures	75
	4.5.4 Finite Element Analysis Program	75
	4.5.5 Summary	84
4.6	Stressing Experiments on Slab-Girder Bridge Model	84
	4.6.1 General	84
	4.6.2 Dimensions and Material Properties.....	84
	4.6.3 Transverse Prestressing	84
	4.6.4 Instrumentation	91
	4.6.5 Test Program	91
	4.6.6 Finite Element Analysis of Bridge Model	91
	4.6.7 Comparison of Experimental and Analytical Results	97
5	VERTICAL AND EDGE LOAD TESTS	105
5.1	Vertical Load Test Program	105
	5.1.1 Introduction	105
	5.1.2 Test Results	112
	5.1.3 Service Load Results	112
	5.1.4 Factored Load Tests	120
	5.1.5 Ultimate Load Tests	128
	5.1.6 Discussion of Test Results	146
	5.1.7 Conclusions	158
5.2	Edge of Slab Posttensioning Stress Distribution Tests	159
	5.2.1 Test Description	159
	5.2.2 Test Results	161
	5.2.3 Design Implications of Data	162

TABLE OF CONTENTS (continued)

Chapter		Page
6	ANALYTICAL PARAMETRIC INVESTIGATIONS OF SLAB-GIRDER AND BOX GIRDER BRIDGES	167
6.1	General	167
6.2	Slab and Girder Bridge	167
6.2.1	Dimensions, Material Properties and Loading	167
6.2.2	Finite Element Modelling	167
6.2.3	Parametric Investigations	167
6.2.4	Possible Method to Account for Diaphragm Effect in Slab and Girder Bridges	184
6.3	Box-Girder Bridges	188
6.3.1	Descriptions of the Bridges Studied.....	188
7	SUMMARY, CONCLUSIONS AND RECOMMENDATIONS	205
7.1	Summary	205
7.2	Conclusions	205
7.2.1	General Conclusion	205
7.2.2	Specific Conclusions	205
7.3	Future Research Needs	207
	REFERENCES	209
	APPENDIX	217

LIST OF TABLES

Table		Page
3.1	Relative amounts of transverse reinforcement in bridge slab	30
4.1a	Material properties of various elements in analysis model	47
4.1b	Material properties assumed for full-scale prototype bridge deck design	47
4.2	A summary of the tested examples	78
4.3	Example 4: skew plates	83
4.4	Concrete mix proportions per cubic yard	89
4.5	Reinforcement for the model	90
4.6	Test cases	96
4.7	Ratios of experimental to analytical stresses	102
5.1	Vertical load test sequence	113
5.2	Planned and actual span lengths and load locations for negative moment tests	150
5.3	West span to east span slab deflection ratios for negative moment tests	151
5.4	Actual slab thicknesses for interior negative moment tests	153
5.5	West span to east span deflection ratios for interior negative moment tests, accounting for actual slab thicknesses	153
5.6	Girder deflections for interior negative moment tests	154
5.7	Comparison of design and experimental transverse slab surface stresses and moments	157

LIST OF TABLES

Table		Page
6.1	Material properties of girders, diaphragms and slab	170
6.2	Slab-girder bridge parametric study cases	174
6.3	Parametric study cases, Part II	190

LIST OF FIGURES

Figure		Page
1.1	Corrosion protection mechanism of prestressing.....	2
1.2	Various components of overall research study deck prestressing	5
1.3	Deck prestressing of a conventional slab-girder bridge	5
2.1	Arching action in concrete slabs	10
2.2	Load deflection relationship for two-way reinforced concrete slab with edges restrained against lateral movement	10
2.3	Arching action in concrete slabs after peak load	12
2.4	Mechanical model of a slab with boundary restraints at punching failure	12
2.5	Transverse and longitudinal posttensioning, Kishwaukee Bridge, Illinois	14
2.6	Partial plan of prestressed roadway slab for I-70 through Glenwood Canyon, Colorado	16
2.7	Section of prestressed roadway slab for I-70 through Glenwood Canyon, Colorado	17
3.1	Transverse prestressing in box girder bridges	29
3.2a	Circular anchorage pattern	29
3.2b	Thin-section anchorage	29
3.3	Transverse reinforcement in bridge decks	30
3.4	Concentrated force at a point of a straight boundary..	33
3.5	Typical locations and types of diaphragms for short-span slab-girder bridges	33

LIST OF FIGURES (continued)

Figure		Page
3.6	Anchorage zones in a thin-webbed box girder section...	34
3.7	Multiple anchorage zones in a transversely prestressed bridge deck	34
3.8	Anchorage plug for corrosion protection	37
3.9	Poor practice in unbonded tendon construction.....	37
3.10	Electrically isolated tendon suggested by Schupack ...	37
4.1	View of prototype bridge	41
4.2	Prototype bridge	43
4.3	Equivalent beam used for two-dimensional finite element analysis	44
4.4	Equivalent lateral springs	45
4.5	Finite element analysis model; one-quarter of bridge	46
4.6	Case 1 stress contours; fixed girder supports; diaphragms included; contours are % of applied edge stress	49
4.7	Case 2 stress contours; fixed girder supports; no diaphragms; contours are % of applied edge stress	50
4.8	Case 3 stress contours; flexible girder supports diaphragms included; contours are % of applied edge stress	51
4.9	Case 4 stress contours; flexible girder supports no diaphragms; contours are % of applied edge stress	52
4.10	Friction losses in posttensioning	56
4.11	Friction test results	57
4.12	Summary of Model bridge slab design philosophy	59

LIST OF FIGURES (continued)

Figure		Page
4.13	Possible strand profiles	60
4.14	Possible splitting failure with middepth tendon profile	60
4.15	Moment envelope and stresses in bridge slab under service plus impact load conditions	62
4.16	Cover and tendon eccentricity in slab	62
4.17	Straight and draped tendon profile	64
4.18	Stress contours for doubling of edge stress in diaphragm regions; contours are percentages of applied edge stress in nondiaphragm region	66
4.19	Factored moment envelope	67
4.20	Prototype slab reinforcement	69
4.21	Tendon spacings in prototype slab	70
4.22	The effects of girders, Webs and diaphragms on transverse prestress distribution, TS	71
4.23	Finite element mesh idealization of the bridges considered in this study	73
4.24a	Eccentricity between girder centroid and slab mid-surface	74
4.24b	Local axes of shell and beam elements	74
4.25	The actual girder-slab connection (a) vs modeled connection (b)	76
4.26	Example 1: 3-girder-slab bridge	79
4.27	Example 2: 4-girder-slab bridge	80
4.28a	Example 3: 6-girder-slab bridge, general plan	81
4.28b	Example 3: experimental and finite element results ..	82
4.29	Example 5: box girder bridge (results at midspan) ...	85

LIST OF FIGURES (continued)

Figure		Page
4.30	Bridge model layout	86
4.31	Model girder reinforcement	87
4.32	Model diaphragm reinforcement	88
4.33	Strips where the prestressing was doubled	92
4.34a	Model slab reinforcement, non-diaphragm regions	93
4.34b	Model slab reinforcement, diaphragm regions	94
4.35	Position, in plan view, of the load cells and surface strain gages	95
4.36	Analytical and experimental middepth transverse stresses in the slab, Test #1	98
4.37	Analytical and experimental middepth transverse stresses in the slab, Text #2R	99
4.38	Analytical and experimental middepth transverse stresses in the slab, Test #3	100
4.39	Analytical and experimental middepth transverse stresses in the slab, Test #4	101
5.1	Vertical load application points	107
5.2	Vertical deflection instrumentation locations for positive moment and minimum positive moment tests	109
5.3	Vertical deflection instrumentation locations for negative moment tests	109
5.4	Locations of existing strain gages used in vertical load tests	110
5.5	Strain gage layout for interior positive moment test on straight-draped side of bridge	111
5.6	Longitudinal relative slab deflection profiles for positive moment service load tests	114
5.7	Transverse relative slab deflection profiles for positive moment service load tests	115

LIST OF FIGURES (continued)

Figure		Page
5.8	Longitudinal relative slab deflection profiles for negative moment service load tests	116
5.9	Transverse relative slab deflection profiles for negative moment service load tests	117
5.10	Longitudinal relative slab deflection profiles for minimum positive moment service load tests	118
5.11	Transverse relative slab deflection profiles for minimum positive moment service load tests	119
5.12	Slab curvature profiles for positive moment service load test on straight and draped tendon section	121
5.13	Longitudinal relative slab deflection profiles for positive moment factored load tests	122
5.14	Transverse relative slab deflection profiles for positive moment factored load tests	123
5.15	Longitudinal relative slab deflection profiles for negative moment factored load tests	124
5.16	Transverse relative slab deflection profiles for negative moment factored load tests	125
5.17	Longitudinal relative slab deflection profiles for minimum positive moment factored load tests	126
5.18	Transverse relative slab deflection profiles for minimum positive moment factored load tests	127
5.19	Slab curvature profiles for positive moment factored load test on straight and draped tendon section	129
5.20	Longitudinal relative slab deflection profiles for positive moment ultimate load tests	130
5.21	Transverse relative slab deflection profiles for positive moment factored load tests	131
5.22	Longitudinal relative slab deflection profiles for negative moment ultimate load tests	132
5.23	Transverse relative slab deflection profiles	

	for negative moment ultimate load tests	133
5.24	Longitudinal relative slab deflection profiles for minimum positive moment ultimate load tests	134
5.25	Transverse relative slab deflection profiles for minimum positive moment ultimate load tests	135
5.26	Longitudinal relative slab deflection profiles for various load levels of interior positive moment ultimate load test with straight and draped strands ..	136
5.27	Transverse relative slab deflection profiles for various load levels of interior positive moment ultimate load test with straight and draped strands ..	137
5.28	Slab curvature profiles for positive moment ultimate load test on straight and draped tendon section	138
5.29	Load-deflection curves for ultimate positive moment tests	139
5.30	Load-deflection curves for ultimate negative moment tests, east slab spans only	140
5.31	Load-deflection curves for ultimate negative moment tests, west slab spans only	141
5.32	Typical cracking in top of bridge slab, positive moment test, straight strand exterior location	144
5.33	Crack patterns on bottom surface of bridge deck, positive moment tests	145
5.34	Crack patterns on bottom surface of bridge deck, outside span of exterior negative moment test locations	147
5.35	Crack patterns on bottom surface of bridge deck, interior negative moment test location, straight strands	148
5.36	Instrumentation and strand utilization for edge of slab posttensioning stress distribution tests	160
5.37	Stress distribution contours for single posttensioning strand at edge of slab	163
5.38	Percent of applied stress in slab near deck edge for various number of tensioned strands	164

LIST OF FIGURES (continued)

Figure		Page
5.39	Area of ineffective prestress between strands at edge of deck	165
6.1	Layout of a typical bridge	168
6.2	Girder and diaphragm dimensions	169
6.3	Finite element mesh configuration	171
6.4	Location of the points studied in the parametric investigation	173
6.5	Transverse stress distribution in deck slab, end- diaphragm case with straight strands, Case = SDE1	175
6.6	Transverse stress distribution in deck slab, all- diaphragm case with straight strands, Case = SDA3	176
6.7	The effect of diaphragm size on slab transverse stresses and diaphragm axial force	177
6.8	Transverse stress distribution in deck slab, end- diaphragm case with draped strands, Case = DDE6	179
6.9	Transverse stress distribution in deck slab, all- diaphragm case with draped strands, Case = DDA8	180
6.10	The effect of diaphragm size on slab trans- verse stresses and diaphragm axial force	181
6.11	The effect of slab Thickness on slab transverse stresses and diaphragm axial force	182
6.12	The effect of span length on slab transverse stresses and diaphragm axial force	183
6.13	Layout of the study bridge, 40° skew case	185
6.14	F.E. mesh configuration of the all-diaphragm case of the study 40° skew bridge	186
6.15	The effect of skew angle on slab transverse stresses and diaphragm axial force	187
6.16	Typical box girder bridge sections	189

LIST OF FIGURES (continued)

Figure		Page
6.17	Typical diaphragm types and locations	192
6.18	1-cell box girder bridge: F.E. idealization of end- and pier-diaphragm regions	193
6.19	2-cell box girder bridge: F.E. idealization of end- and pier-diaphragm regions	194
6.20	3-cell box girder bridge: F.E. idealization of end- and pier-diaphragm regions	195
6.21	1-cell box girder bridge: the effect of end diaphragm on top slab transverse stresses, straight strands	197
6.22	1-cell box girder bridge: the effect of pier diaphragm on top slab transverse stresses, straight strands	198
6.23	1-cell box girder bridge: the effects of end and pier diaphragms on top slab transverse stresses, draped strands	199
6.24	2-cell box girder bridge: the effect of end diaphragm on top slab transverse stresses, straight strands	200
6.25	2-cell box girder bridge: the effect of pier diaphragm on top slab transverse stresses, straight strands	201
6.26	3-cell box girder bridge: the effect of end diaphragm on top slab transverse stresses, straight strands	202
6.27	3-cell box girder bridge: the effect of pier diaphragm on top slab transverse stresses, straight strands	203

C H A P T E R 1

INTRODUCTION

1.1 Problems with Bridge Deck Durability

There are approximately 560,000 bridges in the U. S., of which 45% are structurally deficient or functionally obsolete requiring close to \$50 billion in repair [1,2,3]. Additionally, the interstate highway system that stretches over 40,000 miles across the country will require close to \$500 billion in repairs over the next decade according to the U. S. Department of Transportation [1]. State highway agencies expect bridges to last 50 years or more, but many show signs of corrosion of reinforcement and concrete delamination in five years or less [3]. The problem has become so severe that the phrase "the bridge deck problem" has been coined to specifically imply the distress suffered by bridge decks [3,4].

The cracking suffered by bridge decks under moving vehicular loads facilitates the penetration of water, oxygen, and chloride ions into the concrete, resulting in corrosion of the reinforcement and surface spalling. The mechanism of deterioration has been detailed in the first report in this series [5]. One suggestion for improving bridge deck durability is the application of deck prestressing [6,7]. In composite slab and girder bridges, the decks would be longitudinally and transversely prestressed. In posttensioned box girder bridges, the decks are now longitudinally prestressed and only transverse prestressing would have to be added. "Active reinforcement" of a deck by prestressing would minimize or possibly eliminate cracking of the bridge deck.

Figure 1.1 illustrates the corrosion protection mechanism of prestressing. Since corrosion producing elements can penetrate uncracked concrete with insufficient cover, concrete quality or composition, it is assumed throughout this report that all normal precautions involving provision of adequate cover and concrete quality will be observed. Even in such a well designed and constructed conventional reinforced concrete slab, which more than likely cracks under service load conditions, water, oxygen and salt can penetrate the concrete with subsequent corrosion of the reinforcing steel. However, under the action of prestressing, the applied compressive force prevents cracks from forming or closes the cracks preventing penetration of the corrosion-producing elements.

Unlike many of the other corrosion protection alternatives, there are possible economic advantages in using deck prestressing because of the use of "high efficiency" materials. The utilization of prestressing with smaller, more efficient steel elements would tend to reduce congestion and make concrete placement easier. Moreover, it is

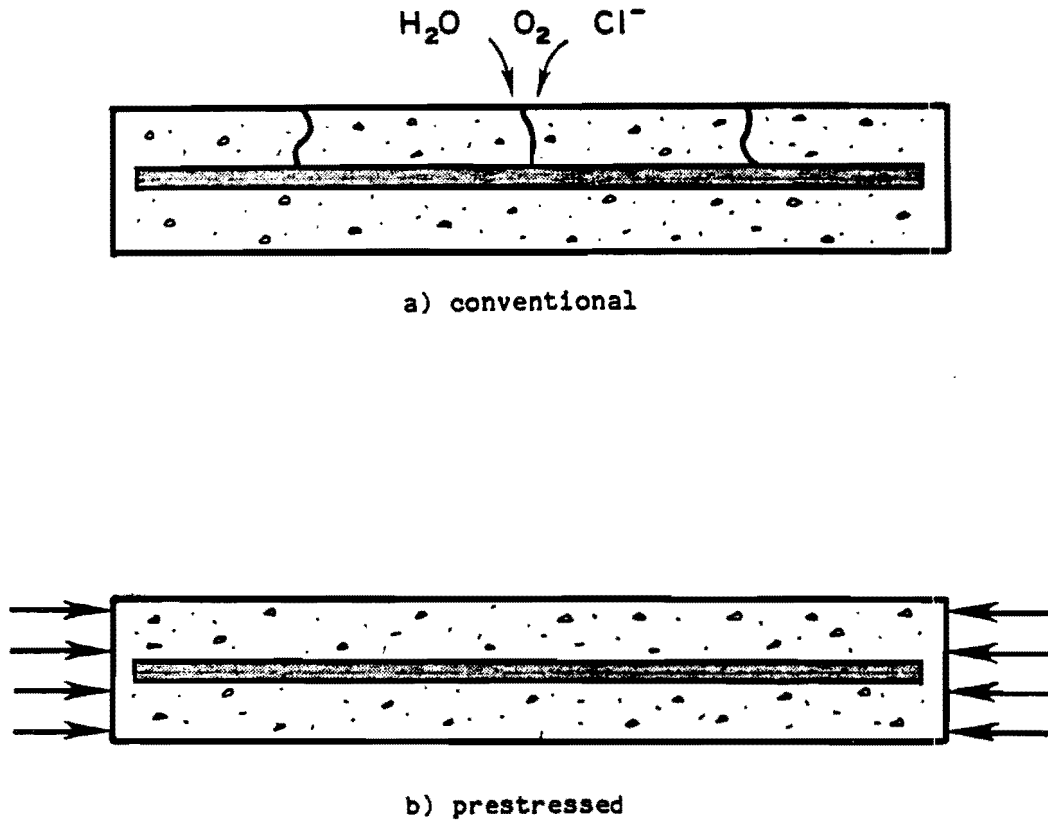


Fig. 1.1 Corrosion protection mechanism of prestressing

believed that the benefits of possible increased durability of bridge decks would more than offset the higher cost of prestressing steel, higher strength concrete and extra labor operations associated with prestressing.

1.2 Design Needs for Transverse Prestressing

Anton Tedesko [7] in 1976 was the first person to clearly expound both the durability and economic benefits of transverse prestressing. Although Tedesko suggested that the advantages of transverse prestressing have a reasonable theoretical basis, there are few documented studies and observations of the actual behavior of such a bridge system [7,8,9,20]. When one examines the present AASHTO Design Specification [11] for prestressed concrete, it is clear that the provisions have been basically developed for longitudinal prestressing. While the provisions may be utilized for transverse prestressing, they do not account for many important variables. For instance, no guidance is given on factors affecting the distribution of prestressing across the slab. Such questions include how much does the lateral stiffness of the longitudinal girders and transverse diaphragms influence the actual distribution of the transverse prestress? If nominal uniform compressive stresses are applied along the edge of the bridge slab, how much is still actually effective at the region over the middle girder? If transverse prestressing is from one edge only, what level of transverse prestressing exists at the far end of the bridge? Additional questions exist which are fundamentally related to the combination of structural effects and durability requirements. Those questions are addressed in the other two reports in this series [5,12].

1.3 Objectives of this Research

The principal objective of the overall research project was to examine the concept of improving the durability of bridge decks with deck prestressing. This principal objective can be further categorized into:

1. Evaluation of the effect of major variables on corrosion protection
2. Evaluation of the structural effects of transverse prestressing
3. Recommendation of design criteria for the economic application of deck prestressing considering the interrelationship between the structural and durability aspects

To help fulfill these objectives, the overall research program was divided into three areas, as shown in Fig. 1.2. The first area was the structural phase summarized in this report in which both analytical and experimental studies were conducted. The second area was the durability phase, in which the main emphasis was the experimental investigation of prestressed concrete exposure specimens. The final area was the formulation of design recommendations for deck prestressing incorporating the results from both the structural and the durability studies.

The scope of the research primarily covers prestressing of composite cast-in-place bridge decks over multiple girders of the general configuration shown in Fig. 1.3. However, many of the conclusions and recommendations relating to the durability aspects are equally applicable to decks of other bridge types. Some examples of structural considerations in box girder bridges are included in this report.

1.4 Report Contents

This report primarily covers the structural effects of the research study shown in Fig. 1.2. A brief review of the basis for current bridge deck design is presented in Chapter 2. A general background of factors affecting transverse prestressing of bridge decks is presented in Chapter 3. Procedures and results of analytical and experimental studies of the effectiveness of transverse prestressing are given in Chapter 4. Procedures and results of both vertical load tests and concentrated edge load tests to determine effectiveness of edge spacing are given in Chapter 5. A brief overview of the results of the analytical parameter studies are included in Chapter 6. The major conclusions from the structural analysis and experimental phases of the research study are summarized in Chapter 7.

Actual design implications, procedures, criteria, and examples are contained in the concluding Report 316-F in this series [12].

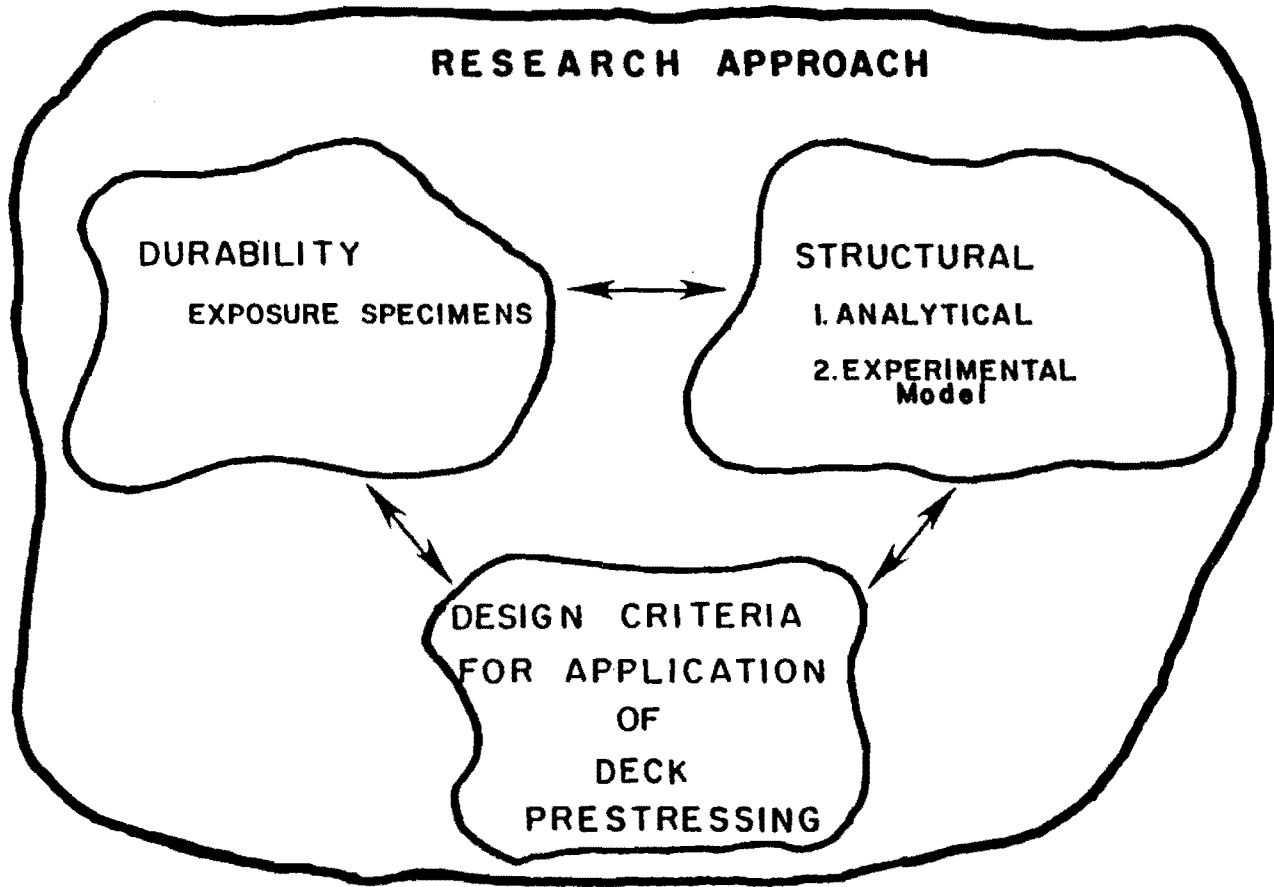


Fig. 1.2 Various components of overall research study on deck prestressing

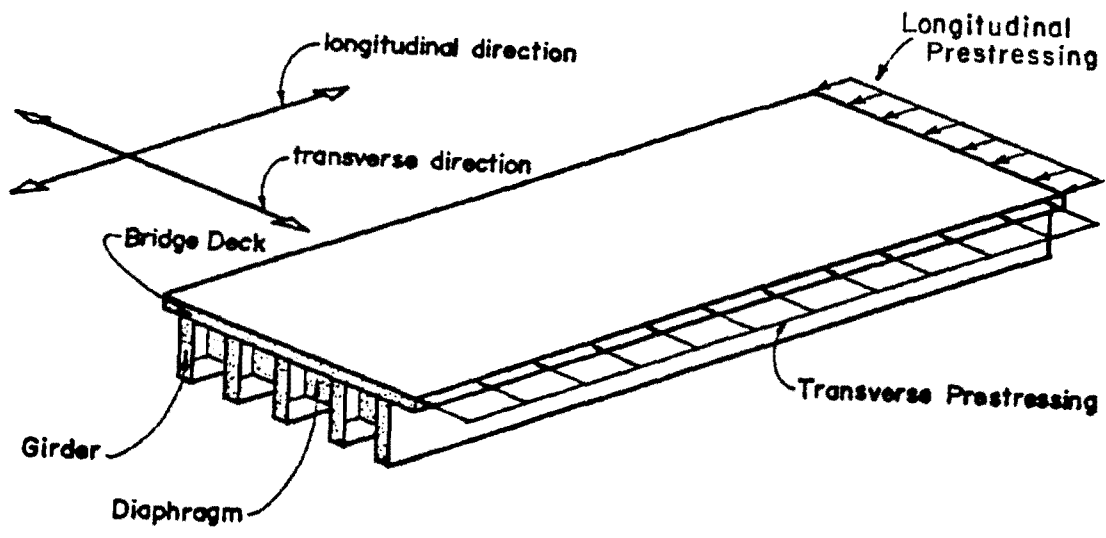


Fig. 1.3 Deck prestressing of a conventional slab-girder bridge

C H A P T E R 2

BACKGROUND OF SLAB DESIGN

Prestressed bridge decks may be considered a special case of concrete slabs. In this chapter, a brief summary of concrete slab behavior and analysis is presented, followed by examples of situations in which concrete slabs have been prestressed to satisfy design requirements. Major research efforts pertaining to concrete bridge decks are discussed, and finally, the current methods of bridge deck design are outlined.

2.1 Review of Concrete Slab Behavior and Analysis

The discussion of concrete slabs may be divided into the areas of elastic and inelastic behavior and analysis. An excellent overview of both these areas of reinforced concrete slabs is given by Park and Gamble [13].

2.1.1 Elastic. At low levels of load, an uncracked, unrestrained concrete slab may be analyzed by classic elastic theory. The basic equation often referred to as "Lagrange's Equation," is a fourth-order partial differential equation relating deflection loading and the flexural stiffness of the slab section. This equation assumes:

- Equilibrium is satisfied at every point in the slab
- The material is linearly elastic and isotropic
- Deflections are small relative to the slab thickness
- Any straight line perpendicular to the middle surface of the slab before bending remains straight and perpendicular to the middle surface after bending
- Direct stresses normal to the middle surface are negligible

Because the boundary conditions are usually complicated for practical cases, direct solution of the differential equation can be quite difficult. Consequently, many approximate analytical techniques have been developed.

For simple cases, "exact" solutions give the deflection of the slab by evaluating enough terms of a suitable series expansion. Internal slab forces are then found using the various derivatives of the deflected shape.

For slabs continuous over flexible supports, numerical moment distribution procedures may be used. Equivalent frame analysis methods are used extensively to analyze slabs in multi-story buildings. A strip of slab, including beams and columns, is used as a two-dimensional frame based on effective member stiffnesses. This "equivalent frame" is then analyzed by conventional means.

Another set of commonly used elastic analysis methods rely on numerical procedures and digital electronic computers. Included in this group is the discrete element technique, where the slab is modeled as a grid composed of beam and torsional elements. This method is especially useful for slabs integral with girders and floor beams. In the finite difference technique, the slab is partitioned using a linear mesh. The intersection of mesh lines is considered a node. Equations can then be written for the deflection of each node in terms of the surrounding nodes, and solved simultaneously for the unknown deflections. Provided the boundary conditions are simple, the finite difference method is good for finding numerical answers to complex slab problems. A very effective analysis technique is the widely known finite element method. The slab is divided into triangular or quadrilateral areas, referred to as elements, connected together at specified nodes. Each element has approximate bending stiffness properties assigned to it. The response of the slab is then found by the solution of equations written for continuity and equilibrium at each of the nodes. The finite element method is well adapted to slab analysis, since a large amount of discretion may be used in selection of the size and type of elements to be used.

2.1.2 Inelastic. As the load on a slab increases, elastic behavior ceases when cracking of the concrete develops. With further load, the critical sections reach the yield moment, maintaining close to that moment capacity with increased curvature, while yielding of the reinforcement spreads to other sections of the slab. The spread of plastic hinging is known as the formation of yield lines. The load level corresponding to the various stages of behavior is primarily influenced by the span to thickness ratio, reinforcement ratio, and edge restraint of the slab. The edge conditions assume particular importance if significant lateral and rotational restraint is provided by the slab surrounding the loaded area and/or the vertical slab supports. Under these circumstances (which occur in most bridge decks) in-plane compressive forces are induced in the slab because as the slab deflects vertically, the edges tend to move outward and react against the bounding elements (Fig. 2.1). Known as compressive membrane action or arching, this effect greatly enhances both the ultimate load capacity and stiffness of the slab.

In the case of a slab without edge restraint, failure will occur when the yield lines extend to the point that further redistribution of moments is no longer possible. For a uniformly loaded underreinforced slab with sufficient edge restraint, behavior is

characterized by three stages, as shown in Fig. 2.2. In the phase from A to B, elastic behavior initially occurs, followed by cracking and the formation of yield lines. During this stage, restraint forces due to arching increase linearly from commencement of loading (A) to the maximum compressive membrane strength at point B. The load at B characteristically is developed at a deflection of approximately one-half the slab thickness. Between points B and C, the geometry of the slab has changed sufficiently such that the in-plane forces detract from slab strength, and contribute to further deflection. As illustrated in Fig. 2.3, this happens because the centroid of compression in the middle of the slab is below the centroid of compression at the slab edges. At point C, enough deflection has occurred to eliminate the horizontal restraining forces and instead, activate the reinforcing as a tensile net. Failure of the slab is at point D when the reinforcement fractures or loses anchorage. When a slab is loaded with a concentrated load instead of distributed load, the failure mode will usually be punching shear before the slab reaches maximum arching strength at point B. The load at which this punching shear failure occurs may also be affected by arching action. Since compressive membrane action reduces the amount of flexural cracking, more concrete is available in compression to resist shear stresses around the periphery of the loaded area, thus increasing shear strength.

The analysis of two-way concrete slabs at ultimate behavior is generally accomplished using either the strip or yield line methods. More recently, techniques have been developed to account for the contribution to flexural and shear strength of arching effects.

The strip method, developed by Hillerborg [14], allows the selection of a distribution of moments such that:

- Equilibrium is satisfied at any point
- Yield moment of the slab at a given section is not exceeded
- Boundary conditions are satisfied

This method ignores torsion and in-plane forces, so that a two-way slab is considered as a series of independent strips spanning in each direction. Applied loads are assigned to each strip by the analyst's judgment, and moments are computed with ordinary beam theory. Such an analysis is considered a lower bound limit analysis in that it can be shown that the true ultimate load is greater than or equal to that calculated.

Limit analysis of concrete slabs by the yield line theory was mainly developed by Johansen [15]. The ultimate load of a slab is found by first postulating a collapse mechanism consisting of a series of plastic hinge lines along which the ultimate moment of the slab has

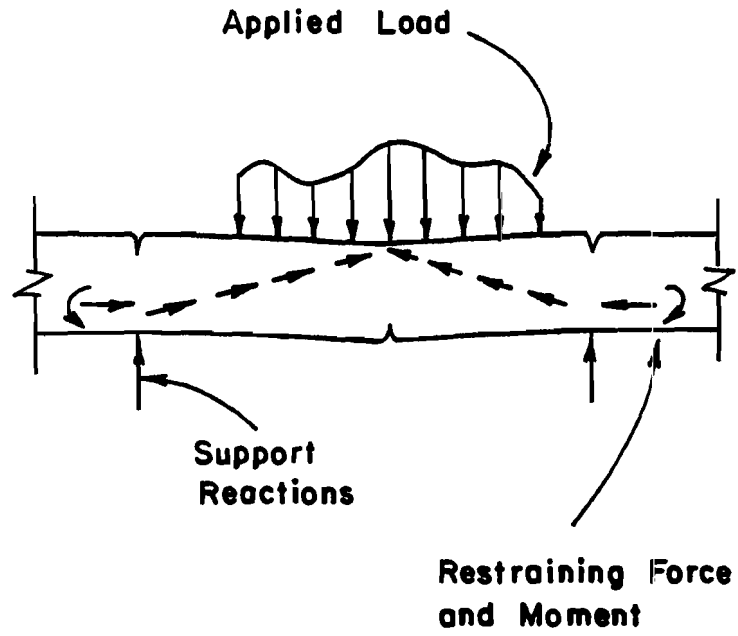


Fig. 2.1 Arching action in concrete slabs

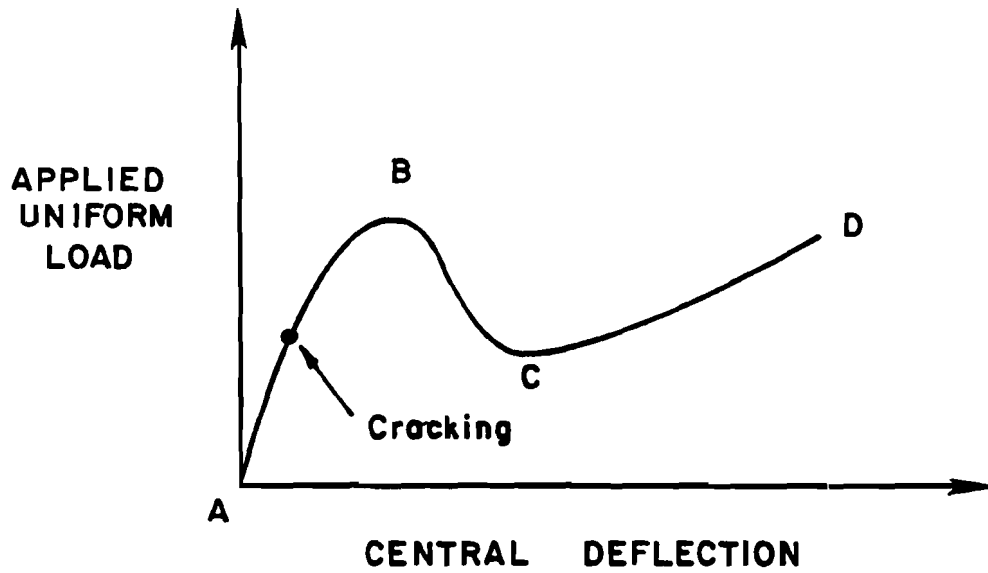


Fig. 2.2 Load deflection relationship for two-way reinforced concrete slab with edges restrained against lateral movement [13]

been reached. Then, either the principle of virtual work or the equations of equilibrium are applied. If virtual work is used, the solution is an upper bound one, giving an ultimate strength of the slab equal to or greater than the actual capacity. If the equations of equilibrium are used, the solution is a lower bound, and the actual capacity is at least that calculated. When the solution satisfies both virtual work and equilibrium, it is unique and equal to the actual slab capacity.

Compressive membrane effects for uniformly loaded slabs may be taken into account in a manner similar to the strip method of analysis [16,17]. The slab is divided into a series of strips spanning in each direction. Yield sections are introduced into each strip near the location of yield lines. The portions of the strips between yield sections are assumed to remain straight and ultimate load is assumed to occur at a deflection of one-half the slab thickness. Using this model with the principles of virtual work, and including axial forces in the strips, the strength of the slab is determined.

The analysis of a concrete slab subject to concentrated loads has been developed [18] for a punching shear mode of failure to include the effects of arching. The idealized mechanical model adopted for this situation is shown in Fig. 2.4. The portion of the slab outside of the failure cone is considered to be loaded through a compressed conical shell beneath the perimeter of the loaded area. Forces acting on the sector element shown in Fig. 2.4(b) are:

- The oblique compression force $T\beta/2\pi$ from the compressed conical shell
- Horizontal forces from reinforcement R_1 and R_2
- Horizontal compressive forces in the concrete, R_3
- Boundary restraints F_b and M_b

The boundary restraint forces are found using assumed maximum boundary stresses and forces modified by a restraint factor ranging from 0 to 1 to account for practical boundary conditions. Considering the sector element equilibrium and adopting an empirical failure criterion based on strain near the shear crack, the theoretical punching load, P , is determined in an iterative process. This theoretical punching load is then corrected for dowel effects to give the ultimate punching load of the slab.

2.2 Previous Applications of Prestressed Concrete Slabs

Prestressed slabs have been used in a number of design situations. These applications can give insight into the successful

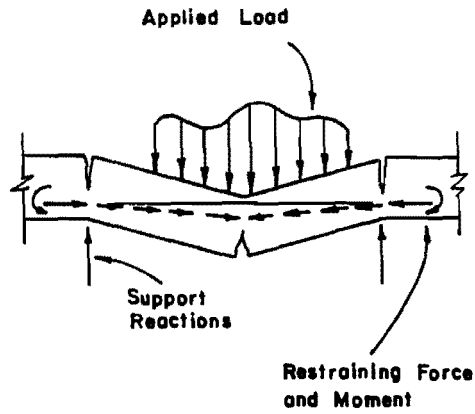
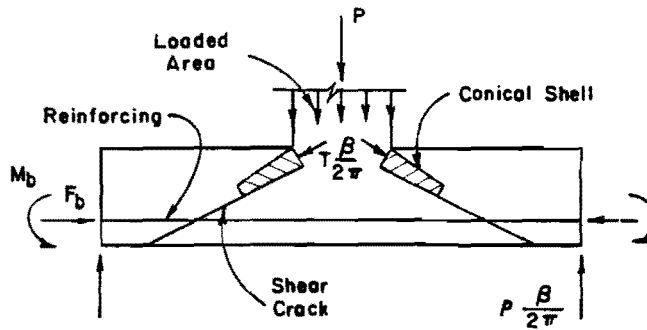
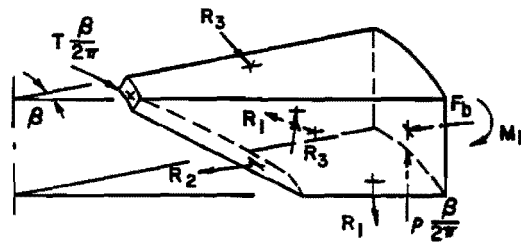


Fig. 2.3 Arching action in concrete slabs after peak load



(a) Section Showing Boundary Forces



(b) Sector Element Showing Slab Forces

Fig. 2.4 Mechanical model of a slab with boundary restraints at punching failure [18]

implementation of transversely prestressed bridge decks. The three main areas of usage for prestressed slabs are bridges, buildings and, more recently, pavements.

2.2.1 Bridges. Longitudinally posttensioned slabs are used for some short span bridges. This system has the advantages of simple construction and very small superstructure depth. By far the more common usage of prestressed slabs in bridges, however, is in bridge decks. This subsection will introduce only a few applications. A much more detailed summary is given in Chapter 3.

Posttensioned box girder bridges are often constructed with transversely posttensioned deck slabs. In such a design the gravity loads imposed on the deck and the transverse shortening of the deck due to posttensioning must be analyzed with respect to the box section as a whole. The resulting deck has the advantage of being in compression both longitudinally and transversely. In addition, the prestressed slab is usually thinner than a conventional deck, thus reducing the superstructure dead load. An example of tendon geometry for a transversely posttensioned deck is shown in Fig. 2.5.

Precast-prestressed concrete deck panels are routinely used as stay-in-place forms for typical slab and girder bridges. The 4-in. thick panels span between adjacent girders and act compositely with the cast-in-place portion of the deck. Use of the panels saves materials and labor normally required for deck formwork.

Several innovative uses of prestressed concrete for bridge decks have been made recently, in addition to the more common applications. In the early 1970's, a bridge was designed and built in Dallas, Texas, which incorporated a concrete deck posttensioned in both directions [20]. To facilitate stressing, measures were taken to ensure the 10-1/2-in. thick slab was free to move horizontally relative to the steel floor beam and girder superstructure. Though a detail installed later connected the slab to the supporting steel beams, composite action was not utilized in the capacity of the bridge. A recent visit to this structure, more than a decade after construction, revealed no signs of cracks or corrosion in the prestressed slab, while adjacent conventional reinforced concrete segments of bridge deck showed significant cracking with evidence of water seepage through the cracks.

In 1983, the deck of the Woodrow Wilson Bridge in Washington, D.C., was replaced by precast, prestressed concrete slabs. The 8-in. thick slabs, measuring approximately 46 ft by 10 to 12 ft, were posttensioned transversely at the casting plant, and longitudinally after installation in lengths of 140 to 285 ft. Lightweight concrete, unbonded tendons and non-composite action were utilized in this design. The advantages of this method of reconstruction were that by working at night traffic was maintained during peak hours, the project

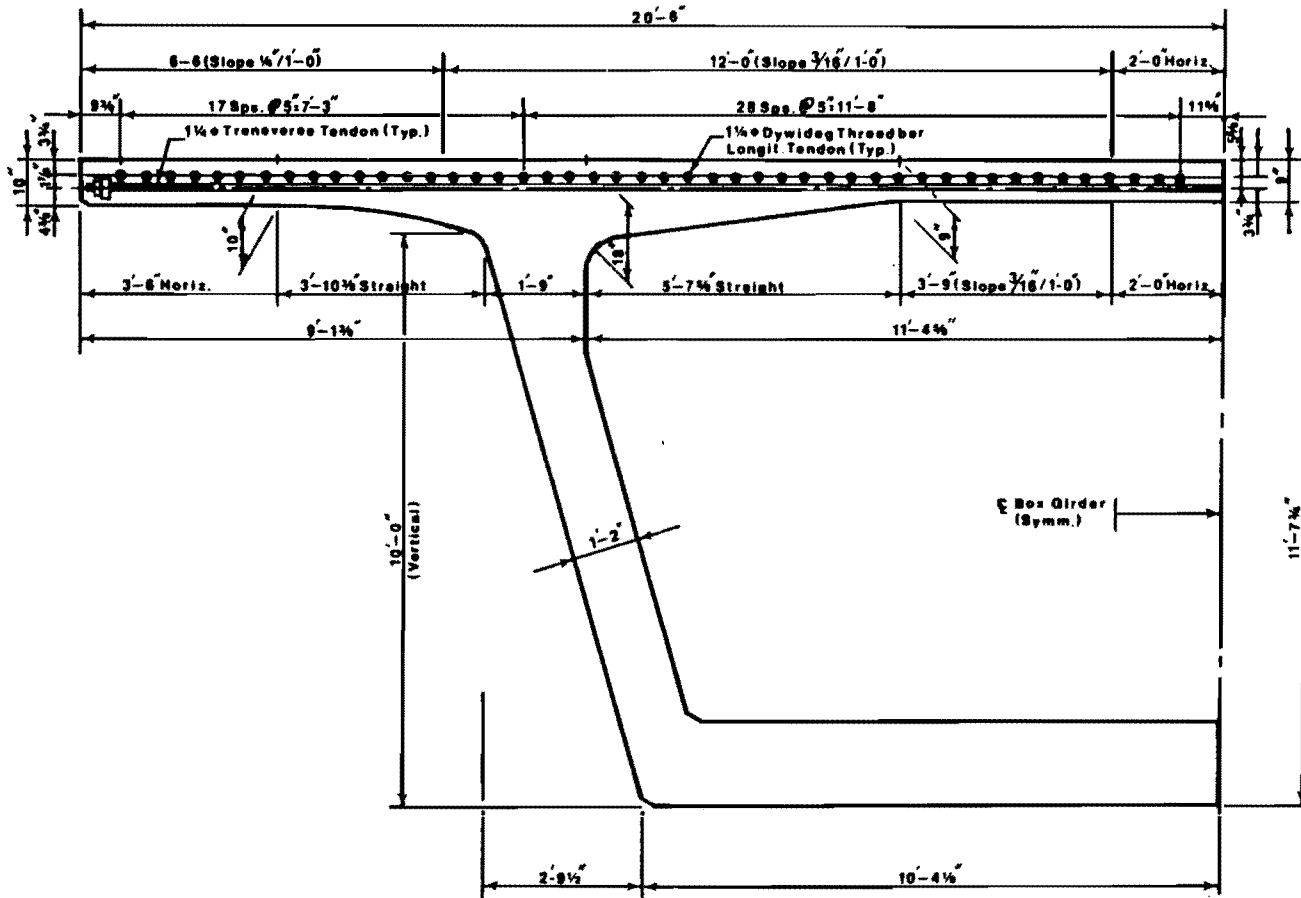


Fig. 2.5 Transverse and longitudinal posttensioning, Kishwaukee Bridge, Illinois [19]

was completed swiftly, the cost was relatively low, and the finished deck was posttensioned in both direction, increasing durability.

2.2.2 Buildings. Posttensioned concrete slabs have become a very popular form of construction for commercial and residential buildings including parking structures, apartments and office buildings. Such designs typically have span-to-depth ratios of 42 to 48, utilize draped tendons, and may be either one-way or two-way slabs. While stiffness of the supporting elements must be taken into account, in general the restraint forces in building slabs are reduced relative to other applications of posttensioning because of the lower compressive stress levels required.

It is useful to note that many parking garages constructed with prestressed concrete have experienced severe deterioration due to chloride induced corrosion [21,22]. Salt and melting ice from parked vehicles tend to accumulate in localized areas of the garage floor. Concrete cracks due to temperature, shrinkage, and creep effects together with insufficient concrete cover, inadequate tendon sheaths, gaps in the grease coating, and incomplete anchorage protection often allow the brine solution to penetrate to the susceptible tendon resulting in heavy corrosion and in some cases tendon failure.

2.2.3 Pavements. From the early 1970's, posttensioned concrete slabs have been used on a limited basis as a roadway surface resting on grade [23]. Typically, such pavements consist of a 6-in. thick slab constructed on a prepared subbase and prestressed in the longitudinal direction only with a single layer of tendons to a level of 200-300 psi. Sections of slab up to 600 ft long are stressed as unit with unbonded tendons. To minimize friction losses between the slab and the ground, a double layer of polyethylene sheeting is provided just beneath the concrete.

An extension of this concept, which also incorporates some features of bridge deck design, was recently constructed as part of Interstate 70 through Glenwood Canyon in Colorado. As Figs. 2.6 and 2.7 illustrate, the roadway slab is posttensioned with two layers of unbonded tendons placed at an angle of 60 degrees to the centerline of the roadway. An 8-in. thick section is used for the on-grade portions, increasing to a 12-in. depth to provide a 6-ft cantilever. Note that protection of the anchorages is provided by casting the concrete barriers over the epoxy-coated anchorage components.

Prestressed pavements built to date are reported to be performing adequately [23]. The one area of difficulty has been the transverse expansion joints, where movements of up to 1-1/2-in. must be accommodated. Typical problems include corroded and frozen expansion hardware, deterioration of the joint sealer, and failure of the joint armor.

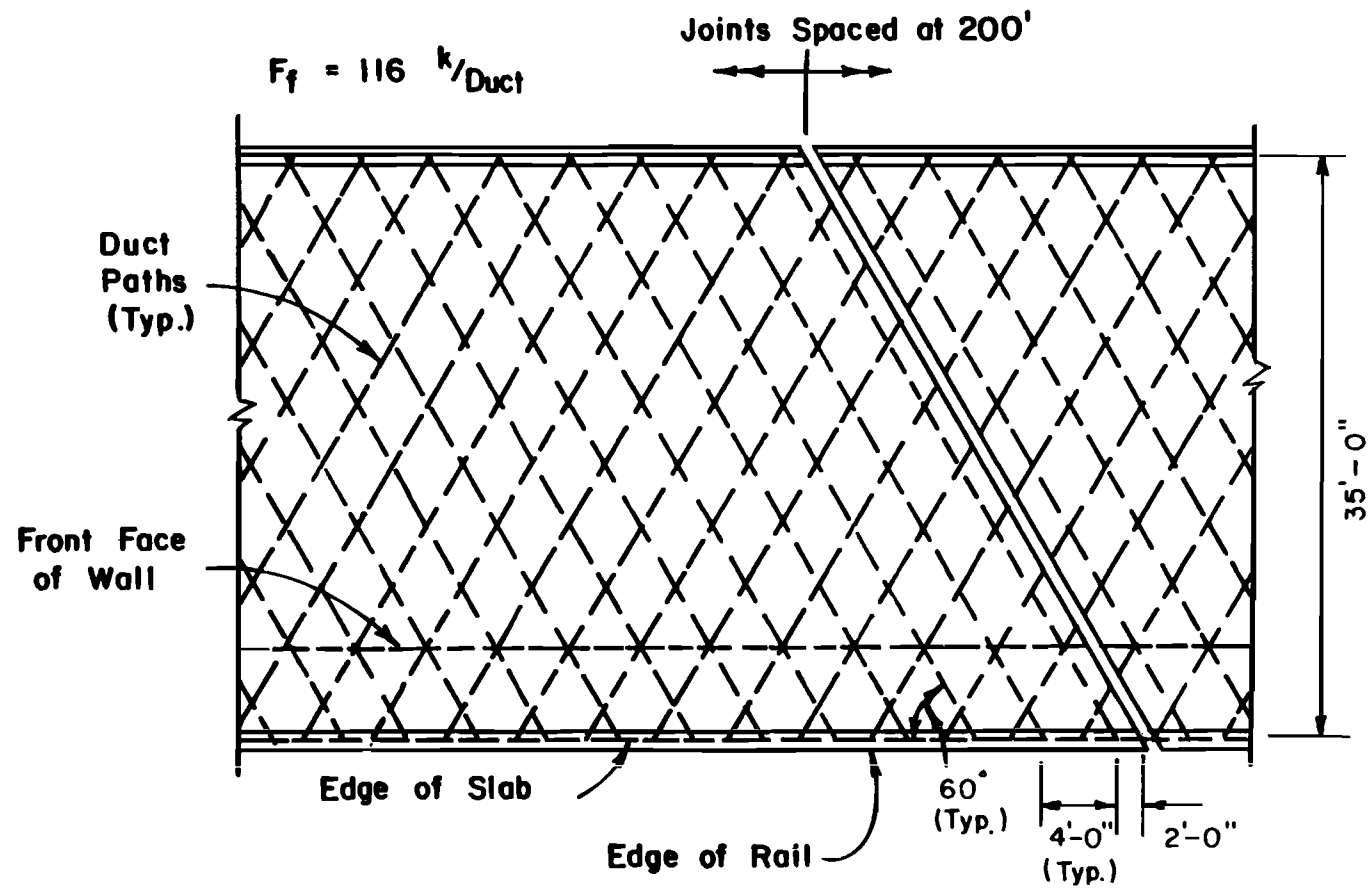


Fig. 2.6 Partial plan of prestressed roadway slab for I-70 through Glenwood Canyon, Colorado [40]

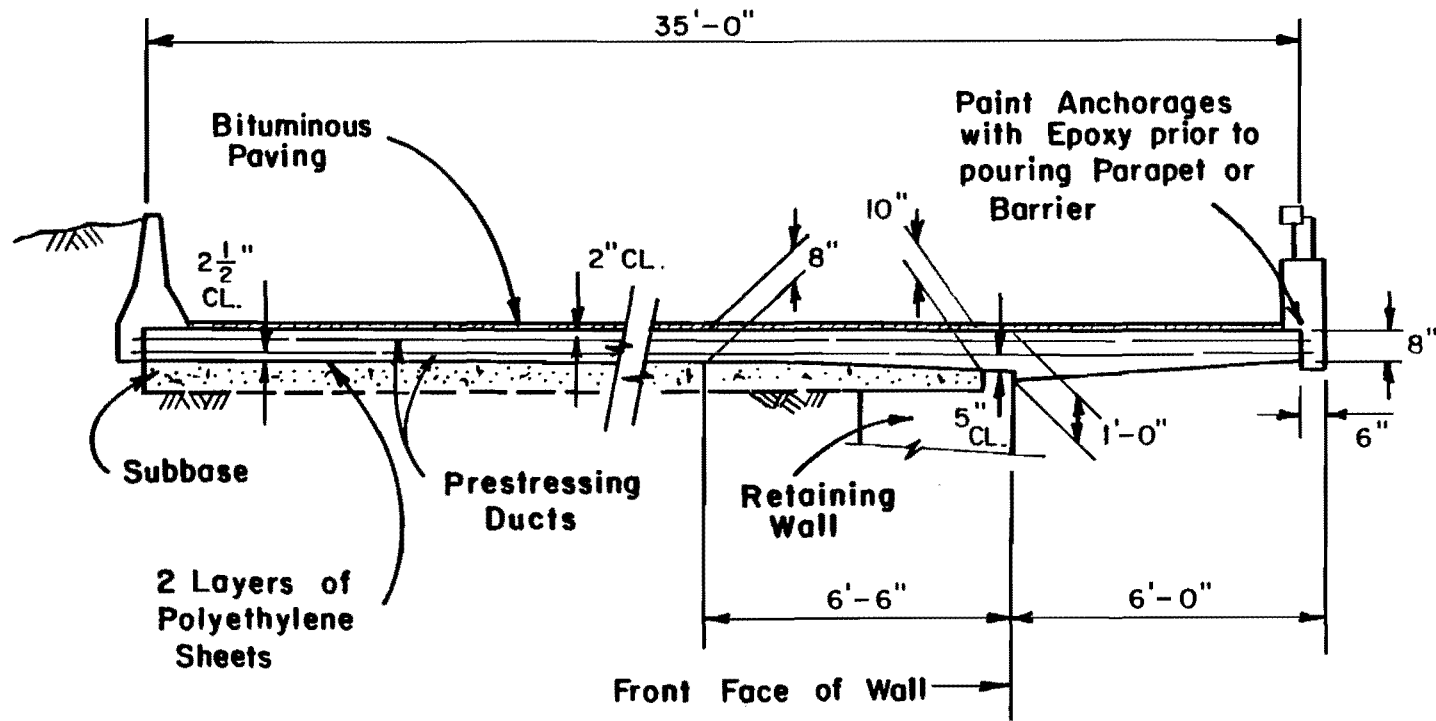


Fig. 2.7 Section of prestressed roadway slab for I-70 through Glenwood Canyon, Colorado [40]

A recent application of prestressing in highways for the specific purpose of improving durability was a prestressed concrete road pavement built in Lubbock, Texas [57]. The town officials allowed the prestressed pavement to be substituted for reinforced concrete because "... they thought prestressing would hold up better to the site's severe conditions." The prestressed concrete pavement was installed at a cost of \$18/sq. yd. instead of \$24/sq. yd. estimated for a reinforced concrete pavement.

2.3 Related Research

Major research investigations involving concrete bridge decks have been carried out by both the University of Illinois [24,25,26,27,28] and the Ontario Ministry of Transportation and Communications [18,29,30,31]. Numerous other studies [32,33,34,35,36,37,38,39] dealing with the distribution of wheel loads through the deck, or with concrete slabs in a more general sense, have also been reported.

2.3.1 The University of Illinois. Westergaard's classic study in 1930 [28] of the effect of concentrated loads on an infinitely wide simple span slab was the forerunner of later research on bridge decks at the University of Illinois. This study developed the concept of replacing concentrated loads with an equivalent small area of uniform load. It then used a classical elastic analysis to obtain an influence surface relating moments in the slab to concentrated loads applied at any location. Although limited by assumptions such as the supports are simple and non-deflecting, this work formed the foundation for later studies and directly influenced the present AASHTO specifications for the distribution of loads in concrete slabs.

A large research program on bridge decks was conducted at the University of Illinois from 1936 to 1954 [27]. The research can be classified into four categories:

1. Fundamental analytical and experimental studies concerned with various aspects of reinforced concrete slabs. Most notable in this category are the studies [24,25] extending Westergaard's work using approximate analytical techniques as discussed in Sec. 2.1.1
2. Investigations of simple-span solid-slab bridges with integrally cast curbs
3. Investigations of slab and girder type bridges
4. Studies of composite construction for I-beam bridges, with special attention to shear connectors

For the purpose of bridge deck design, the most important results of this research are the analytical studies mentioned above [24,25] and the design recommendations published by Newmark [26], all of which form the basis for current AASHTO provisions.

2.3.2 Ontario. Beginning in the mid 1960's, as part of the development of the Ontario Highway Bridge Design Code, the Ontario Ministry of Transportation and Communication sponsored an extensive testing program which eventually led to the incorporation of the effects of compressive membrane action into bridge deck design. Much of this work [18,29] was carried out at Queen's University in Kingston, Ontario.

Conventionally designed reinforced concrete bridge decks were shown to fail in punching shear, not flexure as assumed in design practice, with an average factor of safety of 16, and minimum of 13. This behavior was explained through the concept of compressive membrane enhancement of flexural and shear strength as discussed in Sec. 2.1.2. From this it was decided that concrete bridge deck design should be based on requirements for durability and crack control, rather than the less critical criteria of strength. An empirical deck design, using a minimum thickness of 9-in. and 0.3% isotropic reinforcement in the top and bottom portions of the slab, was proposed, verified through laboratory and prototype tests, and adopted into the Ontario Highway Bridge Design Code. A concise summary of this research may be found in the supplement to the OHBDC [30].

Research is currently (1985) underway at McMaster University in Hamilton, Ontario, to extend the concept of the Ontario Bridge Deck Design using transverse prestressing [31]. This study involves determining the amount of transverse prestressing required in a single layer of a 7-in. thick deck to produce a slab design equivalent to the OHBDC empirical design.

2.3.3 Other Research. In the late 1960's, two major studies were initiated which were closely related to bridge deck design, but not directly applicable. The objective of these programs was to develop lateral load distribution criteria for bridges. The first study, directed by Sanders at Iowa State University, was conducted under the National Cooperative Highway Research Program [37]. It resulted in recommended load distribution factors dependent on the aspect ratio, relative stiffness of beams and floor, relative diaphragm stiffness, and the extent of continuity. For most cases, the proposed distribution factors did not give significantly different values from the current AASHTO Specifications. The second research program was done at Lehigh University by Van Horn et al. [39]. This study also developed recommended lateral load distribution factors. Neither of these studies' recommendations were ever incorporated into the AASHTO bridge design specifications.

Many other studies related to concrete bridge deck behavior but not directly associated with the major efforts at the University of Illinois or Ontario have been reported. Some of these have dealt with membrane action in slabs, such as work by Park [36], Taylor and Hayes [38], Acki and Seki [32], and Brotchie and Holley [34]. Others, such as a recent study by the New York Highway Department [33] and current research at Ferguson Laboratory at The University of Texas [35], have focused on model tests of both conventional and Ontario Bridge Deck designs. The New York study found factors of safety of at least six times the design wheel load. At The University of Texas, researchers are investigating the strength and fatigue characteristics of the Ontario design using full scale bridge span models with both a cast-in-place slab and with a deck slab constructed using precast-prestressed panels as stay-in-place forms.

2.4 Current Design Practice

The design of concrete bridge decks in North America presently follows either the standard specifications published by the American Association of State Highway and Transportation Officials (AASHTO) [11] or the relatively new empirical method of design put forth in the Ontario Highway Bridge Design Code (OHBDC) [30]. In addition, many state highway departments require bridge designs which they review to incorporate more stringent provisions than the design codes.

2.4.1 AASHTO Specifications. The AASHTO requirements which pertain to reinforced and prestressed concrete bridge deck design are summarized in this section. Though many of the provisions for prestressed concrete were intended for applications of longitudinal prestressing of superstructure elements, they are often assumed in this report to apply also to transversely prestressed deck slabs. The numbers in parentheses refer to the corresponding section in the specifications.

Loads: The HS 20 design live load basically consists of a 32 k axle load (3.7), increased by 30% to account for dynamic effects (3.8). The resulting concentrated wheel group load (including impact) of 20.8 k may be considered, for the purposes of more exact methods of analysis, to be applied over an area 8-in. long and 20-in. wide (3.30). When load factor design is used, the Group I ultimate load is computed as (3.22):

$$U = 1.3 (DL + 5/3 (LL + I))$$

where:

DL = dead load

(LL + I) = live load including impact

Analysis: For a slab monolithic with the supporting girders, the span length is taken as the clear distance between slab supports. In the case of steel girder supports, the span length is the distance between the edges of the girder flanges, plus one-half of the flange width (3.24.1).

When analyzing a longitudinal deck edge, the concentrated wheel load is positioned one foot from the face of the curb or rail (3.24.2), while the transverse edge, the load is considered directly at the slab edge and must be supported by a diaphragm or by other means (3.24.9).

Detailed analysis of the central portion of the slab is usually circumvented entirely in ordinary slab and girder bridges through the use of an approximate equation for transverse bending moment in simple spans (3.24.3):

$$M = ((S + 2)/32) P$$

where: M = moment per foot width of slab (ft-lb)
 P = wheel load (lb) (16,000 pounds for H20 loading plus impact allowance).
 S = effective transverse span length (ft).

When the slab is continuous over at least three supports, a continuity factor of 0.8 is applied to the above value and the positive and negative moments are assumed to be equal.

Alternately, a more exact elastic analysis is allowed (3.24.3 and 8.4). The most commonly used method for this is the influence surfaces giving moments per unit length presented by Pucher [41] and Homberg [42]. Once the fixed end moments are found in this way, they may be distributed transversely across the deck to obtain the design moments.

After determining the design moments by either the empirical equation or elastic analysis, the deck is designed in 1-ft wide transverse strips for flexure only. If flexural requirements are satisfied, shear is considered non-critical (3.24.4).

Design: Reinforced concrete decks may be designed by either the service load or load factor method (8.14.1). Certain provisions apply to both methods. Concrete cover is to be taken as a minimum of 2-in. for the top surface and 1-in. for the bottom of the slab (8.22.1). Where analysis indicates reinforcing is required, the minimum area of reinforcement provided must be able to develop a factored moment at least 1.2 times the cracking moment of the section, based on the modulus of rupture of the concrete (8.17.1). In the surfaces of slabs

where reinforcing is not otherwise required, a minimum of 1/8 sq. in. of steel per ft must be provided to control temperature and shrinkage cracking. The spacing of this reinforcing is not to exceed 18-in. or three times the thickness of the slab (8.20). Fatigue considerations are ignored (8.16), but control of crack width is implicitly provided by checking the equation (8.16.8.4):

$$f_s = z/(d_c A)^{1/3} \leq 0.6 f_y$$

where: f_s = stress in reinforcing at service loads (ksi)
 z \leq 170 k/in. for moderate exposure
 \leq 130 k/in. for severe exposure
 d_c = thickness of concrete cover (in.)
 A = effective area of concrete surrounding flexural tension reinforcement (in.²)

Deflection control is established by requiring a minimum thickness in ft of (8.9):

$$((S + 10)/30) \geq 0.542$$

where S = effective transverse span length (ft).

Allowable stresses for service load design are (8.15.2):

$$f_c = 0.4 f'_c$$

$$f_s = 20 \text{ ksi (Grade 40 reinf.)}$$

$$f_s = 24 \text{ ksi (Grade 60 reinf.)}$$

and the strength reduction factor used with factored load design is 0.90 for flexure (8.16.1.2).

As with other applications of prestressed concrete design, prestressed decks must satisfy both stress requirements at service loads and strength criteria (9.13.1). Cover requirements for prestressed and conventional steel in slabs are 1-1/2 in. in the top surface, increased to 2 in. if deicer salts will be used, and 1 in. in the bottom (9.25.1).

Allowable prestressing steel stresses are given as (9.15.1):

$$0.7 f'_s \text{ at release}$$

and

$0.8 f_y^*$ under service loads after losses

where: f_s' = ultimate strength of prestressing steel
 F_y^* = yield point stress of prestressing steel

Concrete compressive stresses are not to exceed $0.55 f_{ci}'$ in posttensioned slabs immediately after release, or $0.40 f_c'$ at service loads after all losses have occurred (9.15.2). Tensile concrete stresses permitted are as follows:

$6 \sqrt{f_c'}$ for normal exposure with bonded reinforcing
 $3 \sqrt{f_c'}$ for severe exposure with bonded reinforcing
 0 without bonded reinforcing

Also, posttensioned anchorage stresses in the concrete are limited to 3000 psi, but not to exceed $0.9 f_{ci}'$.

Prestress losses may be calculated by a simple method presented in the specifications, or a lump sum loss may be assumed (9.16). The maximum amount of prestressed steel allowed is such that (9.18):

$$p^* (f_{su}^*/f_c') \leq 0.30$$

where: $p^* = A_s^*/bd$, ratio of prestressing steel.

The minimum amount of steel necessary is the same as for reinforced concrete slabs.

When calculating the strength requirements of the prestressed section, the strength reduction factor is taken as 0.95 as opposed to the 0.90 for non-prestressed reinforced concrete sections (9.14).

Other Requirements: For both reinforced and prestressed concrete deck slabs, reinforcement parallel to the bridge girders is specified for the bottom of the deck to provide for distribution of concentrated loads. The percentage of the main reinforcement required for this purpose is $220/\sqrt{S}$ (where S = effective transverse span length in feet), not to exceed 67%. This steel must be placed in the middle one-half of the slab span, with an additional amount of reinforcing, at least half again as much, to be distributed in the outer quarter spans of the slab (3.24.10).

2.4.2 OHBDC Provisions. The Ontario Design Code allows the use of elastic or ultimate analysis (but not the empirical moment equation) and design methods similar to the AASHTO provisions for the

design of concrete bridge decks. For decks of common composite beam-slab type bridges, however, an empirical design method may be used provided certain conditions are met.

This empirical design consists of providing a minimum of 0.3% reinforcement in each direction in the top and bottom of the deck (7.8.5.1), which is calculated using an average of the two effective depths in a given slab face. Such a design is assumed adequate for crack control and shear requirements, but must be checked for transverse moment and shears due to differential deflection when used with steel box girders with widely spaced diaphragms. Also, cantilever portions of the deck must be analyzed and designed by conventional means.

Conditions which must be satisfied for the use of the empirical design may be summarized as follows (7.8.5.2):

1. The slab must not span more than 3.7 m (12 ft) and must extend past the centerline of the exterior girder a minimum of 1.0 m (3 ft, 3 in.)
2. Span to thickness ratio is not to exceed 15
3. Minimum slab thickness is 225 mm (9 in.) and maximum spacing of reinforcement is 300 mm (12 in.)
4. Diaphragms in steel I and box girder bridges must be extended throughout the bridge cross section and be spaced less than 8.0 m (26 ft)
5. Spacing of shear connectors is not to exceed 0.6 m (2 ft)
6. Transverse edges of the slab must be supported by diaphragms or other means

The required minimum concrete cover is specified as 50 mm (2 in.) for the top mat and 30 mm (1-1/4 in.) for the bottom layer of reinforcing.

2.4.3 Other Design Requirements. Many state highway departments have requirements for bridge deck design in addition to those found in the AASHTO Specifications for projects funded with state or federal monies. For instance, the Colorado Department of Highways specifies design must be done by the working stress method, with an allowable steel stress, regardless of reinforcing grade, of 20 ksi. In addition, concrete cover is to be 2-1/2 in. for the top reinforcement and all steel within 4-in. of the upper surfaces of bridge decks and parapets must be epoxy-coated [43].

CHAPTER 3

TRANSVERSE PRESTRESSING

3.1 Introduction

Even though the idea of transverse prestressing in bridge decks for improved durability is relatively new, there have been numerous previous applications of transverse prestressing, particularly in box-girder bridges. This chapter reviews previous applications and studies of transverse prestressing as well as current prestressing technology, code provisions and practices which are applicable to its use.

3.2 Previous Applications of Transverse Prestressing

An extensive literature review revealed that the earliest applications of transverse prestressing in bridge decks were apparently in Europe around 1960 [7]. The main reason for its use was to increase the length of cantilever overhangs in box-girder bridges and to reduce the number of interior webs as illustrated in Fig. 3.1. The reduction in number of webs reduced construction costs. Transverse prestressing was also used in pier regions to reduce congestion in reinforcing steel layout, to achieve positive connection between longitudinal beams, and in decks of voided-slab bridges. In the earliest applications, the idea of enhanced durability in bridge decks was not specifically recognized.

In contrast to the early European applications, the first American application was the previously mentioned steel girder expressway bridge built in Dallas, Texas, in the early 1970's [20]. The concrete deck was posttensioned longitudinally as well as transversely. In this case, prestressing was specifically used for crack control and to minimize maintenance. Thus far, the bridge deck has shown no signs of deterioration. Design studies in connection with the Dallas bridge concluded that transverse posttensioning should not be used with composite slab-girder action. This conclusion was reached because of lack of experimental evidence on slab restraint effects. The designers were concerned with possible detrimental interaction between the concrete deck and supporting girders during transverse posttensioning which might severely reduce the effective prestress force. The bridge was designed so that the slab would slide over the beams during posttensioning. In fact, the beam-slab interface was greased to reduce friction. Because of the conservative design philosophy, much of the possible cost reduction was lost due to the prevention of full composite action.

Based partly on this experience with the Dallas bridge, the primary focus of the present investigation was the feasibility of transverse prestressing of composite cast-in-place decks of standard-type slab-girder bridges. At the inception it was felt that noncomposite slabs might have to be cast and stressed with subsequent shear transfer devices installed to produce composite action. However, it is now apparent that for most bridges of interest, the procedures verified experimentally and analytically in this study should permit transverse posttensioning without requiring subsequent major steps to develop composite action.

Since the Dallas bridge, there have been several other transversely prestressed bridges built in the United States [44,45]. These have been box-girder type bridges, with posttensioning used in the cast-in-place bridges, and pretensioning used in the precast segmental bridges. Again, as for their earlier European counterparts, the primary motivation for transverse prestressing in these bridges was to maximize the length of cantilever overhangs and decrease the number of interior webs. Table 4.1 of Ref. 46 summarized approximately 30 bridges built around the world which have utilized transverse prestressing [6,7,44,45,47,48,49,50,51,52,53,54,55,56].

There have been a few studies of transverse prestressing in bridge decks. However, they were primarily conceptual studies with little, if any, information on tests or measurements. They dealt with precast pretensioned units for deck replacements, and completely ignored composite cast-in-place decks [10,58,59]. One study [8] in the 1960's reported on the influence of transverse prestressing on the strength of prestressed concrete bridge slabs. However, this study focused only on flat-plate type slabs with no supporting girders. A detailed literature review revealed no other analytical or experimental investigations concerning the use of transverse prestressing in composite cast-in-place decks.

Several highly detailed theses and dissertations have been completed as part of the present overall research program at The University of Texas at Austin. Details of the study not included in these reports can be found in those references. Poston [46] summarized both the durability experiments and the development of design criteria. Almstafa [60] developed techniques for the analysis of transverse prestressing effects in bridge decks. His study included a parametric investigation of various structural effects using three-dimensional finite element analysis. Results from the design, construction and testing of a model bridge were presented by Mora [61] and Ralls [9]. Their work primarily involved the experimental investigation of structural effects in the application of transverse prestressing to a composite slab-girder bridge model. The experimental behavior of the model bridge to vertical loads and development of design procedures was reported by Phipps [63].

3.3 Prestressing Systems for Bridge Decks

There are three possible systems which can be used for the application of transverse prestressing in bridge decks. The first is the utilization of pretensioning prestressing. This system is best suited for precast deck systems. Pretensioning used in conjunction with a cast-in-place deck would require large structural bulkheads to maintain the prestressing until the deck is cast and the subsequent transfer of force into the hardened concrete can take place. The most common method for pretensioning tendons is mechanical jacking. However, in Russia, the electrothermal method of prestressing has found wide usage in pretensioning. Electric current is used to heat and expand prestressing steel, which is then held at the ends. As the steel cools and tends to shrink, it is stressed [64,65]. In pretensioned systems the details of the protection of the ends of the tendons become critical. They provide a channel for moisture to enter the concrete if not fully encapsulated. Also, the use of unprotected prestressing tendons, which is common in deck pretensioning applications, has been severely limited by federal and state highway agencies until further research indicates no potential for corrosion [66].

The second and third systems applicable to transverse prestressing involve the use of unbonded and of grouted posttensioning, respectively. The use of posttensioning is most prevalent in cast-in-place construction. Stressing is generally mechanical stressing with hydraulic rams. The electrical method has been used but it has been found to be uneconomical [65]. In the bonded system the tendons are posttensioned and then grouted. The degree of protection provided by the grout varies considerably, depending on the grout and grouting procedure [67]. In the unbonded system the tendons are left unbonded but are afforded corrosion protection through external coverings such as extruded plastic-coating and grease or wrapping with sisal kraft paper. The greases which are used sometimes contain anti-corrosives or corrosion inhibitors [68]. Unbonded systems have not been widely accepted in bridge applications because of the concerns for corrosion protection and for control and distribution of cracking due to overloads. Posttensioning systems require protection of the anchors. However, a distinct advantage of the grouted system is that failure of the end anchors should not significantly impair the structural integrity of the bridge if effective bonding has been achieved. The need for complete encapsulation of the tendon system in a corrosion resistant barrier and the need for adequate auxiliary bonded reinforcement to ensure adequate structural integrity are emphasized in the design recommendations in Report 316-3F of this project.

There is a wide variety of systems available for posttensioning applications. These include conventional wire and strand systems as well as the threaded bar system. However, few currently available

anchor systems are specifically designed for thin deck slab construction. A number of unbonded monostrand anchors are available for thin sections. Most of the available multistrand posttensioning anchors are either cone, bell or plate type. Their design generally calls for a capability of handling at least five tendons. In these anchor types the tendons are generally arranged in circular pattern, as shown in Fig. 3.2a. This pattern is not conducive to use in thin sections such as deck slabs. Anchors which place the tendons in only one or two horizontal planes, as shown in Fig. 3.2b, are probably better suited for thin-section applications. Discussions with industry representatives indicate some preliminary designs and prototype testing have been completed for thin-slab section anchors primarily intended for posttensioned flat-plate building structures. However, their comments suggest that this type of anchor should be easily adaptable for applications of transverse prestressing in bridge decks.

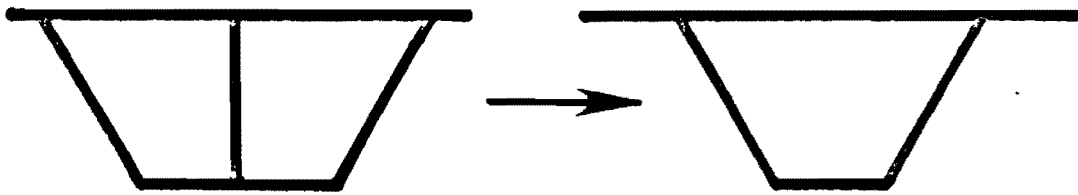
At present, the most common multistrand posttensioning duct is circular. However, industry is designing flat, rectangular ducts, both rigid and flexible, which are compatible with the newly developed thin-section anchors.

3.4 Current Applicable Code Provisions and Practice

3.4.1 Design Bending Moments. The transverse strength of a bridge deck must be adequate to resist the imposed external vertical loads. This strength can be provided by conventional reinforced, prestressed or partially prestressed concrete. In the U. S., the most common approach for the design of bridge decks is according to the AASHTO Specifications [11]. The basis for AASHTO transverse slab design was reviewed in Sec. 2.4.1.

The intent of the AASHTO transverse slab design procedure is to provide for the same moment capacity at positive and negative moment regions. However, there is no definitive guidance in AASHTO regarding the design for possible reversal of moments at a section. It is general practice in the U.S. to place the same amount of reinforcement over the girder regions for negative moment as at the middle section of the slab panel for positive moment. Half of the above amount of reinforcement is used at these sections for the case of moment reversals, as shown in Fig. 3.3.

However, tests performed by Newmark and Siess [27] and others [48,69] indicate that the maximum negative moment in the slab over the girders is smaller than that given by current AASHTO Specifications. Table 3.1 compares the relative amounts of reinforcement suggested by Newmark and Siess to that of current AASHTO practice. This table reveals that AASHTO is conservative for the maximum negative moment in the slab over the girders, and is extremely conservative for the



No Transverse
Prestressing

With Transverse
Prestressing

Fig. 3.1 Transverse prestressing in box-girder bridges

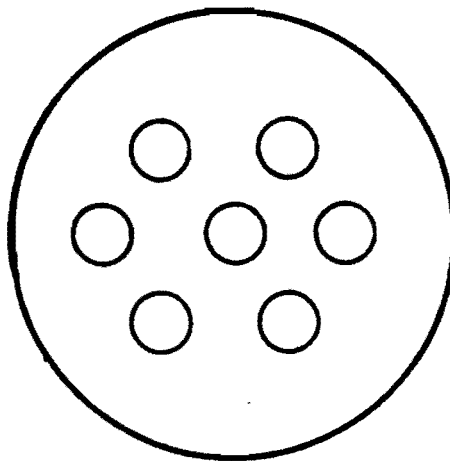


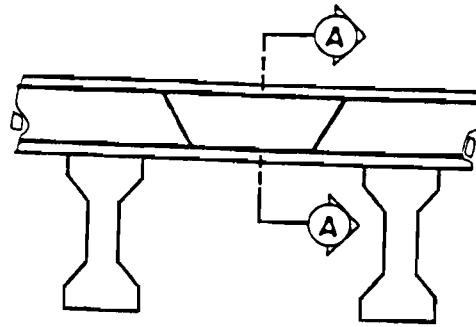
Fig. 3.2a

Circular Anchorage
Pattern

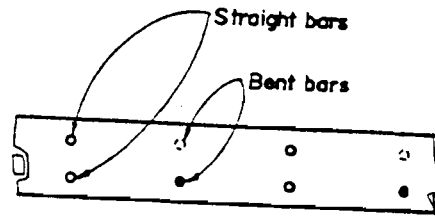


Fig. 3.2b

Thin-Section Anchorage



Straight & Bent bars



Straight & Bent bars

Section A-A

Fig. 3.3 Transverse reinforcement in bridge decks [60]

Table 3.1 Relative Amounts of Transverse Reinforcement in Bridge Slab

Slab Location	AASHTO		Newmark and Siess	
	Middle of Panel	Over the Girders	Middle of Panel	Over the Girders
Bottom (+ Mom.)	1.0	0.5	1.0	0.4
Top (- Mom.)	0.5	1.0	0.2	0.7

maximum negative moment at the middle of the slab. Adoption of smaller maximum negative design moments in the slab would allow a corresponding increase in concrete cover and protection. It would also permit greater tendon spacings for transversely prestressed bridge decks, and thereby reduce costs.

3.4.2 Stress Distributions. Prestressing tendons spaced along the edge of a bridge deck represents a fairly complex analysis problem. There is very little information available in the literature which aids in the analysis of this problem. The physical situation of forces applied at anchor locations on the edge of a bridge deck translates into a mathematical problem of finding stresses in an elastic media where point loads are applied along a straight boundary.

There is a two-dimensional, closed-form theory of elasticity solution for the problem shown in Fig. 3.4 of a concentrated force acting on a horizontal straight boundary of an infinitely large plate [70]. However, this solution is severely limited for the application of transverse prestressing in bridge decks. It is for a single force only, and does not include interaction effects of several point loads, such as the case of many anchor locations along the bridge slab. In addition, it cannot account for lateral stiffness effects of girders and diaphragms in a bridge.

There are several discrete-element computer programs available for the global analysis of conventional slab-girder bridges. However, these programs only permit vertical loads on the bridge deck. They do not consider the possibility of in-plane loads such as is the case for transverse prestressing.

Because of the lack of available analysis techniques for transversely prestressed bridge decks, two- and three-dimensional finite element analysis computer programs were developed as part of the overall research program. These computer programs offer great flexibility for determining stress distributions in transversely prestressed bridge decks. Almstafa, in his work, describes the three-dimensional finite element analysis program which he used for parametric investigations of structural effects in transversely prestressed slab-girder bridges [60].

3.4.3 Use of Diaphragms. Since diaphragms are built perpendicular to the longitudinal girders, and hence parallel to the main reinforcement in a deck slab, they may have a significant restraining effect on the prestressing distribution in a transversely prestressed slab. End diaphragms are usually provided at supports of slab-girder bridges. The end diaphragms "tie" the longitudinal girders together and provide an efficient means of transferring the lateral loads acting on the superstructure to the substructure. Additionally, end diaphragms provide support for the deck slab between the girders at the end regions of a bridge for those cases in which

the slab is not continuous in the longitudinal direction for several spans for live load only. Besides end diaphragms, interior diaphragms are generally used between girders at one or more locations between end supports. Figure 3.5 shows typical locations and types of diaphragms used in current practice for a short span bridge.

The effectiveness of end and interior diaphragms in slab-girder bridges under static and dynamic loading has been investigated by several researchers [71,72]. They conclude that interior diaphragms are not necessary based on the structural behavior of the completed bridge and thus could be omitted. However, interior diaphragms are useful to aid in bridge erection and to provide lateral stability of the structural girder skeleton until the deck is cast.

3.4.4 Anchorage Zone Design. A number of problems have occurred in posttensioned applications in both bridges and buildings which indicated that design procedures and criteria of anchorage zones for posttensioning tendons needed further examination and refinement. Significant cracking occurred in many cases but was controlled by the presence of additional reinforcement in the anchorage zone. Even though capacity of the member was not reduced in these cases, the cracks which appeared provided a path for penetration of aggressive substances resulting in corrosion. The formation of cracks negates one of the principal advantages of prestressed concrete, namely the minimization of service load cracking.

Because of the recent problems with posttensioning anchorage zones, a comprehensive analytical and experimental research program was conducted at The University of Texas at Austin [73,74,75]. That study resulted in recommendations and guidelines for anchorage zone design of thin-web posttensioned members as shown in Fig. 3.6. Because of geometry differences, the recommendations from that study are of limited use in thin-slab applications such as in the case of transversely prestressed bridge decks.

There is one effect that the Texas research study did not include which could be critical for transversely prestressed bridge decks. The recommendations from the study are specifically for single anchorage zones in a thin section and do not directly consider interaction effects of multiple anchorages. The application of transverse prestressing in bridge decks requires the use of multiple anchors along the edge as shown in Fig. 3.7. While some limited tests were run in connection with a prototype structure in this project, further research is needed in this area.

3.4.5 Tendon and Anchor Protection. Even though transverse prestressing in bridge decks has been suggested as a way of improving durability, it is implicit that such a "crackfree" design can only ensure corrosion protection if adequate thickness of concrete cover, adequate concrete quality and adequate compaction exist so that

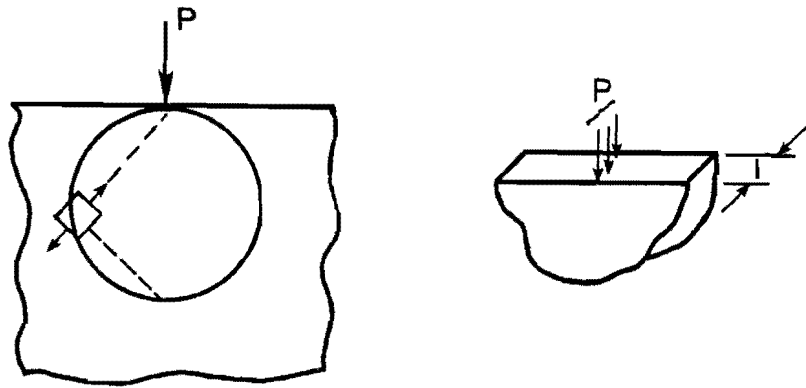
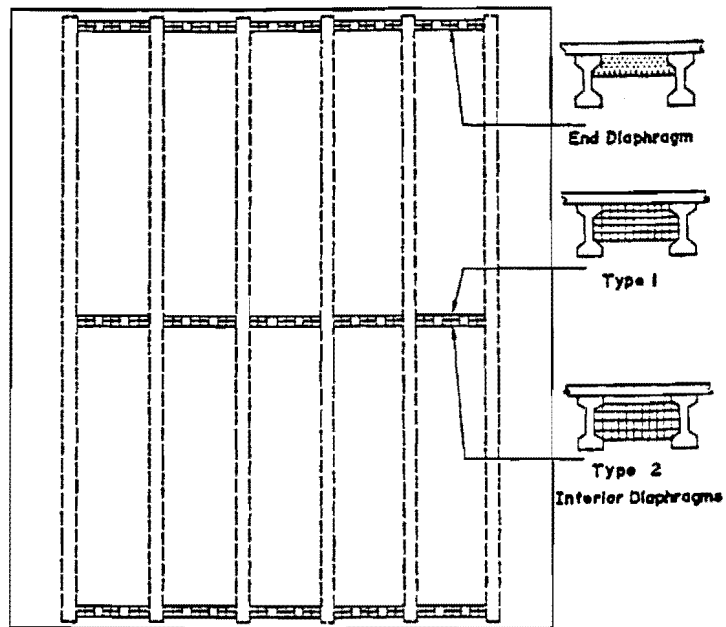


Fig. 3.4 Concentrated force at a point of straight boundary



PLAN VIEW

Fig. 3.5 Typical locations and types of diaphragms for short-span slab-girder bridges [60]

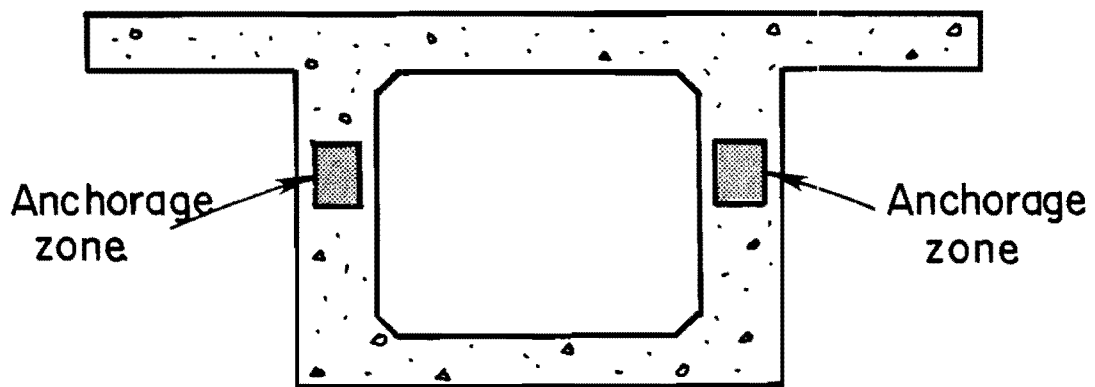


Fig. 3.6 Anchorage zones in a thin-webbed box-girder section

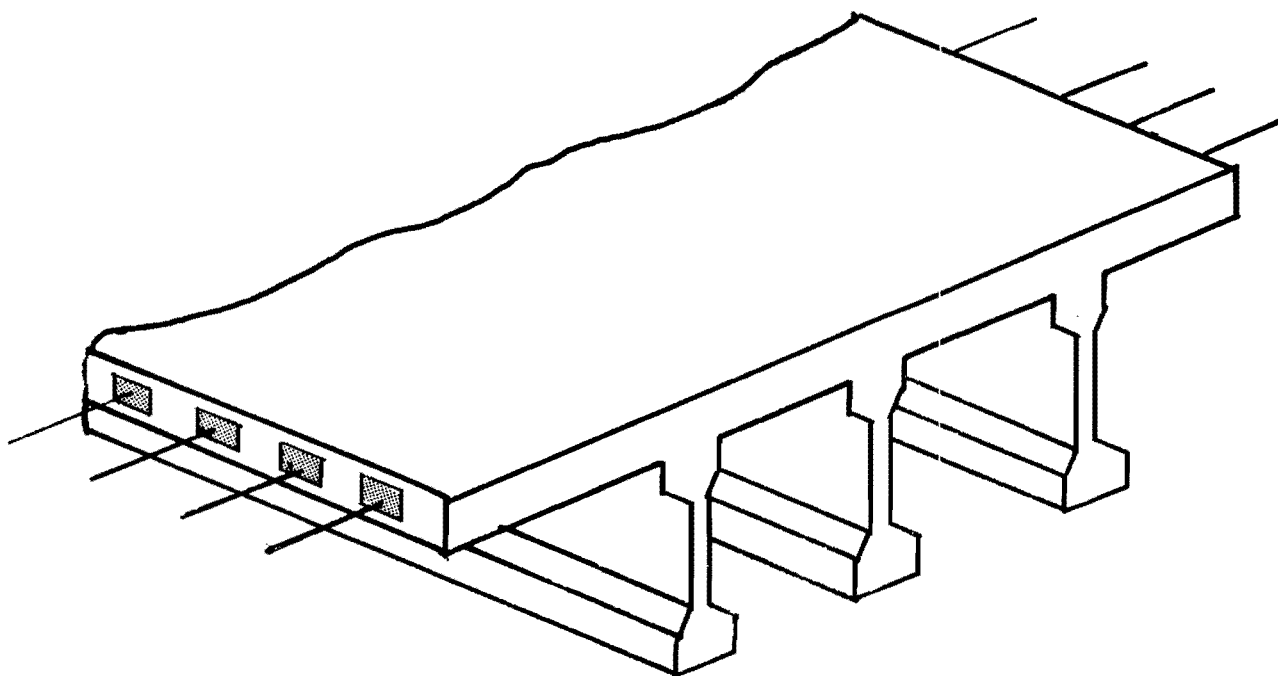


Fig. 3.7 Multiple anchorage zones in a transversely prestressed bridge deck

"uncracked" concrete provides the necessary barrier to inhibit the corrosion mechanism. In addition, its effectiveness depends on adequate corrosion protection of anchors. There are important differences between unbonded prestressing and bonded (grouted) prestressing systems, not only from a structural point of view, but also in regard to protection against corrosion. With bonded tendons the prestressing steel is embedded in a portland cement grout, which results in an alkaline environment with a high pH which should provide good protection. For unbonded tendons, the prestressing steel is surrounded by a heavy grease which results in a chemically neutral environment, which by itself does not provide protection against corrosion. In some cases, the greases used may contain anti-corrosives. Furthermore, the lack of bond is particularly critical for an unbonded tendon since the loss of an anchor or portion of the tendon to corrosion implies the loss of load-carrying capacity and thus overall structural integrity. Authorities [68,76,77] agree on the basic pitfall in the protection of prestressing systems. In general, prestressing tendons are well protected in sound dense concrete. However, the protection can break down because of faulty and careless construction practices which leave prestressing tendons and anchors vulnerable to attack.

There are several common sense practices which ensure a well-protected bonded tendon [77]. The first is to ensure an adequate anchorage plug at the stressing end where the anchor is recessed as shown in Fig. 3.8. FIP [76] recommends a normal portland cement mortar with low-shrinkage properties. Adhesion of the mortar to the concrete hardened in the pocket is improved by using a resin bonding agent on the sides of the pocket. Secondly, proper grouting provides adequate protection for the prestressing tendon. There are no known cases of catastrophic failure of bonded tendons due to corrosion in which proper grouting techniques had been used. A good grout calls for no bleed voids, which is a separation of the cement and water before initial set. The use of an expansive agent and an admixture that controls bleeding also produces superior grout.

However, in unbonded construction, corrosion failures produce dramatic failures. Schupack's [77] description of the failure is as follows:

...Failed unbonded tendons, because of the sudden release of energy, tend to shoot out of their enclosure. The projectile nature of this type of failure is obviously a hazard to life, besides the overall structural concern...

The problem is especially critical because if an unbonded tendon fails, the total tendon is lost. FIP [76], HERON [68] and PTI [78] recommendations call for the unbonded tendon to be covered with a water impermeable grease and then wrapped in a tough protective sheathing such as polyethylene. Furthermore, the common practice of

leaving that portion of the strand adjacent to the anchor exposed to concrete as shown in Fig. 3.9 should be discontinued. The gap between the end of the sheath and the stressing anchorage contradicts the basic intent of the grease and sheathing. As for the case of bonded tendons, the anchor plug for unbonded tendons should be painted with a resin bonding agent, then packed using a suitable non-shrink mortar. Finally, current practice calls for special care in tendon placement to ensure no punctures or indentations in the sheathing leaving the strand unprotected.

Schupack [77] recently presented an excellent idea for protecting prestressing tendons, as shown in Fig. 3.10. His concept calls for the encapsulation of the tendon completely from end to end which electrically isolates the tendon. This isolation requires a tough plastic to take the bearing stresses under the anchor plate. He estimates that the costs of this protection would be as low as 1% of the total cost for a parking structure. The same functional concept is recommended by the recent HERON and PTI reports [68,78]. With the tendon isolated by a plastic sheathing, the HERON and PTI reports recommend use of an epoxy capping around all steel components at the ends of the strand and at the anchorages. This functionally results in an electrically isolated tendon. However, the concept of the electrically isolated tendon, which was developed by Schupack and Suarez [77], is patented in the U.S. and is under patent review in various other countries.

The Post-Tensioning Institute recently completed a specification for unbonded tendons [78]. This specification also recommends the idea of a fully encapsulated tendon at all locations, and the need for complete water tightness. Additional recommendations are provided for minimum material properties and construction procedure which should provide unbonded tendons with corrosion protection. Specific performance requirements for corrosion preventative coatings and greases which surround unbonded tendons are also included. The relative fragility and the generally low cost of plastic sheathings argue strongly for thicker, tougher sheathings which can better resist shipping, handling and local tie tendencies to produce cuts or slits in the sheathing.

3.4.6 Transverse Prestressing Specifications. The current AASHTO Specifications [11] relating to prestressing were developed principally for longitudinal prestressing. The early authors of the AASHTO Specifications for prestressed concrete envisioned the use of prestressing principally only in the longitudinal direction in precast girders and box-sections. The present AASHTO Specifications are severely limited in the coverage of transverse prestressing. This, of course, is one principal reason why the present research program was initiated. Report 316-3F [12] provides definitive guidance for the utilization of transverse prestressing in bridge decks.

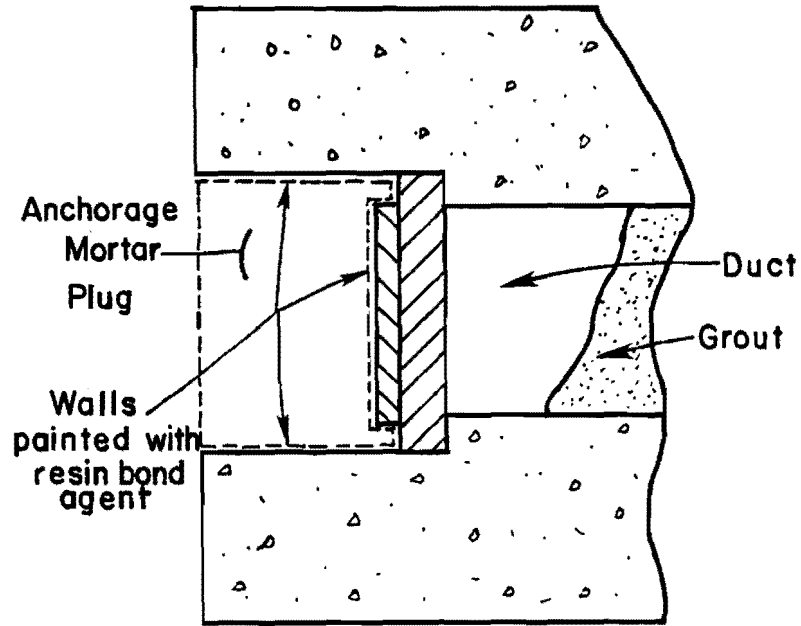


Fig. 3.8 Anchorage plug for corrosion protection

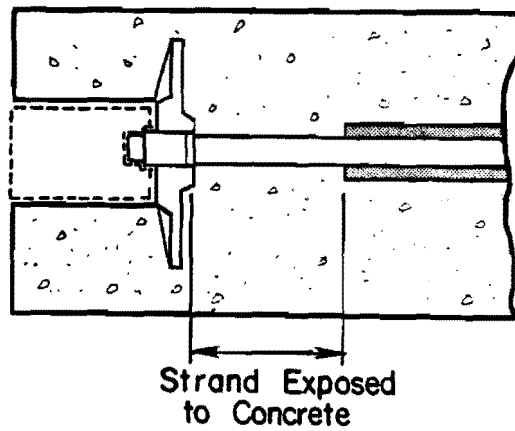


Fig. 3.9 Poor practice in unbonded tendon construction

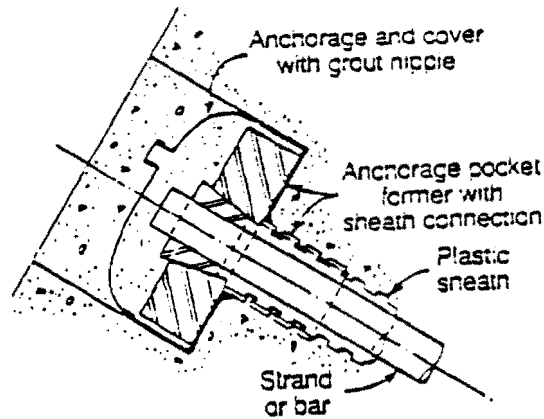


Fig. 3.10 Electrically isolated tendon suggested by Schupack [77]

CHAPTER 4

STRUCTURAL BRIDGE MODEL

4.1 Introduction

As previously shown in Fig. 1.2, one major component of the overall research program was the experimental testing of a laboratory model bridge to assess the structural effects of transverse prestressing. This chapter briefly summarizes the experimental testing which was conducted to determine the effective distribution of the prestress force, and discusses the design of the transversely posttensioned deck of the laboratory bridge model. Since the bridge model had to be designed before detailed results were available, the design process reported herein may be considered provisional. After interpretation of the test results, a design process was finalized and is reported in Report 316-3F [12]. Generalized analytical results, detailed experimental data from testing the model bridge, and comparisons between analytical and experimental results, can be found in other studies [9,46,60,61,63] which were a part of the overall research program on transverse prestressing. The major results affecting prestress force distribution are briefly summarized in this chapter. The results pertaining to slab behavior under vertical load and under single concentrated edge loads are reported in Chapter 5. The important design implications are discussed in Report 316-3F [12].

4.2 General Description

Models are routinely used in structural engineering. In cases where the structure or material is too complex to represent analytically, where the structure which must be tested is too large for laboratory conditions, or where a check of analytical procedures is required, a model test is very useful.

Under service load conditions, a prototype bridge structure is subjected to vehicular loads amounting to as much as 100 kips per lane of traffic. At an ultimate limit state, this translates into loads exceeding 225 kips per lane. Considering the size of a prototype bridge as well as the level of applied loads, it would have been difficult to test a full-scale transversely prestressed prototype bridge. Therefore, a 0.45 scale true model of a prototype bridge was constructed and tested.

The bridge model utilized transverse prestressing in the deck, but otherwise was conventional in design. It was constructed using precast, prestressed concrete girders and exterior and interior concrete diaphragms. Moreover, the model bridge was designed to take advantage of composite action between the deck and girders, which is

standard bridge design practice. The primary objective of the testing was to experimentally determine the state of stress in the model bridge deck which was transversely prestressed. Supplemental testing of the model bridge included vertical load tests simulating vehicular traffic. This testing was conducted primarily to complete the overall design verification of a bridge which utilizes transverse prestressing.

4.3 Model Prototype Design

The prototype structure selected for modeling in the laboratory was a single span of a conventional multispans bridge designed by the Texas State Department of Highways and Public Transportation (TSDHPT) and to be located over Oso Bay in Corpus Christi, Texas. The superstructure of the prototype bridge consists of TSDHPT Type C prestressed concrete girders, simply supported between bents with a reinforced concrete deck slab. Figure 4.1 illustrates a typical layout of the prototype bridge. It is common practice to sometimes use a continuous deck slab over interior bents even though the girders are simply supported. Continuous slabs are primarily used to reduce the number of articulated expansion joints. These expansion joints require routine maintenance, and thus fewer expansion joints mean lower maintenance costs. In addition, fewer expansion joints provide for a smoother riding surface on a bridge. However, since the laboratory model was only a single span, the model deck slab necessarily represented those cases in which the deck slabs are not fully continuous at interior bridge bent locations.

The use of a particular prototype bridge as the focal point of the laboratory study was appropriate for several reasons. First, it represents the most common bridge structural system used by the TSDHPT. Secondly, the bridge is located in a marine environment which will challenge the durability of the slab. Third, the bridge possesses features which highlight some of the concerns and questions with respect to the application of transversely prestressed bridge decks. In particular, the question concerning the effect of the lateral stiffness of girders and diaphragms on the stress distribution over the bridge deck. Finally, it was hoped that a portion of the actual prototype bridge could be built following the recommendations derived from the research study. This would have permitted a direct field comparison of the performance of a conventional reinforced concrete and a transversely prestressed concrete deck system. Unfortunately, the timing of the research program to that of the bridge construction did not permit this.

The prototype structure was first designed and the model dimensions determined by scaling for similitude requirements. The bridge was designed for AASHTO [11] HS20-44 live load and for an unshored construction procedure. An excellent account of the modeling

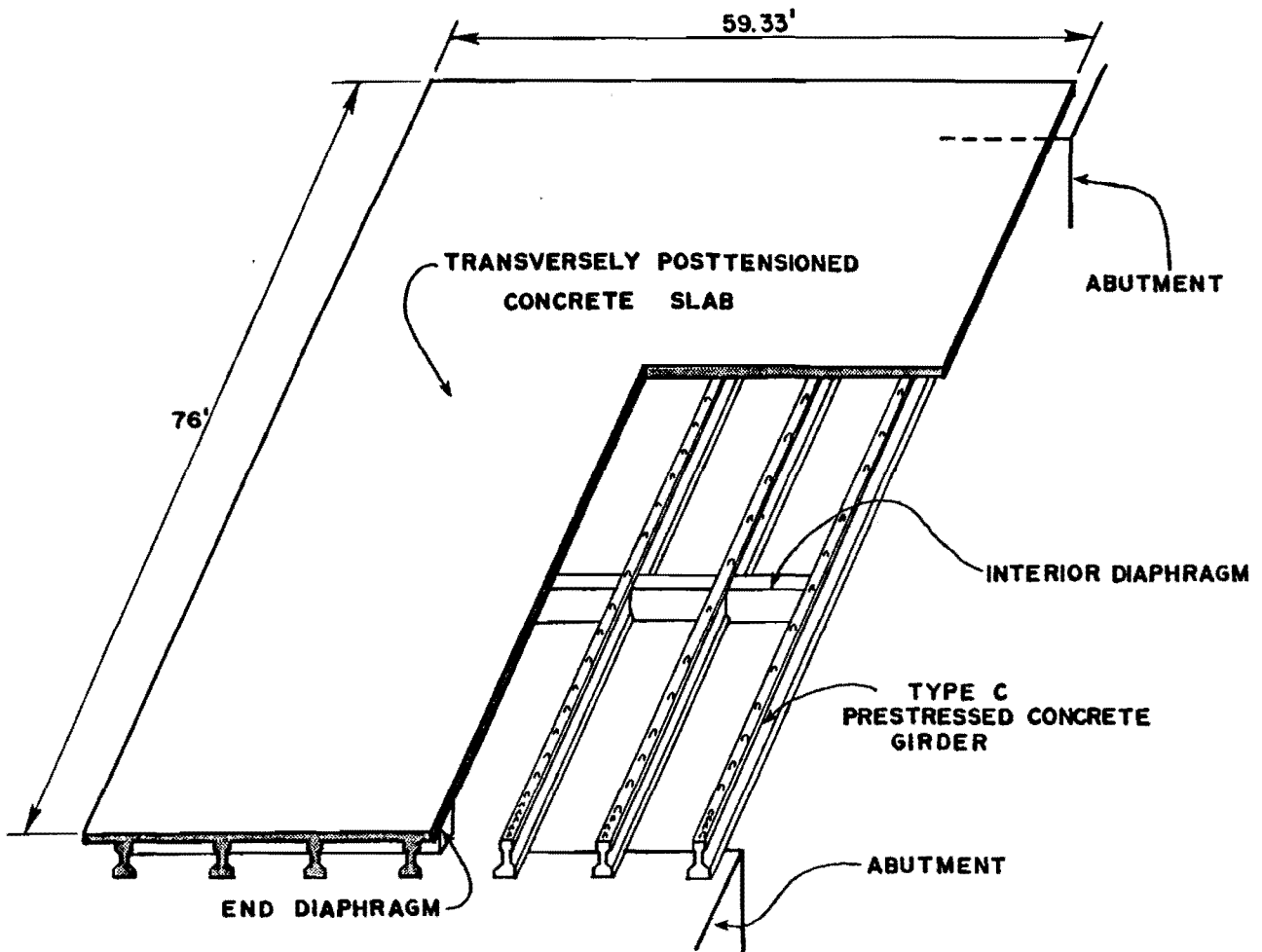


Fig. 4.1 View of prototype bridge

requirements and of the overall design and construction of the bridge model is provided by Mora in Ref. 61.

Two series of tests were conducted on the bridge model. The first series involved the determination of stresses introduced into the slab with the application of transverse prestressing. Taking advantage of symmetry in the model, each half of the bridge slab was constructed with a different transverse strand profile, namely straight tendons and a combination of straight and draped tendons. A total of four transverse posttensioning tests were conducted on the model: two on each half of the bridge, one with end and interior diaphragms in place, the other with the interior diaphragms removed.

The second series of tests consisted of single lateral load applications to determine tendon spacing effects and of vertical load testing of the bridge model to simulated vehicular live load. These latter tests were conducted for loads representing service, factored design and ultimate conditions. All are reported in the next chapter.

4.4 Deck Design

4.4.1 Two-Dimensional Finite Element Analysis of Structural Effects. A two-dimensional finite element analysis was conducted to aid in the deck design of the model bridge. A two-dimensional analysis seemed appropriate because of the belief that the lateral girder stiffness effects on the transverse stress distribution of the bridge deck were predominately in-plane.

Figure 4.2 illustrates a cross section and plan view of the prototype bridge. The structural skeleton of the prototype bridge consists of seven TDSHPT Type C prestressed concrete girders and exterior and interior concrete diaphragms. For purposes of the finite element analysis, the Type C girders were modeled as rectangular beams of equivalent lateral stiffness as shown in Fig. 4.3. It was important for analysis purposes to model the 14-in. top girder flange width of the Type C girder for the equivalent rectangular beam. This resulted in an equivalent rectangular girder depth slightly greater than the Type C girder depth. However this had no effect on the analysis since there were no vertically applied loads in the two-dimensional model. The girders rest on neoprene bearing pads on the bridge abutments. Equivalent lateral springs, as developed in Fig. 4.4, were used in the analysis to model the support conditions. Because of symmetry, it was possible to analyze only one-quarter of the bridge shown in Fig. 4.2. The resulting finite element model used in analysis is shown in Fig. 4.5. The material properties assumed for the different elements are provided in Table 4.1a. The bridge slab was modeled using an eight-node quadratic quadrilateral plane stress element with properties shown in Table 4.1a. Axial stiffening elements with the properties shown in Table 4.1a represented the

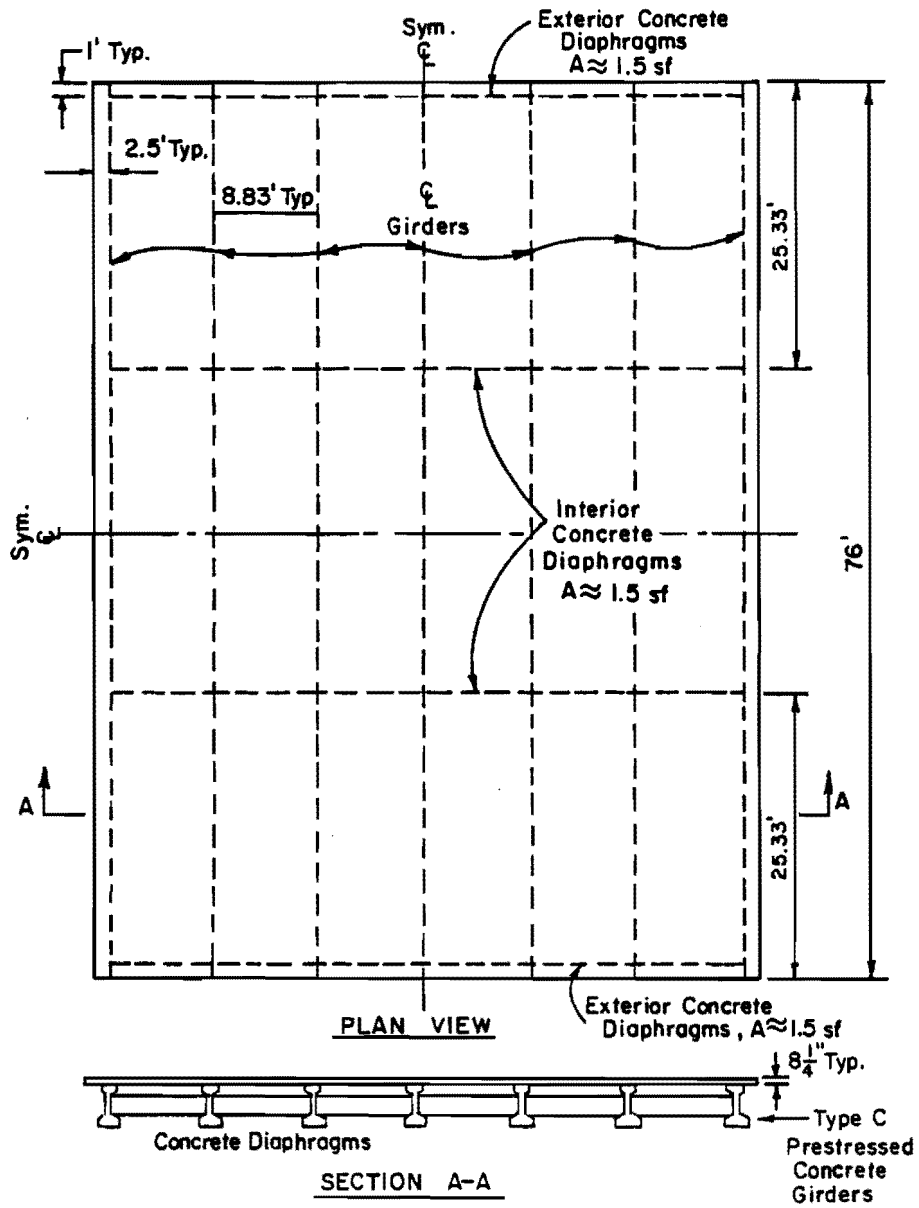
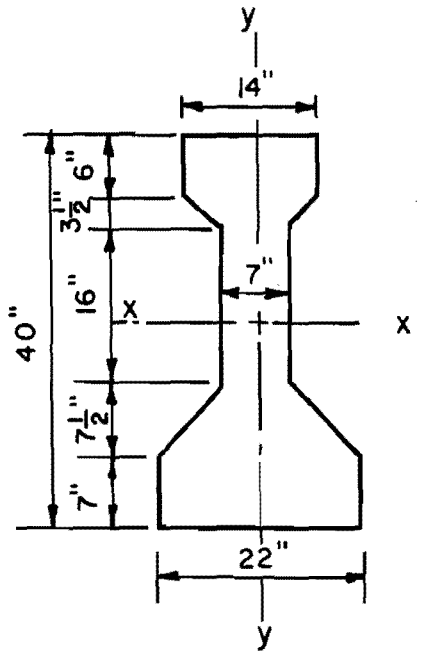
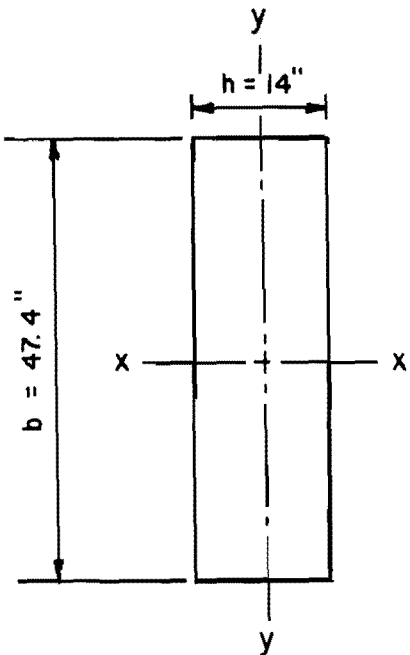


Fig. 4.2 Prototype bridge



$I_x = 82,602 \text{ in.}^4$
 $I_y = 10,830 \text{ in.}^4$
 $A = 494.9 \text{ in.}^2$

Texas Type C Girder



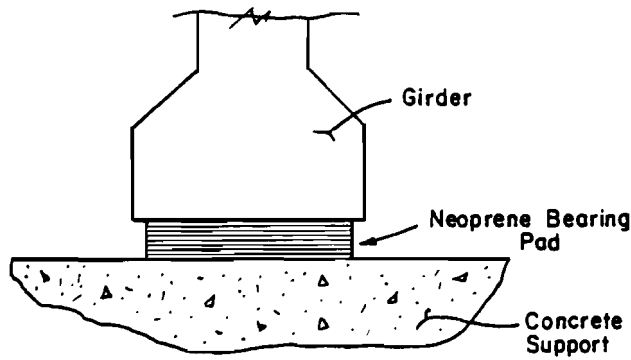
$$I_y = \frac{bh^3}{12}$$

$$10,830 = \frac{b(14)^3}{12}$$

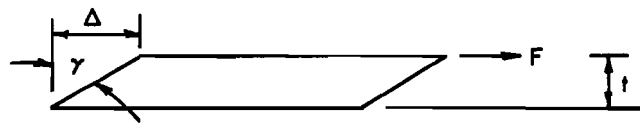
$$b = 47.4''$$

Rectangular Beam with Equivalent Lateral Stiffness

Fig. 4.3 Equivalent beam used for two-dimensional finite element analysis



a) Girder Support Condition



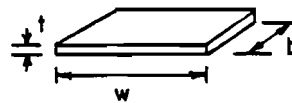
b) Shear Distortion of Neoprene Pad

$$\tau = G \gamma$$

$$\tau = G \frac{\Delta}{t}$$

$$F = \tau \text{ Area}$$

$$F = \frac{Gbw\Delta}{t}$$



$$K_L(\text{ATERAL}) = \frac{F}{\Delta}$$

[Ref. 62]

$$K_L = \frac{Gbw}{t}$$

$$G = 160 \text{ psi}$$

$$t = 4 \text{ in.}$$

$$w = 20 \text{ in.}$$

$$b = 12 \text{ in.}$$

$$K_L \approx 10,000 \text{ lb/in.}$$

c) Calculations for Spring Constant

Fig. 4.4 Equivalent lateral springs

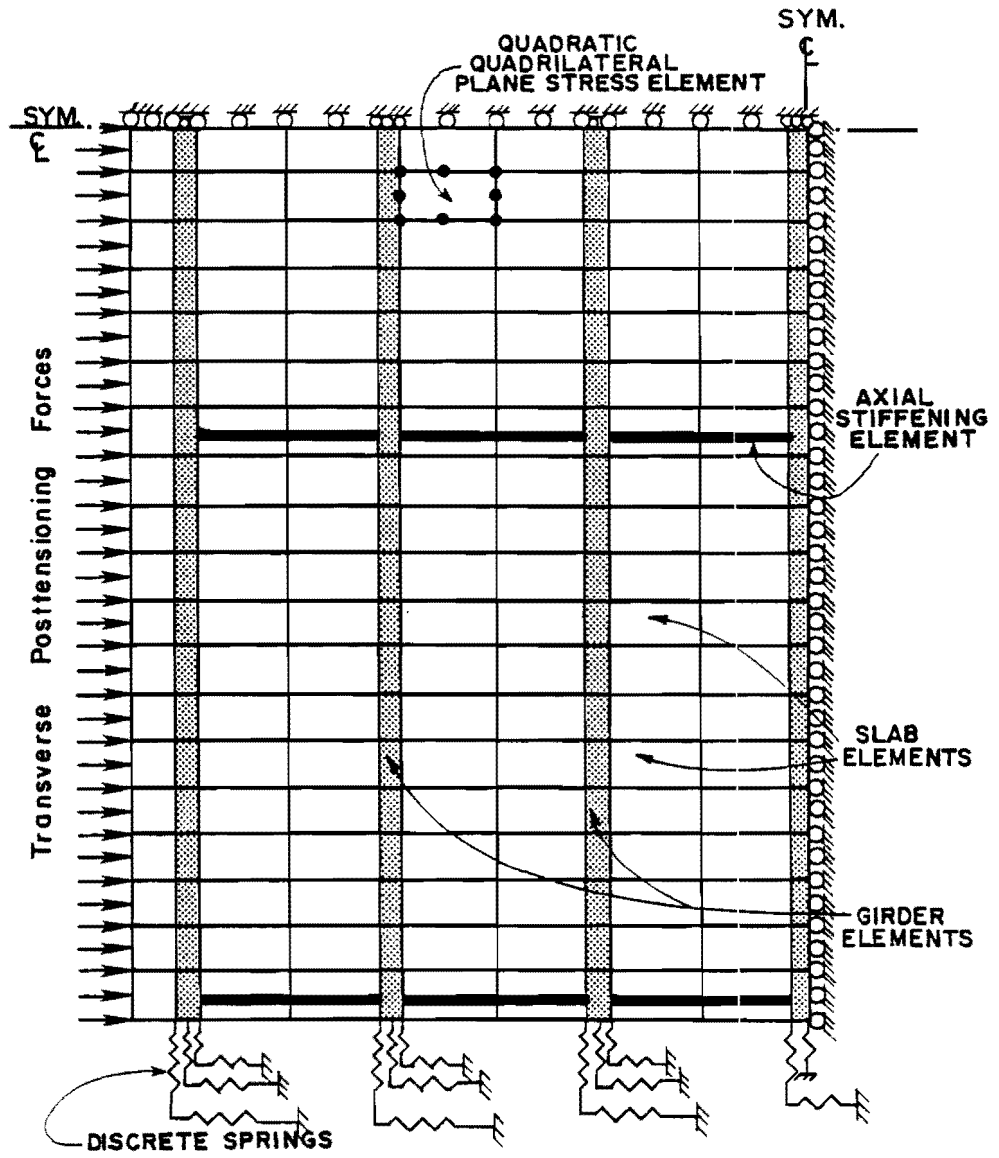


Fig. 4.5 Finite element analysis model; one-quarter of bridge

TABLE 4.1(a) Material properties of various elements in analysis model

Element	Modulus of Elasticity (ksi)	Poisson's Ratio	Thickness (in.)	Area (in. ²)
Slab	4000	0.15	8.25	----
Girder	4000	0.15	55.65*	----
Diaphragm	4000	----	-----	216

*Total thickness = equivalent rectangular girder depth + slab thickness = 47.4 + 8.25 = 55.65 in.

TABLE 4.1(b) Material properties assumed for full-scale prototype bridge deck design.

Concrete compressive strength, f'_c	5 ksi
Nonprestressed reinforcement yield strength, f_y	60 ksi
Prestressed reinforcement	
1/2-in. diameter prestressing tendon	
Ultimate strength, f_{pu}	270 ksi
Area, A_{ps}	0.153 ksi
Effective prestress after losses, f_{pe}	150 ksi

concrete diaphragms. The girders were also modeled using eight-node elements having properties shown in Table 4.1a. Transverse posttensioning was modeled as uniformly distributed point loads along the edge of the bridge deck as shown in Fig. 4.5.

Four analyses were carried out using the two-dimensional finite element analysis model. The first case was for restrained movement at the girder supports and with the diaphragms in place. Case 2 was the same as Case 1 except with all diaphragms removed. Case 3 was for calculated spring stiffness values corresponding to the girders resting on neoprene pads as shown in Fig. 4.4, and with all diaphragms in place. Case 4 was similar to Case 3 except with the diaphragms removed.

The resulting stress contours resulting from each analysis case are shown in Figs. 4.6 through 4.9. The contours shown in these figures are for the same one-quarter symmetry analysis model of Fig. 4.5. The values shown in these figures represent a percentage of the nominal uniform stress applied along the edge of the bridge slab which is considered to be 100%. For example, > 70% implies that the average compressive stresses in the transverse direction are at least 70% of the applied edge stress in the region bounded by the contour lines. Case 1 represents a lower bound solution since the girders are completely restrained. For this case, Fig. 4.6 shows that the normal stresses are as low as 10% of the applied edge stress in some isolated regions near the support ends of the girders which is also the location of the end diaphragms. Figure 4.6 also shows that the transverse compressive stresses are below 50% of the edge stress for a substantial portion of the deck. The stress contours shown in Fig. 4.7 for Case 2 are similar to those for Case 1 except that a substantially larger portion of the slab is stressed to a value greater than 90% of the edge stress. This is primarily due to the absence of the diaphragms. However, the the slab regions near the support end of the girders, the transverse stresses are as low as 10% of the applied edge stress even though no diaphragms are present. This points out a basic problem when the girder supports are fixed. The girder fixity locally restrains slab shortening at the end of the bridge, and thus the transverse compressive stresses are significantly lower than the applied transverse edge stress. Since the slab stress contours for Case 1 and Case 2 are similar at the abutment end of the bridge, it can be concluded that in this case girder fixity has a much more pronounced effect on transverse stress distribution than the presence of end diaphragms. However, at interior slab locations, comparing the stress distribution for Cases 1 and 2 reveals that the presence of interior diaphragms does significantly change the transverse stresses in the regions near the line of interior diaphragms. For Case 1, the interior diaphragms locally restrain slab shortening, and thus the stresses are smaller than those for Case 2 in a large portion of interior slab locations.

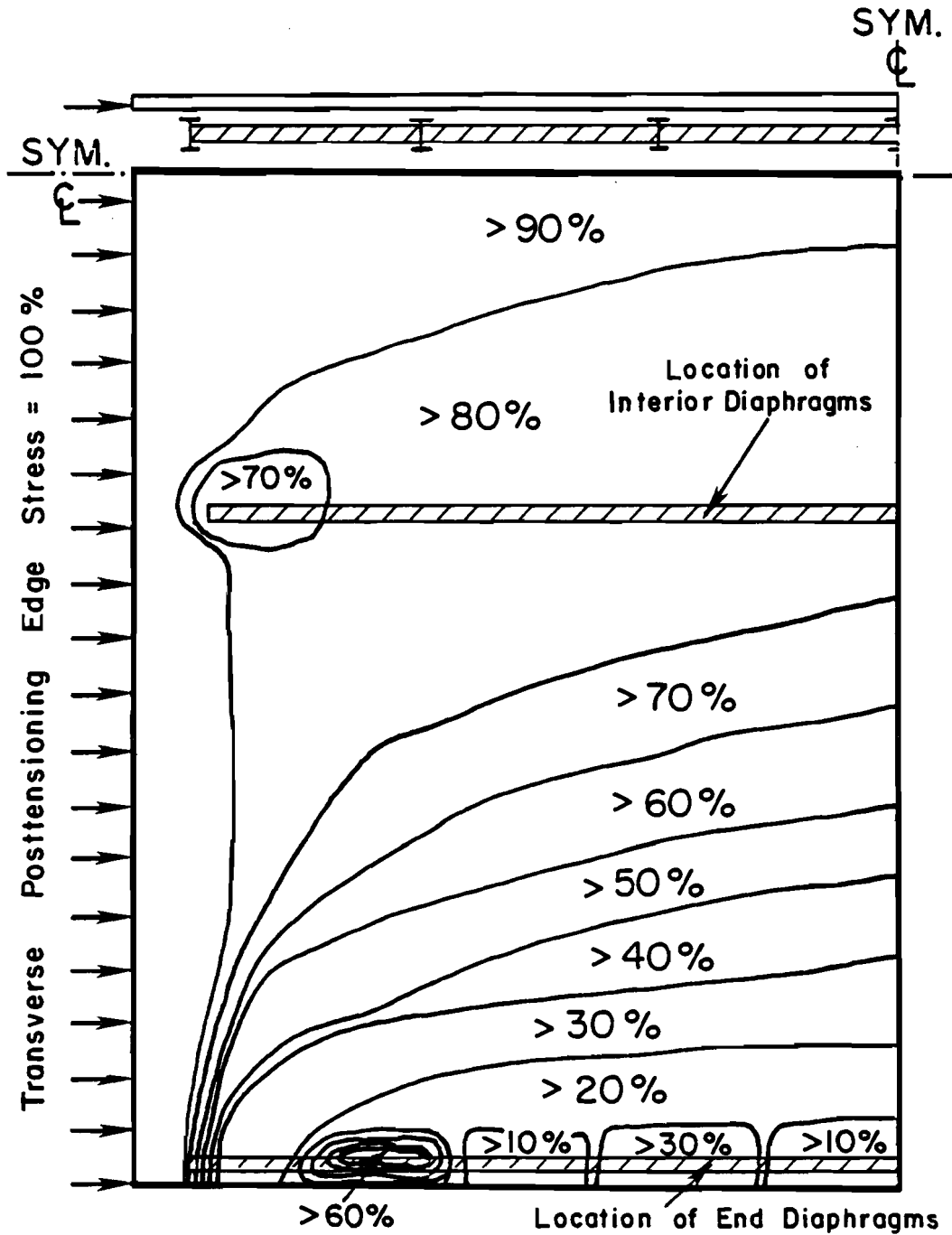


Fig. 4.6 Case 1 stress contours; fixed girder supports; diaphragms included; contours are % of applied edge stress

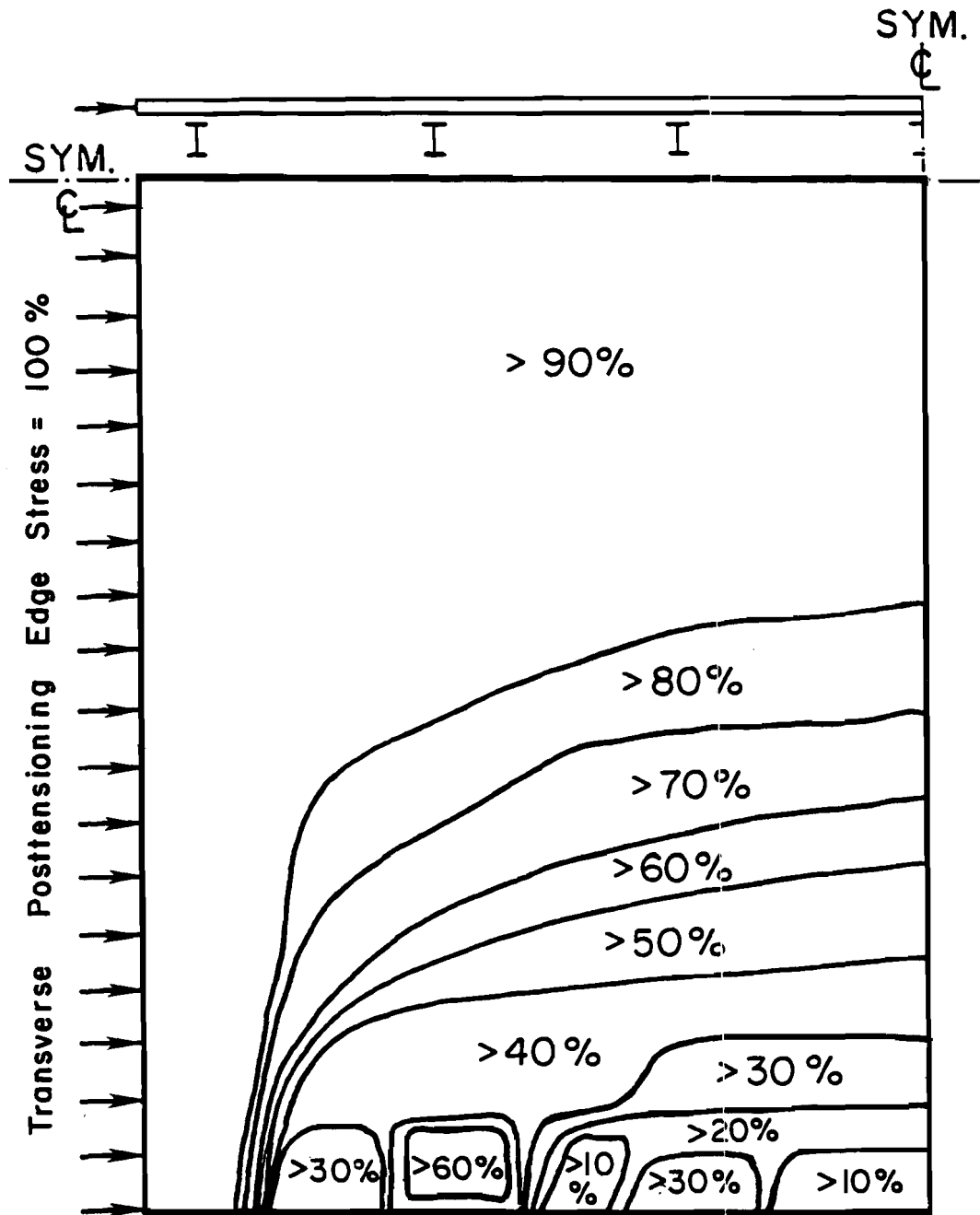


Fig. 4.7 Case 2 stress contours; fixed girder supports; no diaphragms; contours are % of applied edge stress

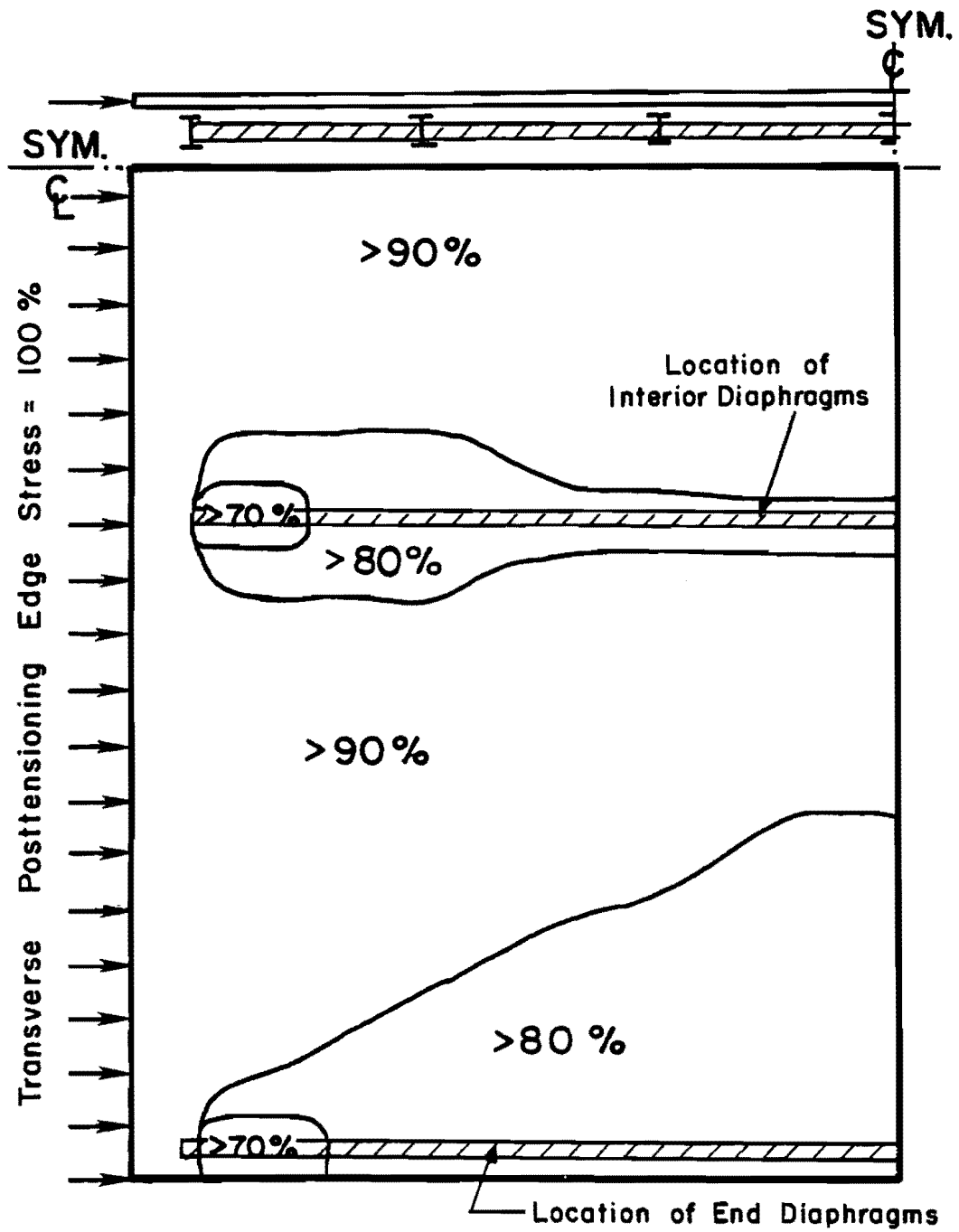


Fig. 4.8 Case 3 stress contours; flexible girder supports; diaphragms included; contours are % of applied edge stress

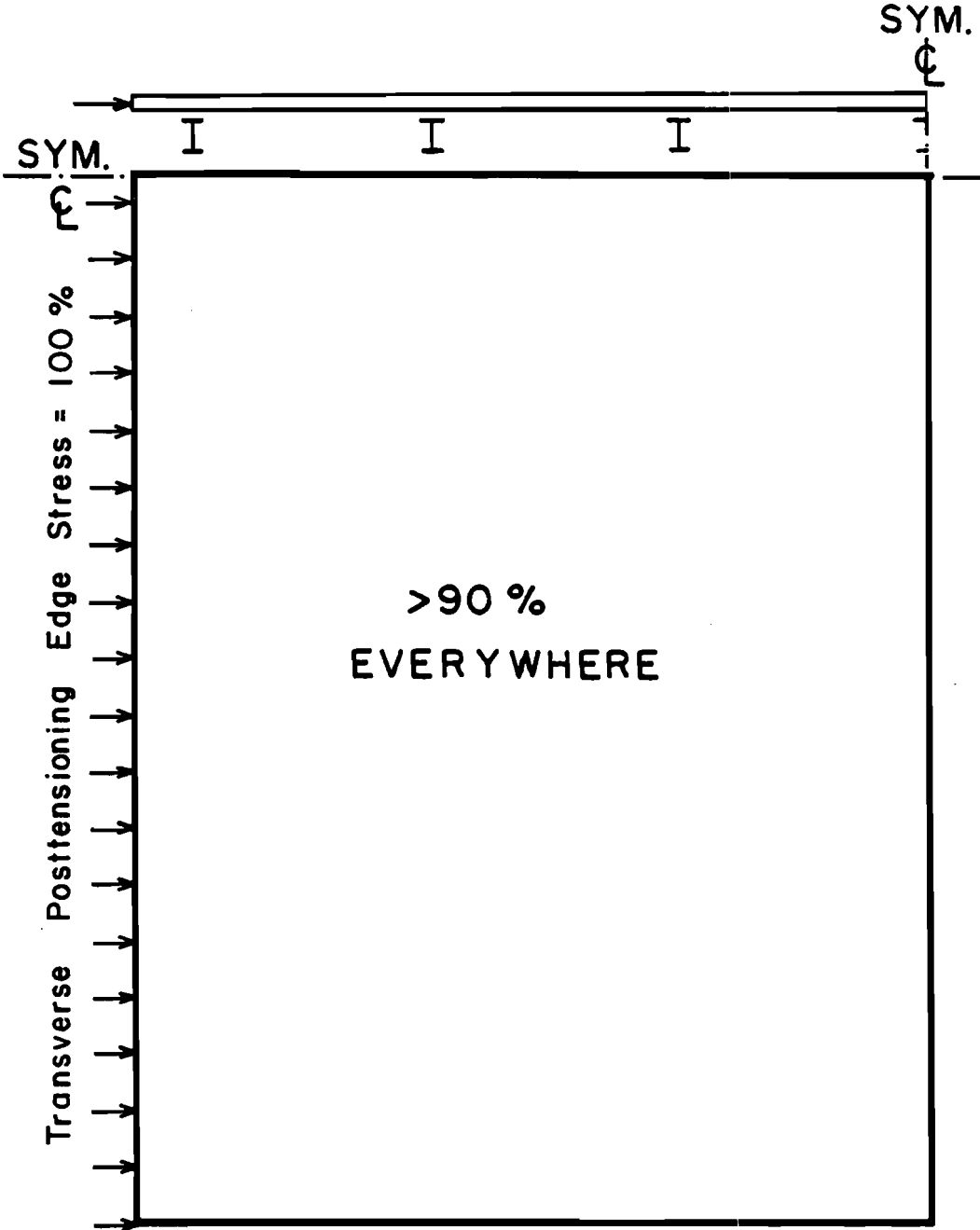


Fig. 4.9 Case 4 stress contours; flexible girder supports; no diaphragms; contours are % of applied edge stress

However, Cases 3 and 4 represent more realistic analyses for transverse prestressing of a bridge deck. The analysis results shown in Fig. 4.8 for Case 3, which is for flexible girder supports and diaphragms, indicate that in the diaphragm regions there are some stress zones where there is a significant reduction in the applied edge stress. However, nowhere are the transverse stresses below 70%. The transverse stresses are well above 80% and 90% of the compressive edge stress for most of the bridge deck. The results shown in Fig. 4.9 for Case 4, which is for flexible girder supports and no diaphragms, are even more encouraging. These results show that the transverse stresses do not fall below 90% of the applied edge stress anywhere in the bridge deck when the diaphragms are removed.

The results for Case 4 clearly indicate that the lateral stiffness effects of the girders on the transverse stress distribution are negligible if girders are on flexible supports. The results from Case 3 reveal that the diaphragms do locally restrain slab shortening, and thus reduce the compressive stresses in the bridge deck near the location of the diaphragm. However, there is at most only about a 30% reduction in transverse stresses in the regions near the diaphragms. These reductions in stresses in the regions near the diaphragms can easily be accounted for by locally increasing the prestressing in the diaphragm regions as was done for the laboratory bridge model.

The magnitude of the elastic shortening along the edge of the bridge deck for Case 3 approached that obtained from Eq. (4.1):

$$\delta = PL/AE \quad (4.1)$$

where δ = the transverse elastic shortening,
 P = the total load applied along the edge of the bridge deck,
 L = width of the bridge deck,
 A = cross-sectional area of the bridge deck, and
 E = modulus of elasticity of the concrete bridge deck.

For Case 4 where the diaphragms are excluded, the elastic shortening along most of the edge of the slab is numerically equal to that given by Eq. (4.1). The values of elastic shortening obtained for Cases 3 and 4 again indicate that there is very little restraint provided by either the diaphragms or girders.

Cases 3 and 4 also provided interesting results for design considerations in the longitudinal direction for in-plane forces. The

analysis results indicate that the maximum principal longitudinal in-plane tensile stresses due to transverse posttensioning of the bridge slab are only of the order of 7% of the applied transverse compressive stresses. These results suggest that for in-plane forces there is little need for reinforcement in the longitudinal direction to actively control cracking, since the tension stresses are small. However, there may be a need for longitudinal reinforcement for controlling cracking due to vertical loads.

4.4.2 Design Philosophy. The AASHTO Specification [11] is quite definitive in its guidance for the transverse design moments in a concrete bridge slab. AASHTO implicitly assumes that the behavior of a concrete bridge slab is elastic at service load levels. The distribution and magnitude of the design moments should not be affected by whether the slab is a conventionally reinforced deck or is transversely prestressed. Some studies [48,71] indicate that the AASHTO design moments for bridge decks are quite conservative and could be reduced. However, since it was not the major purpose of this study to reevaluate current AASHTO provisions for slab loads, the design of the transversely prestressed model bridge deck followed the present AASHTO provisions for the design slab moments. In fact, all applicable provisions in the current AASHTO Specification [11] were followed for design of the deck.

Perhaps the most important aspect of the posttensioned model bridge slab design was the assumption of the limiting tensile stresses. The fundamental precept for improving the durability of bridge decks with transverse prestressing assumes that the concrete remains essentially uncracked. Thus, it follows that the extreme fiber slab stresses must remain below a realistic tension stress index. The index assumed in the current AASHTO provisions is $6\sqrt{f'_c}$ for normal exposure conditions.

The present $6\sqrt{f'_c}$ tension index is really based on flexural cracking consideration [79]. The allowable tension was changed from $3\sqrt{f'_c}$ in the 1969 AASHTO Specifications to $6\sqrt{f'_c}$ in the 1971 Interim AASHTO Specifications. The change was made since experience from the building industry showed that at a stress level of $6\sqrt{f'_c}$ prestressed concrete remains essentially uncracked. However, this change ignored fatigue considerations. Since 1971, research and experience in the bridge industry has shown that at a tension stress of $6\sqrt{f'_c}$ cracking occurs [79]. At crack locations, prestressing tendons can experience large stress ranges which result in mechanical fatigue fracture, and thus reduces the capability of a member to carry design loads. For corrosive environments, the current AASHTO Specifications [11] limit tension stresses to $3\sqrt{f'_c}$ which was the allowable tension index for normal exposure conditions in the 1969 AASHTO Specifications [11]. At $3\sqrt{f'_c}$ there appeared to be no problems with fatigue [79]. Adopting the 1969 AASHTO Specifications philosophy for normal exposure conditions would suggest that for severe corrosive exposure

conditions, the allowable tension stress index should be even smaller than $3\sqrt{f'_c}$. A more conservative tension stress index would be 0 psi, thereby assuring that no cracks form. Additionally, since the critical path for deicing salt penetration into a bridge slab is from above, it is reasonable to assume a more restrictive requirement for the top fiber than the bottom fiber of a transversely prestressed bridge deck. The different criteria for the top and bottom of the slab would allow some additional economy in the required tendon spacings. With these considerations, the decision was made to limit the top slab tensile stresses to 0 psi and the bottom slab tensile stresses to $2\sqrt{f'_c}$. The value $2\sqrt{f'_c}$ seemed to be a reasonable limiting tension stress index which is below the $3\sqrt{f'_c}$ limit for fatigue considerations.

After establishing limiting tensile stresses, the required tendon spacings for the model bridge slab were calculated. Besides satisfying the assumed limiting tensile stresses, the calculated tendon spacings also reflected the results from the plane stress finite element analysis previously discussed in this chapter. The reduced stress zones in the near regions of the diaphragms required extra tendons to compensate for the restraining effect. Extra tendons would produce more compression, and thus would compensate for the transverse stress reductions due to the presence of diaphragms. More closely spaced tendons in the diaphragm regions would result in a more uniform state of stress in the slab.

The tendon spacings also required modification to account for friction losses in the posttensioning system. Friction losses are a function of several variables and can be evaluated analytically from equations if material-dependent friction constants are available [11,64,65]. Since prestressing tendons can be draped or straight, the friction losses depend on the cumulative angle change which occurs in the tendon direction, known as curvature effect, and also on local irregularities in the duct profile which is referred to as "wobble." Figure 4.10 illustrates the idea of friction losses for a posttensioning tendons due to both wobble and curvature effects.

The model bridge slab utilized prestressing tendons in grease-filled plastic ducts because of cost considerations, ease of construction, availability, and because it was to be a structural model and corrosion resistance was not a concern. However, since reliable information on the magnitude of friction losses for this type of prestressing system was not available, an experimental friction test program was conducted. The testing and results of this friction study are reported in detail in Ref. 9 and are summarized in Fig. 4.11. For a tendon length of 60 ft, which is approximately the width of the prototype bridge deck, the straight tendons show a 10% loss of force at the dead end compared to the jacking end. In contrast, for a tendon which consists of seven full cycles of draping as shown pictorially in Fig. 4.11 for the seven-girder prototype

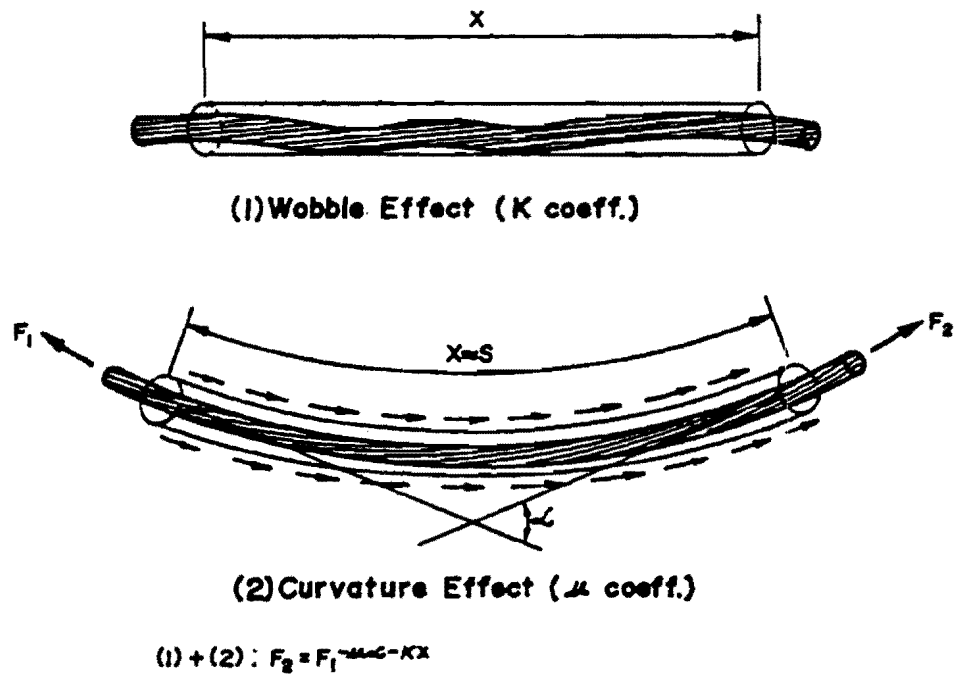
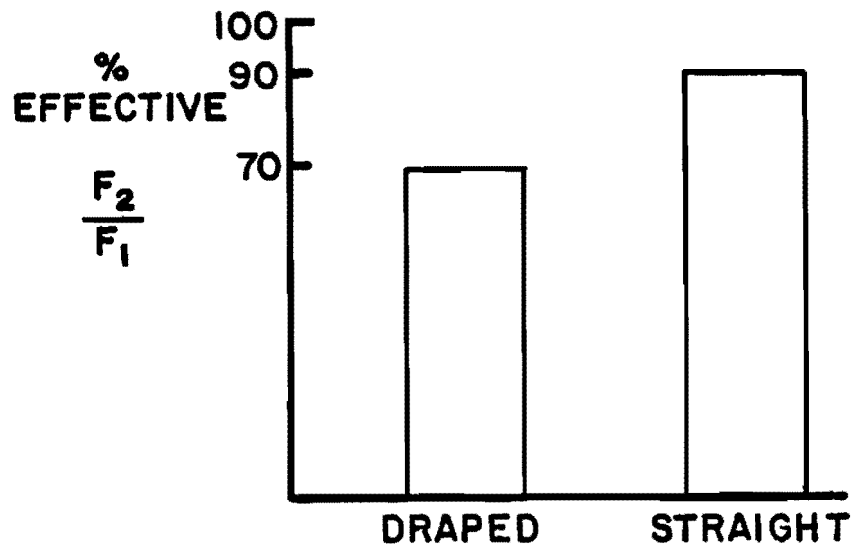
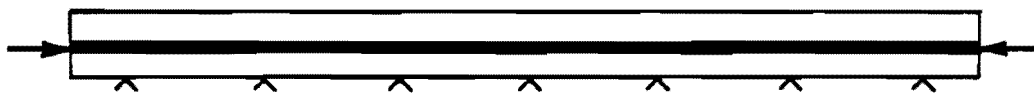


Fig. 4.10 Friction losses in posttensioning



F_1 = force at stressing end

F_2 = force at dead end



Straight Tendon



Draped Tendon

Fig. 4.11 Friction test results

bridge, the force at the dead end is only about 70% of the jacking force. Even though the experimental friction test was conducted for full-scale prototype dimensions, it was reasonable to assume a direct translation of the friction losses for the tendon system used in the model bridge slab. Therefore, the friction loss values shown in Fig. 4.11 were used for the design of the slab.

Finally, the model bridge slab was designed to ensure adequate strength at the factored load condition. Also, the current ACI [80] recommendations for minimum bonded reinforcement were used in the model bridge design in order to assure overall structural integrity.

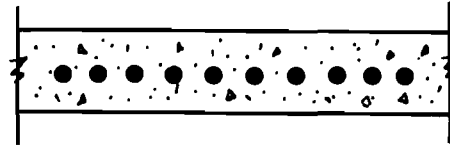
Figure 4.12 summarizes the design philosophy followed in the design of the transversely prestressed model bridge slab. Highlights of the design calculations for the model bridge slab are presented in Sec. 4.4.4. More detailed calculations are presented in Appendix A.

4.4.3 Other Design Considerations. A preliminary design of the slab identified three possible layouts for the prestressing in the transverse direction as shown in Fig. 4.13. These profiles included straight middepth tendons (Fig. 4.13a), eccentric straight tendons (Fig. 4.13b), and a combination of eccentric straight and draped tendons (Fig. 4.13c). The first profile offers ease of construction and a "fail-safe" design for ultimate strength considerations since the tendons are equally effective in resisting both negative and positive moments. The second profile offers a more efficient design for strength since the internal slab resisting couple utilizes a larger moment arm than that for middepth tendons. The last profile requires fewer posttensioning strands since some of the tendons are draped according to the need for negative or positive moment reinforcement.

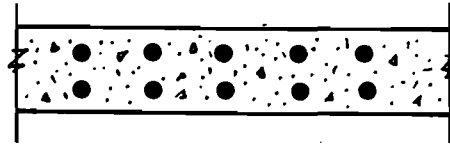
However, a closer look at the profiles revealed that only the latter two were viable alternatives for the laboratory model. The first strand profile, which utilized middepth tendons, was eliminated from further consideration for several reasons. The internal resisting moment arm was inefficient for the middepth tendons and required a slab design dominated by strength considerations. The design using this tendon profile required far more tendons for strength than needed for limiting service load stresses at the extreme slab fibers. A good design would strive for more of a balance between the prestressing tendons required for service and ultimate loads. In addition, the required prestressing steel for factored loads exceeded the maximum allowable steel percentage as specified by AASHTO 1.5.10(A) [11]. Finally, there was a real concern for the tension splitting stresses generated by multiple in-line anchorage zones as shown in Fig. 4.14. Depending on the stress levels, number of anchorages, and their proximity to each other, a splitting type failure, as illustrated in Fig. 4.14, could occur.

- AASHTO SPECIFICATIONS FOR TRANSVERSE LOAD DISTRIBUTION
- LIMIT TENSILE STRESSES
 - TOP - 0 PSI
 - BOTTOM - $2 \sqrt{f'_c}$
- TENDON SPACING
 - TENSILE STRESSES
 - FEA STRESS DISTRIBUTION
 - FRICTION TEST RESULTS
- ADEQUATE STRENGTH
- BONDED REINFORCEMENT FOR INTEGRITY

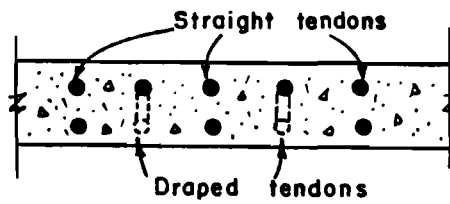
Fig. 4.12 Summary of model bridge slab design philosophy



(a) Middepth straight tendons



(b) Eccentric straight tendons



(c) Combination straight and draped tendons

Fig. 4.13 Possible strand profiles

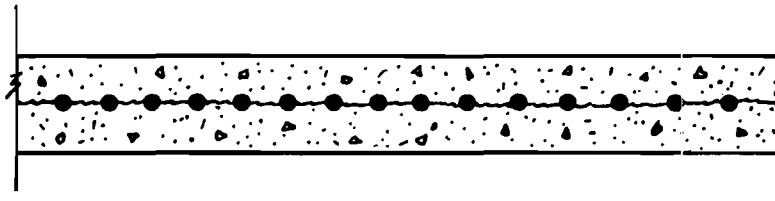


Fig. 4.14 Possible splitting failure with middepth tendon profile

A major deviation from the current AASHTO provisions was made concerning the required amount of longitudinal distribution steel. AASHTO [11] would have required a large amount of longitudinal steel. However, the analytical study by Almustafa [60] concluded that there was no need for flexural reinforcement in the longitudinal direction. Accordingly, only the minimum steel for temperature, shrinkage, crack control and structural integrity was specified for the longitudinal direction.

4.4.4 Design Calculations. The design of the transversely posttensioned model bridge slab was carried out following the guidelines and considerations outlined in the previous sections. The approach was to design the slab for the full-scale prototype bridge, and then to scale the design according to the similitude requirements of the model. A 1/2.23 scale was chosen for the laboratory bridge model based on cost, available laboratory facilities, accuracy and ease of construction. Only highlights of the calculations follow. More detailed calculations are presented in Appendix A.

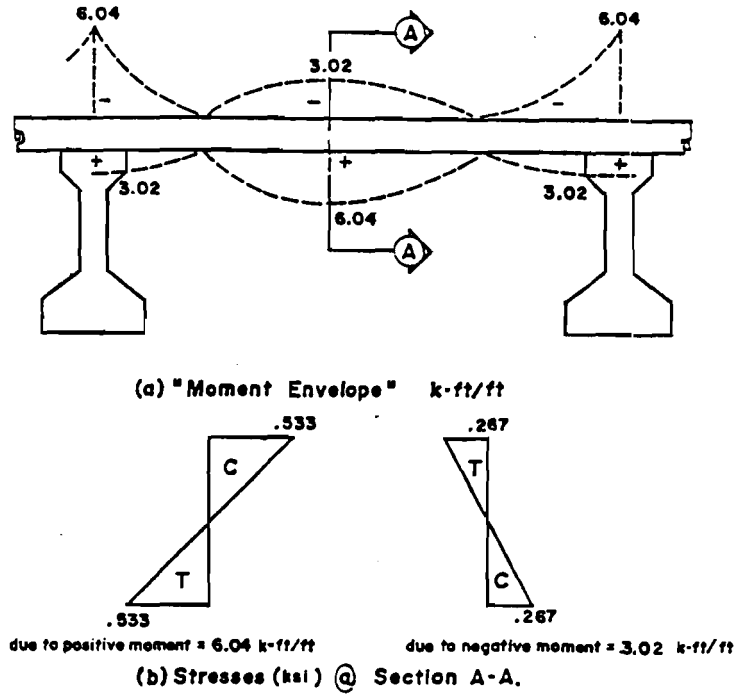
4.4.4.1 Full-Scale Prototype Deck. The material properties assumed for design of the prototype bridge deck are shown in Table 4.1(b).

The maximum positive and negative service load plus impact moment was computed according to AASHTO for HS20-44 loading for an 8.25 ft slab span as 6.04 k-ft/ft. The corresponding moment envelope for a typical interior span is shown in Fig. 4.15a. Current design practice calls for a moment reversal of half this value at critical sections.

The maximum concrete stress, f_c , was computed for the service load moment as ± 0.533 ksi assuming a gross uncracked concrete section. The stresses are shown for the slab midspan in Fig. 4.15b.

Straight Tendon Profile. The limiting tension stresses assumed for design were 0 psi at the top of the slab, and $2\sqrt{f'_c}$ (140 psi for $f'_c = 5000$ psi) at the bottom of the slab. The prestressing was designed to ensure that these limiting stresses were not exceeded for the service load moment.

The critical sections for design were at the girders for the maximum negative moment, and at midspan for the maximum positive moment. An assumed 2-in. clear concrete cover allowed a maximum tendon eccentricity of 1.875 in. as shown in Fig. 4.16. The previously calculated concrete stress was increased to account for the friction loss expected in straight tendons as shown in Fig. 4.11. According to Fig. 4.11, the stress at the far end of a straight tendon is expected to be 0.90 of the stressed end because of friction losses. Using elastic beam theory, the following two equations were written to solve for the required top and bottom tendon forces which satisfy the limiting tension stresses:



Stresses Based on Gross Concrete Section

Fig. 4.15 Moment envelope and stresses in bridge slab under service plus impact load conditions

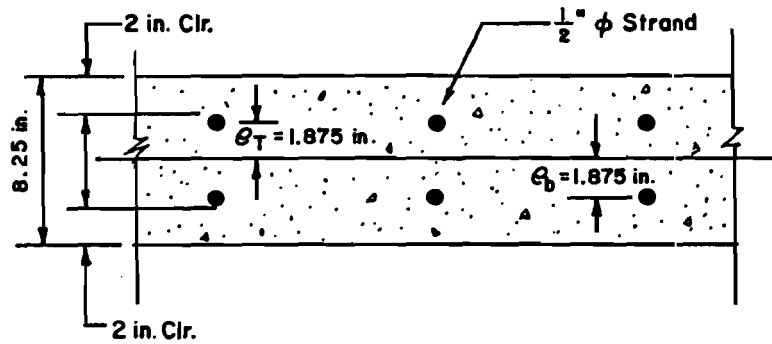


Fig. 4.16 Cover and tendon eccentricity in slab

$$-0.9P_T/A - 0.9P_{Te}/S - 0.9P_B/A + 0.9P_{Be}/S + 0.533 = 0 \quad (4.2)$$

$$-0.9P_T/A + 0.9P_{Te}/S - 0.9P_B/A - 0.9P_{Be}/S + 0.533 = 0.140 \quad (4.3)$$

where P_T = required tendon force per foot width of slab
for the top of the slab, kips

P_B = required tendon force per foot width of slab
for the bottom of the slab, kips

A = area per foot width of slab, in.²

S = section modulus per foot width of slab, in.³

and e = tendon eccentricity, in.

Solving these equations for P_T and P_B resulted in:

$$P_T = 28.3 \text{ kips}$$

$$P_B = 23.2 \text{ kips}$$

These forces were used to compute the required tendon spacings assuming the effective prestress force shown in Table 4.1(b).

Bottom tendon spacing = 11-7/8 in.

Top tendon spacing = 9-3/4 in.

The unequal tendon spacings for the top and bottom of the slab would result in secondary moments in the slab. However, an analysis showed that the secondary moment effects were negligible in this case.

Straight and Draped Tendon Profile. For ease of construction, it was decided to utilize an equal spacing between straight and draped tendons. Accordingly, the more restrictive 0 psi criterion was used for both slab faces. In addition, the decision was made to use an equal number of straight and draped tendons for a given section as shown in Fig. 4.17.

According to Fig. 4.11., the effective stress at the far end of a combination of straight and draped tendons would be between 70% and 90% of the stress at the stressing end. For design purposes, an average value of 80% was assumed. With the same definition of variables as in Eqs. (4.2 and (4.3), Eq. (4.4) was written to satisfy the limiting tension of 0 psi under superimposed loads at the critical negative moment section:

$$-0.8P_T/A - 0.8P_{Te}/S - 0.8P_B/A + 0.8P_{Be}/S = 0.533 = 0 \quad (4.8)$$

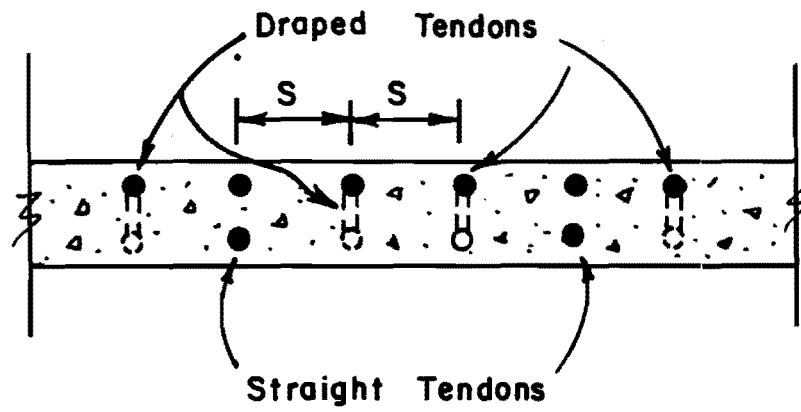


Fig. 4.17 Straight and draped tendon profile

But, $P_B = P_T/3$ in this case as shown in Fig. 4.17, and thus solving for P_T resulted in:

$$P_T = 29.1 \text{ kips}$$

Based on this prestressing force, the required tendon spacing was computed as 9-1/2 in. For a given repeating section, the design required one straight tendon top and bottom, and two draping tendons.

An analysis of this tendon profile also revealed that the secondary moment effects were negligible.

According to the results of the finite element analysis shown in Fig. 4.8, the stresses in the regions near the diaphragms are as low as 70% of the applied edge stress. Thus, to compensate for the restraining effects, the previously calculated tendon spacings were conservatively cut in half in the diaphragm regions. This reduced tendon spacing was extended over a 4-ft. region at both the end and interior diaphragm locations. Figure 4.18 shows the results from the finite element analysis in which the transverse posttensioning was doubled in the 4-ft region surrounding the diaphragms. The transverse slab stresses in the diaphragm regions are in general at least equal to or greater than the applied edge stress in the nondiaphragm regions. A check of the compression concrete stresses reveals that even in this diaphragm region the concrete compressive stresses are well below the $0.4 f'_c$ limit specified in AASHTO.

The current ACI recommendations [80] for the use of bonded reinforcement with unbonded prestressing tendons were followed to ensure overall structural integrity of the bridge slab. Even though the ACI recommendation is primarily for buildings, some bonded reinforcement is required in bridges to ensure overall flexural performance at ultimate conditions, to control cracking at service loads, and to provide strength during construction until the posttensioning is completed. This requirement translated into the use of #4 reinforcing bars at 12-in. spacing for both the top and bottom of the bridge deck in the transverse direction. Since Almustafa's [60] finite element analysis revealed that the AASHTO requirement for longitudinal distribution steel was excessive, it was decided to use the bonded reinforcement requirement for this direction as well. This would provide for an easier construction since both the top and bottom mats of steel in both directions would have the same reinforcing bar spacing.

A check of the AASHTO requirement for temperature and shrinkage steel revealed that the bonded reinforcement satisfied the required $1/8 \text{ in.}^2$ of reinforcement per foot width of slab.

The factored moment envelope for a typical interior deck span of the bridge was computed according to AASHTO and is shown in Fig. 4.19.

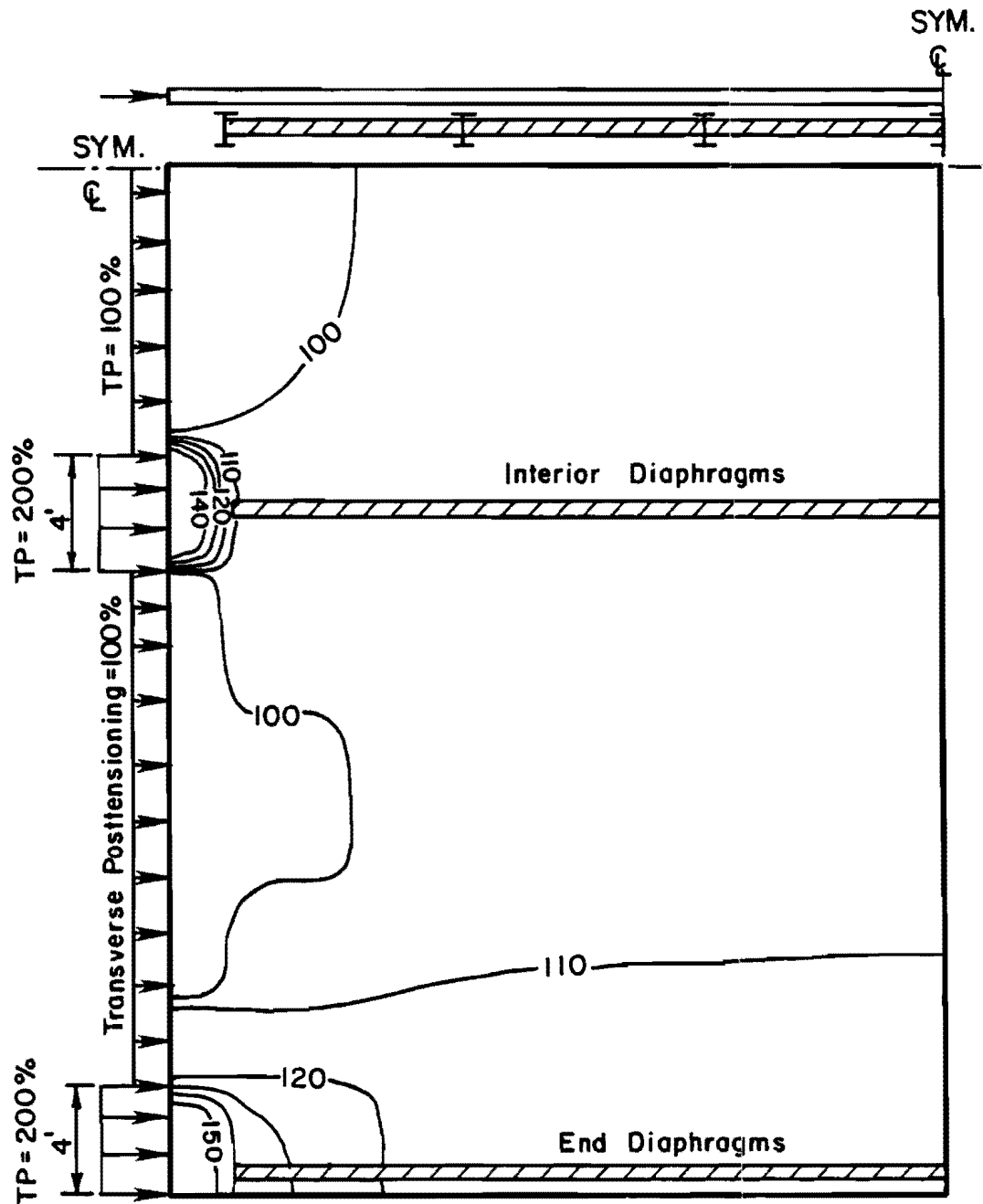
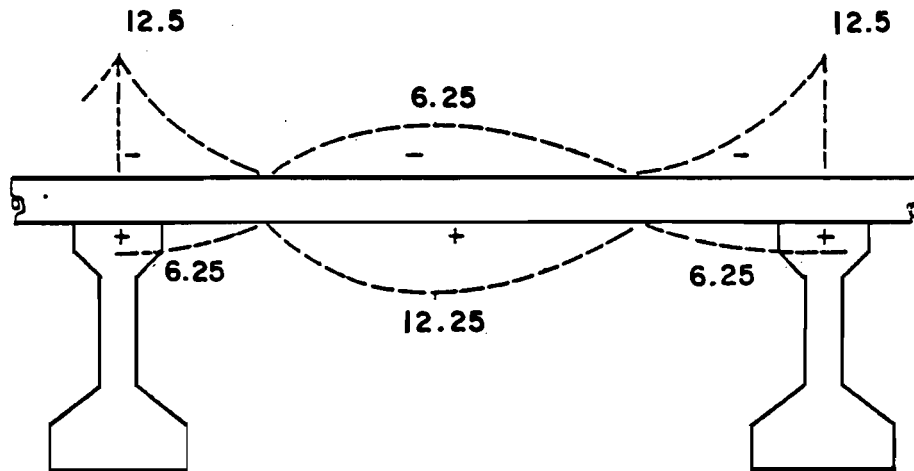


Fig. 4.18 Stress contours for doubling of edge stress in diaphragm regions; contours are percentages of applied edge stress in nondiaphragm region



Units Kip-ft./ft.

Fig. 4.19 Factored moment envelope

A check of ultimate strength showed that for both tendon profiles, the prestressing alone was not quite enough to meet the strength requirement. However, the ultimate strength of the deck was satisfied by including the bonded reinforcement in the calculations. Ultimate moment calculations are shown in detail in Appendix A.

Finally, a check of both strand profiles revealed that the minimum and maximum steel percentages of AASHTO were satisfied as shown in Appendix A.

The details of the reinforcement for the transversely prestressed prototype bridge deck are shown in Fig. 4.20. As outlined in the design, in the near regions of the diaphragms, the tendon spacing was reduced to one-half of that in the nondiaphragm regions, as shown in Fig. 4.21.

4.5 Method of Analysis

4.5.1 General. In order to provide a realistic analysis of any structure, it is necessary that the analytical method used be sufficiently rigorous to model all significant behavior of the structure under the specified loads. Since the objective of this study is to determine the transverse stress distribution in a bridge slab due to the application of the transverse prestress loading, the most important characteristic to be analyzed is the in-plane behavior of the slab. As shown in Fig. 4.22, this in-plane behavior may be affected by the existence of longitudinal girders in a slab-girder bridge and the existence of nonrigid diaphragms at the ends or intermediate locations in the bridge. Furthermore, the in-plane behavior of the slab may be affected by the bending actions of the slab itself, especially when draped prestress is used, because of the existence of the girders and diaphragms. Thus, any analytical method must be capable of modeling the in-plane and bending behavior of the slab and the influence of the girders and diaphragms.

Since it seemed that the diaphragms may be the most influential variable on the transverse stress distribution in the slab, the finite element method was the most practical choice since the bridge slab, longitudinal members and diaphragms can be easily modeled under any specified loading.

4.5.2 Finite Element Method. The finite element method is a discretization technique which replaces a structural system with infinite degrees of freedom by one with finite degrees of freedom. The original structure is discretized into a finite number of structurally deformed elements interconnected together at the nodal points where continuity and equilibrium are to be satisfied. In the displacement formulation of the finite element method, the stiffness matrix of each element of the discretized structure is basically

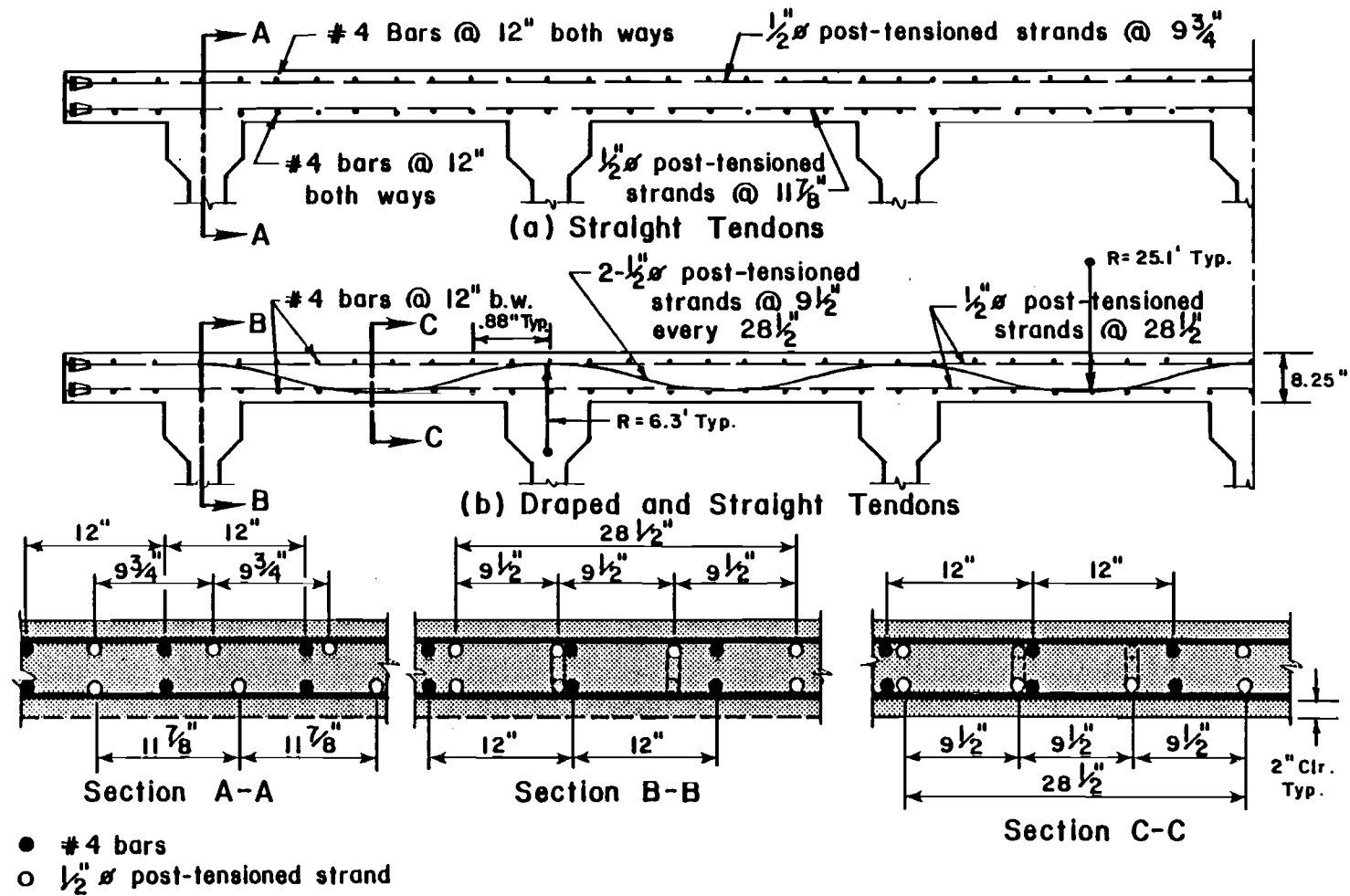


Fig. 4. 20 Prototype slab reinforcement

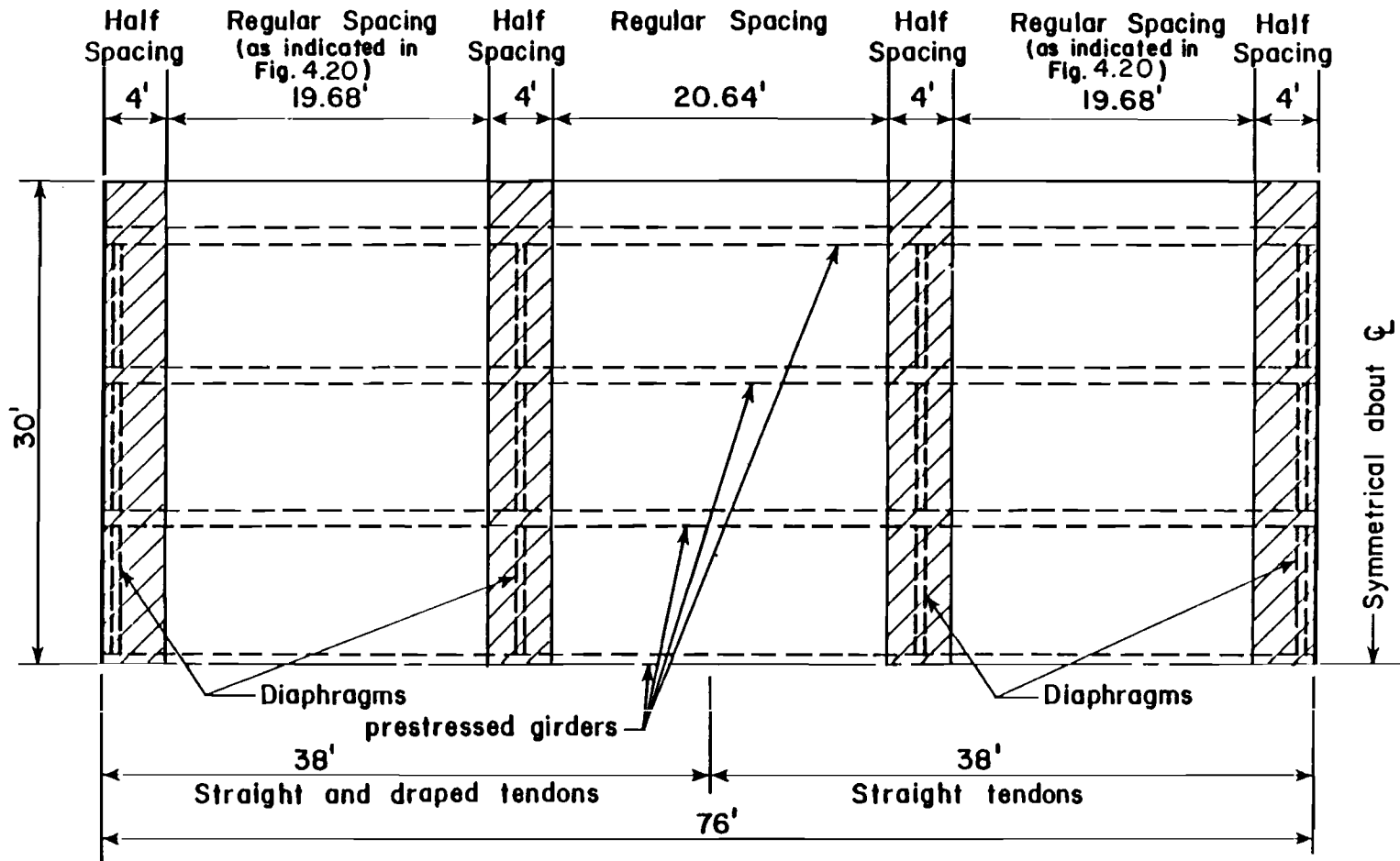


Fig.4 .21 Tendon spacings in prototype slab

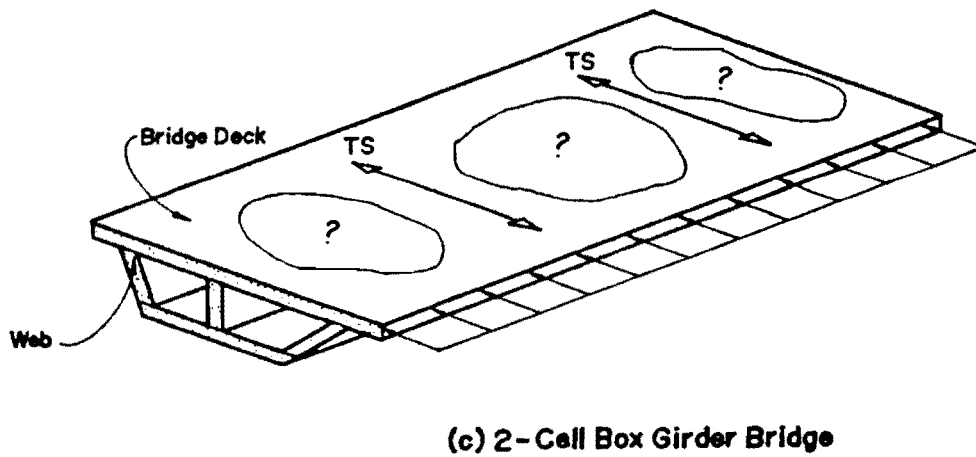
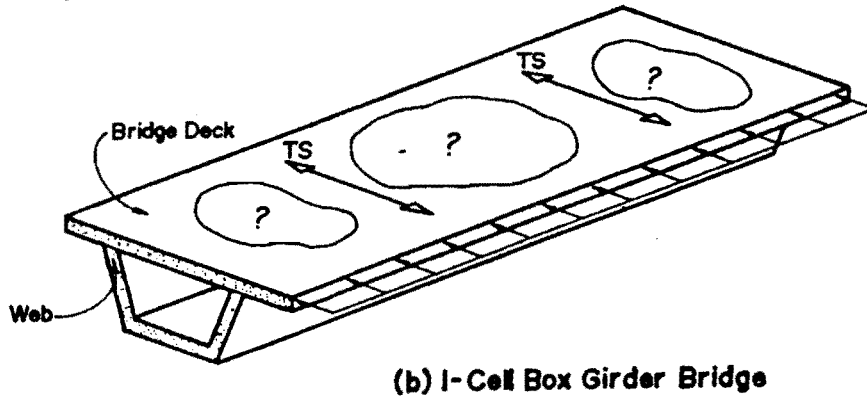
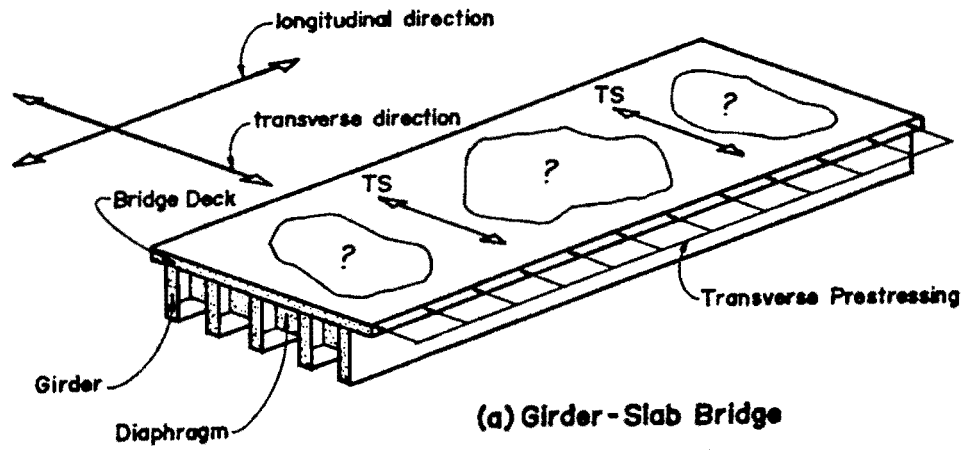


Fig. 4.22 The Effects of Girders, Webs and Diaphragms on Transverse Prestress Distribution, TS

derived from an assumed displacement function. The stiffness of the entire structure is then obtained by the usual direct stiffness technique. Along with the specified displacement boundary conditions and the applied nodal loads, this global stiffness matrix is solved for the unknown displacements and stresses.

The stiffness of a bridge structure consists of three stiffness systems:

1. In-plane and bending stiffnesses of the bridge deck (modeled by shell elements)
2. Beam stiffnesses of longitudinal members and diaphragms
3. Stiffness due to eccentricity between the deck and the supporting beams

Fig. 4.23 illustrates the finite element modeling of girder-slab and box girder bridges.

Both the shell and beam elements are developed to account for the first two of the above stiffness systems, respectively. The stiffness matrix for beam elements is first derived referring to nodal points on the local axes of the beam elements and subsequently transformed to common nodal points at the midsurface of the bridge deck by a usual stiffness matrix transformation. For the deck shell elements, no transformation is necessary because the local and global axes coincide. To account for stiffness system 3, which essentially represents the true composite action, a special transformation of the beam stiffness matrices (which are formulated on their local axes) to that of the midsurface of the deck shell elements [81], is necessary and shown in Fig. 4.24. This eccentricity transformation will introduce suitable coupling between the in-plane and bending stiffnesses of the bridge structure.

The basic assumptions in deriving these elements are:

1. The material is isotropic, homogeneous and linearly elastic.
2. Small deformation theory is adopted but the Kirchhoff hypothesis is relaxed so that normals to the midsurface before deformation remain straight but not necessarily normal to the midsurface after deformation.
3. The stress normal to the shell midsurface is equal to zero.

Since the proposed solution is fully three-dimensional, no special consideration has to be given to such effects as torsion, shear lag and other local effects. Isoparametric formulation was used to derive both elements. The shell element is a four-node quadrilateral with

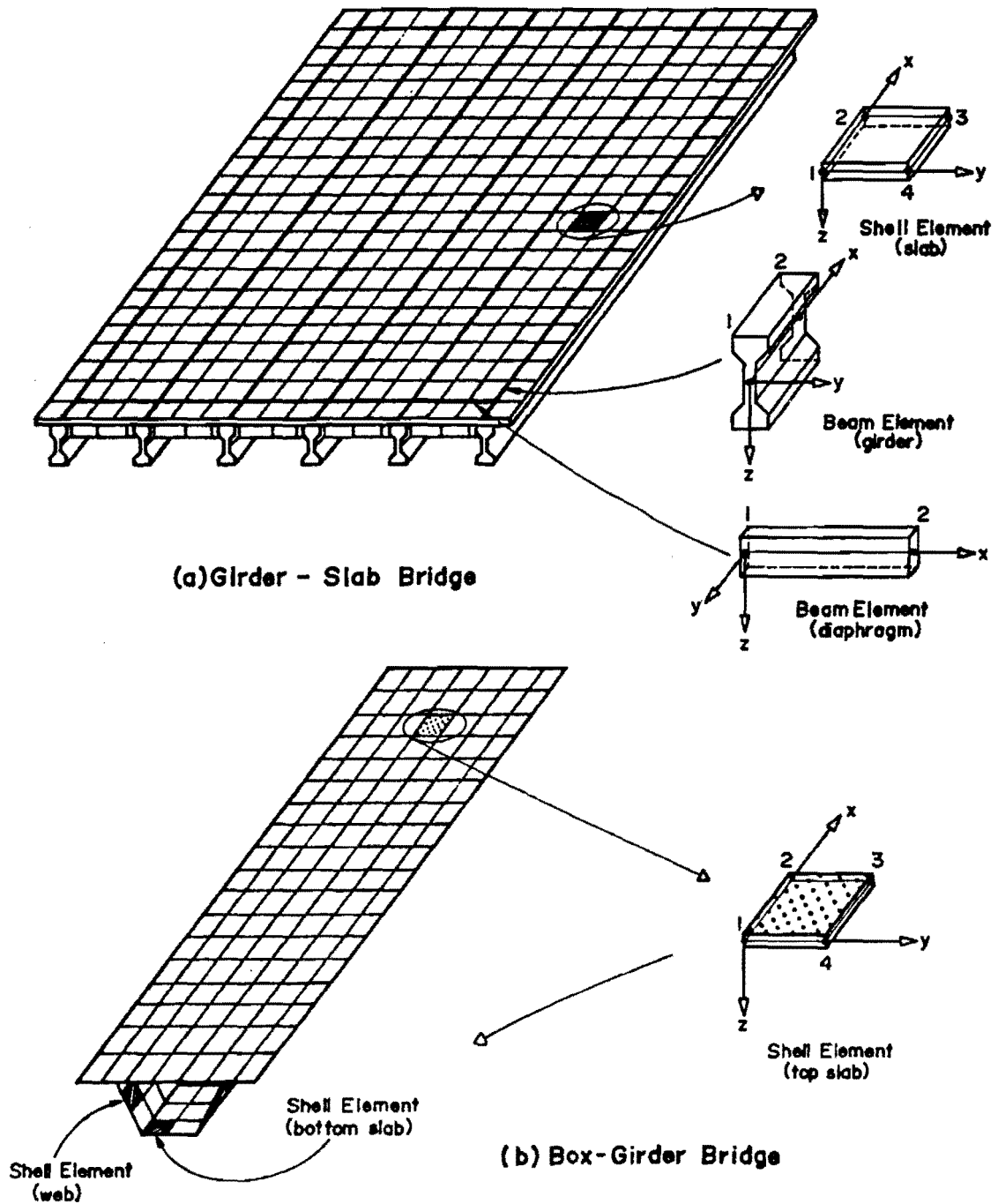


Fig. 4.23 Finite element mesh idealization of the bridges considered in this study

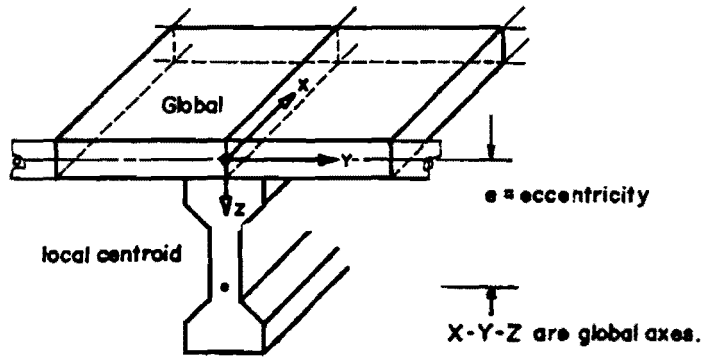


Fig. 4.24a Eccentricity between girder centroid and slab mid-surface

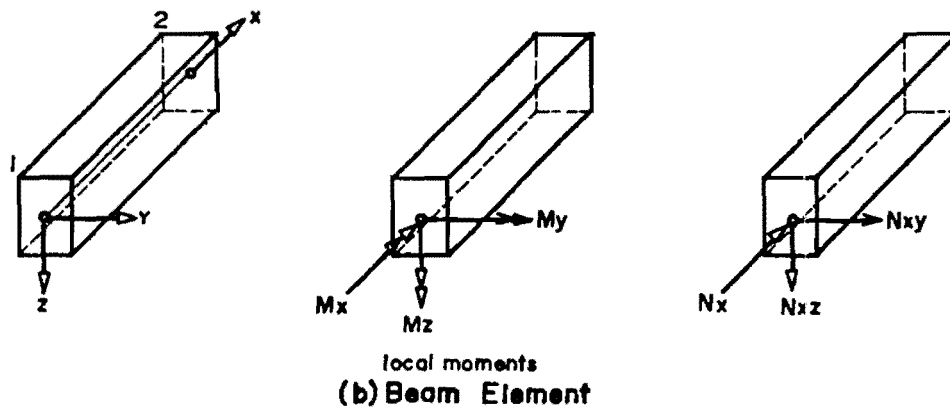
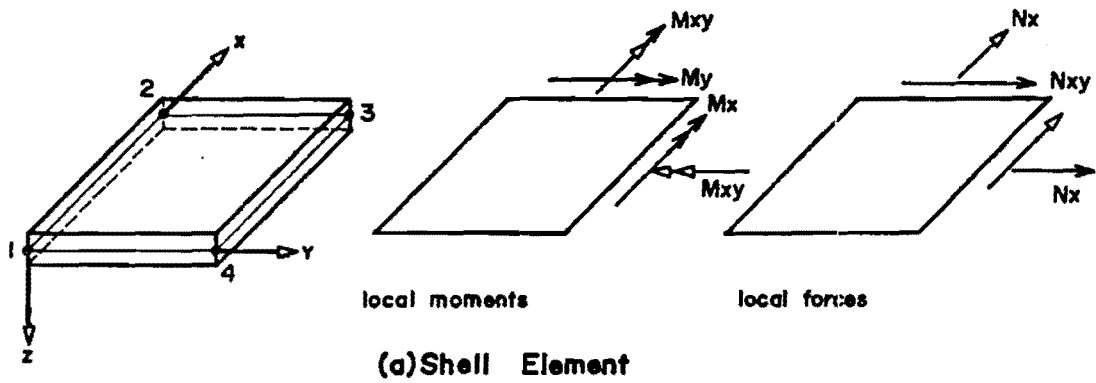


Fig. 4.24 b Local axes of shell and beam elements

six degrees of freedom per node. The beam element is a two-node straight element with six degrees of freedom per node. The shape functions for displacement and rotation for shell and beam elements are assumed to be independent linear functions. The thickness of the shell element is assumed constant for each element and structures with smooth variations in thickness are appropriate with abrupt steps in thickness.

4.5.3 Finite Element Modeling of Bridge Structures. As shown in Fig. 4.23, the slabs of slab-girder and box girder bridges are idealized as shell-type elements. The girders and end and interior diaphragms of a slab-girder bridge are idealized as beam-type elements with special eccentricity transformation to account for the composite action. In the modeling used for the slab-girder bridge members, the width of the slab panel between the girders was taken from girder center-to-center. This assumes that the girders are one-dimensional line elements, as shown in Fig. 4.25. The girder-slab connection is idealized as a point connection on the vertical axis of the girder and not as a real finite-width connection. This results in a local distortion of the actual transverse stresses in the slab in the vicinity of these connections. The webs of a box girder bridge are idealized as shell-type elements. Plane stress elements are used to model the end diaphragms in a box girder bridge. More realistic boundary conditions are imposed in the finite element idealization used than those usually assumed in folded plate and finite strip methods. Because of the actual idealization of the diaphragms, they are not assumed to be infinitely stiff in their own plane and perfectly flexible normal to their own plane. At the end diaphragm nodal supports, the nodes are prevented from vertical movement only.

In this study, the bridges considered will be subjected to transverse prestress loading prior to grouting only. Thus, no bond stresses are developed between the tendons and slab concrete. Consequently, the transverse posttensioned tendons exert pure external loads. In modeling the posttensioned tendons forces, conventional allowance was made for tendon losses. Draped transverse posttensioned tendons press against the concrete slab and thus subject the slab to horizontal and vertical loads and possibly end moments. These forces are calculated using the "equivalent load concept" [65] and input as external loads.

4.5.4 Finite Element Analysis Program. The development of the finite element computer program UTSCA and a listing are detailed in Ref. 60. The computer program is coded in standard FORTRAN IV and is practically machine independent.

The computer program UTSCA provides a powerful tool for the analysis of a wide variety of structural problems. Several examples relevant to this study have been chosen to illustrate the application of the program and the validity of the results obtained. The results

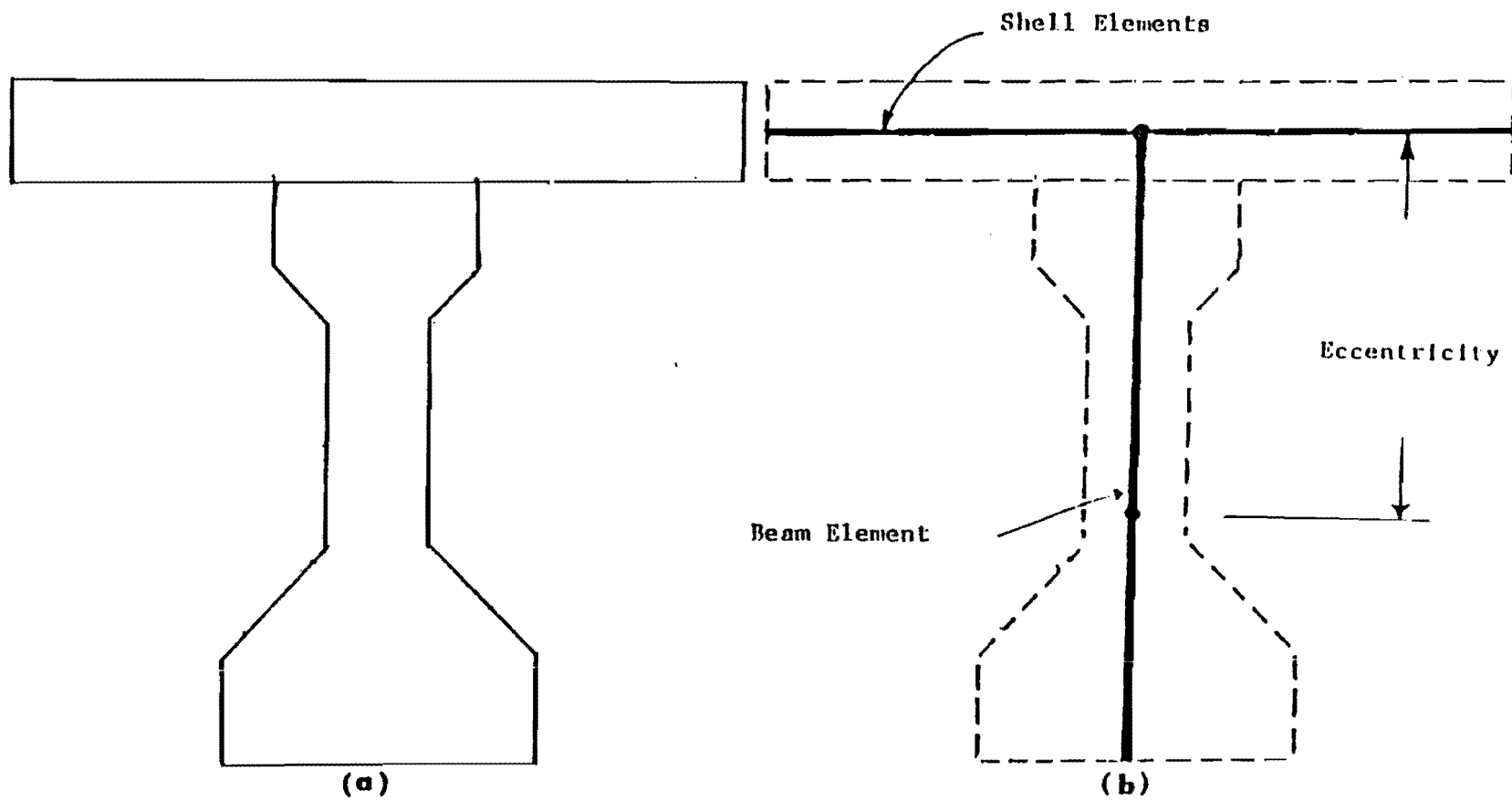


Fig. 4.25 The actual girder-slab connection (a) vs modeled connection (b)

obtained are compared with values obtained from either other analytical solutions or experimental tests. These examples are shown, for reference, in Table 4.2.

Example 1, shown in Fig. 4.26(a), was taken from a report by Mehraïn (82). The three-beam-slab bridge has been chosen to compare the present shell and beam elements to more complicated folded plate elements used in the original report. This example provides an adequate verification of the performance of both the eccentric beam and shell elements. As shown in Fig. 4.26, the agreement with the folded plate method is very good despite the relatively small number of elements used to idealize the bridge.

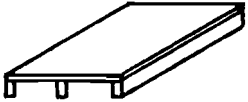
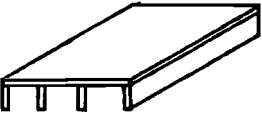
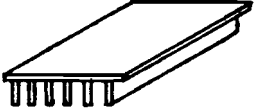

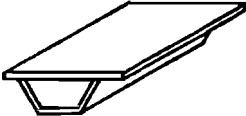
Example 2, shown in Fig. 4.27, was taken from a report by Willam and Scordelis [83] who used folded plate theory for the analysis. This four-beam-slab bridge has been chosen to illustrate the applicability of the present computer program when the structure is subjected to different types of loadings, especially horizontal transverse loading. The three loading cases are analyzed using a very crude mesh (6x6 elements), and the results are shown in Fig. 4.27. The results of the present computer program are in good agreement with those of the folded plate method.

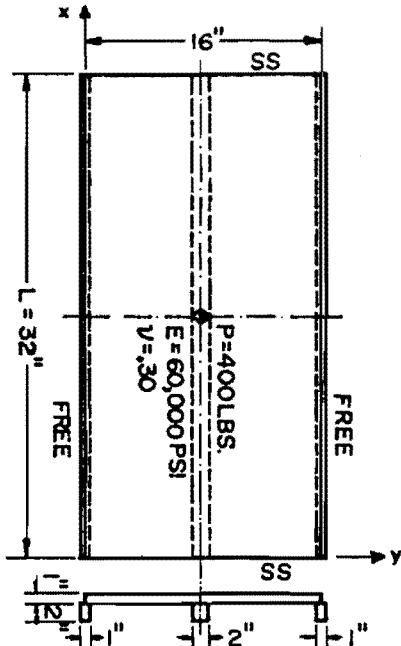
Example 3, shown in Fig. 4.28(a), was taken from a report by Sengupta and Breen [84]. The six-girder-slab bridge, with and without end and interior diaphragms, has been chosen to verify the applicability of the beam element when it is used to model a diaphragm in a girder-slab bridge. Different cases of diaphragms are analyzed and the results obtained are compared to the results obtained from experimental tests. Since the values originally given by Sengupta and Breen are experimentally determined influence-line-type values, the values obtained from the present program are only compared to three girder points for each case. Figure 4.28(b) shows that the results from the computer program are in good agreement with the experimental results.

Example 4 has been chosen to demonstrate the adequacy of the present shell element to idealize skew plates, without even referring to a special skew formulation. Due to the lack of orthogonality and the presence of singularity at the obtuse corners, the analysis of skew plate is more complicated than that of rectangular plates. The results of the present program obtained for different skew angles and boundary conditions are compared to those obtained by Morley [85], and shown in Table 4.3. Since convergence of the finite element results is very slow in the case of skewed plates, a highly refined mesh is required to provide acceptable results. The convergence can also be improved by releasing the corner rotations from clamping.

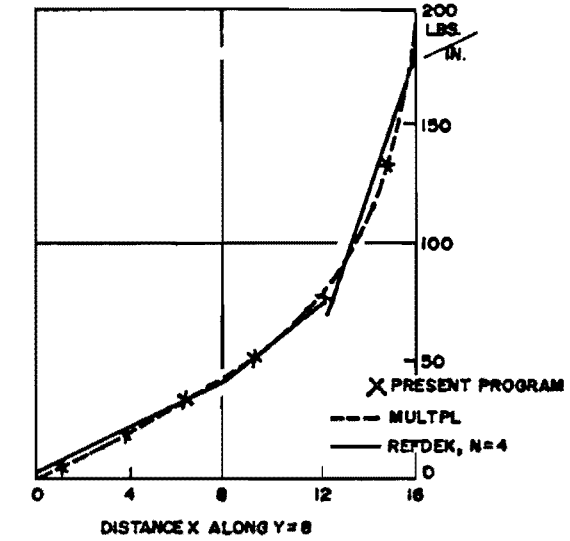
The last example, Example 5, was taken from a report by Kabir and Scordelis [86] to demonstrate the efficiency of the present shell

Table 4.2 A summary of the tested examples

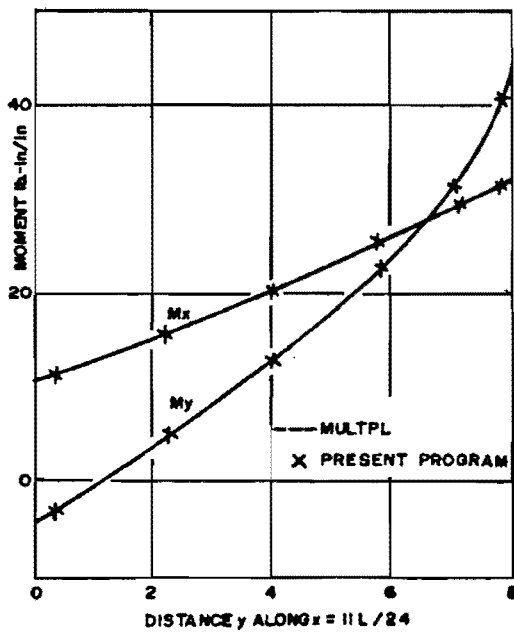
Test	Type	Bridge	Plan	Load
1	Anal.	3 - Girder - Slab		Point
2	Anal.	4 - Girder - Slab		Uniform Vert. Point Hor. Point
3	Exp.	6 - Girder - Slab *w/ Diaphragms *w/o Diaphragms		Point
4	Anal.	Skew Slab *Clamped *Simply S. *Simple/Free		Uniform Point
5	Anal.	Box Girder		Point



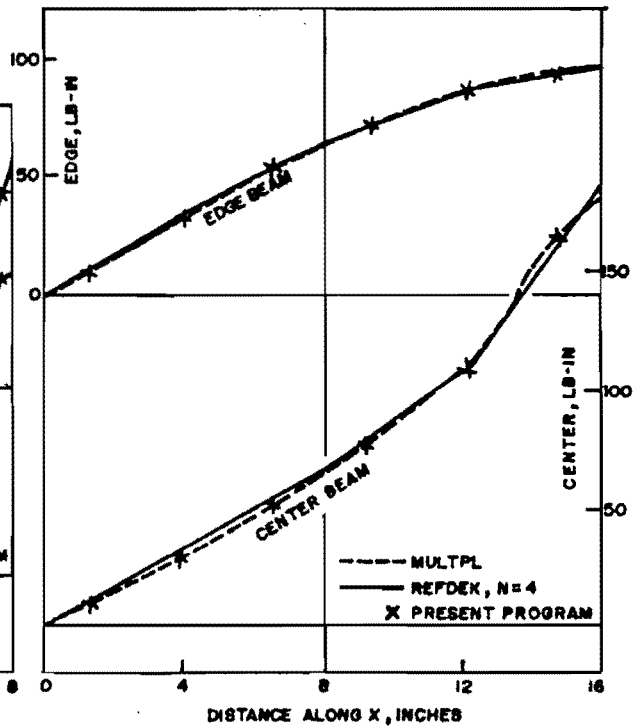
(a) 3-Girder-Slab Bridge



(b) Distribution of N_x in Deck Plate

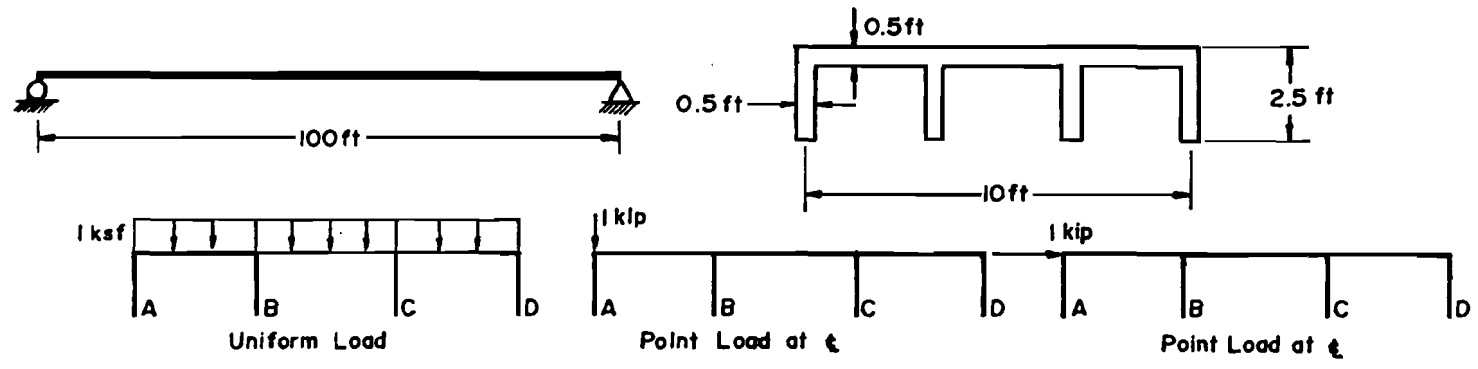


(c) Distribution of M_x & M_y in Deck Plate



(d) Center & Edge Beam Moments

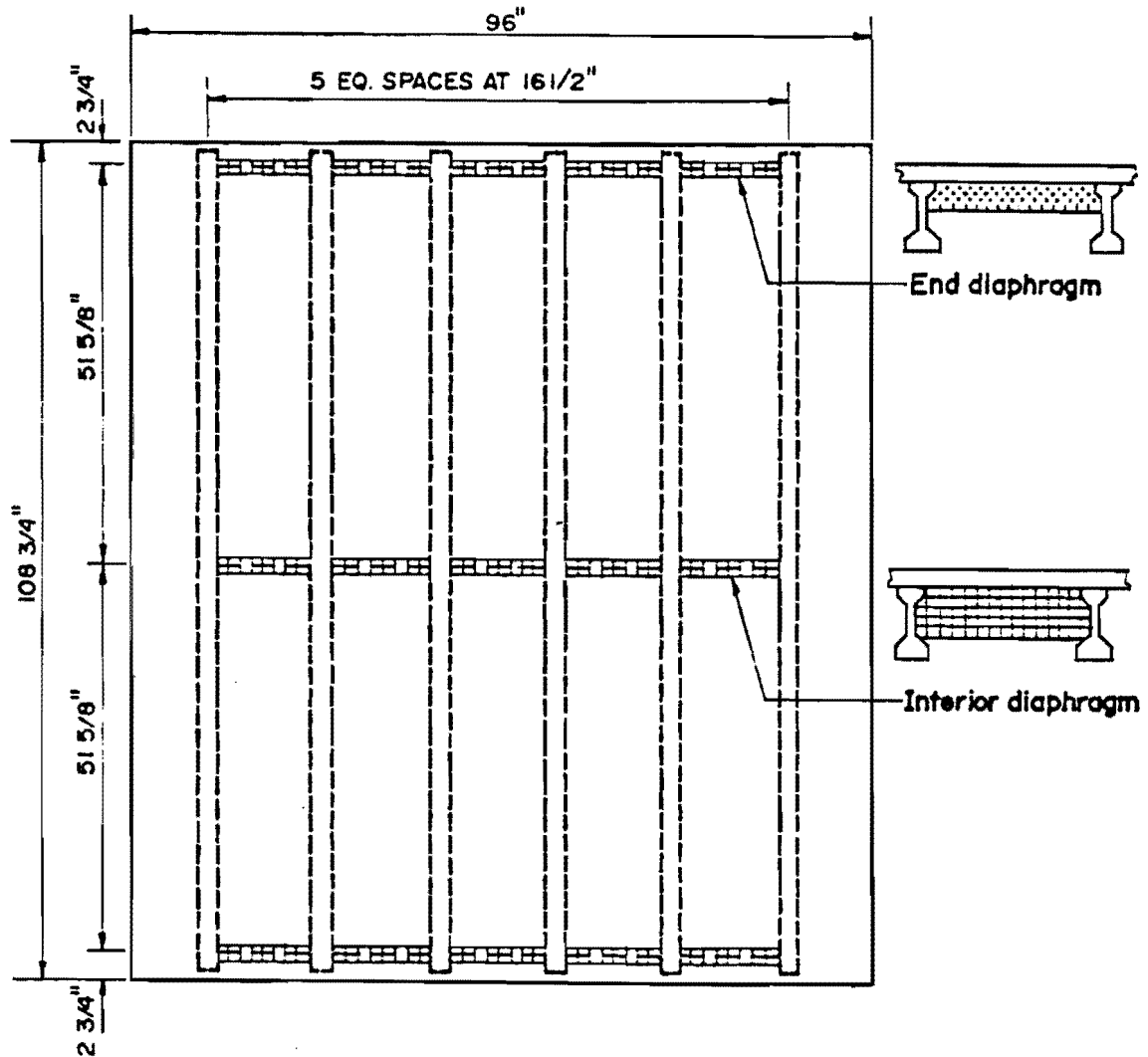
Fig. 4.26 Example 1: 3-girder-slab bridge



		A	B	C	D	A	B	C	D	A	B	C	D
u @ support	FP	1.49	1.48	1.48	1.49	.00301	.00248	.00196	.00145	.00111	.00035	-.00037	-.00111
	FE	1.57	1.56	1.56	1.57	.00318	.00262	.00208	.0015	.00105	.00035	-.00035	-.00105
v @ ϵ	FP	.0328	.0109	-.0109	-.0328	-.0596	-.0601	-.0604	-.0606	-.00793	-.00788	-.00786	-.00785
	FE	.0347	.0115	-.0115	-.0377	-.0608	-.0613	-.0617	-.0620	-.0074	-.0074	-.0075	-.0075
w @ ϵ	FP	87.1	87.0	87.0	87.0	.185	.154	.124	.095	.00596	.00194	-.00207	-.00606
	FE	87.71	87.68	87.68	87.71	.191	.157	.124	.093	.0062	.0021	-.0020	-.0061
T_{slab} @ ϵ	FP	-1340	-1330	-1330	-1330	-5.00	-3.06	-2.00	-1.02	-1.808	-.404	.460	1.400
	FE	-1397	-1394	1394	-1397	-3.92	-3.15	-2.23	-1.36	-1.13	-.5	.3	1.12

FP = Folded Plate Theory (Ref. 30) FE = Present Program

Fig. 4.27 Example 2: 4-girder-slab bridge



PLAN VIEW

Fig. 4.28a Example 3: 6-girder slab bridge, general plan

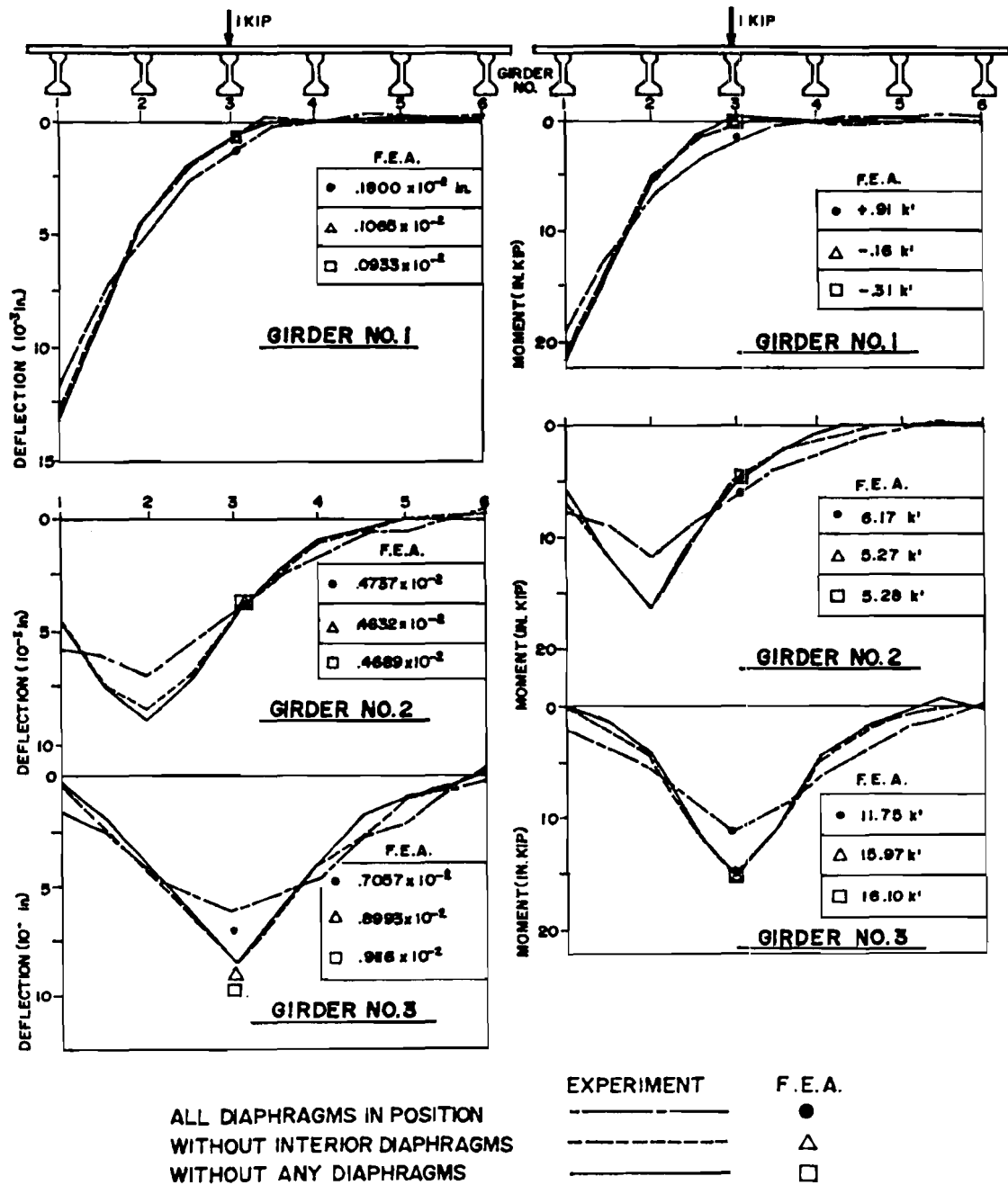
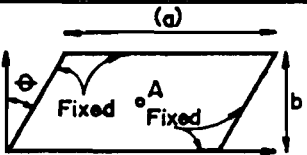

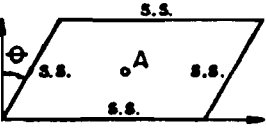
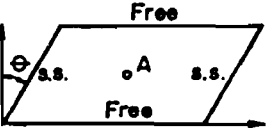


Fig. 4.28b Example 3: experimental and finite element results

TABLE 4.3 EXAMPLE 4: SKEW PLATES

Case	Plan	Θ	Mesh	Deflection @ A F.E.A./Morley
1		30°	8 x 12	0.94
2		30°	16 x 24	0.98
3		45°	4 x 6	0.82
4	$a/b = 2$	45°	8 x 12	0.96
5	 $a/b = 2$	45°	8 x 12	0.91
6	 $a/b = 2$	45°	8 x 12	0.95

element in modeling box girder bridges. The single cell composite box, shown in Fig. 4.29(a), has been previously analyzed using the folded plate and finite strip methods. The results for the three methods, shown in Fig. 4.29(b), are in good agreement.

4.5.5 Summary. The present finite element program has been tested as outlined in Section 4.5.4 using five different structures. The results obtained from the present program compare favorably with other analytical and experimental results. Therefore, the computer program developed for this study can be adequately used to analyze girder-slab and box girder bridges of different geometries under different types of loadings.

4.6 Stressing Experiments on Slab-Girder Bridge Model

4.6.1 General. The basic purpose of the experimental study was to use the physical model to verify the results obtained using the mathematical model, thus providing a "calibration" for the mathematical models.

A direct model at approximately half scale of the prototype slab-girder bridge outlined in Section 4.3 was constructed, instrumented and measurements were made during stressing to corroborate the transverse stress distribution in the model slab to that predicted using the finite element model. Based on cost, available laboratory facilities, accuracy of instrumentation and material availability, a 1/2.23 scale was chosen for this model.

4.6.2 Dimensions and Material Properties. The structural model consists of seven prestressed Texas Type-C girders with end diaphragms and interior diaphragms at third points. The model had a 3.78-in. thick slab and the spacing between girders was 47.06-in. Model layout and girder and diaphragm reinforcement are shown in Figs. 4.30 to 4.32.

The concrete mix design was made using 3/8-in. maximum size of aggregate for the girders, diaphragms and for the slab. Conventional sand was employed in all mix designs. Table 4.4 shows the final proportion of cement, water and aggregates employed during construction.

In addition to the modeling of concrete material, the reinforcement was also scaled as shown in Table 4.5. Where exact scaling of reinforcement area was not possible, spacings were changed to provide the correct force relationship.

4.6.3 Transverse Prestressing. As outlined in Section 4.3, two different prestress profiles were used to provide the required transverse strength. One-half of the model slab was provided with

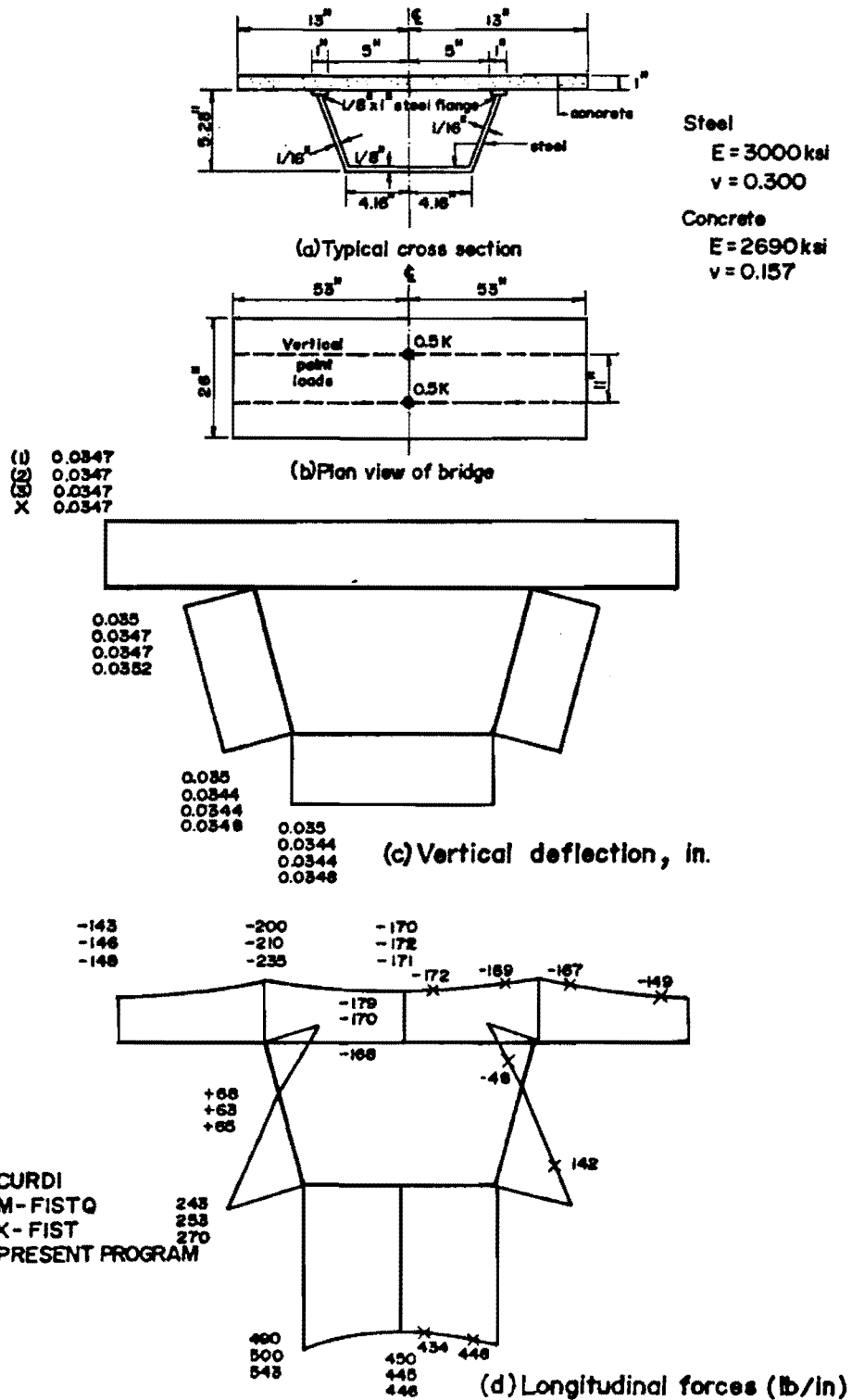


Fig. 4.29 Example 5: box-girder bridge (results at midspan)

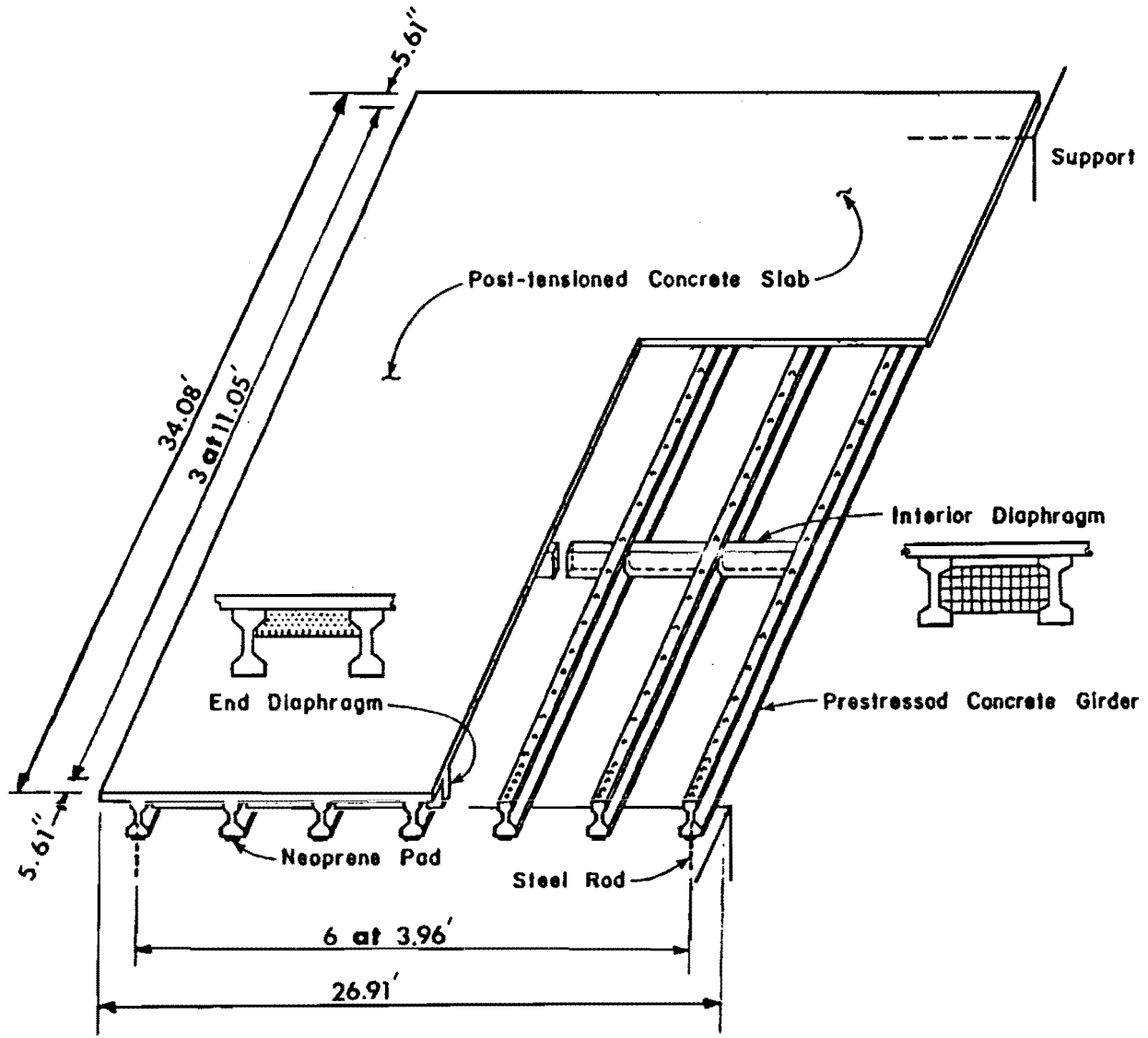
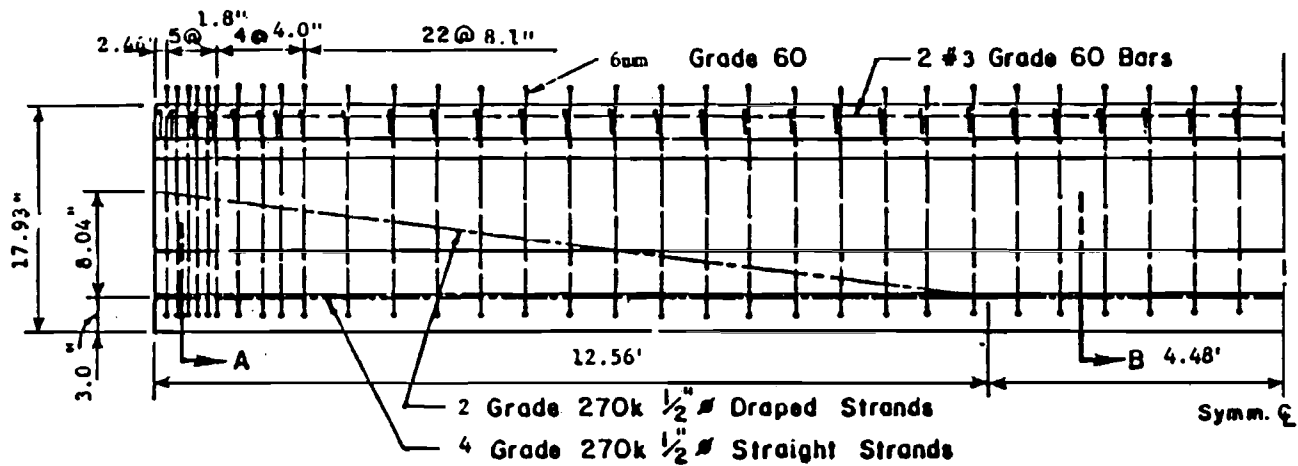


Fig. 4.30 Bridge model layout



(a) Longitudinal and Shear Reinforcement

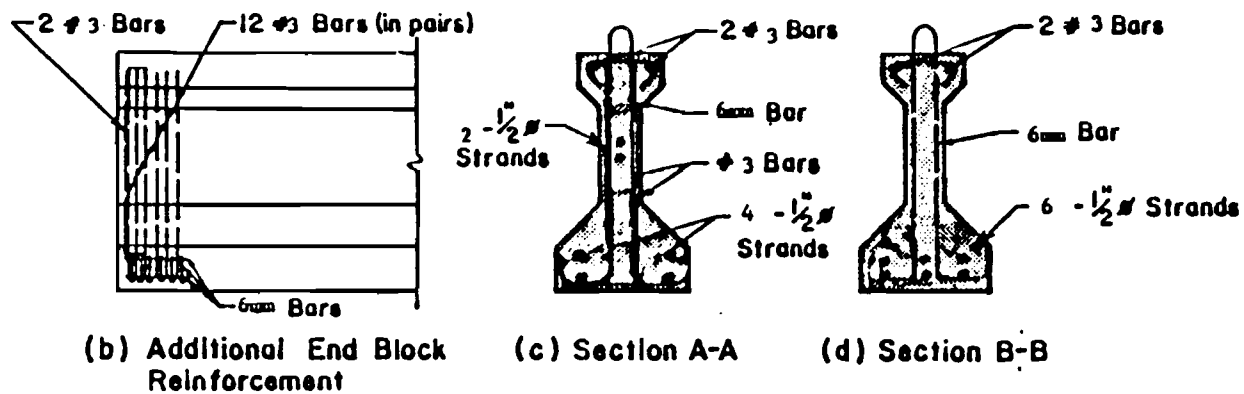
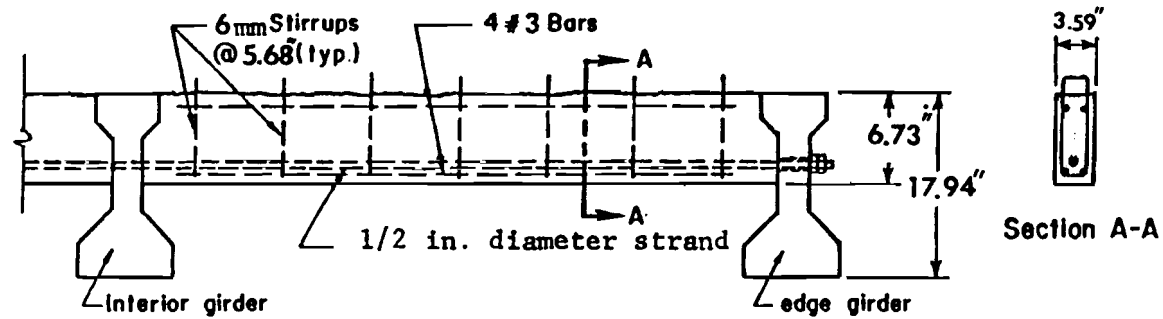
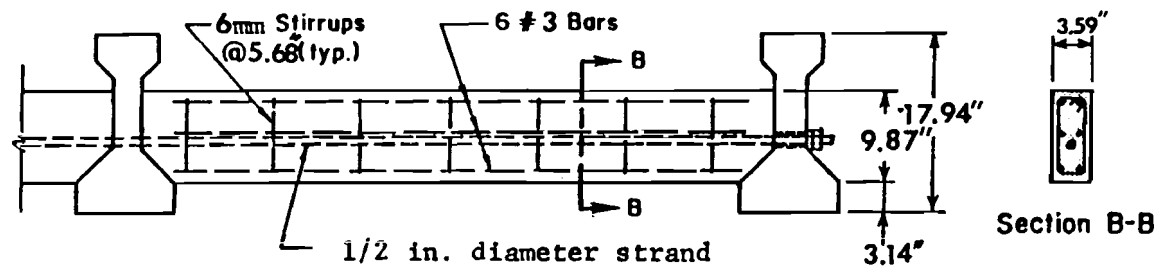


Fig. 4.31 Model girder reinforcement



(a) End Diaphragm Reinforcement



(b) Interior Diaphragm Reinforcement

Fig. 4.32 Model diaphragm reinforcement

TABLE 4.4 CONCRETE MIX PROPORTIONS PER CUBIC YARD

Component	Girder	Slab	Diaphragms
Cement type I, lb.	800	658	565
Water, gals.	34	36	36
3/8" max. size agg., lb.	1590	1590	1546
Sand, lb.	1273	1400	1473
Admixtures		Tricene L 4 oz./sack	

Concrete Compressive Strengths

Member	28-Day psi	90-Day (Stressing) psi
Slab, straight-draped strand half	5400	5850
Slab, straight strand half	4500	4950
Girders	5000	----
Diaphragms	4000	----

TABLE 4.5 REINFORCEMENT FOR THE MODEL

Type of reinforcement in prototype	Type of reinforcement in model		
	Girder	Slab	Diaphragm
1/2" dia. prestressing strand, grade 270K	1/2" dia. prestressing strand, grade 270K	1/4" dia. prestressing strand, grade 250K	---
#3 bars, grade 60	6 mm deformed bars, grade 60	---	---
#4 bars, grade 60	6 mm deformed bars, grade 60	6 mm deformed bars, grade 60	6 mm deformed bars, grade 60
#5 bars, grade 60	#3 bars, grade 60	---	#3 bars, grade 60
#6 bars, grade 60	#3 bars, grade 60	---	---
#8 threaded steel rod	---	---	1/2" dia. prestressing strand

straight strands and the other half with a combination of straight and draped strands. Based on the indications of the finite element analysis, the amount of transverse prestressing steel in the slab was doubled in the diaphragm regions to account for the diaphragm restraint effects, as shown in Fig. 4.33. The transverse prestressing reinforcement is shown in Fig. 4.34. One-quarter in. diameter Grade 250K strands were used for the transverse prestressing.

4.6.4 Instrumentation. The basic purpose of the model study was the comparison of measured slab transverse prestress distribution with that predicted by the finite element analysis. Two quantities need to be accurately measured; the transverse strand force and the concrete strain on the top and bottom surfaces of the slab. The forces in the strands were sampled and monitored using a large number of small load cells. All strands had load cells while tensioning. Approximately 10% of the strands in Test 1, 38% of the strands in Tests 2 and 3, and 30% of the strands in Test 4 had load cells left in position to sample subsequent load changes. The concrete strains were determined using electrical resistance strain gages. The positions of surface strain gages and permanent load cells in Test 1 are shown in Fig. 4.35.

4.6.5 Test Program. Four basic tests were conducted using the bridge model. These tests are listed in Table 4.6. The first two tests had both end and interior diaphragms in place and are termed the all-diaphragm cases. The last two tests had only end diaphragms in place and are termed the end-diaphragm cases. After finishing the first two tests, the interior diaphragms were destroyed in order to test the end-diaphragm cases. Every test was conducted separately from the others. This means that only one-half of the model bridge slab was prestressed in each test.

Each test consisted of very carefully tensioning each strand while monitoring slab deformations. All results are reported for completed stressing of all tendons in the half span.

4.6.6 Finite Element Analysis of Bridge Model. Using the actual measured dimensions and experimentally sampling material properties for each bridge model, finite element analyses for the four tests were performed. Except in the analysis of Test 1, where average value of the monitored strand forces as used to model the transverse prestress forces, step-wise strand force distribution, as sampled from the permanent load cells, was used to model these forces [60]. In Tests 1 and 4 with straight strands, the very low levels of friction loss (less than 2%) were neglected so that only one-half of the model need be considered in the analysis. For Tests 2 and 3, the entire bridge was analyzed in order to model the more substantial friction losses along the draped strands. Note Test 2R (a repeat test) was used for all comparisons because strand forces were in question in Test 2.

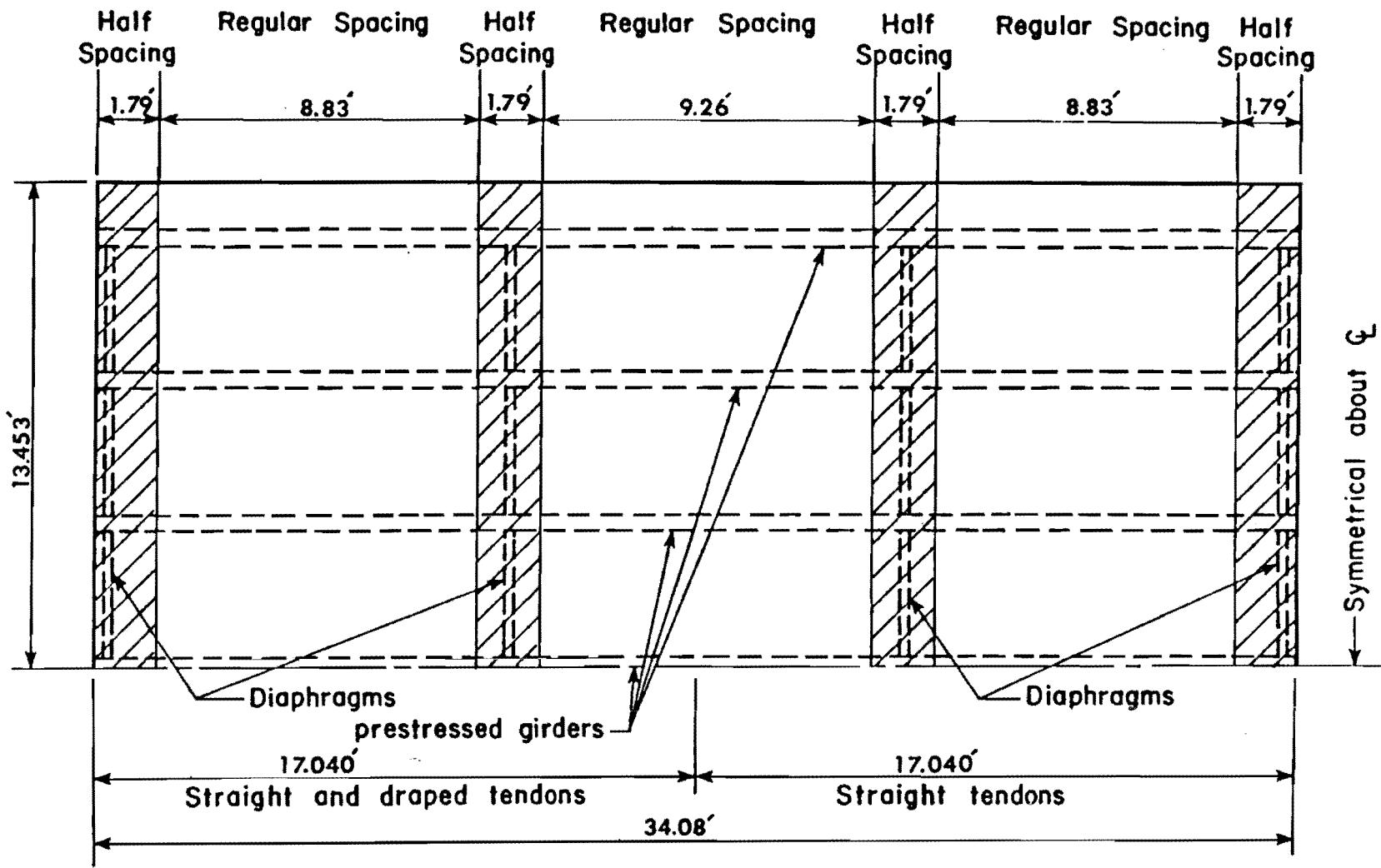


Fig. 4.33 Strips where the prestressing was doubled

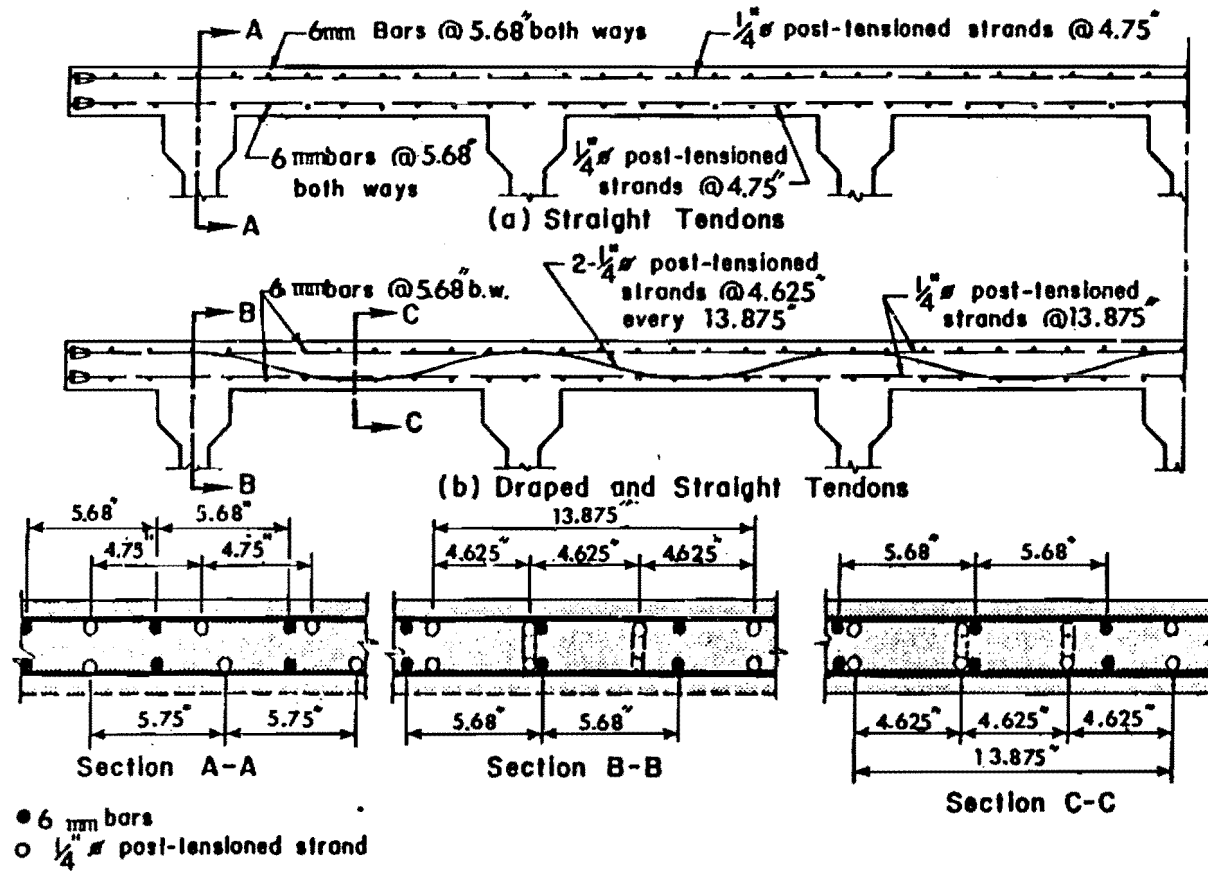


Fig. 4.34a Model slab reinforcement, non-diaphragm regions

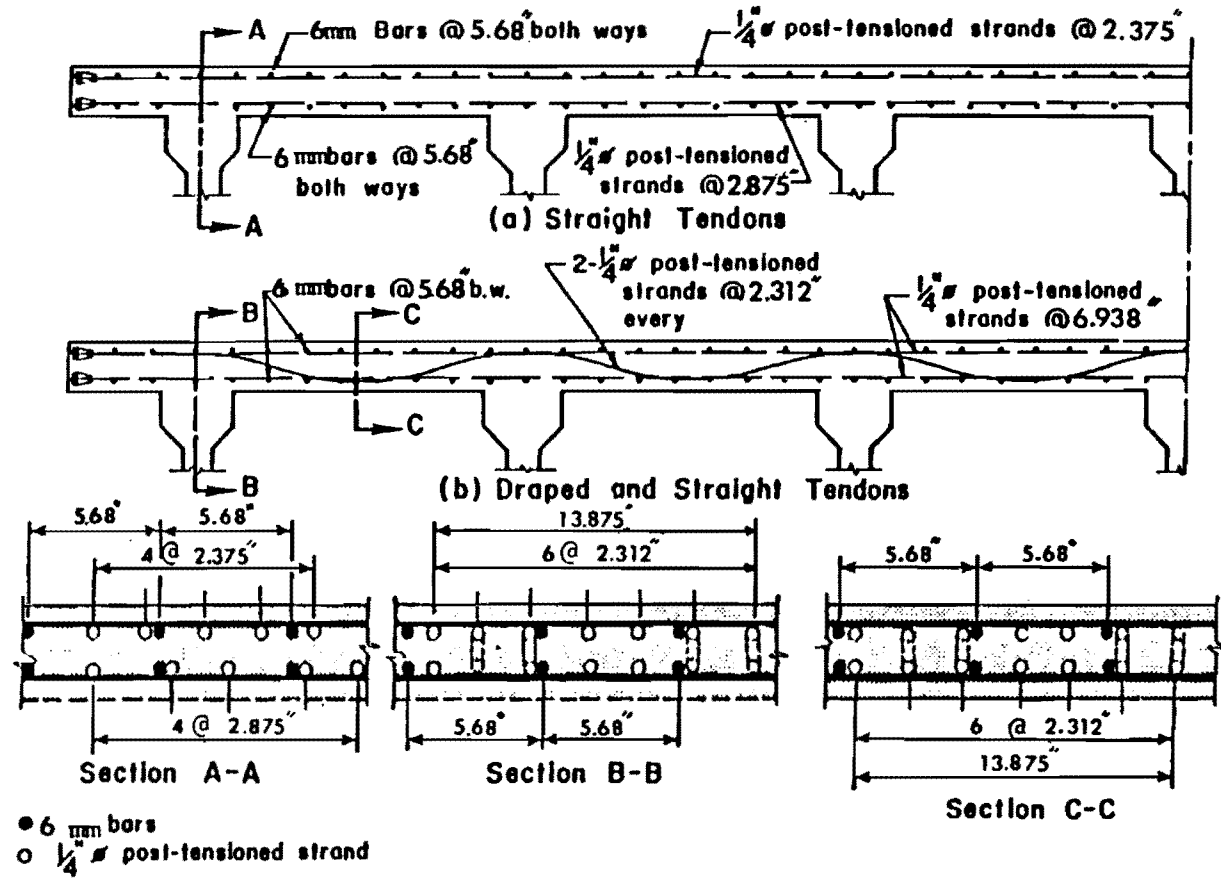


Fig. 4.34b Model slab reinforcement, diaphragm regions

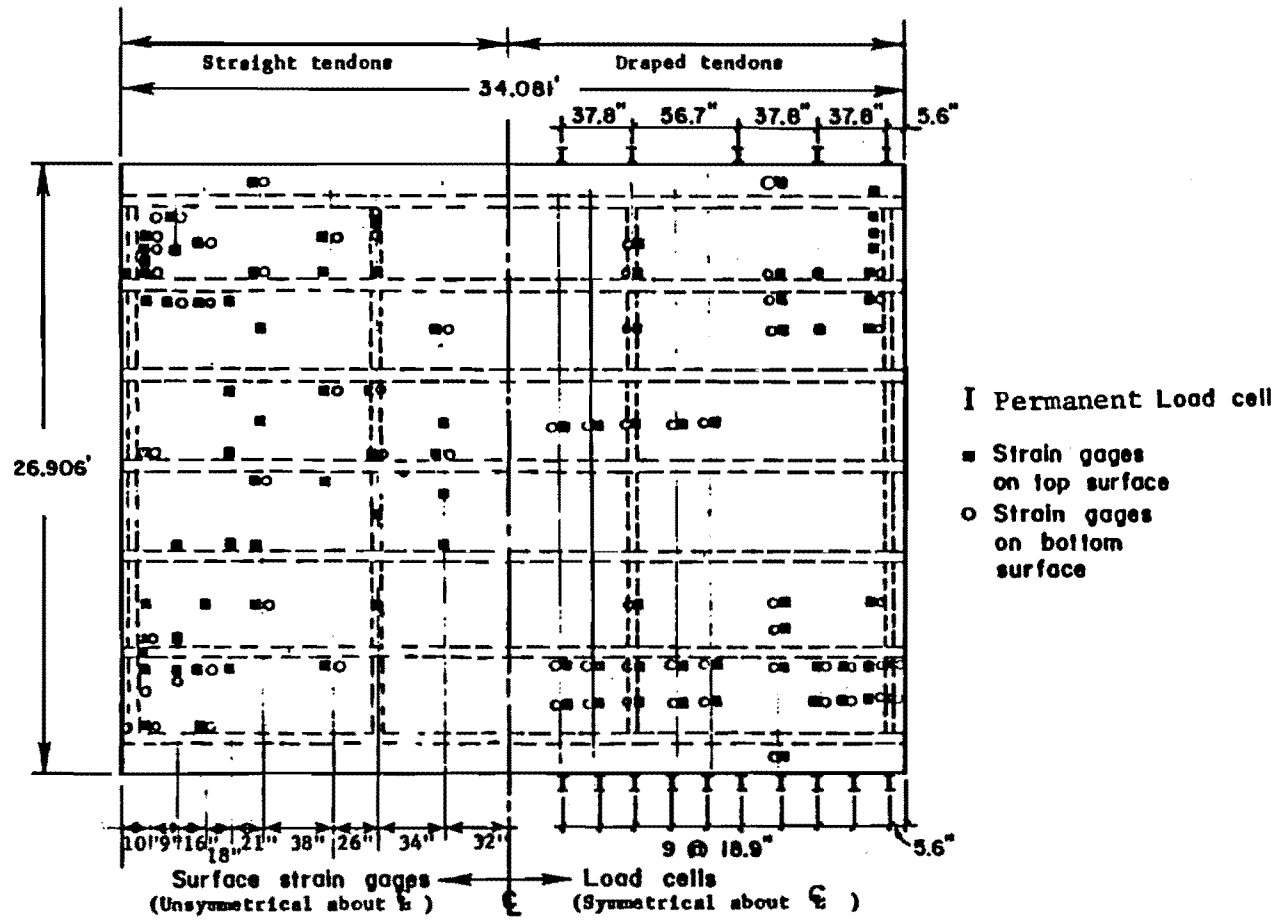


Fig. 4.35 Position, in plan view, of the load cells and surface strain gages

Table 4.6 Test Cases

Test	Bridge Case	Prestress Profile
# 1	All-Diaphragm	Straight
# 2	All-Diaphragm	Straight and Draped
# 2R	All-Diaphragm	Straight and Draped
# 3	End-Diaphragm	Straight and Draped
# 4	End-Diaphragm	Straight

4.6.7 Comparison of Experimental and Analytical Results. Since only half of the model deck was transversely prestressed in each test, concrete strains were only measured in the stressed half. Therefore, in comparing the experimental and analytical results, the transverse stress distribution in the slab is only given for the stressed half. Each tested half was also divided into tendon jacking or "live" end and tendon anchored or "dead" end sides.

The comparison between test and analytical results is illustrated in Figs. 4.36 to 4.39. Triangles indicate the measured stress percentage from gages located at the solid circle while the analytical values are plotted as contours. All values are shown as percentages of the applied edge stress. The experimental values correspond to the mid-depth stress determined by averaging results from top and bottom surface strain gages to cancel local slab bending effects. As indicated in Sec. 4.5.3, the method of modeling the girder-slab connection distorts the local bending effects in the slab in the vicinity of the girders. In computing the stress percentages, the stresses obtained from the analytical and experimental results were divided by an average nominal compressive stress. The average nominal compressive stress is the average edge P/A stress based on measured stressing loads. The values of P/A were 597 psi for Tests 1 and 4, and 450 psi for Tests 2 and 3.

Actual slab top and bottom stress values were very sensitive to both prestressing force effects and to local bending effects due to tendon eccentricity. Tendon eccentricity in the thin model slab was very difficult to control due to possible placement errors of the strands. Very small eccentricities can greatly affect local bending stresses. Tendon placement errors on the order of 1/8-in. can cause extreme fiber stress changes of about 15%. Such errors are cancelled out by consideration of the average middepth stresses. Because both analytical modeling and experimental errors cast doubt on accuracy of slab bending stresses, in arriving at general assessment of the measure of agreement between the experimental and analytical results, most weight was given to the mid-surface stress ratios.

In spite of taking all possible precautions, some errors in experimental tests are unavoidable. It is difficult to draw any definite quantitative conclusions regarding the verification of the analytical results from direct comparison with the experimental results using only Figs. 4.36 to 4.39. However, an approximate indication or measure of the general agreement between the analytical and experimental results can be determined. Since for an ideal situation, the experimental values ought to equal the analytical values, the ratios of these values should be close to 1. An indication of agreement may then be obtained from examining the mean value of these scattered values and the corresponding standard variation for each test. These ratios and their mean and standard deviation values are given in Table 4.7 for Tests 1 to 4. The effects

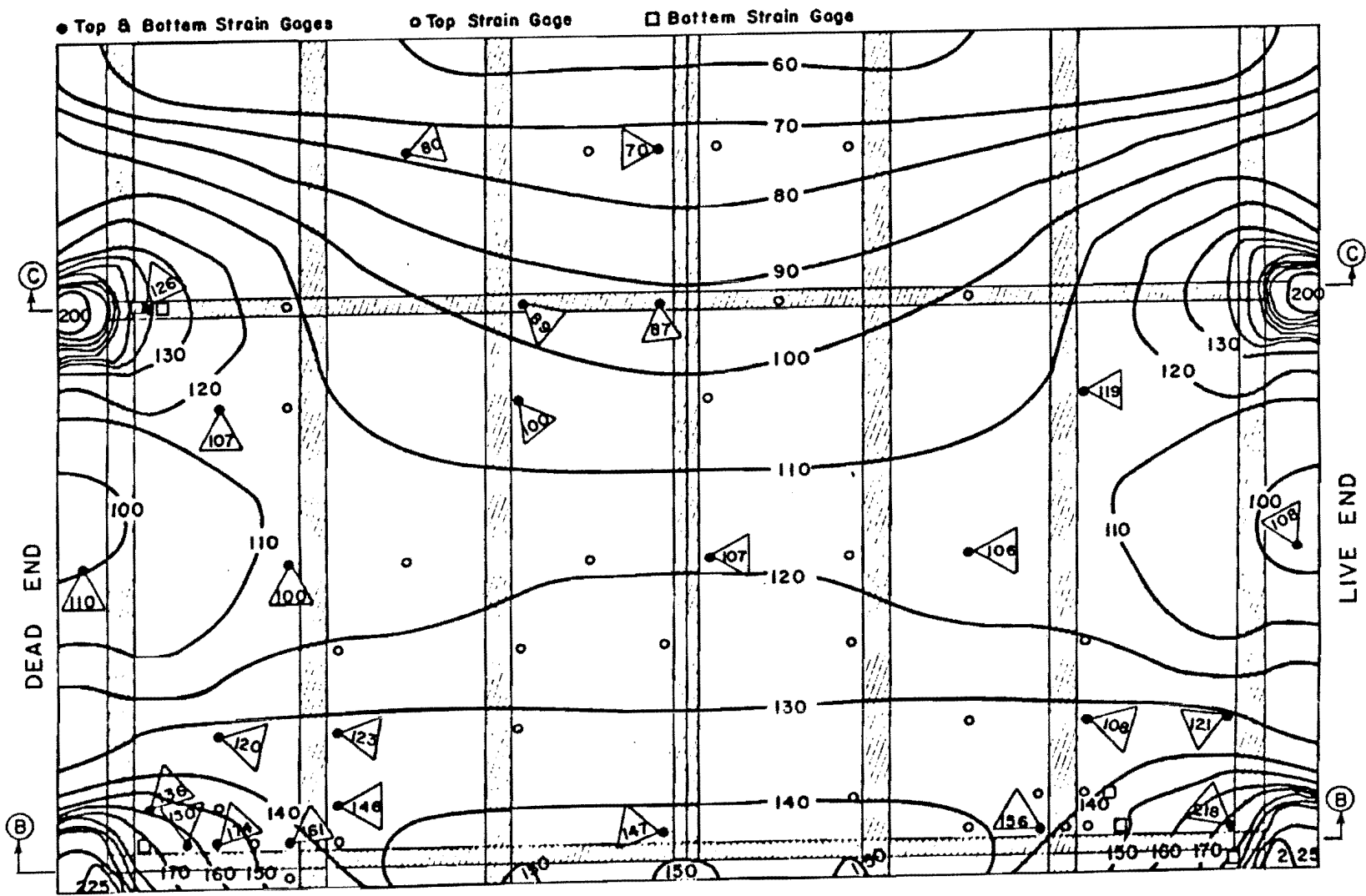


Fig. 4.36 Analytical and experimental middepth transverse stresses in the slab, Test #1. (all diaphragms in place - straight strands)

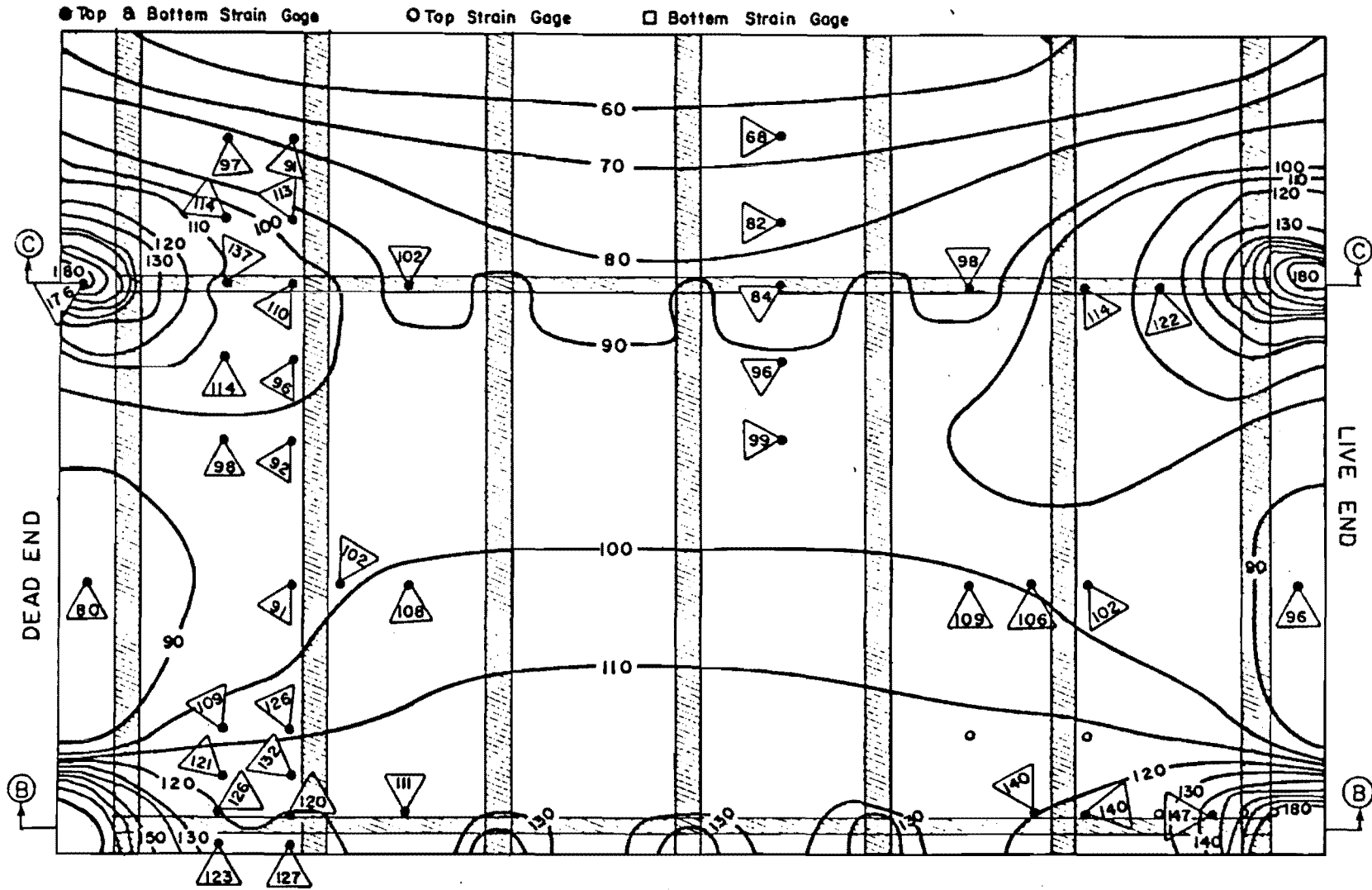


Fig. 4.37 Analytical and experimental middepth transverse stresses in the slab, Test #2R.
 (all diaphragms in place - straight and draped strands)

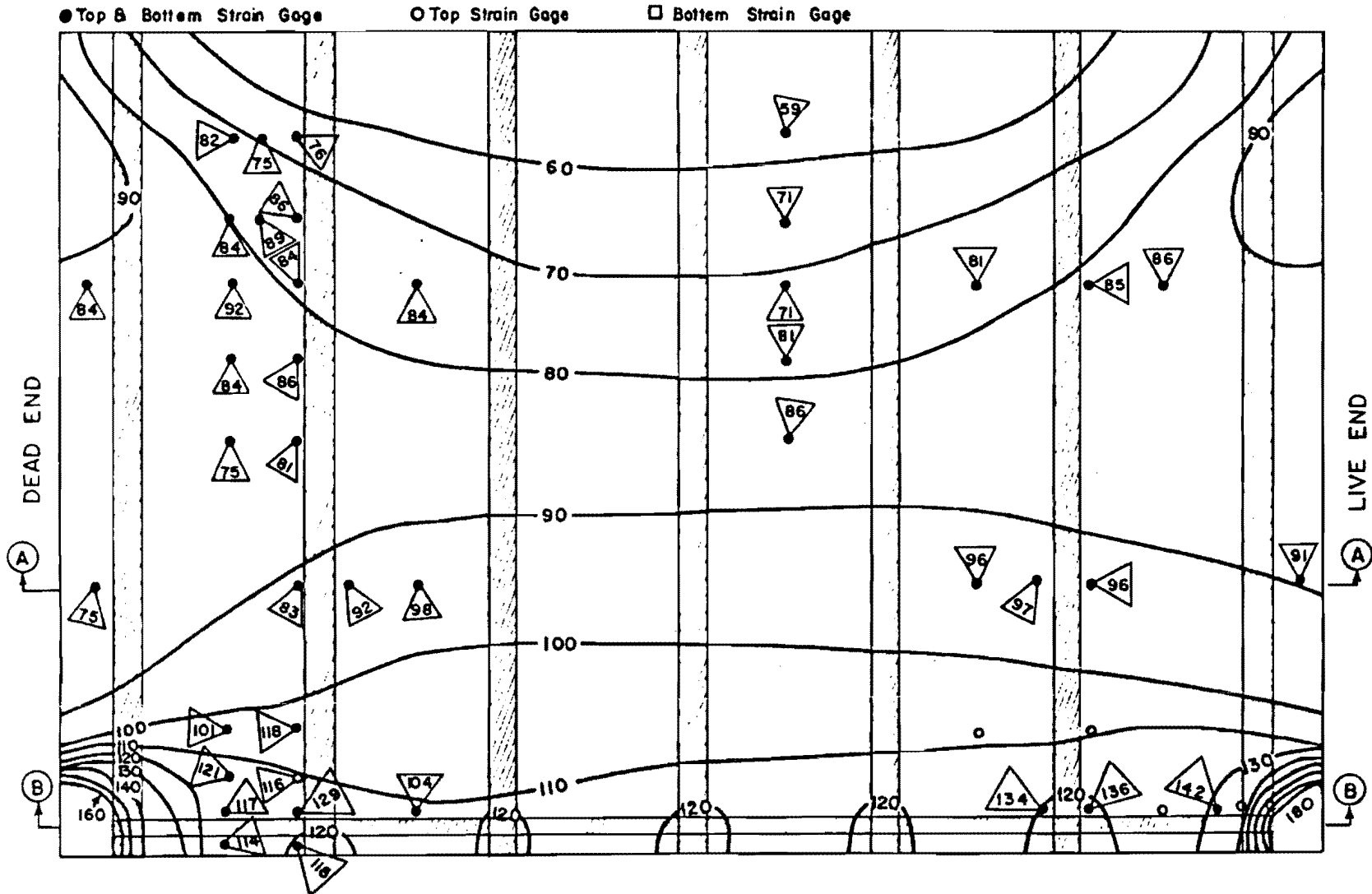


Fig. 4.38 Analytical and experimental middepth transverse stresses in the slab, Test #3.
(end diaphragms in place - straight and draped strands)

Table 4:7 Ratios of Experimental to Analytical Stresses

	Total Points	Mean (Exp. / Anal.)	Standard Deviation	
Test 1	Top Stresses	53	0.98	0.19
	Bottom Stresses	31	0.99	0.19
	Middle Stresses	25	0.99	0.10

	Total Points	Mean (Exp. / Anal.)	Standard Deviation	
Test 2R	Top Stresses	47	1.12	0.46
	Bottom Stresses	42	1.23	0.46
	Middle Stresses	42	1.14	0.07

	Total Points	Mean (Exp. / Anal.)	Standard Deviation	
Test 3	Top Stresses	49	1.26	0.44
	Bottom Stresses	44	1.12	0.44
	Middle Stresses	44	1.11	0.07

	Total Points	Mean (Exp. / Anal.)	Standard Deviation	
Test 4	Top Stresses	53	1.00	0.18
	Bottom Stresses	37	1.13	0.18
	Middle Stresses	32	1.08	0.07

of the experimental and analytical modeling uncertainties on the slab top and bottom stresses can be clearly seen in Table 4.7 where the standard deviation values for the draped tendon slabs is extremely high as compared to the straight tendon slabs. However, the mean values and the standard deviations for the averaged middle stresses are very acceptable. The overall average for all four tests for the middle stresses are 1.08 for the mean and 0.08 for standard deviation. These comparisons definitely show the analytical procedures to be powerful predictors of transverse stress distribution.

From the comparison of the analytical and experimental results, the following conclusions were reached.

1. The maximum discrepancy observed occurs in the slab extreme fiber stresses due both to modeling errors of the girder-slab connection and of experimental discrepancies such as the effects of tendon placement errors. Verification of the finite element program has been totally based on the comparison of slab middepth stresses, which are not affected by placement errors and local bending effects.
2. An accurate step-wise distribution of strand forces should always be used in modeling transverse prestress forces.
3. As predicted by the finite element program, the effect of the lateral resistance of the girders, without diaphragms, on the slab transverse stress distribution was confined to the regions of the slab which are over the girders.
4. The test results accurately confirmed the stress peaks in the end and interior diaphragm regions predicted by the finite element program, as shown in Figs. 4.36 to 4.39 along sections B and C. It also shows that the slab transverse stresses are mostly affected by the existence of the diaphragms.

C H A P T E R 5

VERTICAL AND EDGE LOAD TESTS

5.1 Vertical Load Test Program

5.1.1 Introduction. Lateral posttensioning stress distribution tests on the bridge model, carried out as outlined in Section 4.6 showed that transversely prestressing the deck of a slab-girder bridge can effectively develop compressive stresses in the slab to counteract tensile stresses that would occur due to shrinkage and to live loads. The vertical load tests presented in this section address the performance of the transversely prestressed bridge deck under various levels of dead and live load.

Specific objectives of the vertical load test program were:

1. To document the behavior of the transversely prestressed bridge deck under various levels of loading up to failure including service and factored load
2. To identify modes of failure and the load levels at which they occur
3. To determine and quantify design factors from a structural standpoint, including critical loading conditions, distribution of concentrated loads and stresses induced by live loads

A bridge deck is subject to a great number of loading conditions. Selected for particular study were load placements which would produce maximum positive and maximum negative moments in both interior and exterior transverse slab spans, as well as minimum positive moment in the interior region of the slab. Minimum positive moments were a concern due to the possibility of stress reversal occurring when a high ratio of live to dead load exists, particularly where a draped strand profile has been used. Minimum positive moments in the exterior slab span were not chosen for testing since analysis indicated the magnitude of these moments to be significantly less than in the interior region. Also, punching shear was not selected for separate study because if it were a critical load condition, it would be apparent in the other tests.

One final simplification of the testing program was that the effect of intermediate diaphragms was excluded from study. These diaphragms influence slab behavior only through a slight increase in distribution of the load among the girders. Therefore, only the more severe case of a slab and girder bridge without intermediate diaphragms was examined.

Using the Westergaard [28] contour surface, it was found that for the girder spacing under consideration, the effect of other axles of an AASHTO HS20-44 truck on the transverse and longitudinal slab moments 14-ft away would be negligible. Therefore, only a single axle of each truck was modeled.

The positioning of individual wheel loads relative to the girders to represent a given loading condition was determined by elastic analysis of a simply supported continuous beam. In most instances, placement of one wheel in a critical loading location resulted in the other wheel on the axle being located on top of a bridge girder. Such loads acting directly over the girder have only a secondary effect on the moments in the slab, and thus were excluded from the tests. Consequently, each loading condition was modeled using just one or two wheel loads. The actual locations of vertical load application were chosen to minimize the effects of one test on another. Vertical load application points for each test are shown in Fig. 5.1.

The loaded area representing each wheel load was established using criteria set forth in the AASHTO Specifications, Section 3.30. For a wheel load of 16 k, the tire print is taken as 8 in. in the direction of traffic and 20-in. wide. Applying the model scale factor of 2.23 to this, each wheel in the tests was modeled as a loaded area measuring 3.59 by 8.97 in.

In a direct model where the stress in the prototype is equivalent to the stress in the model, the scale factor for concentrated loads is equal to the linear dimensions scale factor squared. Thus, for the dimension scale factor of 2.23, a wheel load of 16 k, and allowance for live load impact of 30%, the service level live load applied to the model was taken as:

$$\text{Service (LL + I)} = (16) (1.3) / (2.23)^2 = 4.18 \text{ kips}$$

Factored load using AASHTO Specifications is:

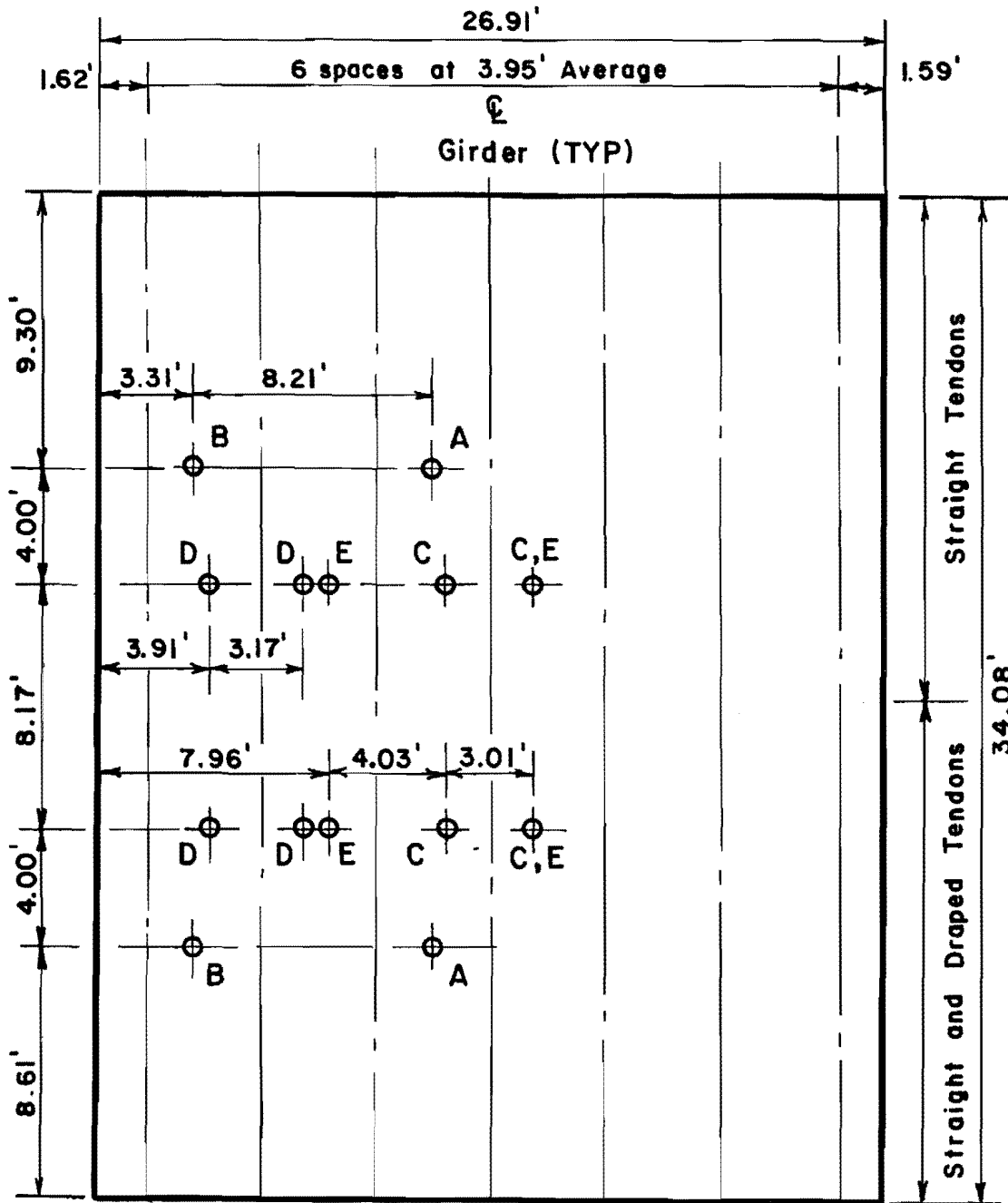
$$U = 1.3 (DL + 5/3 (LL + I))$$

Similarly then, factored live load applied in the model tests was calculated as:

$$\text{Factored (LL + I)} = (1.3) (5/3) (4.18) = 9.06 \text{ kips}$$

For tests involving live loads equal to or greater than factored load, the equivalent dead load was increased 30% from service to factored level. This was accomplished by decreasing the spacing of the compensation dead load blocks on top of the model bridge deck.

Loads were applied to the deck at the specified points by pulling from beneath the bridge using rams and tension rods which were



- A - Interior Positive Moment
- B - Exterior Positive Moment
- C - Interior Negative Moment
- D - Exterior Negative Moment
- E - Minimum Positive Moment

Fig. 5.1 Vertical load application points

anchored to the floor and which passed through drilled holes in the deck. The magnitude of the applied load was monitored by measuring hydraulic pressure at the pump. A pressure transducer of either 5 ksi or 10 ksi capacity was utilized for this purpose and read with a strain indicator.

Three categories of data were collected during the vertical load tests: vertical deflections of the bridge model slab and girders, strains at selected locations on the bridge deck surfaces, and tension force in some of the slab prestressing tendons. Instrumentation details are reported in Ref. 63. Vertical deflection measurements were obtained using a combination of linear potentiometers and mechanical dial gages, positioned as shown in Figs. 5.2 and 5.3.

Surface concrete strains were measured with electrical resistance strain gages of either 30 mm or 60 mm gage length and were read manually using a strain indicator. For most of the vertical load tests, concrete strain readings were obtained only at locations near the load application points where strain gages had been installed previously for the posttensioning stress distribution tests. These locations are shown in Fig. 5.4. To obtain data on slab curvature, a pattern of strain gages was placed around the maximum positive interior moment load position on the straight and draped tendon side of the bridge only. The locations of these gages are detailed in Fig. 5.5.

In order to account for the slab behavior analytically, the force in the transverse posttensioning strands must be known. Therefore, the forces in the strands were sampled using a large number of small load cells especially fabricated for this model. Approximately 31% of the straight strands and 41% of the straight and draped strands were monitored on the live end with the load cells.

The sequence in which the vertical load tests were performed was determined by three factors. First, only enough strand anchors were available to stress one-half of the bridge deck at a time. Thus, a complete set of tests was carried out on the straight strand side of the bridge model (north end) while the straight and draped strand side of the deck remained unstressed. Then the straight posttensioning tendons were released, the straight and draped tendons stressed, and the series of tests repeated on the other side of the bridge (south end). The second factor affecting test sequence was that the compensating dead load blocks had to be moved after the service load tests to increase the dead load to factored level. Finally, in order to minimize the possibility of structural damage produced by one test influencing the results of another test, it was desirable to complete all other tests before beginning the ultimate load tests. These last two considerations required that for a given side of the bridge model, all the service load tests be performed first, followed by all the

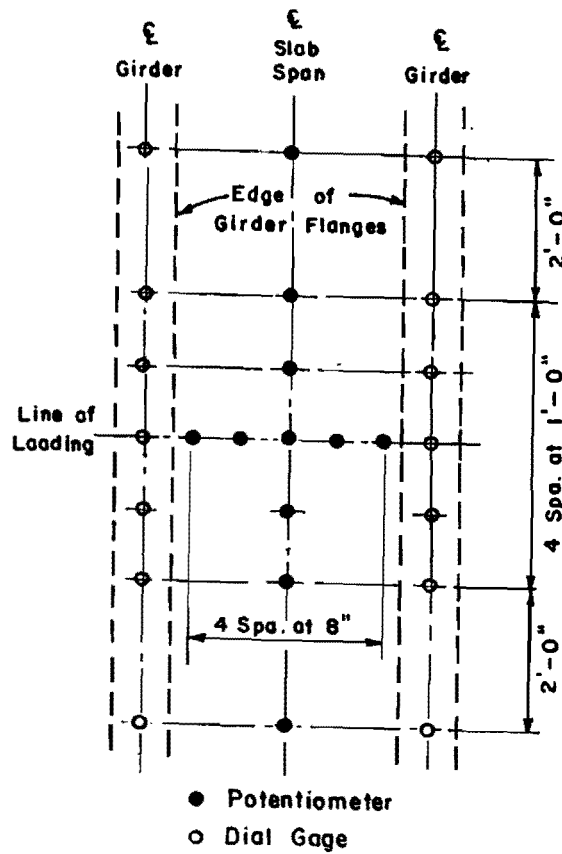


Fig. 5.2 Vertical deflection instrumentation locations for positive moment and minimum positive moment tests

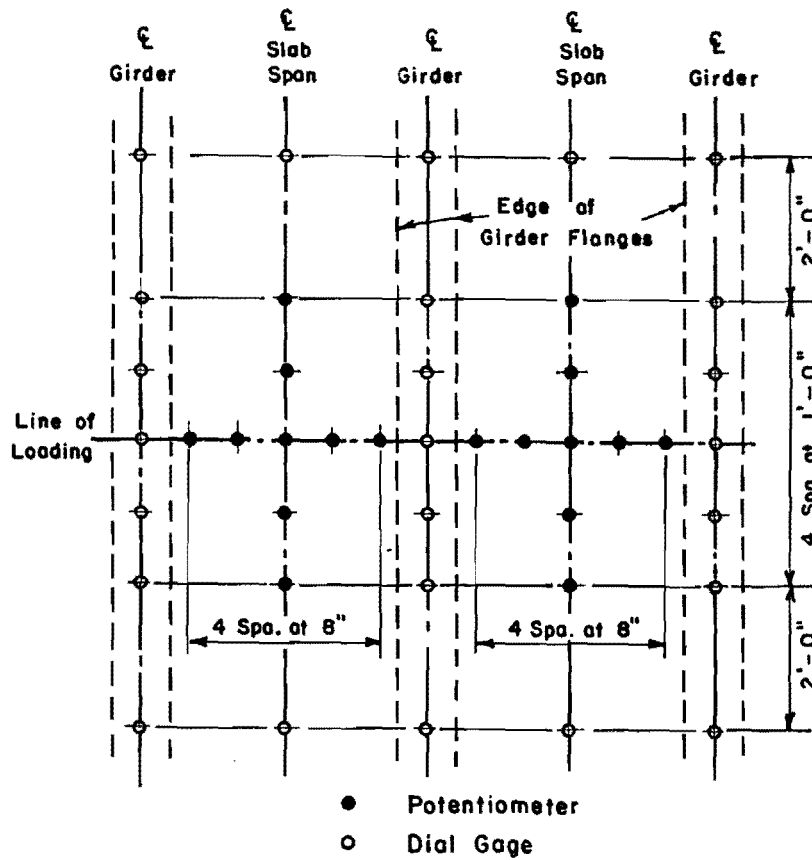


Fig. 5.3 Vertical deflection instrumentation locations for negative moment tests

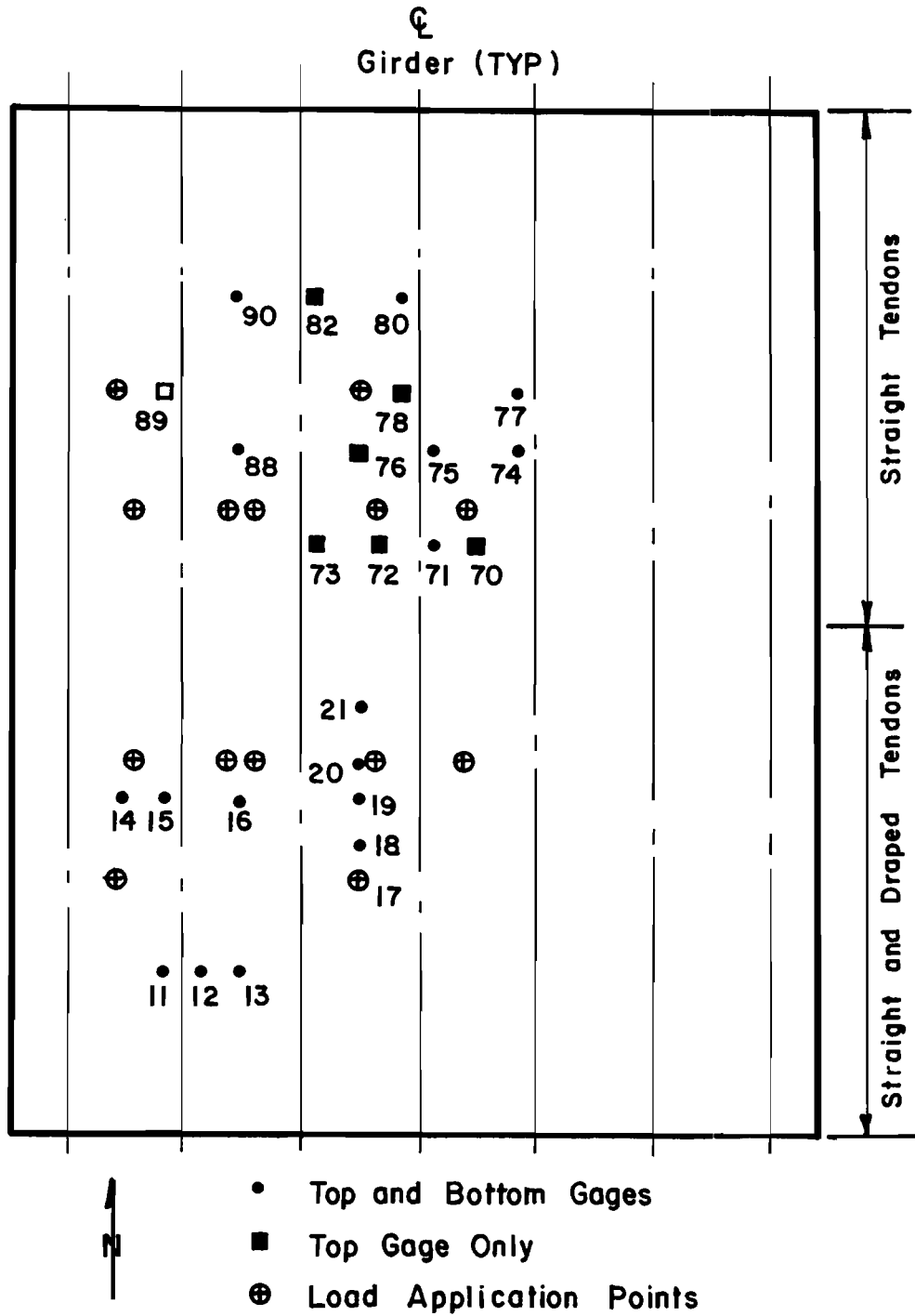


Fig. 5.4 Locations of existing strain gages used in vertical load tests

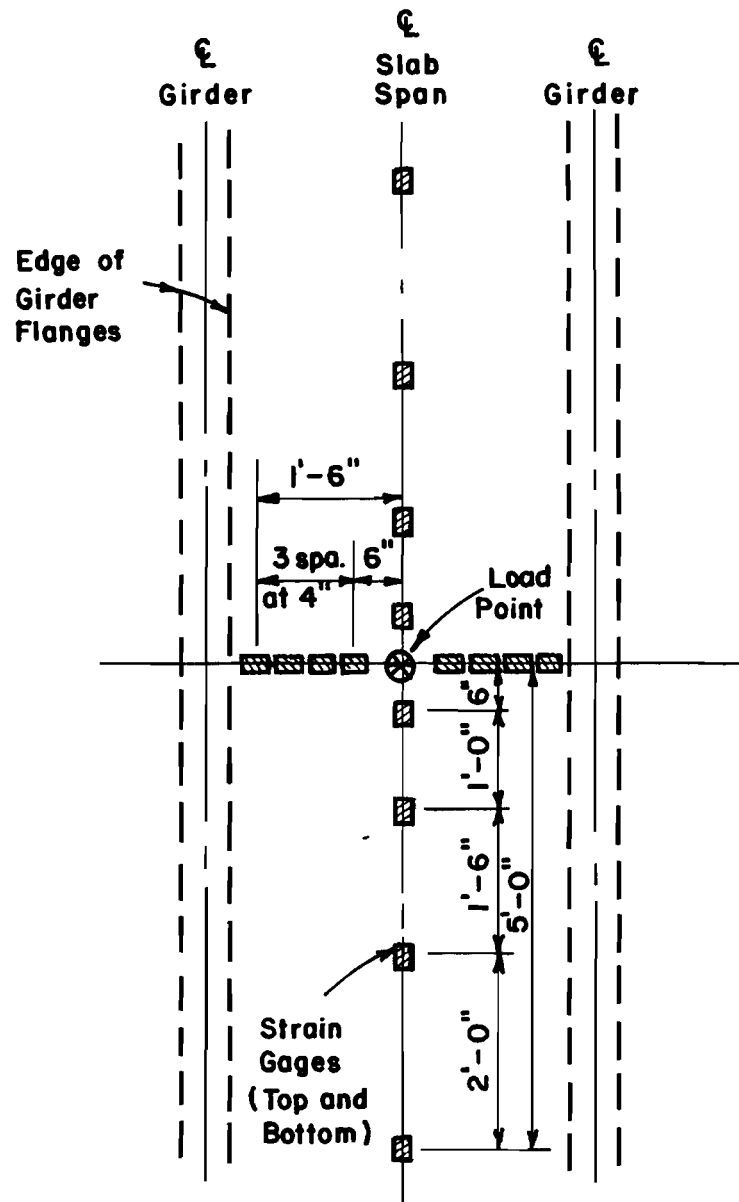


Fig. 5.5 Strain gage layout for interior positive moment test on straight-draped side of bridge

factored load tests, before the ultimate loadings were applied. A summary of the vertical load test sequence is given in Table 5.1.

At the beginning of each test, zero readings were taken for the potentiometers, dial gages and strain gages. The load cells measuring strand forces were only read at the start of the test. Predetermined load increments were then applied with deflection and strain measurements taken after each loading increment. For service and factored load tests, the load increments were one-fourth of the full 4.18 and 9.06 kip loads, respectively. In ultimate load tests, the loading sequence duplicated that of the factored load test up to factored load level. Load increments were then set at one service live load each (4.18 k) until the factored moment capacity of the adjacent girders or the limit of the loading system was reached. This peak load level was always at a point where the load-deflection curve indicated significant stiffness remained in the slab. All tests were terminated after the maximum load was achieved.

5.1.2 Test Results. Data gathered during the vertical load tests were primarily either vertical deflections of the bridge model slab and girders, or surface strains of the deck under a given load. This information was processed into the more useful form of slab deflections relative to the girders, stresses and curvatures of the bridge deck [63].

Instead of including the entire volume of data collected during the vertical load tests in this report, only a portion representative of the overall results will be presented. Complete vertical load test data may be found in Ref. 63.

5.1.3 Service Load Tests. Profiles of the relative bridge slab deflections in both the longitudinal and transverse directions for all the service load tests are shown in Figs. 5.6 through 5.11. Note that for the transverse slab profiles, relative deflection is by definition zero where the slab intersects the girder flanges.

In viewing the slab deflection profiles, the accuracy of the relative deflections must be considered. This is especially true in the service load tests where the magnitude of the deflections, only a few thousandths of an inch, approach the accuracy limitations of the instrumentation. Positive moment tests indicate a slight tendency for greater deflection with straight and draped strands than for straight strands only. Also, the slab deflected more in the area towards the midspan of the bridge than it did in the area towards the bridge supports. However, neither of these tendencies are apparent in the results from the negative moment tests as shown in Figs. 5.8 and 5.9. Another trend in the positive moment tests is that deflections for the interior load locations were slightly larger than those for the exterior load locations for both strand arrangements. As expected for the exterior negative moment tests, deflections in the outside slab

TABLE 5.1 Vertical Load Test Sequence

Test No.	Strand Pattern	Load Pattern	Load Level
1	straight	M + ext.	service
2	"	M + int.	"
3	"	M + min.	"
4	"	M - int.	"
5	"	M - ext.	"
6	"	M - ext.	factored
7	"	M - int.	"
8	"	M + min.	"
9	"	M + int.	"
10	"	M + ext.	"
11	"	M + ext.	ultimate
12	"	M + int.	"
13	"	M + min.	"
14	"	M - int.	"
15	"	M - ext.	"
16	straight and draped	M + ext.	service
17	"	M + int.	"
18	"	M + min.	"
19	"	M - int.	"
20	"	M - ext.	"
21	"	M - ext.	factored
22	"	M - int.	"
23	"	M + min.	"
24	"	M + int.	"
25	"	M + ext.	"
26	"	M + ext.	ultimate
27	"	M + int.	"
28	"	M + min.	"
29	"	M - int.	"
30	"	M - ext.	"

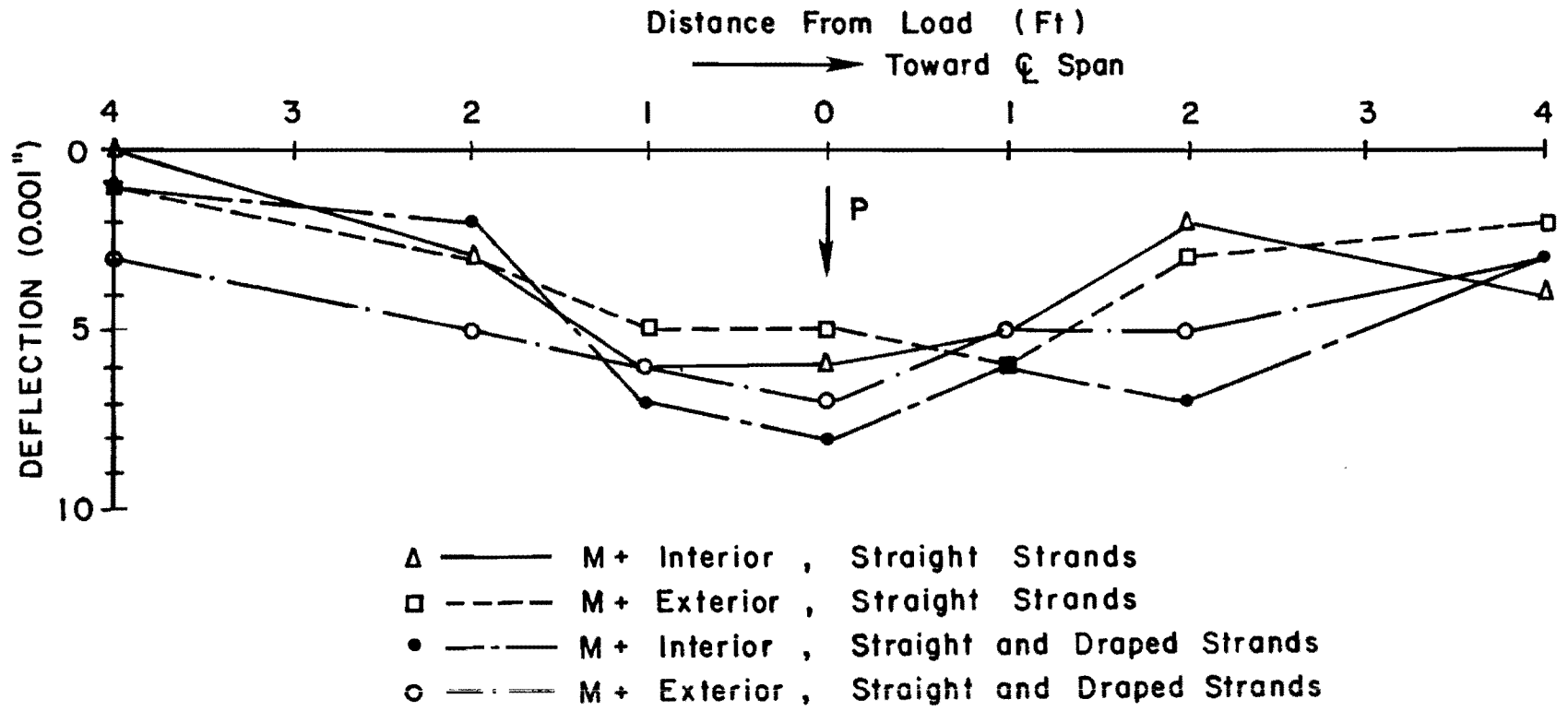


Fig. 5.6 Longitudinal relative slab deflection profiles for positive moment service load tests

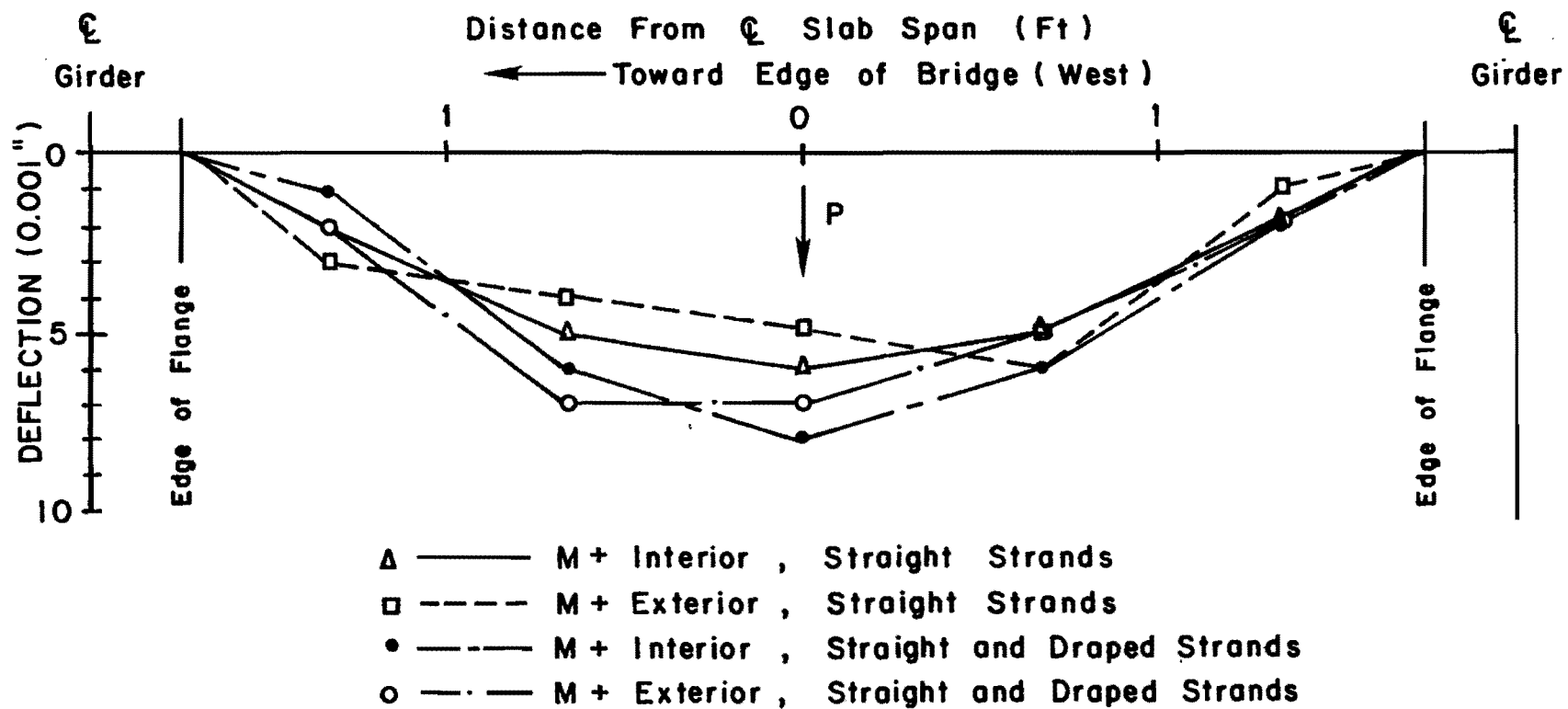


Fig. 5.7 Transverse relative slab deflection profiles for positive moment service load tests

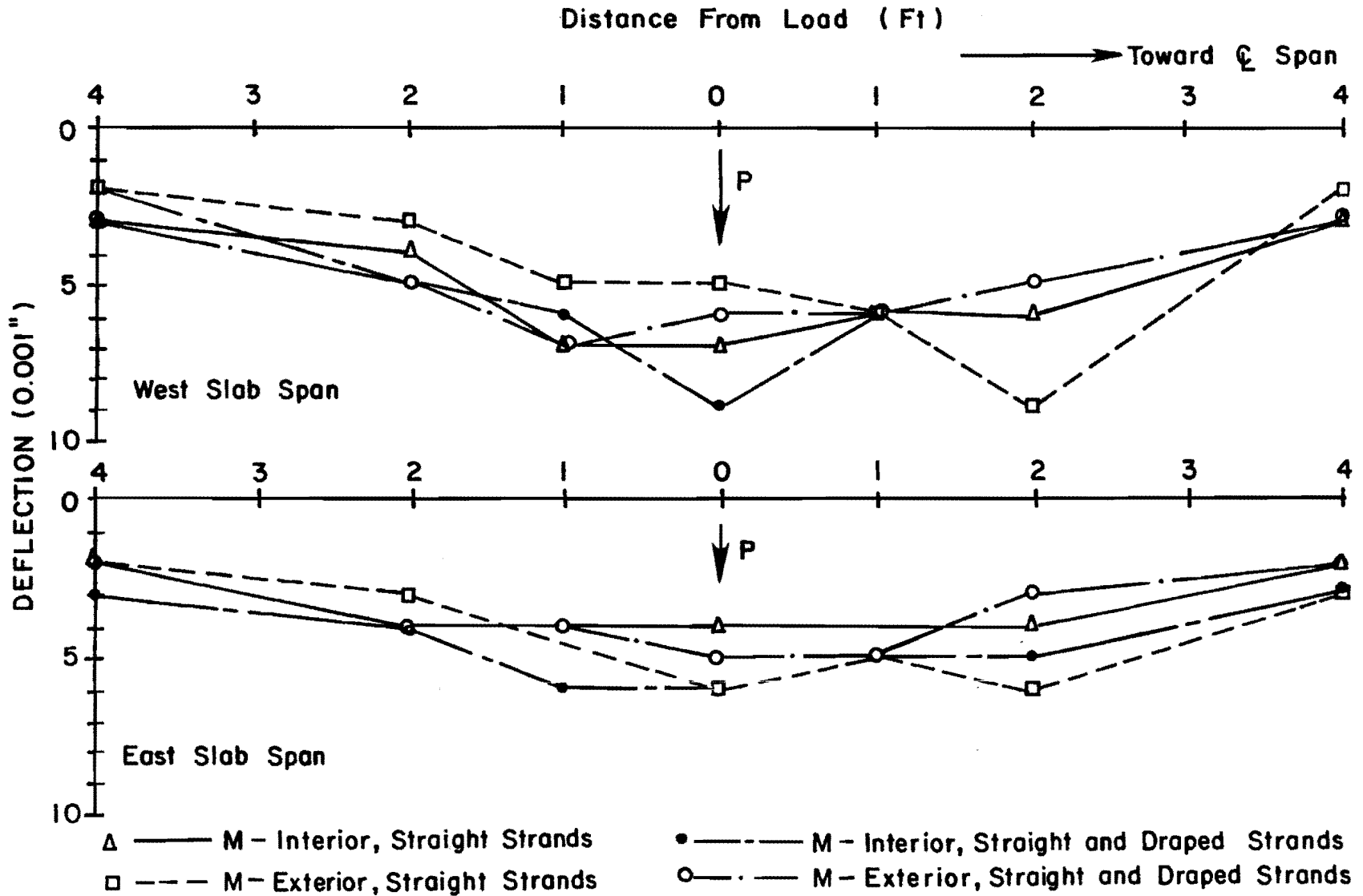


Fig. 5.8 Longitudinal relative slab deflection profiles for negative moment service load tests

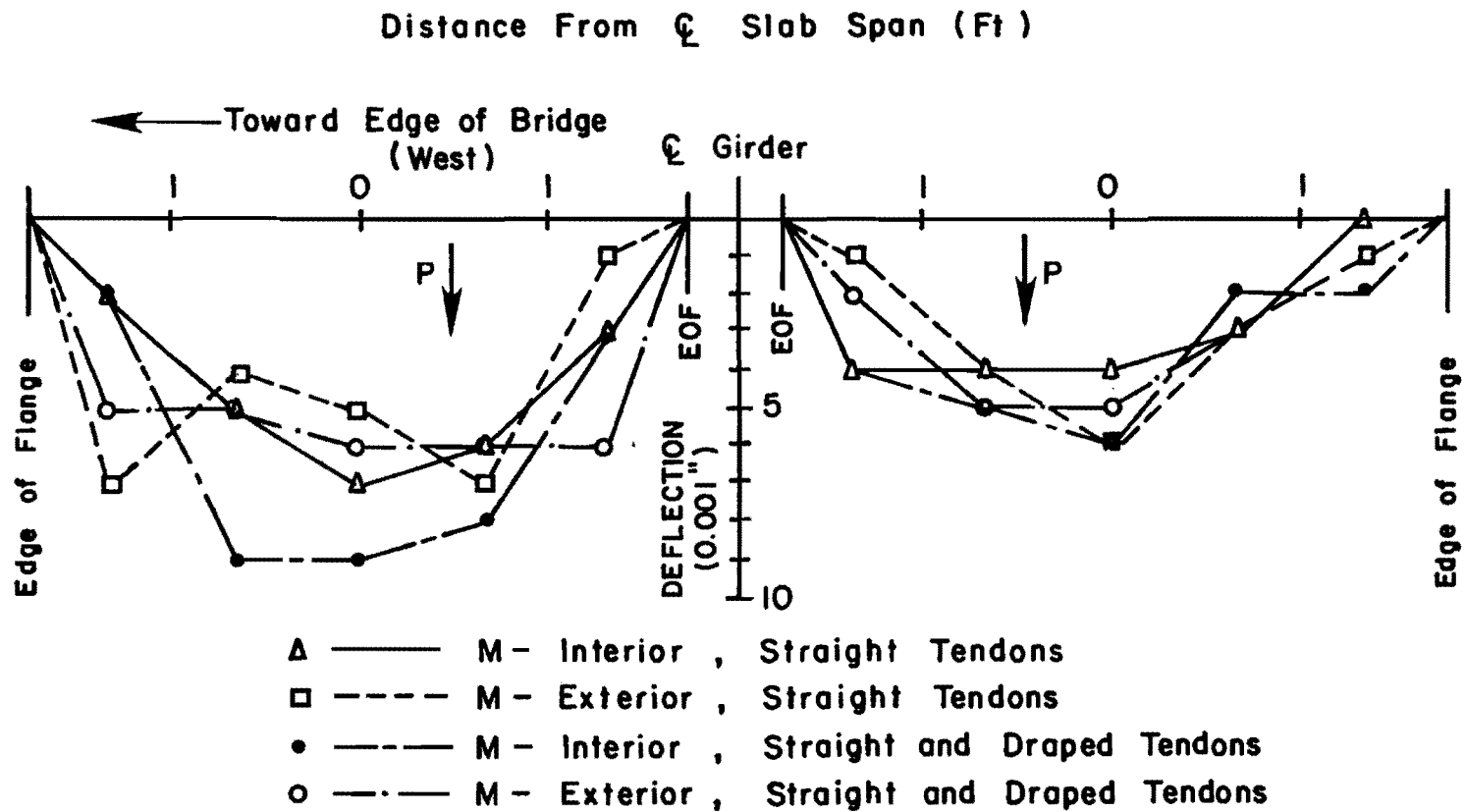


Fig. 5.9 Transverse relative slab deflection profiles for negative moment service load tests

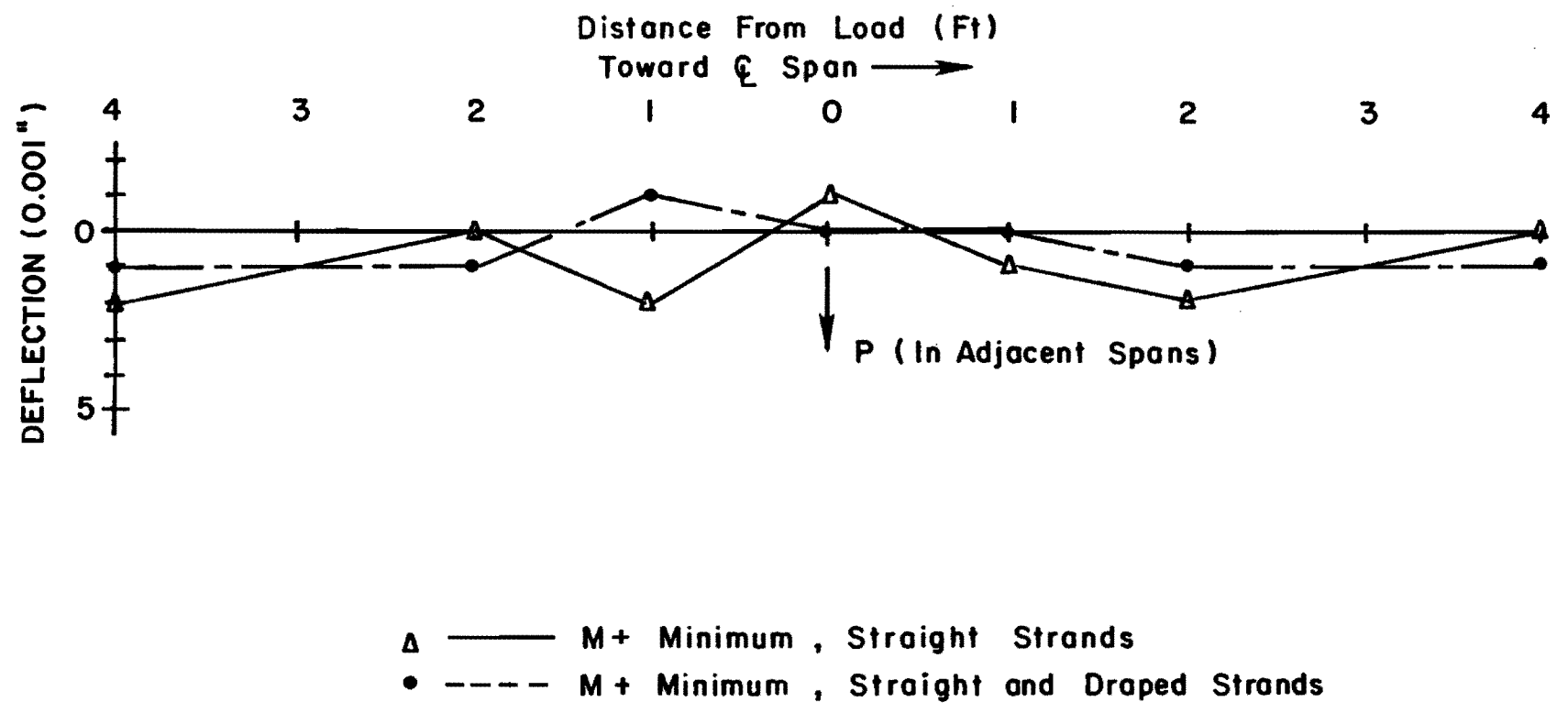


Fig. 5.10 Longitudinal relative slab deflection profiles for minimum positive moment service load tests

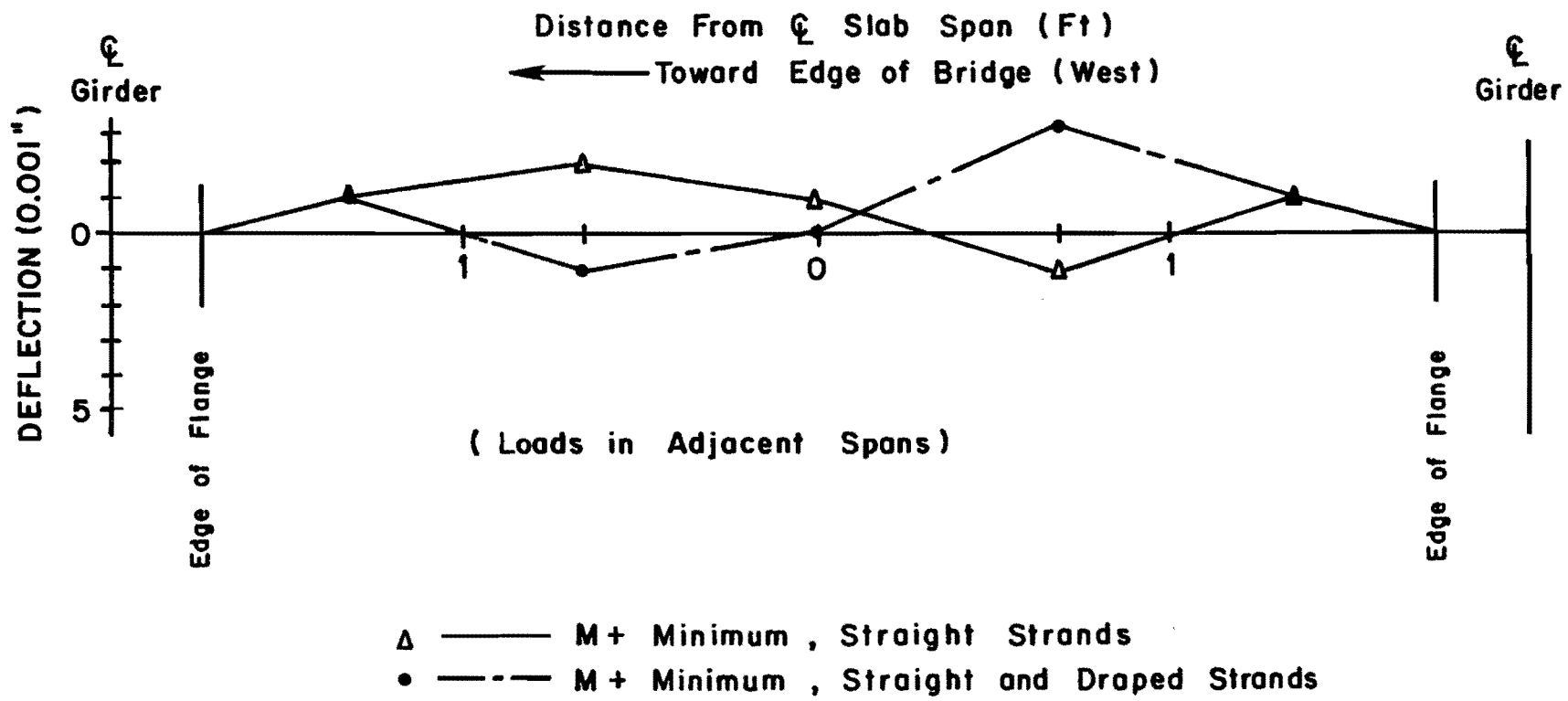


Fig. 5.11 Transverse relative slab deflection profiles for minimum positive moment service load tests

span were somewhat larger than those in the interior span. Surprisingly, though, the west span of the slab in the interior negative moment tests experienced significantly greater deflection than the east slab span. Profiles for the minimum positive moment loading shown in Figs. 5.10 and 5.11 indicate a very slight uplift tendency adjacent to the load and a tendency for downward deflection in areas either direction along the span from the load. In both the negative moment and the minimum positive moment tests, there was no observable difference in the behavior of the straight strands versus the straight and draped strands.

Again, it should be pointed out that because of the magnitude of the relative deflections and the limited sensitivity of the instrumentation, trends observed at the service load level may not be statistically significant. It is significant, however, that these deflections are of such small magnitude. The maximum deflection of 9/1000 of an inch is equivalent to slightly more than 1/64 of an inch in the full scale bridge, or a transverse span to deflection ratio of almost 4600 under service loads.

Stresses determined from measured strains on the surfaces of the bridge deck due only to service live load ranged from 104 psi tension to 345 psi compression for the top surface and from 324 psi tension to 78 psi compression for the bottom of the slab. Figure 5.12 shows slab curvature in the longitudinal direction as a function of longitudinal distance from the load and curvature in the transverse direction as a function of transverse distance from the load. Note that the curvature in the longitudinal direction is greater toward the midspan of the bridge than in the slab nearer the abutments. This correlates well with the earlier observation of deflections in the positive moment tests.

There was no visible cracking in the bridge deck during any of the service level load tests. Examination of load-deflection curves presented later on confirms that the slab indeed remains uncracked past service load levels.

5.1.4 Factored Load Tests. Relative slab deflection profiles similar to those presented earlier are shown for the factored load tests in Figs. 5.13 through 5.18.

As in the service load tests, there was a tendency for greater deflections in the portions of the slab towards the midspan of the bridge than in the area nearer the abutments, especially in the positive moment tests. Unlike the service load tests, however, there was no clear difference in deflections between the straight strand and the straight and draped strand positive moment tests.

In the negative moment tests, the trend observed earlier for the west slab span to display significantly larger deflections than the

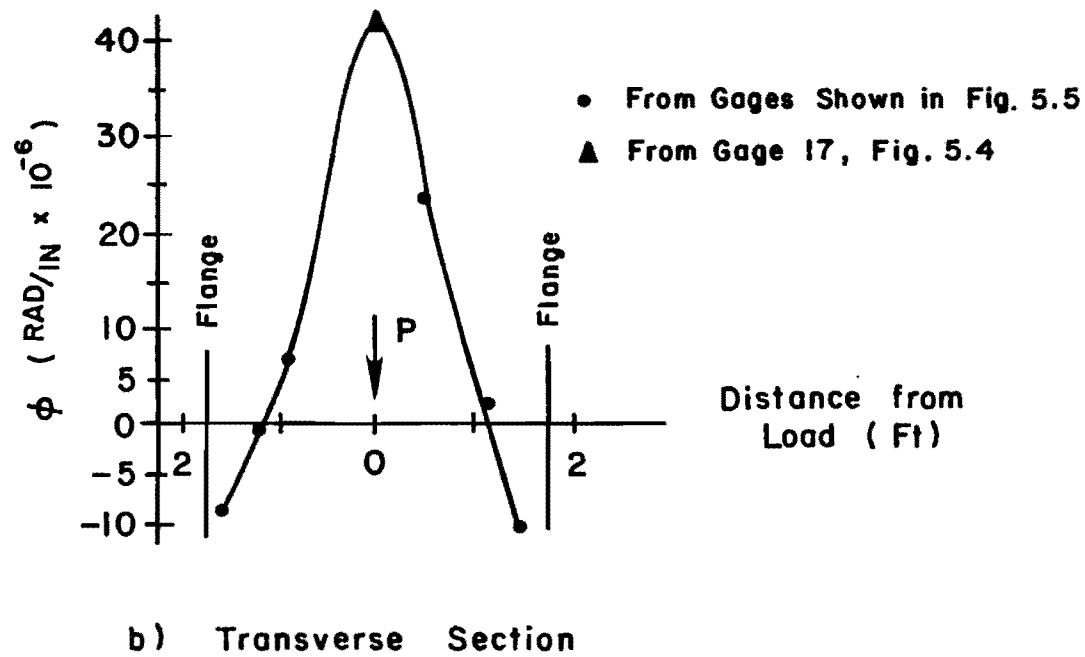
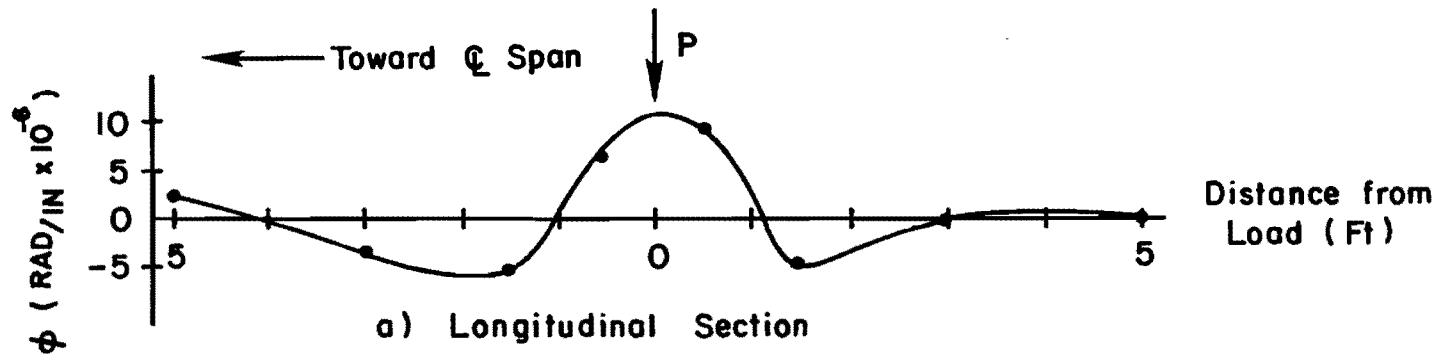


Fig. 5.12 Slab curvature profiles for positive moment service load test on straight and draped tendon section

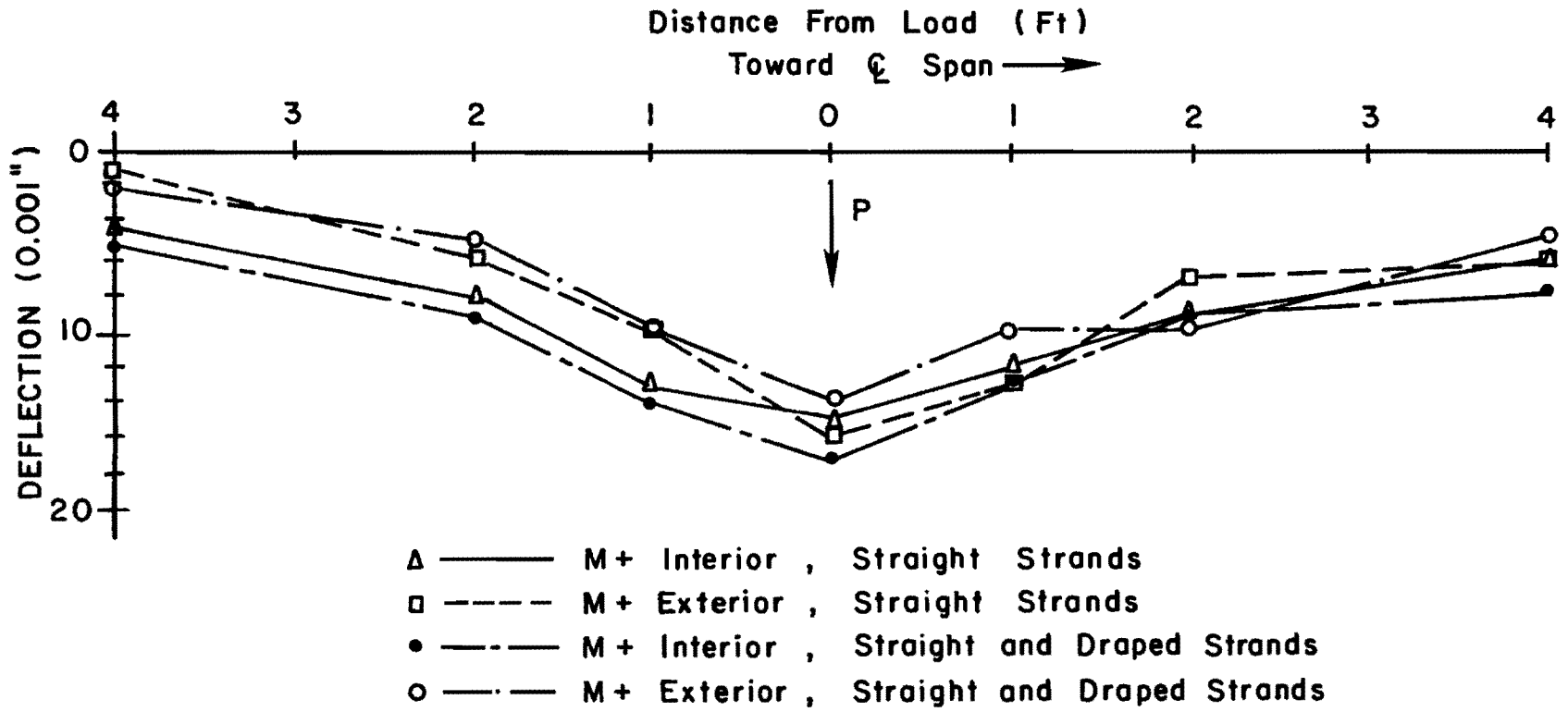


Fig. 5.13 Longitudinal relative slab deflection profiles for positive moment factored load tests

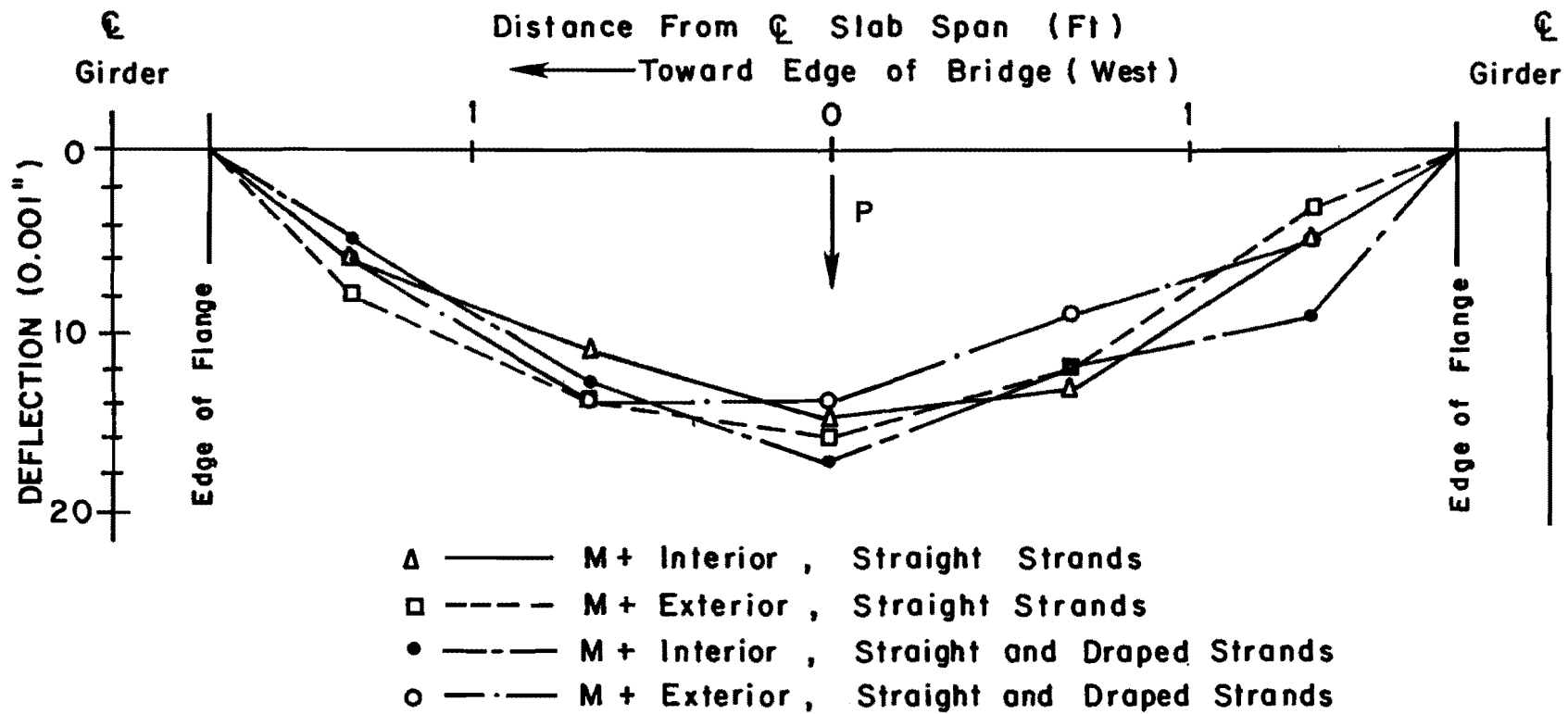


Fig. 5.14 Transverse relative slab deflection profiles for positive moment factored load tests

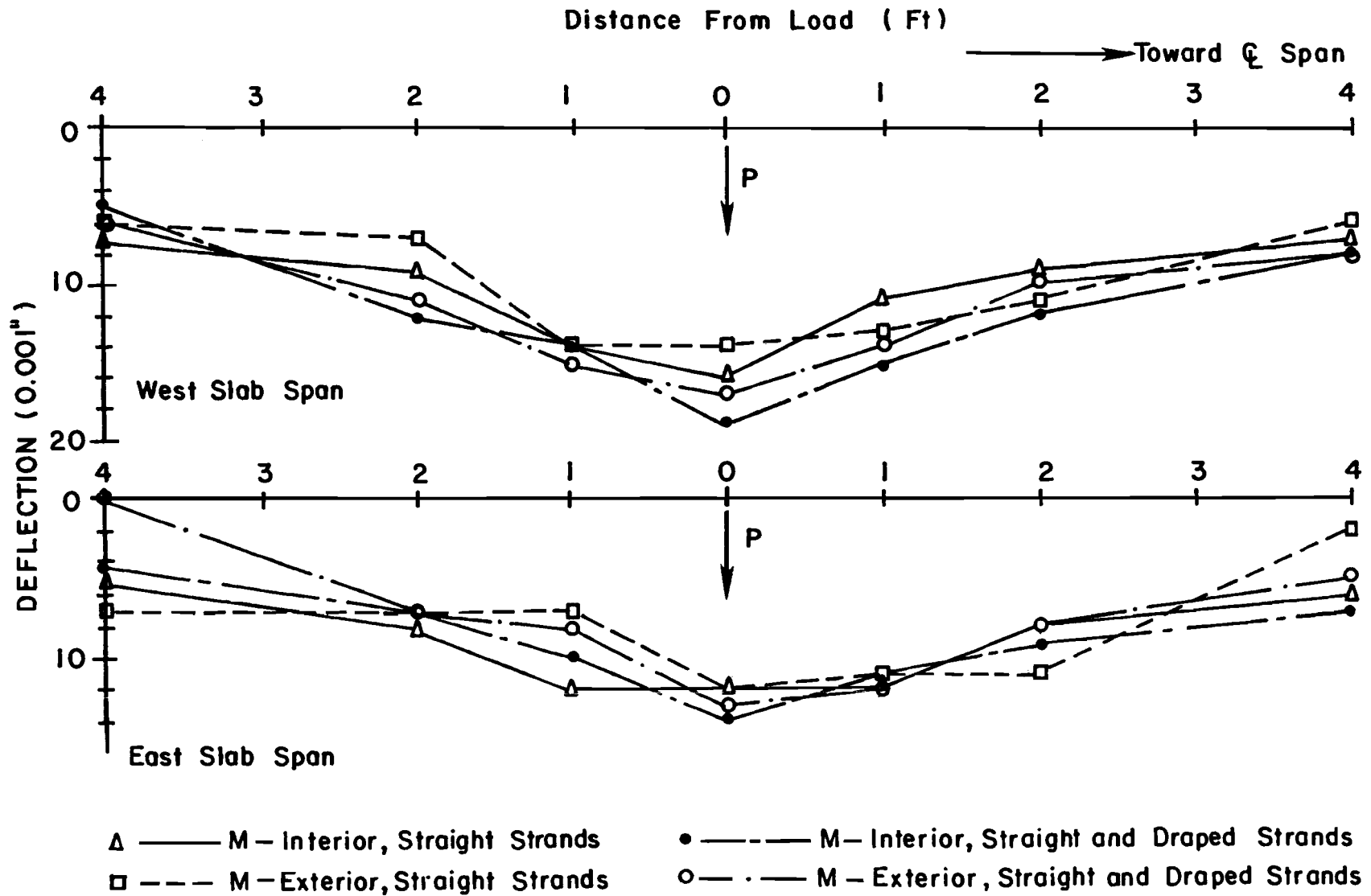


Fig. 5.15 Longitudinal relative slab deflection profiles for negative moment factored load tests

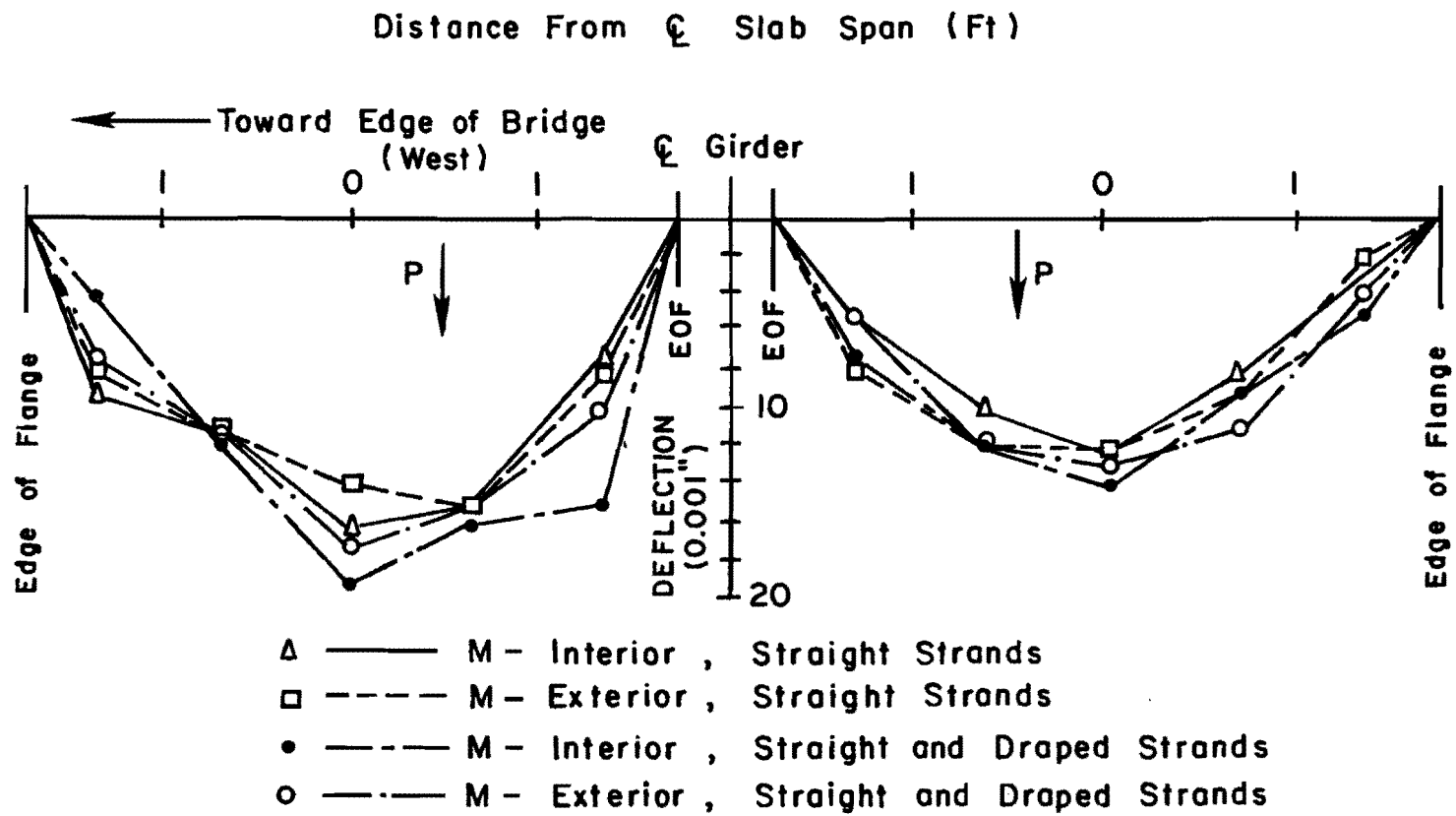


Fig. 5.16 Transverse relative slab deflection profiles for negative moment factored load tests

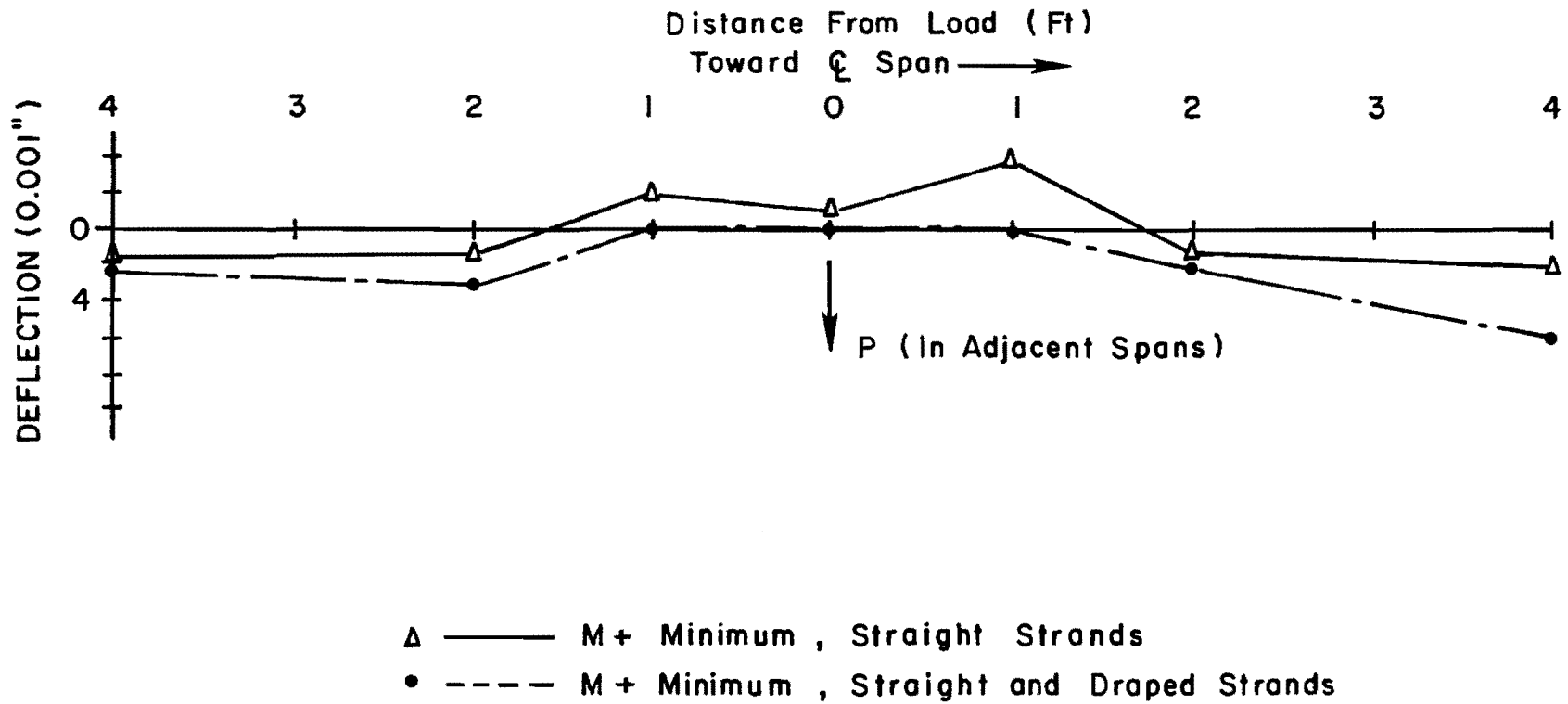


Fig. 5.17 Longitudinal relative slab deflection profiles for minimum positive moment factored load tests

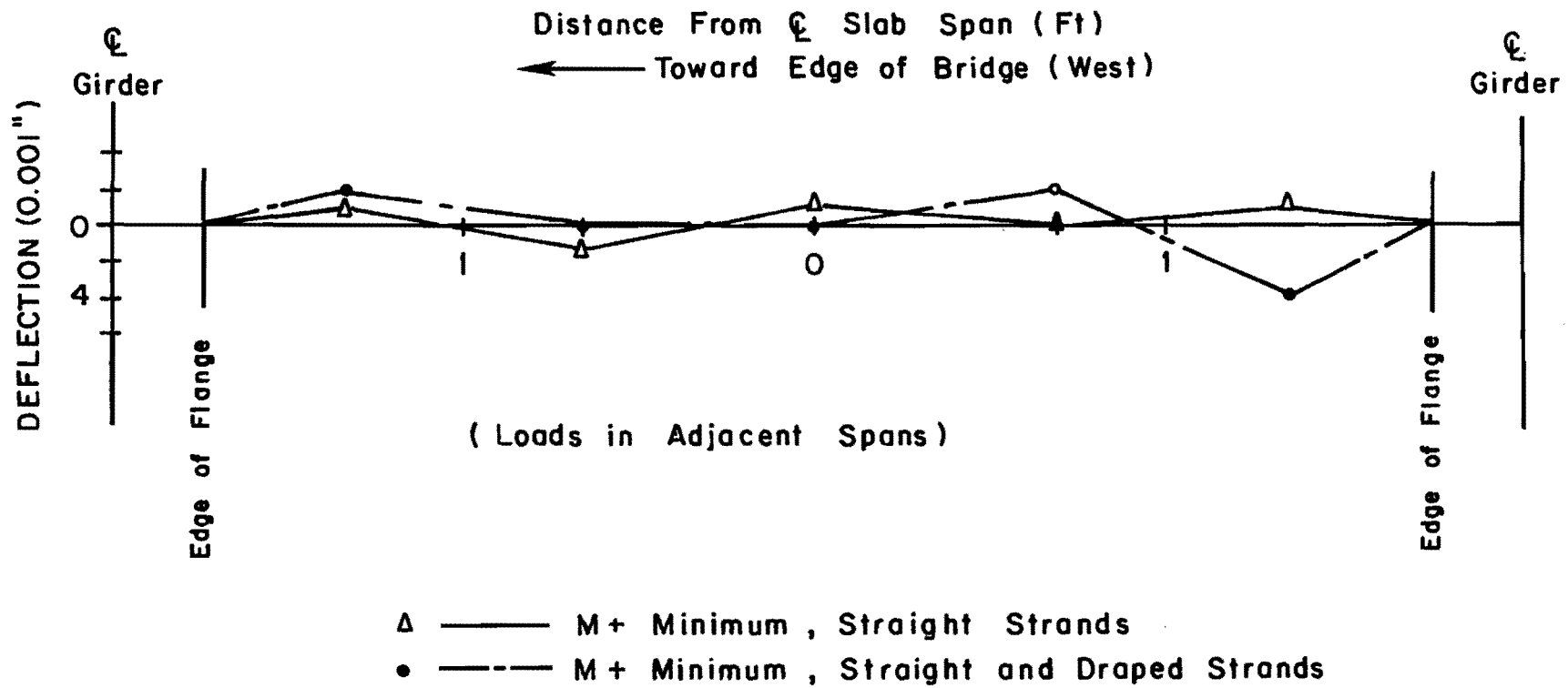


Fig. 5.18 Transverse relative slab deflection profiles for minimum positive moment factored load tests

adjacent loaded span was again very prominent. Also, at factored loads there was a tendency for the deck with straight and draped strands to deflect slightly more than the deck with straight strands only. This characteristic was not evident in the service load tests.

Only a small amount of uplift was observed in the minimum positive moment tests. The longitudinal slab profile shown in Fig. 5.17 indicates more uplift for the straight strands than for the straight and draped strands, but the transverse slab profile shown in Fig. 5.18 tends to contradict this.

Overall, there was no consistent difference found in the deflection characteristics between the interior and exterior slab spans, contrary to what might be expected. None of the factored load tests results in appreciable deflections. The maximum deflection of 0.019 in. corresponds to a live load transverse span to deflection ratio of 2500 at factored load levels.

Surface strains indicate slab surface stress due to factored live load between 246 psi tension and 747 psi compression on top and between 704 psi tension and 203 psi compression on the bottom. Slab curvatures for the positive moment test for straight and draped strands under factored load are presented in Fig. 5.19. Again, it is apparent that the curvature in the longitudinal direction is slightly greater towards the midspan of the bridge than towards the supports.

Visible cracking of the bridge deck did not occur in any of the factored load tests. There is some evidence, however, that small amounts of localized cracking did occur at factored loads: slab strains adjacent to the load increased in greater proportion from service to factored loads than did the magnitude of the load; the gradient of transverse slab curvature is very high near the load; and the load-deflection curves in Figs. 5.26 through 5.31 show a slight nonlinearity near factored load.

5.1.5 Ultimate Load Tests. Relative bridge slab deflection profiles for all the ultimate load tests are shown in Figs. 5.20 through 5.25. Two factors should be remembered when interpreting the data from these tests. First, absolute ultimate load (the load at which further deflections of the structure are not accompanied by an increase in load) was never reached under any of the test conditions. The experiments were terminated when either the calculated ultimate capacity of the girders was reached (in order to preclude a girder failure), or the loading system approached its maximum limit. Second, the maximum load applied to each test location varied slightly, as indicated on the figures. The greatest difference between load levels for a given type of loading was 6.4% for the positive moment tests.

The slab profiles for the ultimate tests again show a tendency for higher deflections in that portion of the slab towards the midspan

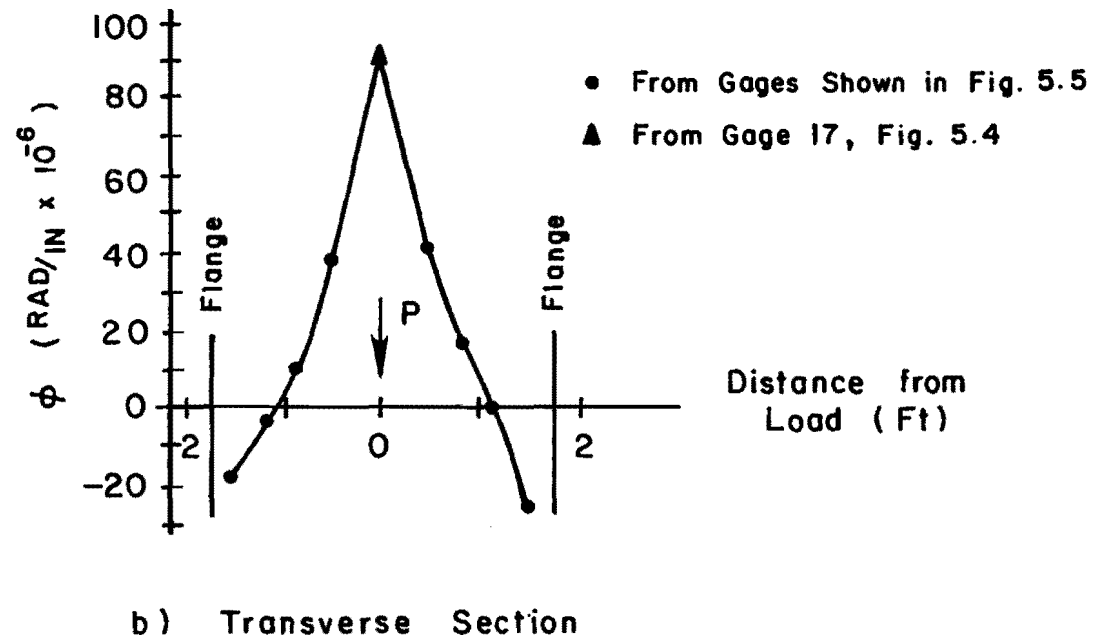
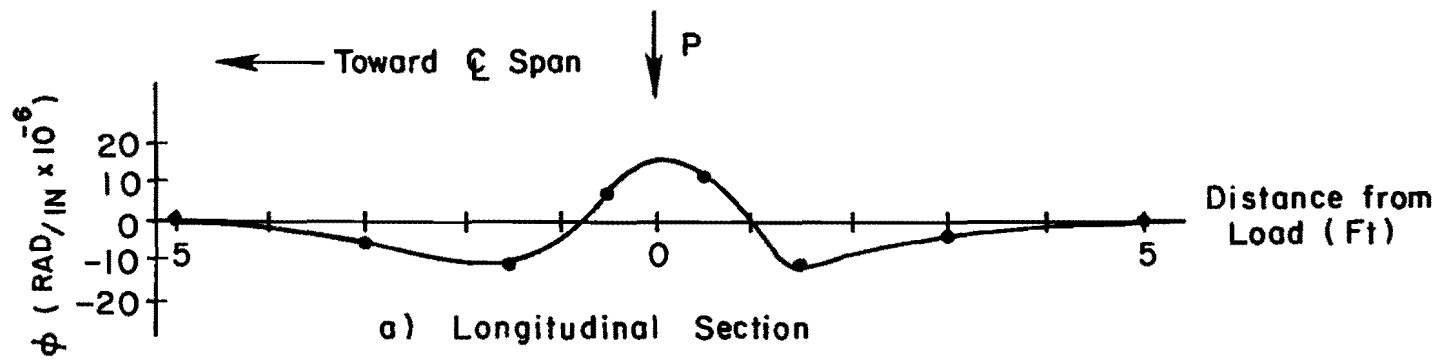
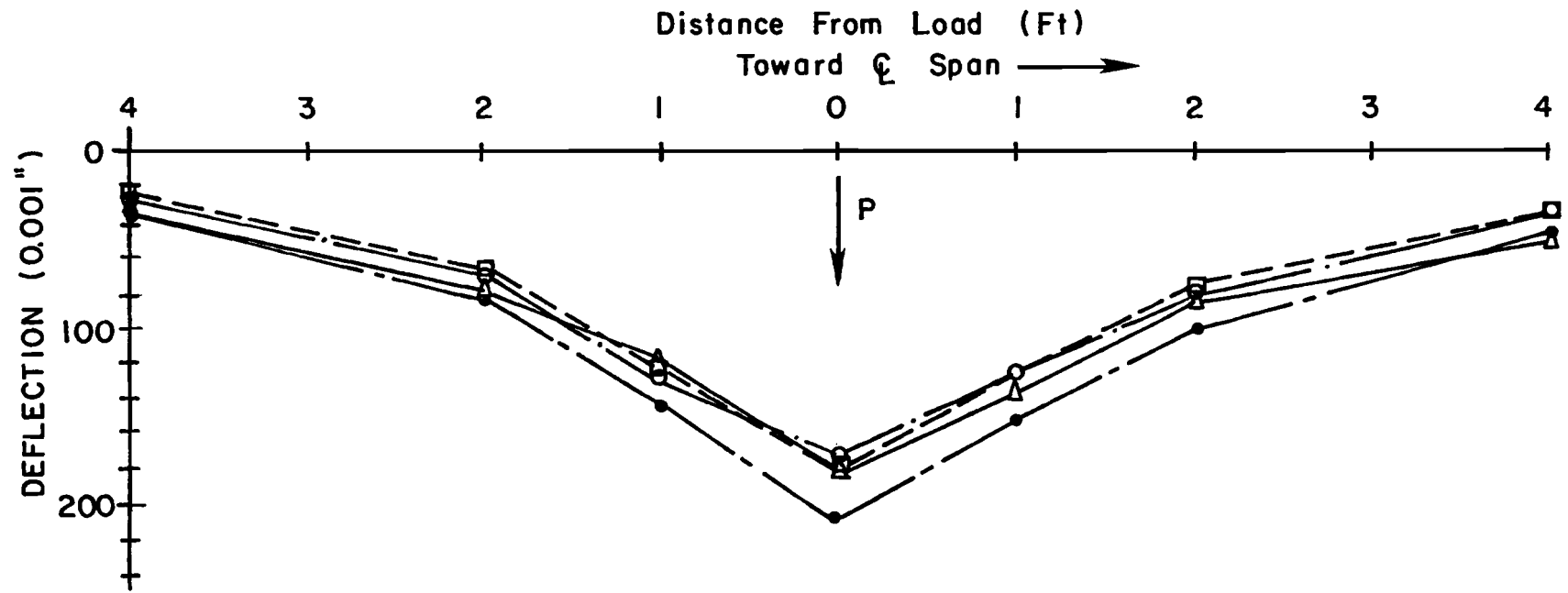


Fig. 5.19 Slab curvature profiles for positive moment factored load test on straight and draped tendon section



- Δ ——— M+ Interior , Straight Strands (50.18 K)
- - - - - M+ Exterior , Straight Strands (48.00 K)
- - - - - M+ Interior , Straight and Draped Strands (51.07 K)
- - · - · M+ Exterior , Straight and Draped Strands (50.46 K)

Fig. 5.20 Longitudinal relative slab deflection profiles for positive moment ultimate load tests

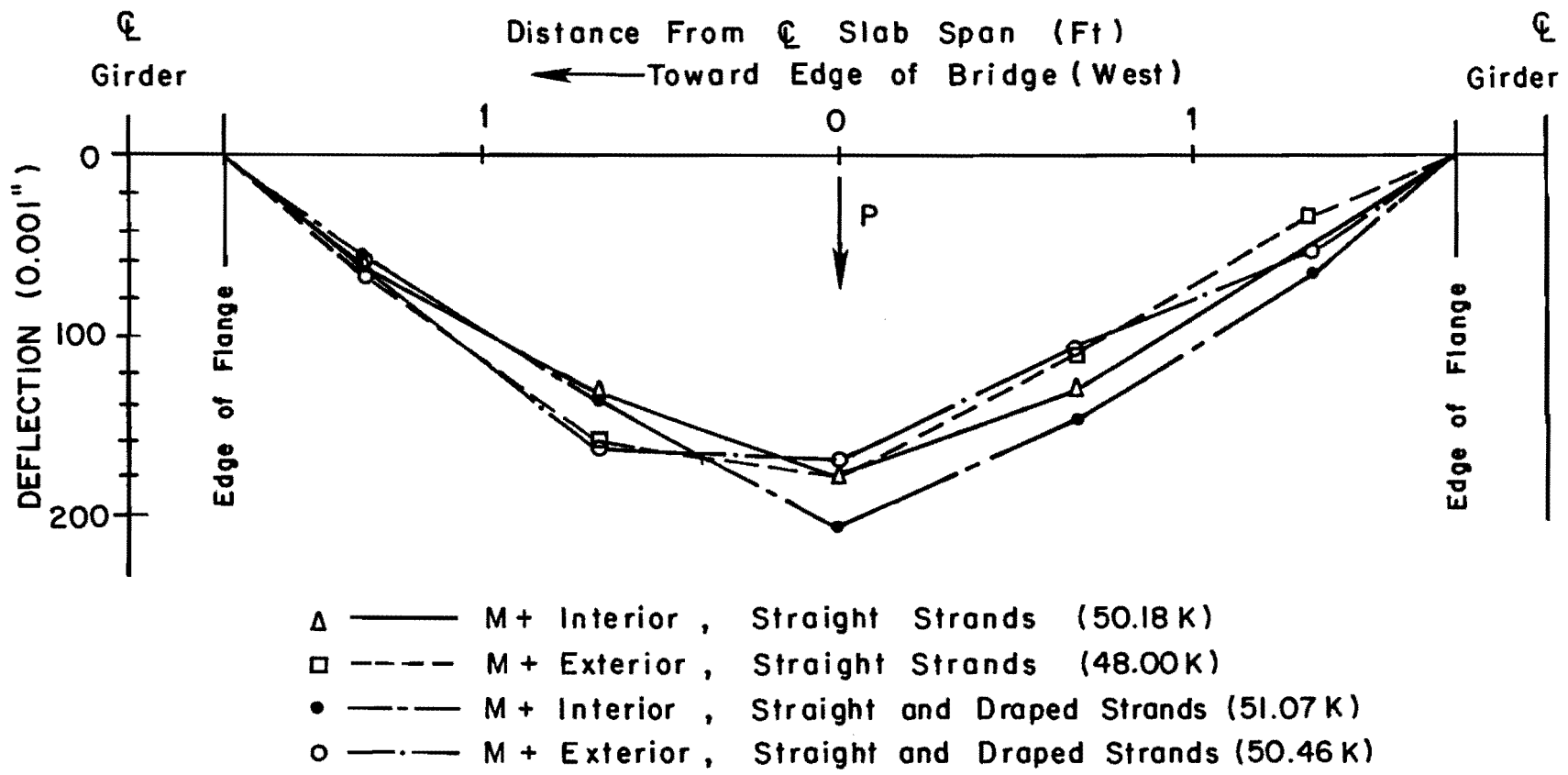


Fig. 5.21 Transverse relative slab deflection profiles for positive moment factored load tests

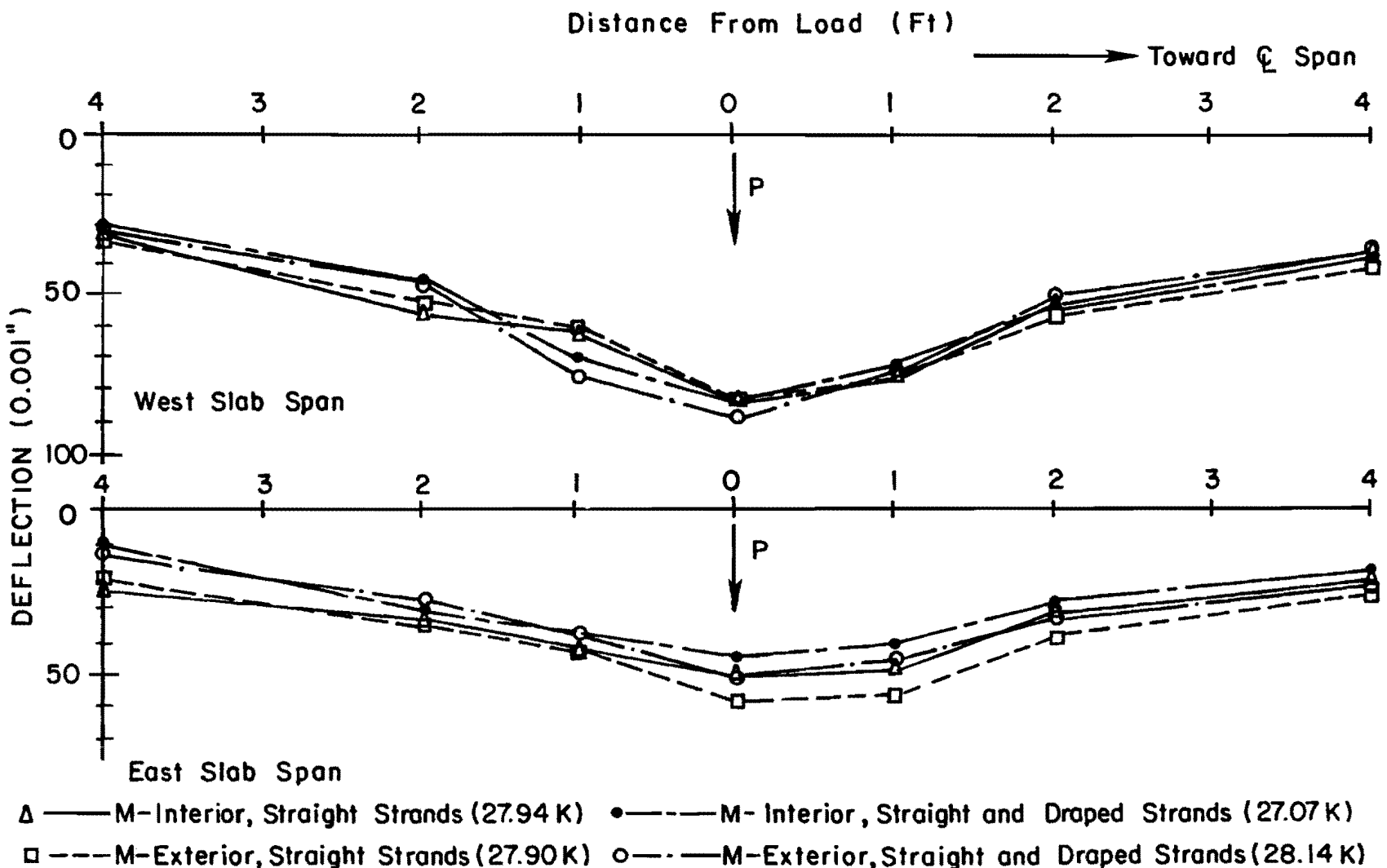


Fig. 5.22 Longitudinal relative slab deflection profiles for negative moment ultimate load tests

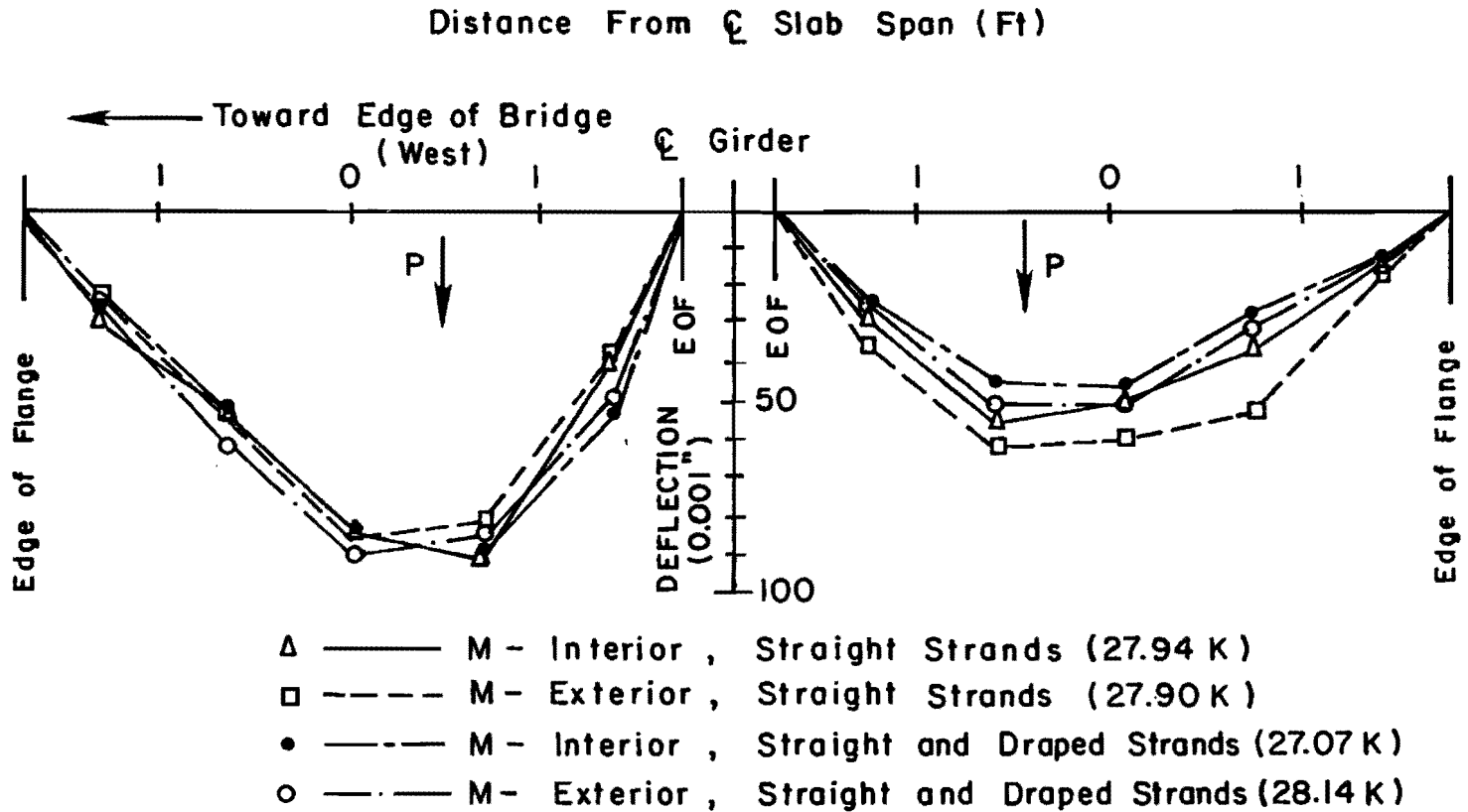


Fig. 5.23 Transverse relative slab deflection profiles for negative moment ultimate load tests

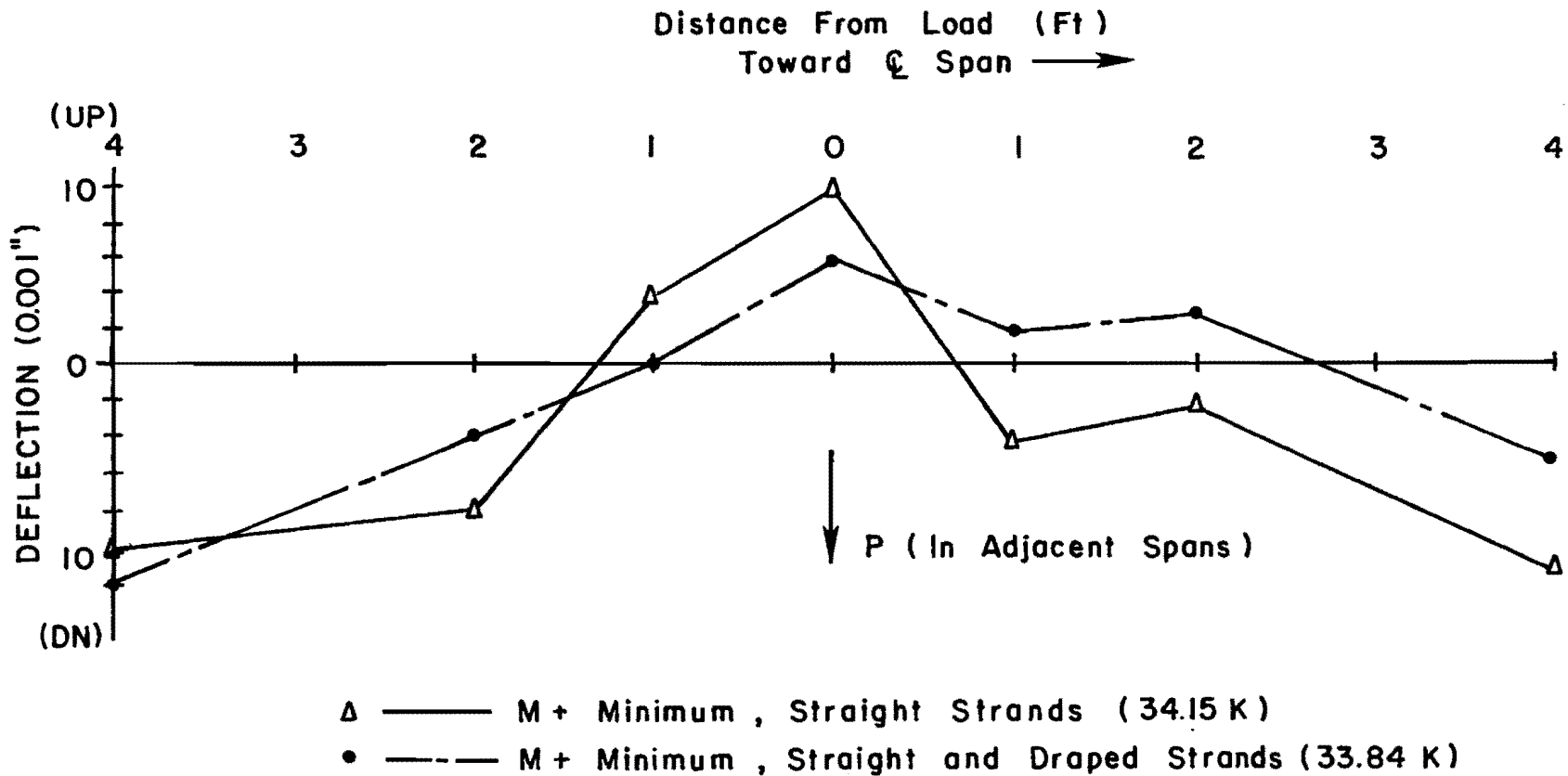


Fig. 5.24 Longitudinal relative slab deflection profiles for minimum positive moment ultimate load tests

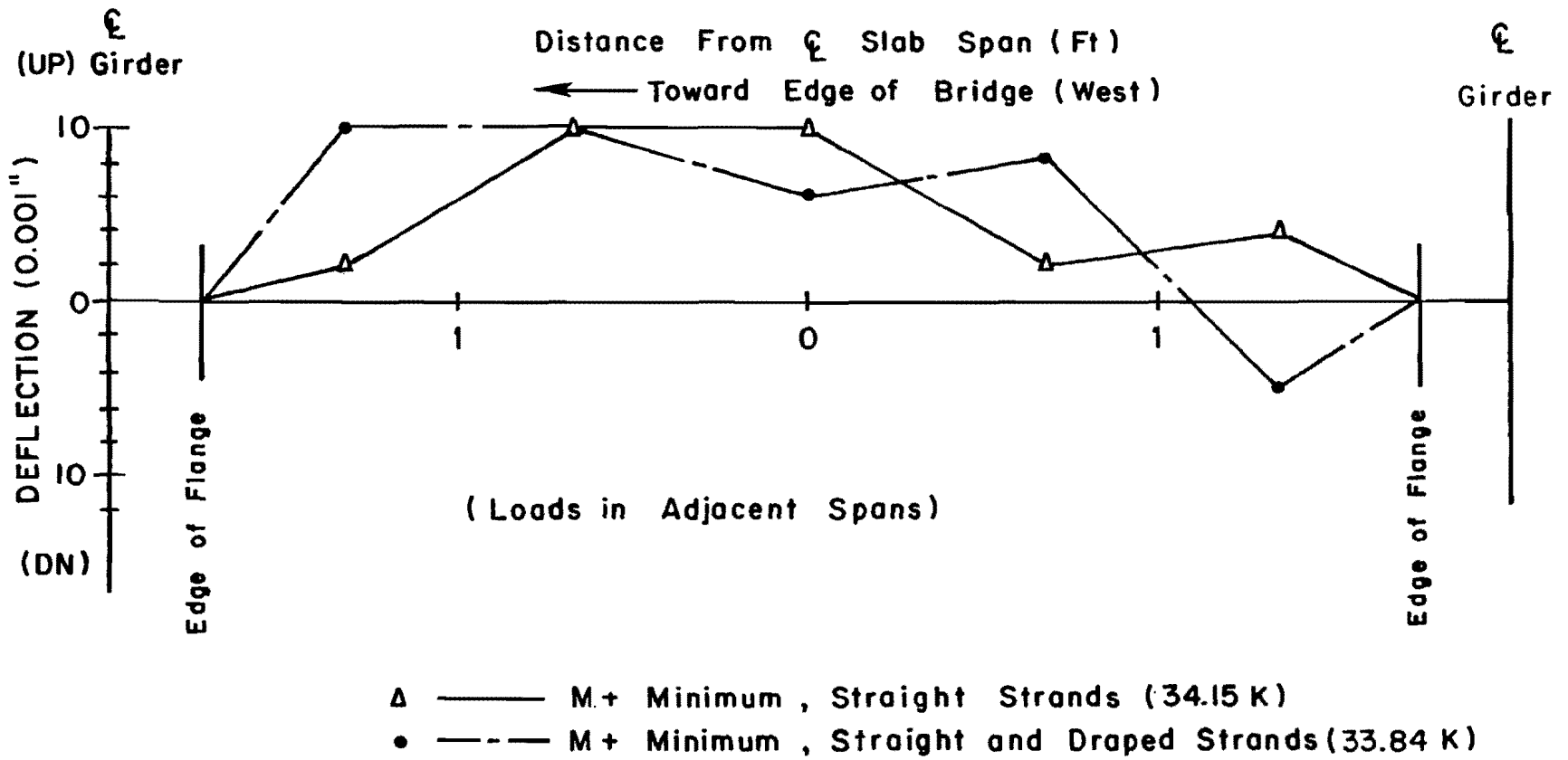


Fig. 5.25 Transverse relative slab deflection profiles for minimum positive moment ultimate load tests

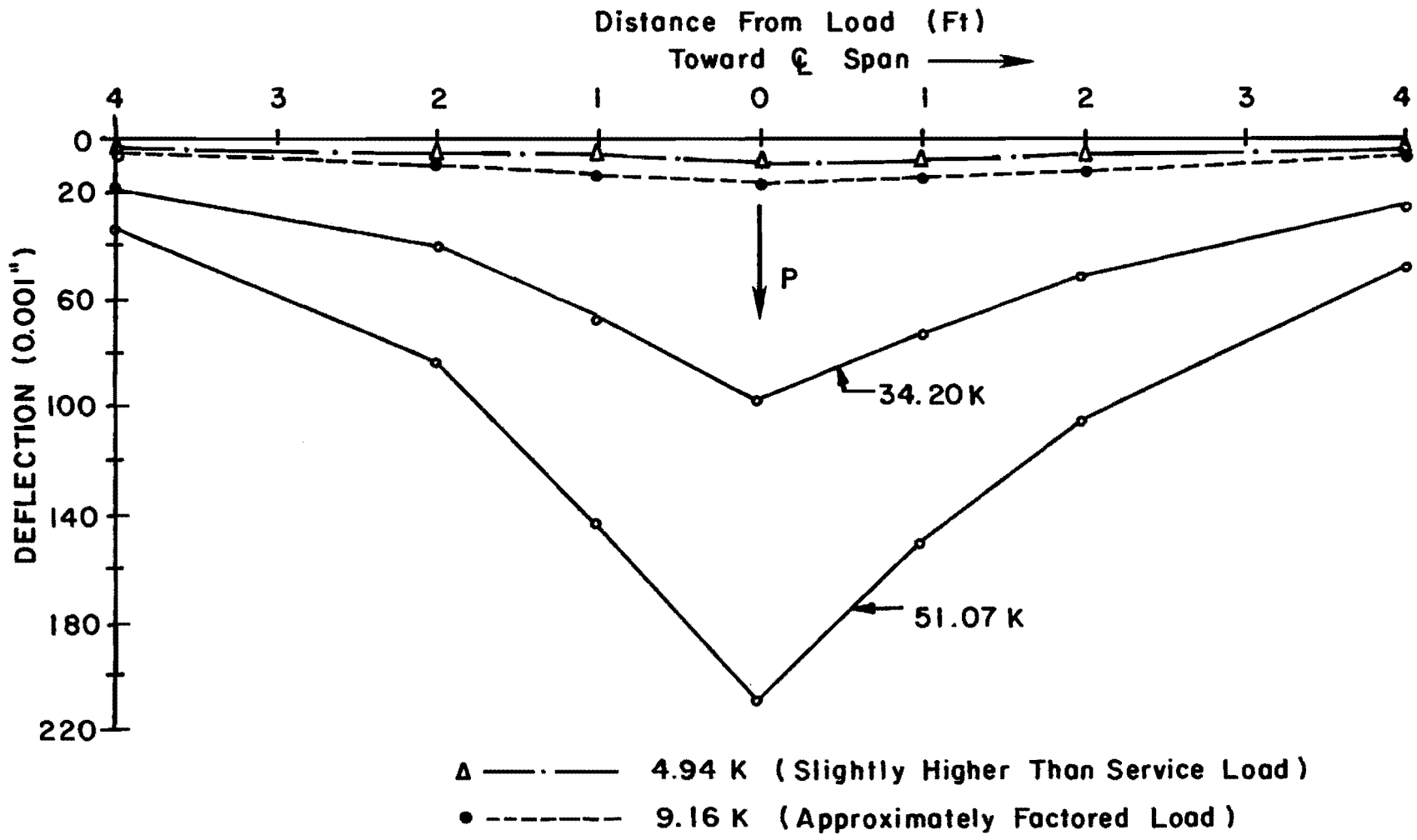


Fig. 5.26 Longitudinal relative slab deflection profiles for various load levels of interior positive moment ultimate load test with straight and draped strands

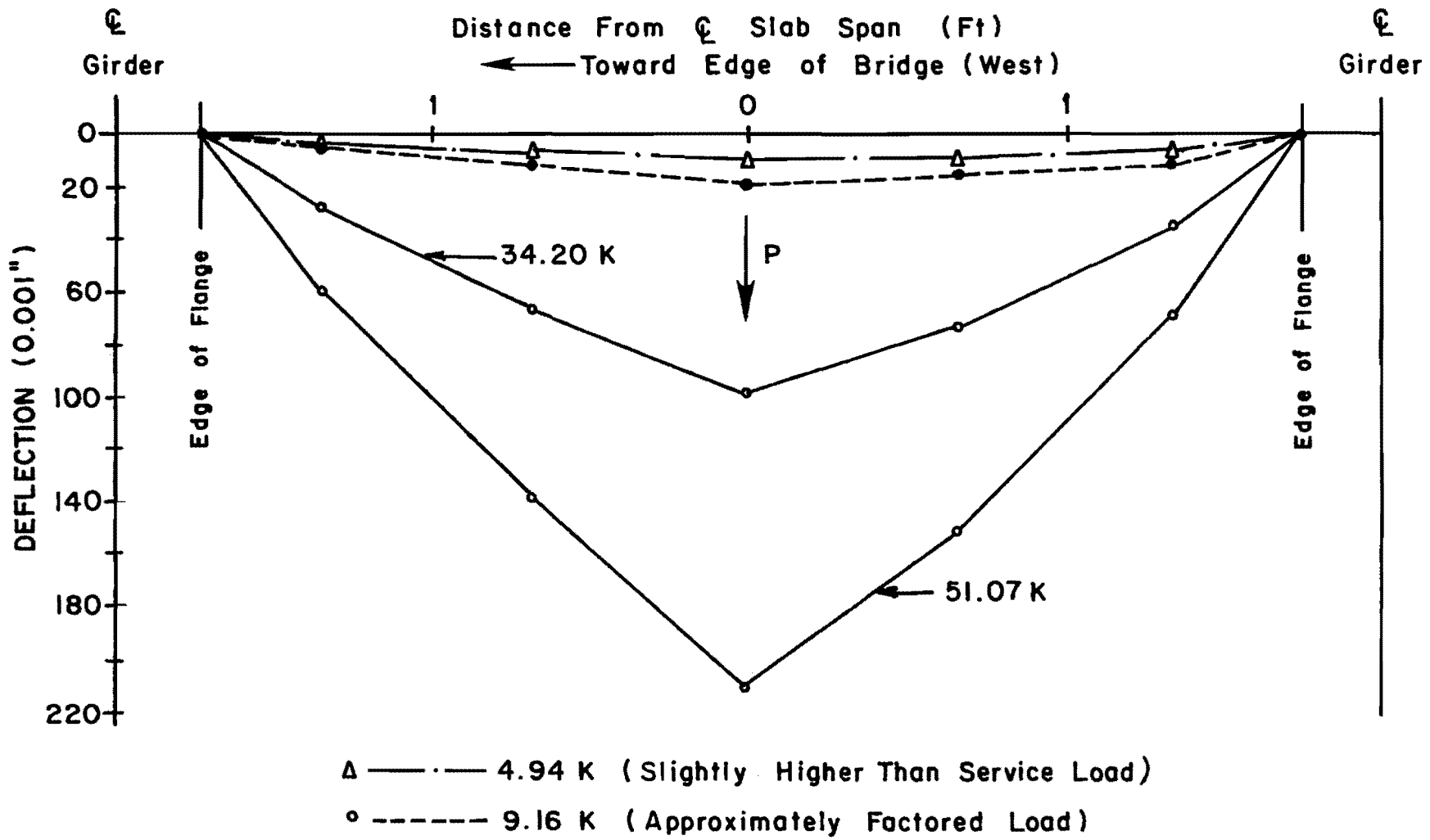
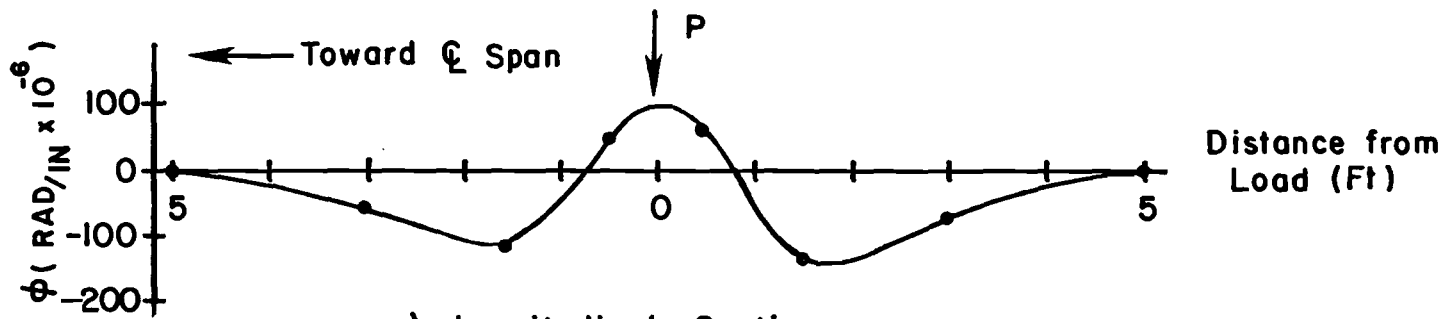
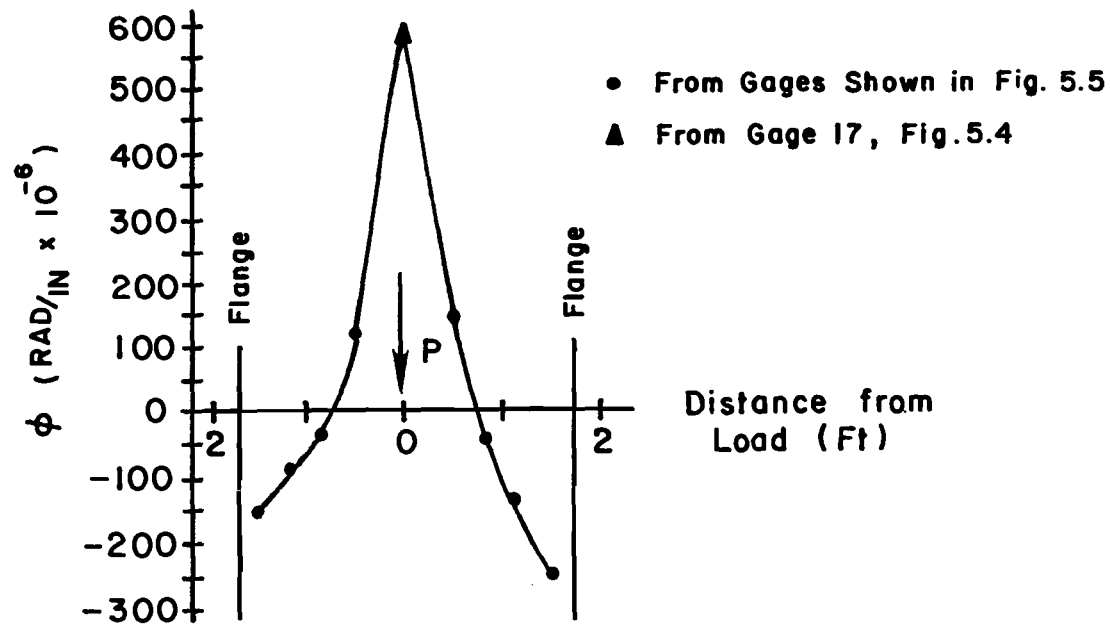


Fig. 5.27 Transverse relative slab deflection profiles for various load levels of interior positive moment ultimate load test with straight and draped strands



a) Longitudinal Section



b) Transverse Section

Fig. 5.28 Slab curvature profiles for positive moment ultimate load test on straight and draped tendon section

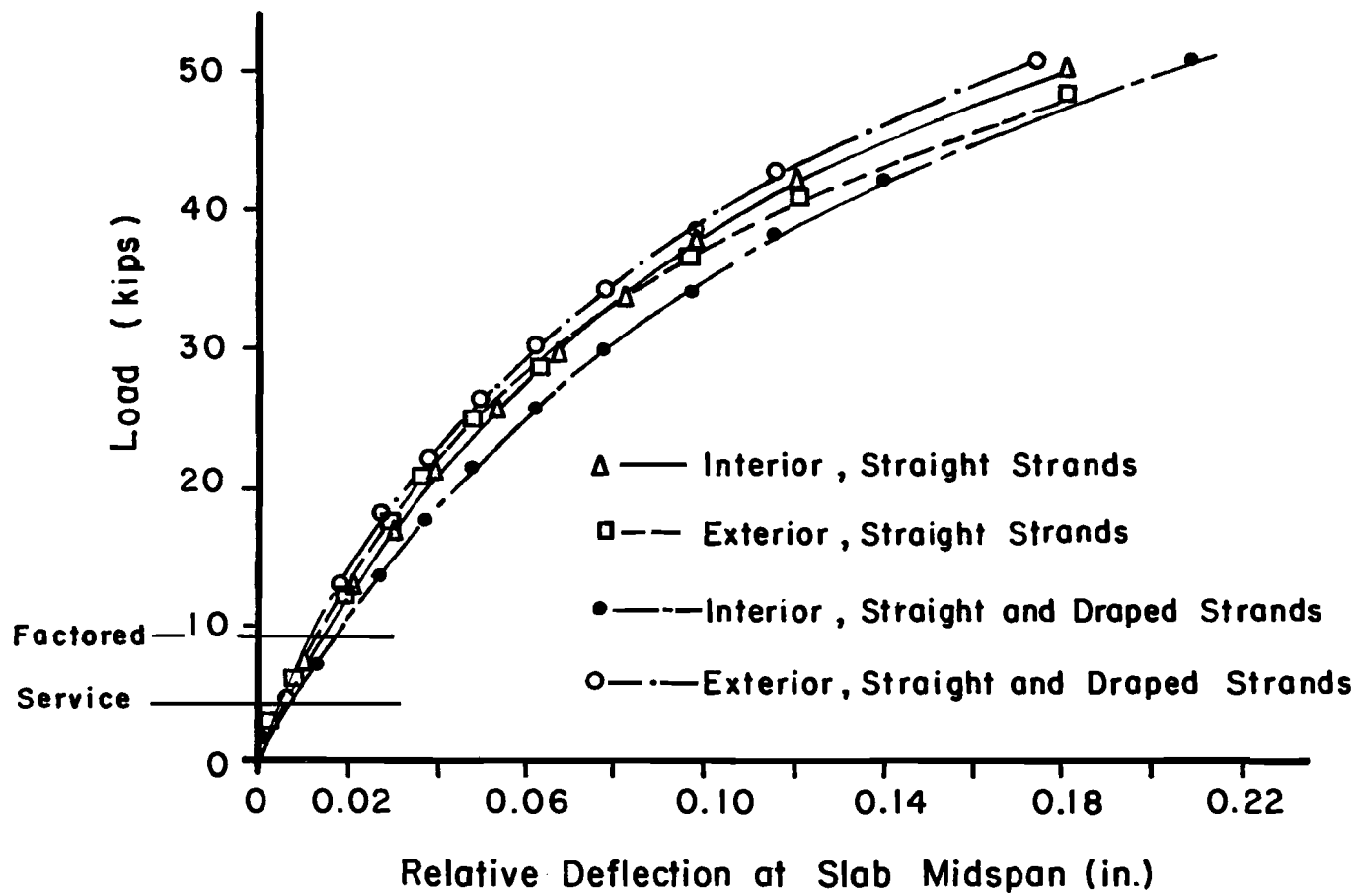


Fig. 5.29 Load-deflection curves for ultimate positive moment tests

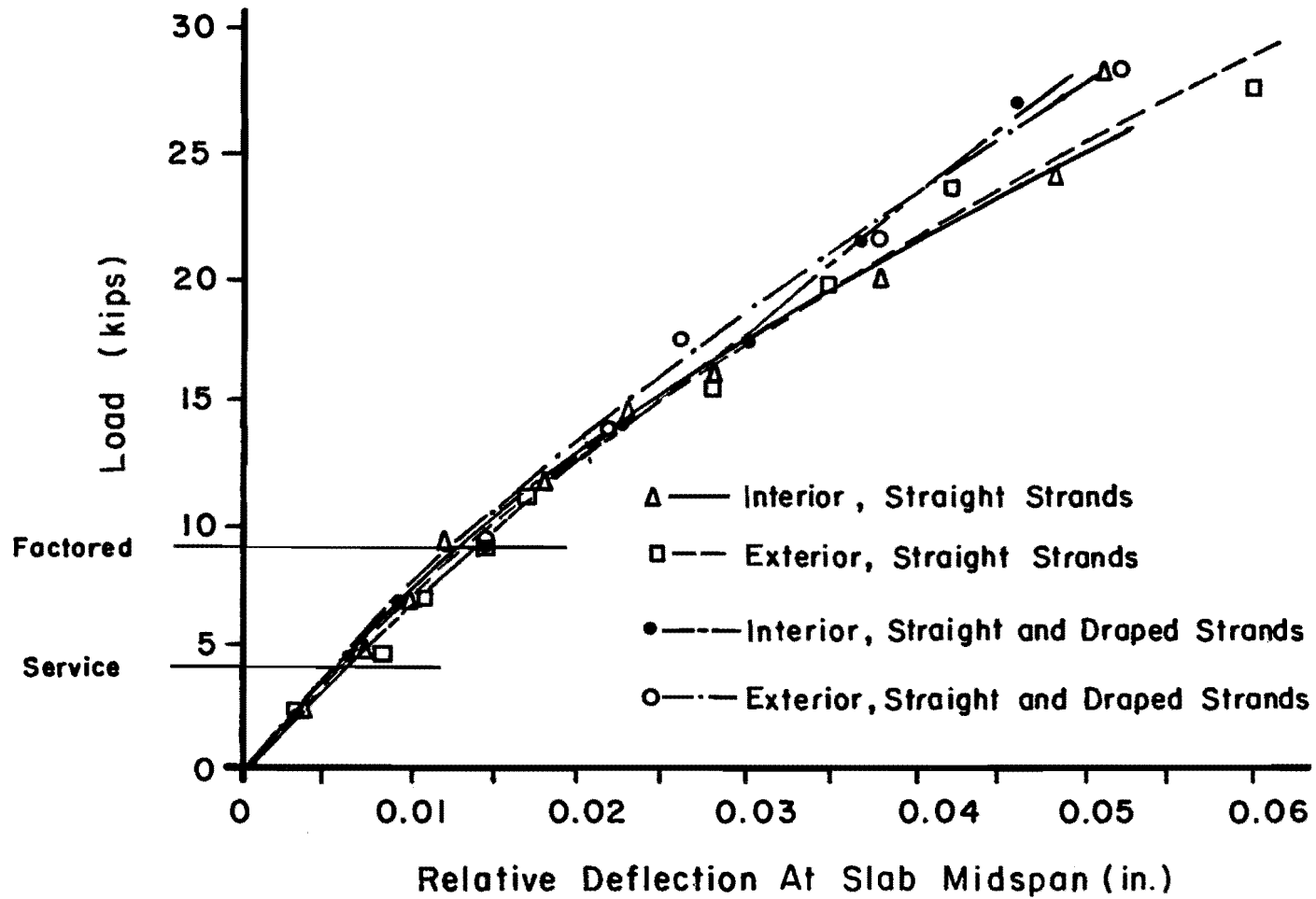


Fig. 5.30 Load-deflection curves for ultimate negative moment tests, east slab spans only

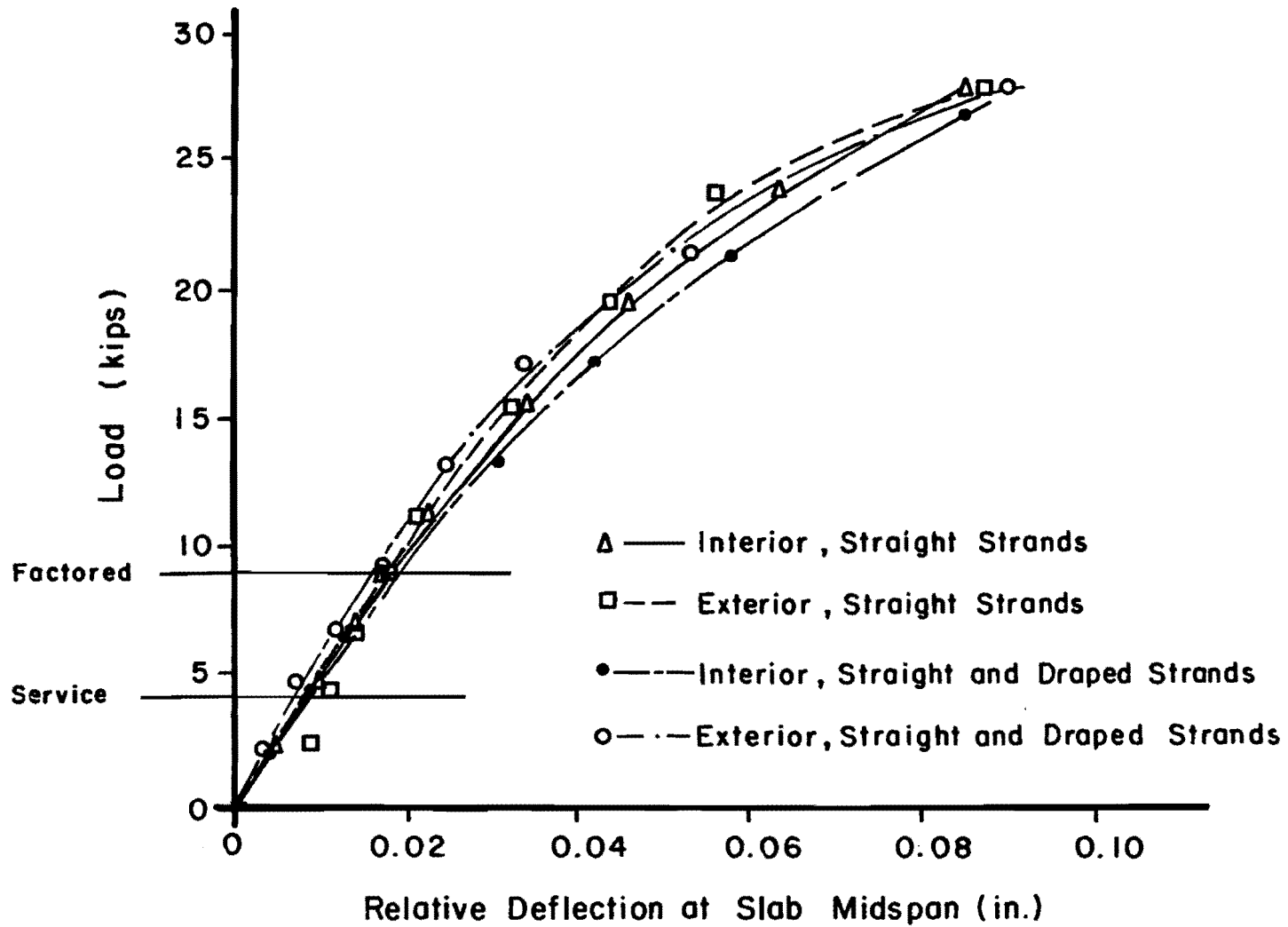


Fig. 5.31 Load-deflection curves for ultimate negative moment tests, west slab spans only

of the bridge in both the positive and negative moment tests. Similar behavior was exhibited at all of the positive moment test locations, except at the interior location with straight and draped stands, where somewhat larger deflections were observed.

Continuing the trend observed earlier, the west slab span of all the negative moment tests displayed significantly larger deflections than the corresponding test slab span (Figs. 5.22 and 5.23). At the exterior straight strand location for the negative moment tests, the east slab span experienced larger deflections than the other test locations. In general, however, all locations tested for negative moment behaved similarly.

The longitudinal slab profiles for minimum positive moment shown in Fig. 5.24 seem to indicate a greater sensitivity to uplift for the straight strands than for the straight and draped strands. The transverse slab profiles in Fig. 5.25, however, do not support this assertion. This same situation was also observed during the factored load tests.

Overall, the only deflection characteristics consistently observed through all levels of load were the tendency for slightly greater deflections towards midspan of the bridge than towards the bridge abutments, and the significantly larger deflections in the west span compared to the east span in the negative moment slab tests.

Once again, the relatively small deflections observed at even the very high loads in these tests are notable. In the positive moment tests, at 5.6 times the factored live load, the maximum relative deflection was 0.210 in., or a transverse span to deflection ratio of about 225. Similarly, in the negative moment tests, at 3.1 times the factored live load, a maximum relative deflection of 0.091 in. corresponding to a transverse span to deflection ratio of approximately 520 was observed. Though the magnitude of these deflections in the ultimate tests seems small, it is helpful to note that they are significantly larger than the deflections observed during the service and factored load tests. This is illustrated in Figs. 5.26 and 5.27 where typical deflection profiles are shown for various load levels of a positive moment test.

Calculated surface stresses from strains measured in the ultimate load tests are of limited usefulness since many of the strains measured are beyond the elastic range of the system. The strain measurements are still a valid indicator of slab curvature, however, and curvatures for the same test location used previously are plotted in Fig. 5.28 for the ultimate load case. In contrast to the service and factored load tests, the curvature in the longitudinal direction shows a tendency to be slightly greater toward the bridge abutment rather than toward the midspan of the bridge.

Relative deflection data for points at the slab midspan along the tranverse line of loading were used to plot load-deflection curves. The load-deflection curves for the positive moment tests are shown in Fig. 5.29, and the curves for the east and west slab spans of the negative moment tests are presented in Figs. 5.30 to 5.31, respectively. Curves for the minimum positive moment tests were of limited value because of the very small magnitude of the deflections. The data for positive moment tests indicate very similar behavior for all the test locations. Response of the slab in all cases was largely linear through factored load, except for a slight change in stiffness between service and factored loads. Load-deflection curves for the negative moment tests showed similar behavior for all locations, but markedly less stiffness for the west slab span in all tests, due to the larger deflections in those spans, as previously discussed. The data for these tests does not lend itself to smooth curves as well as that for the positive moment tests. However, the same type of behavior is again observed in that all test locations performed similarly, and response was fairly linear through factored load, except for a slight decrease in stiffness between service and factored loads. It is notable that even at the high load levels at which the ultimate tests were terminated, significant stiffness still remained in the bridge deck system.

The final observations made during the vertical load tests were of the cracking patterns of the concrete. Although the load-deflection curves indicate initial cracking probably occurred in most tests around loads of 10 to 15 kips (approximately three times full design live load plus impact), visible cracks in the top of the slab, when they were evident, appeared at load levels around 25 to 30 kips for negative moment and 40 kips for positive moment tests. Cracking on the bottom of the bridge deck could not be observed during the test because of the proximity of the instrumentation. Instead, after the highest load level had been achieved and deflection measurements taken, cracks visible beneath the bridge deck were marked with a felt-tipped pen and the load removed.

In general, cracking on the top of the slab was limited, as shown in Fig. 5.32, and cracking on the bottom face of the slab extended radially outward from the point of load, primarily in the longitudinal direction as shown in Fig. 5.33. These cracks in the longitudinal direction also tended to be greater in length in the direction of the bridge midspan than towards the bridge abutments.

In the positive moment tests, cracks approximately 2-ft long appeared in the top of the slab over the edge of one of the girder flanges in all the test locations except for the straight and draped strand interior location. Cracking beneath the slab was modest in the positive moment tests for the straight strands, with only minor cracks in the exterior location and moderate cracks up to 2 ft long in the

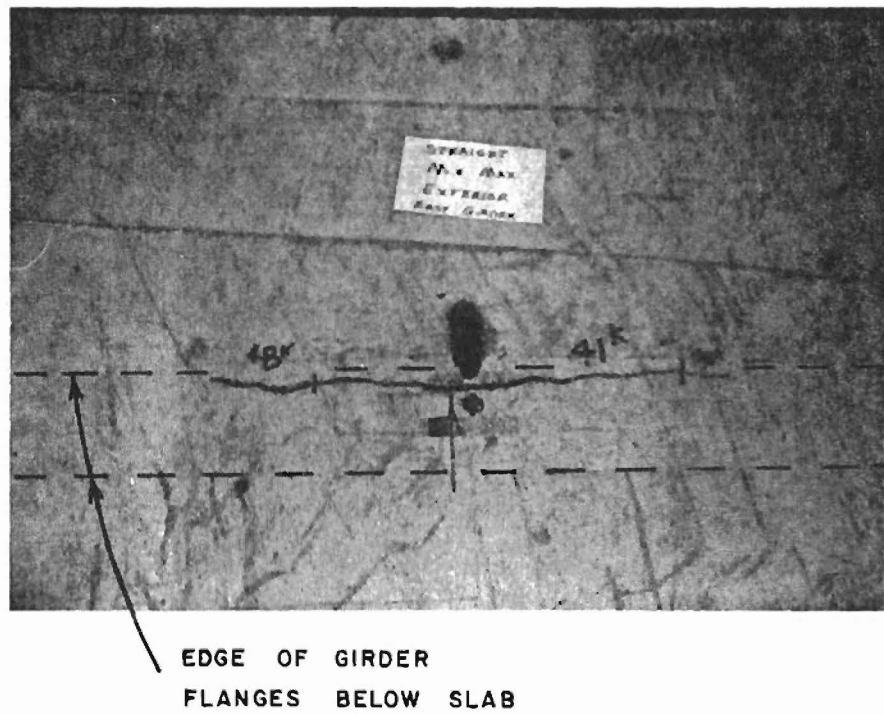
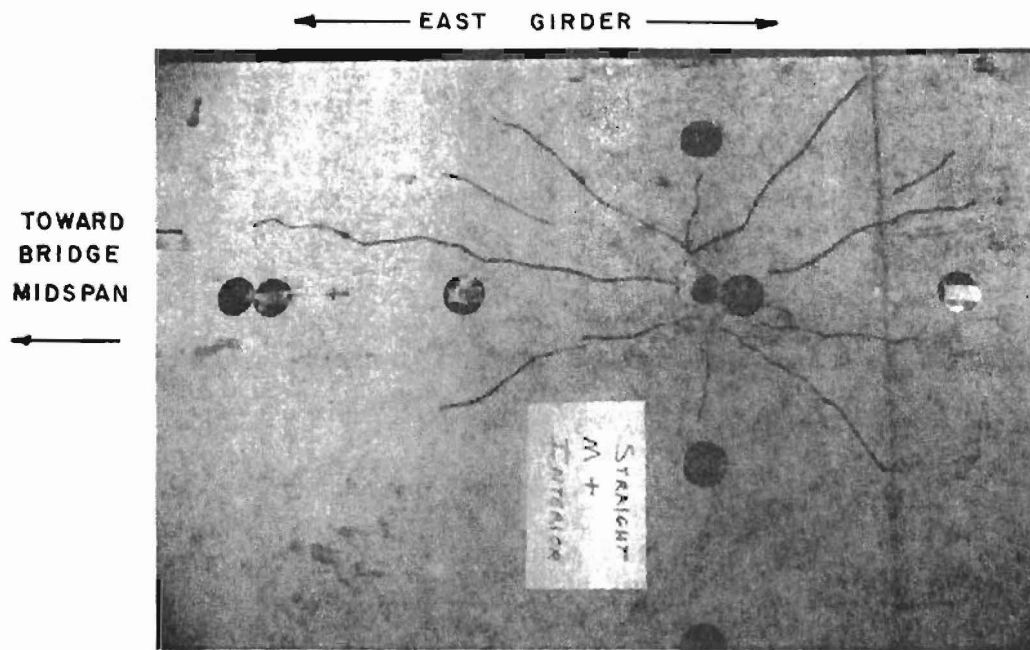
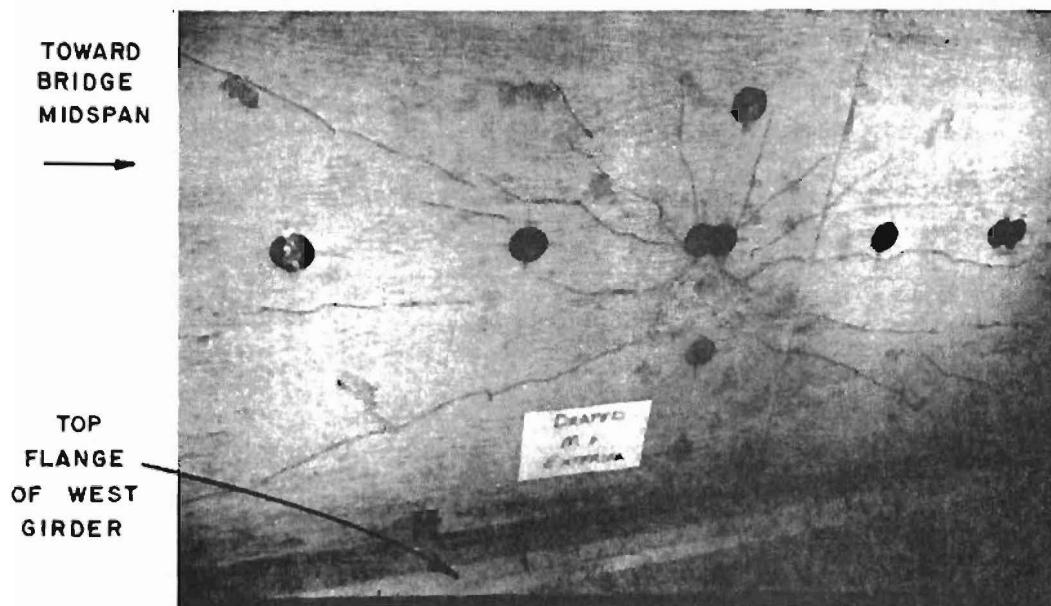


Fig. 5.32 Typical cracking in top of bridge slab, positive moment test, straight strand exterior location



(a) straight strands, interior location



(b) straight and draped strands, exterior location

Fig. 5.33 Crack patterns on bottom surface of bridge deck, positive moment tests

interior location. Cracks beneath the slab for the straight and draped strand locations were more pronounced than for the straight strand locations. Both the interior and exterior positive moment tests yielded widespread cracking, with transverse cracks 8 to 12 in. long and longitudinal cracks 2 to 3 ft in length. Typical crack patterns are shown for the positive moment tests in Figs. 5.32 and 5.33.

Cracks in the top of the slab occurred at only the interior straight and draped tendon location in the negative moment tests. As in the positive moment case, the crack appeared over the edge of a girder flange in the longitudinal direction for about 2 ft. On the bottom surface of the slab, cracks emanated from the points of loading and varied in number and length substantially between each negative moment test. Cracking at the straight and draped strand locations was lighter than at the other end of the bridge with practically no cracks at the interior location, and minor to moderate cracking at the exterior location. On the straight strand end of the bridge, cracking was more severe at the interior location, especially in the west slab span where longitudinal cracks exceeded 4 ft in length. In the exterior negative moment tests, cracking for both strand arrangements was more pronounced in the outside slab span.

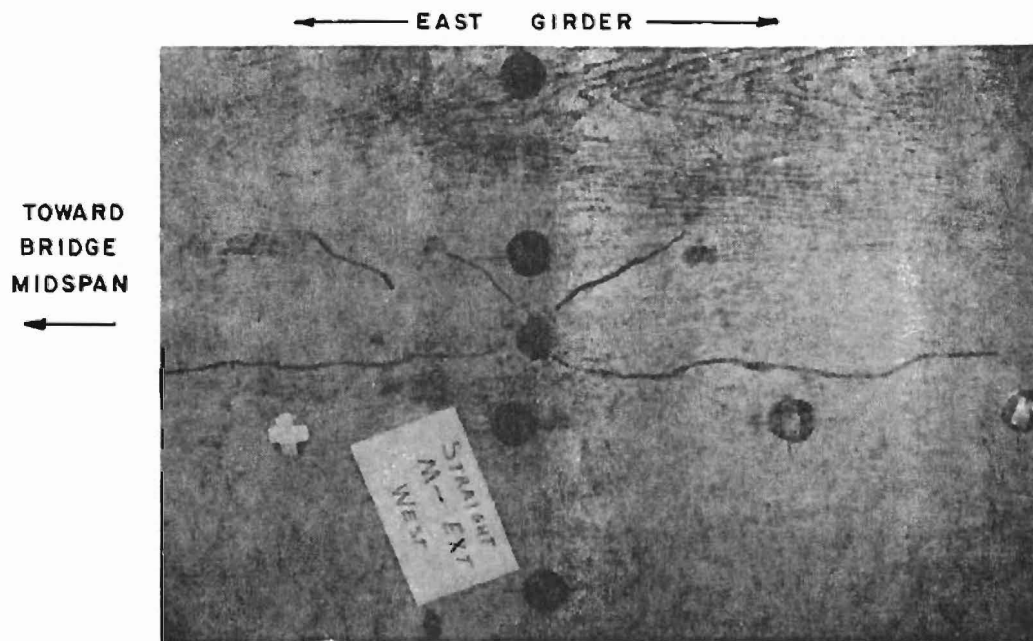
Figure 5.34 shows cracking in the outside spans of the exterior negative moment tests, and Fig. 5.35 presents crack patterns in both slab spans at the interior straight strand negative moment test location.

The minimum positive moment tests at both ends of the bridge produced some cracking on the bottom of the bridge slab at the points of loading, but no visible cracking was observed in the slab span of interest in either test.

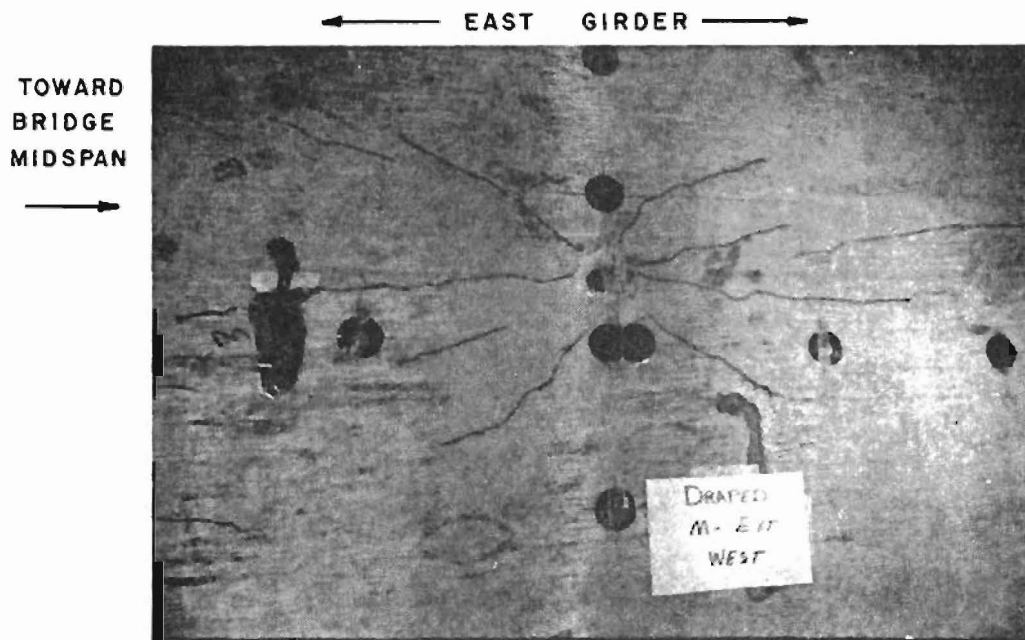
In general for all of the tests, cracking on the top surface of the deck could be classified as hairline cracking, while cracks observed on the bottom of the slab were wider, but definitely less than serviceable crack widths. Again, it should be noted that cracking did not occur whatsoever in most tests before an applied load of at least 2.5 times the service live load plus impact, and that the maximum crack widths described above were for loads from approximately 6.5 to 12 times the service live load plus impact.

5.1.6 Discussion of Test Results

5.1.6.1 System Accuracy. Results of the vertical load tests must be interpreted with respect to the accuracy and precision of major data such as deflections, stresses, and loads. The deflections as measured by linear potentiometers and mechanical dial gages were susceptible to the introduction of errors from several sources such as electrical stability, slippage, human error, and mounting flexibility.

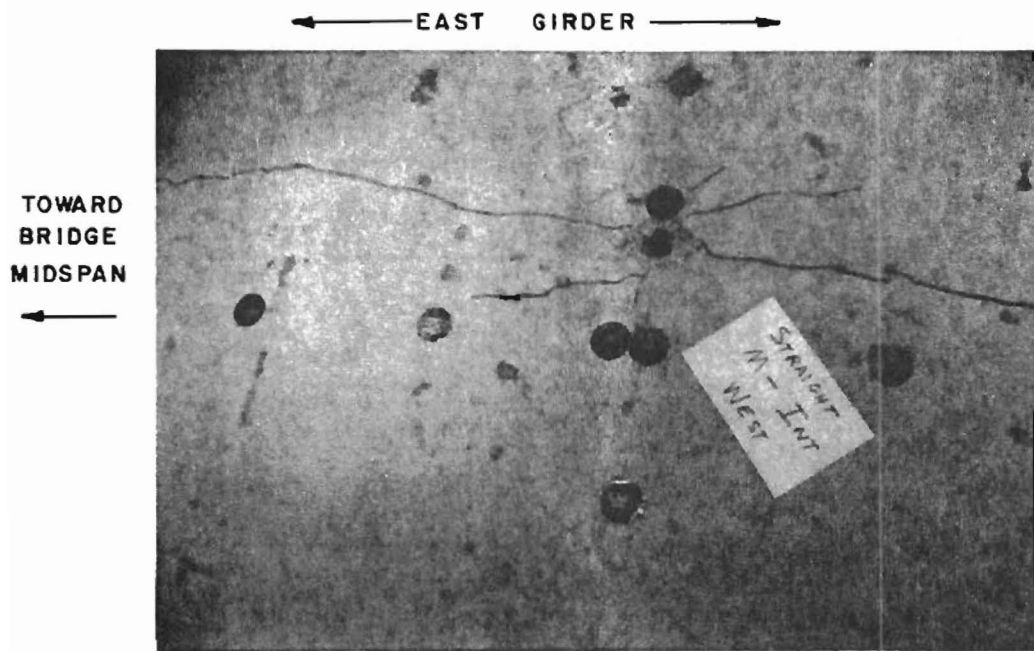


(a) straight strands

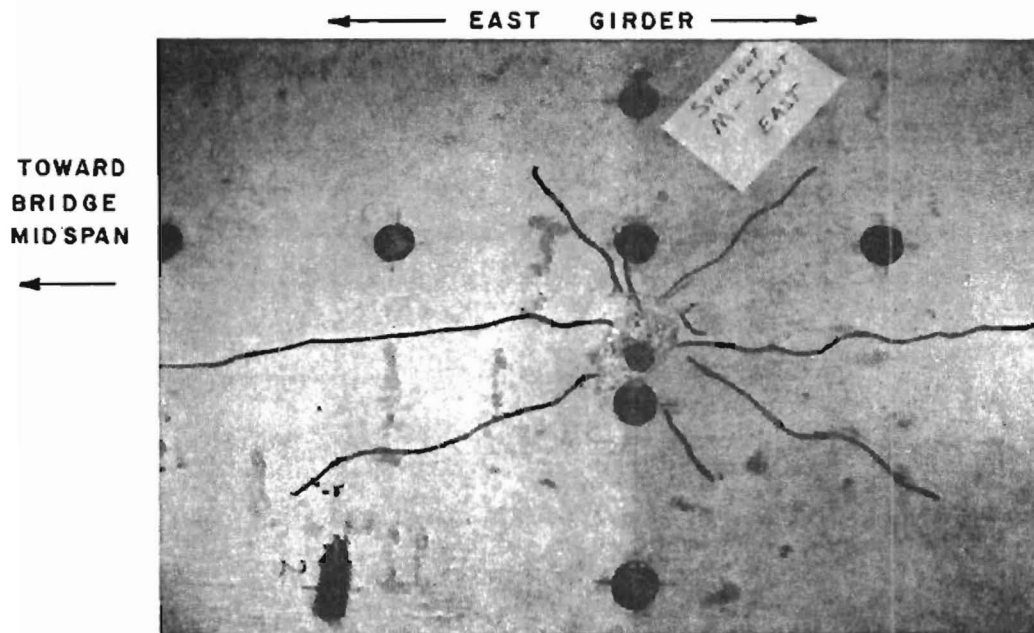


(b) straight and draped strands

Fig. 5.34 Crack patterns on bottom surface of bridge deck, outside span of exterior negative moment test locations



(a) west span



(b) east span

Fig. 5.35 Crack patterns on bottom surface of bridge deck, interior negative moment test location, straight strands

The combined effect of the above error factors on the measured deflections was normally within the range of $\pm 0.003-0.004$ in. While this is only 5 to 15% of the gross deflection values under service load, it is 50 to 100% of relative service load deflections and 2 to 7% of relative ultimate load deflections.

The concrete surface stresses reported for service and factored live loads were also subject to a margin of error due to gage variation, mounting error and concrete modulus variation. Overall, the accuracy of the concrete stress values reported is estimated as $\pm 15\%$.

Load variations were induced by small pressure losses in the hydraulic system, calibration errors, and mismatch effects when parallel rams were used. The combination of these factors then indicates that the applied load at any location was actually 5 to 7% less than that reported.

5.1.6.2 Irregular test results. Some of the slab behavior observed was not what might be expected and requires explanation. Greater relative slab deflections occurred towards the midspan of the bridge than towards the bridge abutments. Two factors can account for this. First, since only half of the bridge slab was prestressed at any given time, the lower stiffness of the adjacent unstressed slab resulted in the prestressed deck near midspan carrying more load, and thus exhibiting more deflection. Second, the girder deflections are greater towards the midspan region, increasing support deflections for the slab, and thus reducing restraint moments acting on a slab span over the girders. Consequently, the transverse positive moment carried by the slab is increased, along with the corresponding deflection.

Also, relative slab deflections in all the negative moment tests were always significantly greater for the west than for the east slab spans. This can be explained by examining the actual transverse span lengths and load locations, variations in the slab thickness, and differential girder deflections transversely.

The influence of each of these factors can be evaluated qualitatively by modeling the deck as a six-span continuous beam on simple supports, and comparing the experimental and calculated ratios of west to east slab span deflections. Table 5.2 gives the actual dimensions for transverse slab span length and load location for each of the negative moment tests. Using these dimensions, west to east slab span deflection ratios were computed and are shown along with the experimental ratios in Table 5.3. For the exterior negative moment tests, the experimental ratio was less than that calculated for service and factored loads, but very near the calculated value for the maximum load. This is because the stiffness of the exterior girder-slab connection reduces the west span deflection at the lower loads,

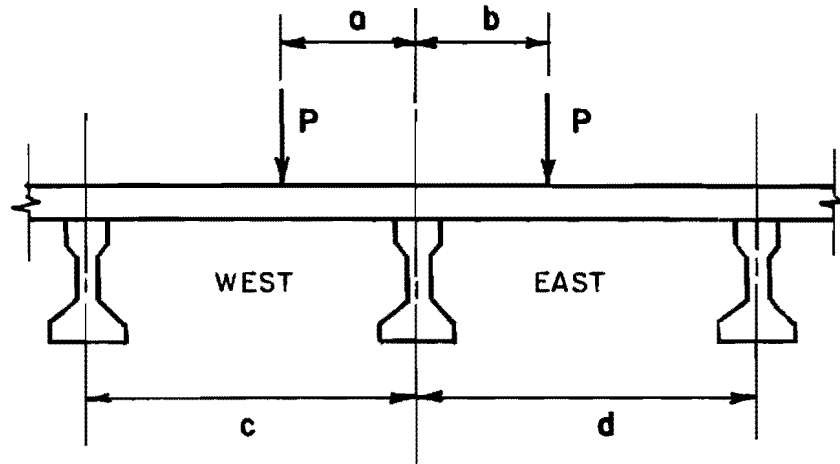


TABLE 5.2 Planned and Actual Span Lengths and Load Locations for Negative Moment Tests

	Dimensions (in.)			
	a	b	c	d
Planned Interior	18.05	18.05	47.53	47.53
Planned Exterior	20.07	18.08	47.53	47.53
Interior, Straight	18.19	17.81	47.88	46.75
Exterior, Straight	19.69	18.06	47.63	47.13
Interior, Straight and Draped	18.69	17.56	48.00	47.00
Exterior, Straight and Draped	20.19	17.69	47.75	47.25

TABLE 5.3 West Span to East Span Slab Deflection Ratios
for Negative Moment Tests

Test	Load Level	Max. Exp. West	Δ (in.) East	Exp. $\Delta W/\Delta E$	Calc. $\Delta W/\Delta E$	$\frac{\text{Exp.}}{\% \text{ Calc.}}$
Interior, Straight Strands	Service	0.007	0.004	1.75	1.10	159
	Factored	0.016	0.012	1.33	1.10	121
	Max	0.085	0.051	1.67	1.10	152
Exterior, Straight Strands	Service	0.005	0.006	0.83	1.63	51
	Factored	0.014	0.012	1.17	1.63	72
	Max	0.087	0.060	1.45	1.63	89
Interior, Straight and Draped Strands	Service	0.009	0.006	1.50	1.14	132
	Factored	0.019	0.014	1.36	1.14	119
	Max	0.085	0.046	1.85	1.14	162
Exterior, Straight and Draped Strands	Service	0.006	0.005	1.20	1.72	70
	Factored	0.017	0.013	1.31	1.72	76
	Max	0.090	0.052	1.73	1.72	101

but after cracking at maximum load levels, the behavior is better modeled as the simple support assumed in the calculations. While accounting for the slab behavior at the exterior negative moment test locations, using actual span lengths and load positions still does not fully account for deck behavior at the interior negative moment test locations.

Actual slab thicknesses, as measured at the load application points, for west and east spans of the interior negative moment tests are shown in Table 5.4. The slab was again analyzed using the continuous beam analogy with the measured span lengths and load locations, and assuming a uniform concrete thickness as given in Table 5.4 for the east and west spans and of 3.75 in. for all other spans. Results from this analysis are given in Table 5.5. Good agreement between analytical and experimental ratios is obtained for service and factored load levels with the exception of the straight strand service load test. As discussed earlier, however, the results at service load levels are especially sensitive to the accuracy of the system. At maximum load levels, the discrepancy between east and west slab span deflections is not fully accounted for by considering actual slab spans, loading positions, and slab thicknesses.

Table 5.6 presents the measured girder deflections along the transverse deck section of interest in the interior negative moment tests. Note that at service and factored load levels, the girder deflections are symmetric around the middle girder. At maximum load for both test locations, however, the west girder deflects approximately 10% more than the east girder, possibly due to differences in cracking of the two girders. When the slab analysis is repeated with inclusion of support displacements (girder deflections), the percent experimental over calculated west to east slab span deflections ratios becomes 57% for straight strands and 55% for draped strands. Apparently because of cracking in the slab, the full effect of differential girder deflections is not reflected in the slab behavior.

From the preceding discussion, then, it can be said that the unexpected differences between the west and east span relative slab deflections are the result of actual slab span lengths, loading positions, slab thicknesses, and of differential girder deflections.

5.1.6.3 General Behavior. From the load-deflection plots given in Figs. 5.29 through 5.31, it can be seen that for all of the load tests, behavior of the deck slab was essentially linear elastic through factored load levels. A slight change in stiffness, probably due to initial cracking, did occur in some of the tests between service and factored load levels. However, because of the prestressing, these cracks close after removal of the factored load, and the slab regains its initial stiffness. This behavior is demonstrated by the fact that the deck had already been tested at

TABLE 5.4 Actual Slab Thicknesses for Interior Negative Moment Tests

Test	Slab Thickness (in.)	
	West Span	East Span
Planned	3.78	3.78
Straight Strands	3.69	4.00
Straight and Draped Strands	3.63	4.13

TABLE 5.5 West Span to East Span Deflection Ratios for Interior Negative Moment Tests, Accounting for Actual Slab Thicknesses

Test	Load Level	Exp. $\Delta W/\Delta E$	Calc. $\Delta W/\Delta E$	% $\frac{\text{Exp.}}{\text{Calc.}}$
Straight Strands	Service	1.75	1.33	132
	Factored	1.33	1.33	100
	Max.	1.67	1.33	126
Straight and Draped Strands	Service	1.50	1.55	97
	Factored	1.36	1.55	88
	Max.	1.85	1.55	119

TABLE 5.6 Girder Deflections for Interior Negative Moment Tests

Test	Load Level	Girder Deflection (in.)		
		West	Middle	East
Straight Strands	Service	0.039	0.053	0.038
	Factored	0.083	0.116	0.083
	Max.	0.400	0.567	0.366
Straight and Draped Strands	Service	0.033	0.048	0.033
	Factored	0.083	0.115	0.081
	Max.	0.349	0.507	0.315

factored loads prior to the tests for which Figs. 5.29 through 5.31 are plotted.

Although actual failure of the deck slab was never achieved in any of the vertical load tests, several statements can be made about the deck behavior at failure. The radial crack patterns observed on the bottom of the deck as shown in Figs. 5.33 through 5.35 are similar to the patterns observed in other tests [18,29] of slabs under concentrated loading in which the eventual failure mode was punching shear. This, in combination with the fact that the flexural cracking on the top slab surface was fairly light, indicates that the failure modes for these vertical load tests would have been punching shear had that level of load been applied.

The level of load required to cause such a failure is again difficult to identify for these tests since failure was never achieved. However, it can be noted that at termination of testing, the deck was loaded with an average of 11.9 times service (5.5 times factored) live loads in the positive moment tests, and 6.6 times service (3.1 times factored) live loads in the negative moment tests, including impact. Even at these levels of load, as discussed in Section 5.1.5, the observed cracking was within serviceable limits and the load-deflection curves indicated substantial remaining stiffness in the deck.

In determining the critical loading condition for design it can first be seen from Figs. 5.24 and 5.25 that the minimum positive moment load case produces such small upward deflections that it can be ignored. Furthermore, examining Figs. 5.29 through 5.31, there appears to be no substantial difference between the behavior of decks with straight strands only and straight and draped strands, nor between interior and exterior test locations. The question of whether positive or negative moment loading is more critical is not answered conclusively by these data, since at the load level at which the negative moment tests were terminated, the east slab spans of the negative moment test locations had the largest stiffness, while the west slab spans of the same tests had the least stiffness. The stiffness of the deck in the positive moment tests fell between the other two.

The applied concentrated loads were well distributed longitudinally within the bridge slab. At service and factored load levels, the relative slab deflections at a distance of one slab span length away from the load in each direction were approximately half the deflections at the load point (Figs. 5.6, 5.8, 5.13, 5.15). At higher loads, the slab response was more localized due to cracking (Figs. 5.20 and 5.22). In looking at the slab curvatures for the interior positive moment tests on straight and draped strands (Figs. 5.12, 5.19, and 5.28), it can be seen that the maximum longitudinal slab moment is approximately 1/4 to 1/6 the maximum transverse moment.

Note that for this bridge, following AASHTO requirements, longitudinal distribution reinforcement in the center portion of the slab amounting to 67% of the provided transverse reinforcement would be required. This is more than twice what is needed according to these data.

The strain measurements taken at the interior positive moment test with straight and draped strands also allow a comparison between the slab stresses and moments assumed in the design, and those outlined in Section 5.1.2, along with the measured slab thickness at the test location of 3.68 in., experimental transverse live load stresses and moments were calculated for service and ultimate load levels. These values, which already include impact, were adjusted for the scale factor and are shown in Table 5.7 along with the values calculated using the AASHTO design procedure. The design values exceed the experimental values by 36 to 44%, indicating that the slab moments given by the AASHTO formula are quite conservative for a bridge of these proportions and construction.

5.1.6.4 Comparisons with Analysis and Other Tests. The most commonly used analytical technique for the design of bridge decks is influence surfaces based on elastic theory, as published by Pucher and Homberg [41,42]. The prototype bridge deck, with dimensional modifications to simulate the laboratory model proportions, was analyzed using these influence surfaces following the procedure given in Ref. 87. This involved modeling the live load as distributed load, finding transverse fixed end moments for a unit width continuous beam simply supported across the girders, finding the equivalent vertical load on the unit width slab from the fixed end moments, and finally calculating the actual transverse slab moments given the distributed moments and equivalent vertical load. For the maximum positive moment at the interior location with straight and draped strands, this procedure predicted a service load moment of 3.48 k-ft/ft. This value is only 7% below the 3.75 k-ft/ft calculated from the test results. One factor which was not accounted for in this analysis, however, was the differential girder deflections. When measured deflections of girders adjacent to the load were included in the analysis (assuming other girder deflections as 1/2 that of the next girder closer to the loaded slab span), the calculated maximum positive transverse slab LL + I moment became 3.90 k-ft/ft at service load and 8.56 k-ft/ft at factored load. From Table 5.7 it can be seen that these moments are in good agreement with the experimental values, being 4.0 and 5.2% greater for service and factored load levels, respectively. The method of elastic analysis by influence surfaces, then seems to predict fairly well the behavior of the bridge deck through factored loads, especially when girder deflections are accounted for.

Tests of reinforced concrete slabs subjected to concentrated loads, reported by Batchelor et al. [18] and Csagoly et al. [29] confirm that the data obtained in the vertical load test program are reasonable. In the tests by Batchelor, 1/8 scale models of composite

TABLE 5.7 Comparison of Design and Experimental Transverse Slab Surface Stresses and Moments

	AASHTO Design Service Factored		Experimental Service Factored		% Design/Exp. Service Factored	
Tensile Stress (psi)	469	1017	324	704	145	144
Compressive Stress (psi)	469	1017	345	747	136	136
Positive Moment (k-ft/ft)	5.33	11.55	3.75	8.14	142	142

slab and steel girder bridges were loaded to failure. Those specimens which modeled conventional deck designs failed in punching shear at approximately 16 times the service live load plus impact. This compares to the load of 12 times service live load plus impact at which the positive moment vertical load tests were terminated without failure.

Csagoly subjected the decks of various types of existing bridges to a single load of 100 kips and measured vertical deflections. For the two bridges tested which were of composite concrete deck and prestressed I-girder design, the transverse slab span to thickness ratios were 13.2 and 11.6, and the slab span to deflection ratios were 1410 and 1740. In the model bridge, the transverse slab span to thickness ratio was 12.6 and 20.1 kip load represents a full scale load of 100 kips. From Figs. 5.29 through 5.31, it can be seen that at this load level, the slab span to deflection ratios ranged from 913 to 1440. Thus, the stiffness of the model slab appears to be somewhat less than that of the actual bridge decks tested by Csagoly, but nevertheless within the same range.

The question remains that if the slab behavior is so well predicted by elastic analysis through factored load, why does the actual ultimate load capacity of the slab so grossly exceed that predicted? As discussed in Section 2.1.2, while the concrete remains uncracked (as it does through factored loads in this case), behavior of the slab is elastic and in-plane forces in the slab have not developed. Any analysis of the ultimate strength of the slab, however, must take into account the strength enhancement due to significant in-plane forces (arching action) which develop along with the concrete cracking.

5.1.7 Conclusions. The major conclusions which can be drawn from the vertical load tests concerning the behavior of the transversely prestressed bridge deck are as follows:

1. The results of the vertical load tests are reasonable in relation to other reported tests of concrete bridge decks subjected to concentrated loads.
2. No substantial difference between the behavior of the deck constructed with straight strands only and with straight and draped strands was observed. There also appeared to be no significant difference in slab behavior at interior and exterior locations.
3. Uplift in the slab due to the minimum positive moment loading conditions was negligible. It is unclear from these tests whether positive or negative moment loading conditions are more critical for the prototype bridge

4. The transversely prestressed slab exhibited essentially linear elastic behavior through factored load levels. Based on a limited amount of data, it may be further said that: a) the empirical formula given by AASHTO for estimation of transverse moment in deck slabs yields values conservative by 35 to 45% in this elastic range of behavior; and b) methods of analysis based on elastic theory, such as the use of influence surfaces, predict slab behavior fairly well in the range of loading through factored, especially if differential girder deflections are taken into account. Otherwise, the results may be slightly unconservative
5. Failure of the slab was never achieved, but concrete crack patterns indicated the eventual failure mode would be punching shear. Though the ultimate load capacity of the slab is not known, proof loads of 11.9 and 6.6 times the service live load plus impact were applied in the positive and negative moment tests, respectively, without the occurrence of failure. This high factor of safety above what was calculated for the design is due to the development of significant compressive membrane forces in the slab after cracking
6. Based on a limited amount of data, the maximum longitudinal slab moment is on the order of $1/6$ to $1/4$ the maximum positive transverse slab moment

5.2 Edge of Slab Posttensioning Stress Distribution Tests

5.2.1 Test Description. The objectives of the edge of slab posttensioning stress distribution tests were: first, to investigate the effect of strand spacing on the distribution of horizontal slab stresses near the deck edge; and second, to determine if stresses induced in the slab by one strand are decreased significantly by the subsequent stressing of an adjacent strand.

To accomplish these objectives, two tests were carried out on the laboratory model described in Section 4.6.2. At a location along the west slab edge where straight and draped strand construction was used, closely spaced 30mm electrical resistance strain gages were installed on the top and bottom slab surfaces as shown in Fig. 5.36. All of the posttensioning strands within a longitudinal distance of 20 in. (roughly the amount of slab overhang, measured from the center of the exterior girder) from the gages were instrumented with the small load cells used in previous tests of the model. Both of the tests involved stressing the strands within this 40-in. long region and reading the strain gages so that the resulting slab stresses could be calculated.

In the first test, a single strand in the upper portion of the slab was stressed. Load cell and strain gage readings were taken. The strand was then released. This process was repeated for each upper strand in the test area.

For the second test, readings were again taken after each strand was stressed. However, the tensioned strands were not destressed. Strands in the bottom portion of the slab were stressed as well as those in the top portion. Referring again to Fig. 5.36, the order of strand tensioning began with strand 5, then went to strands 4 top and bottom, then to strand 6, and so forth, alternating on each side of the center strand, until strands 1 (top and bottom) through 9 had been stressed.

5.2.2 Test Results. The top and bottom concrete surface strains measured in the first test were averaged at each gage location to eliminate the effects of bending in the data. From these average strains, average concrete stresses were computed assuming the compressive strength of the concrete to be 5000 psi. The calculated stresses were then normalized as a percentage of the applied stress as follows:

$$\text{percent stress} = 100 \times (t_c) / (F / (T \times S))$$

where: T_c = calculated stress from measured strains
 F = measured strand force
 T = slab thickness
 S = strand spacing

Finally, since data from strands symmetrical about the strain gages (strands 2 and 8, for instance) are for the same distance from the tensioned strand, the averages of the percent stress values for such strands were used for the particular distance from the stressed strand.

The values obtained for percentage of stress in the slab due to a single tensioned strand by the data reduction process described above are plotted in Fig. 5.37. Using these values, contour lines representing equal stress in the deck overhang were constructed as shown in the figure. Note that the pair of strain gages located at a distance of 7 in. from the deck edge gave consistently unreasonable values of strain, and thus were ignored for the purpose of constructing the contour lines.

In the second test, the percentage of applied stress in the slab was calculated slightly different because both upper and lower strands

were stressed, and strands were not destressed during the test. The formula used to determine the percentage of applied stress was:

$$\text{percent stress} = 100 \times \tau_c ((x F) / (3/4 \times T \times S \times N))$$

where: τ_c , F, T, S = as before

N = number of tensioned strands

The values of percent of applied stress in the slab are plotted in Fig. 5.38 for various numbers of tensioned strands. Note that data from the erratic strain gages 7 in. from the slab edge were again ignored. As expected, stresses near the strand anchorage are fairly high, and not greatly affected by tensioning of additional strands. There are two instances where tensioning additional strands decreases the slab stresses. First, when strands adjacent to the center strand (No. 5) are tensioned, the stress decreased from 140.1% to 134.7%, a relative reduction of 4%. This is due to the elastic shortening of the deck in the vicinity of the center strand. Second, when strands located three and four strand spacings away from the center strand were tensioned, slab stresses 3 to 5 in. from the deck edge decreased slightly. This is to be expected in light of the tensile stresses induced by strand tensioning as shown in Fig. 5.37. It is also interesting to note that through the duration of this test, the tension in the center strand decreased by only 1%, from 5202 to 5142 lb.

5.2.3 Design Implications of Data. Because the posttensioning forces are applied to the deck in a discretized manner due to the spacing of the strands, there will be areas along the edge of the deck between strands where the prestressing is ineffective. The extent of this area must be known so that other means of resisting the imposed loads may be provided. Referring again to Fig. 5.38, it can be seen that the slab stresses near the deck edge do not change appreciably after the adjacent tendons have been tensioned (this corresponds to 4 tensioned strands in this test). Therefore, by examining the slab stresses between two adjacent tendons, an estimation can be made of the size of the ineffectively prestressed area. Figure 5.39 shows superimposed stress contours, from Fig. 5.37, for two adjacent tendons at the edge of the slab. By inspection, it is found that the inadequately stressed area is bounded roughly by an equilateral triangle with the slab edge as its base and a side length equal to the tendon spacing. This area extends into the slab a distance from the edge equal to the strand spacing times the sine of 60° , or approximately 0.85 times the prestress tendon spacing. Depending on the tendon spacing, overhang amount, slab thickness, and curb and rail attachment, this area may or may not require special attention in design.

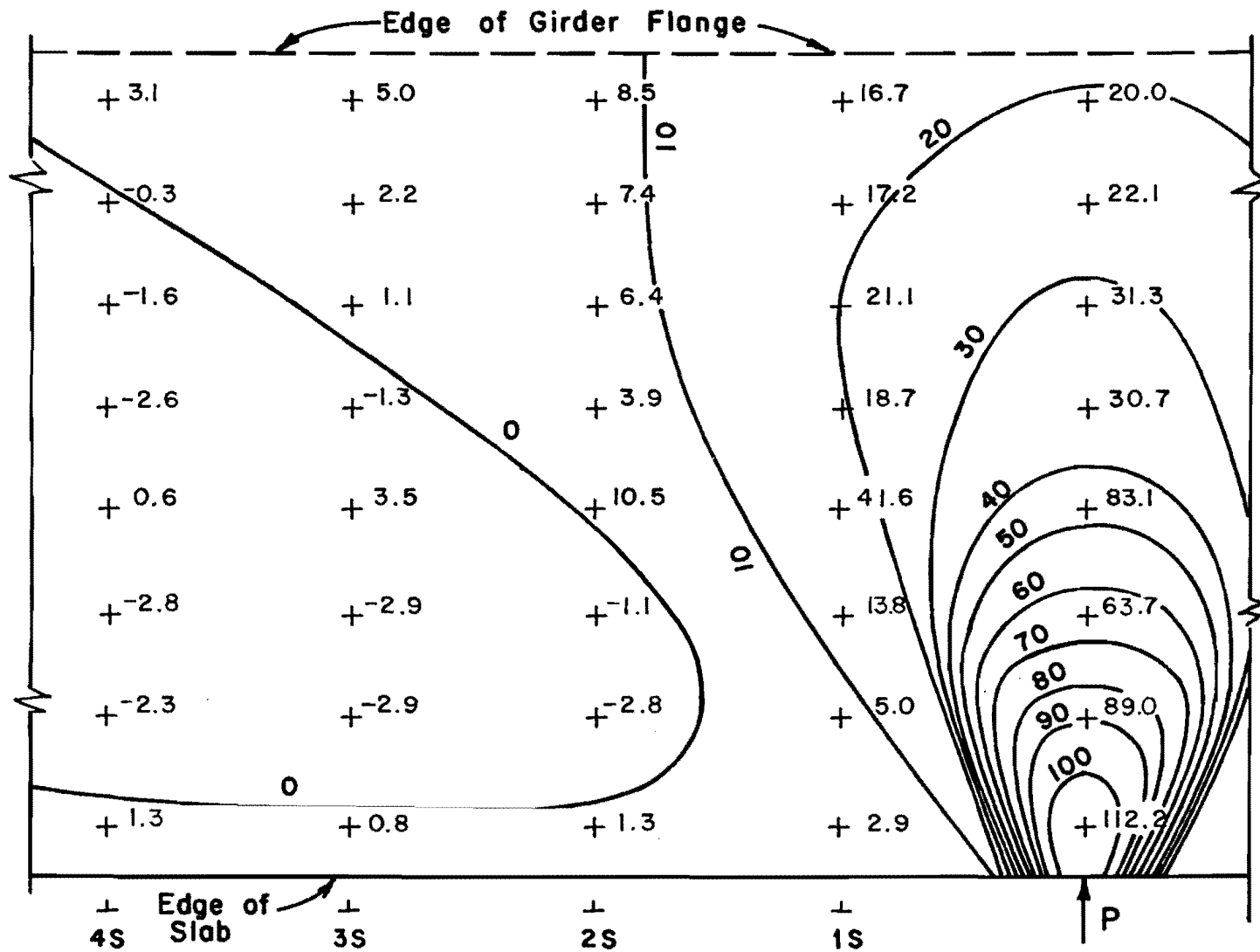


Fig. 5.37 Stress distribution contours for single posttensioned strand at edge of slab

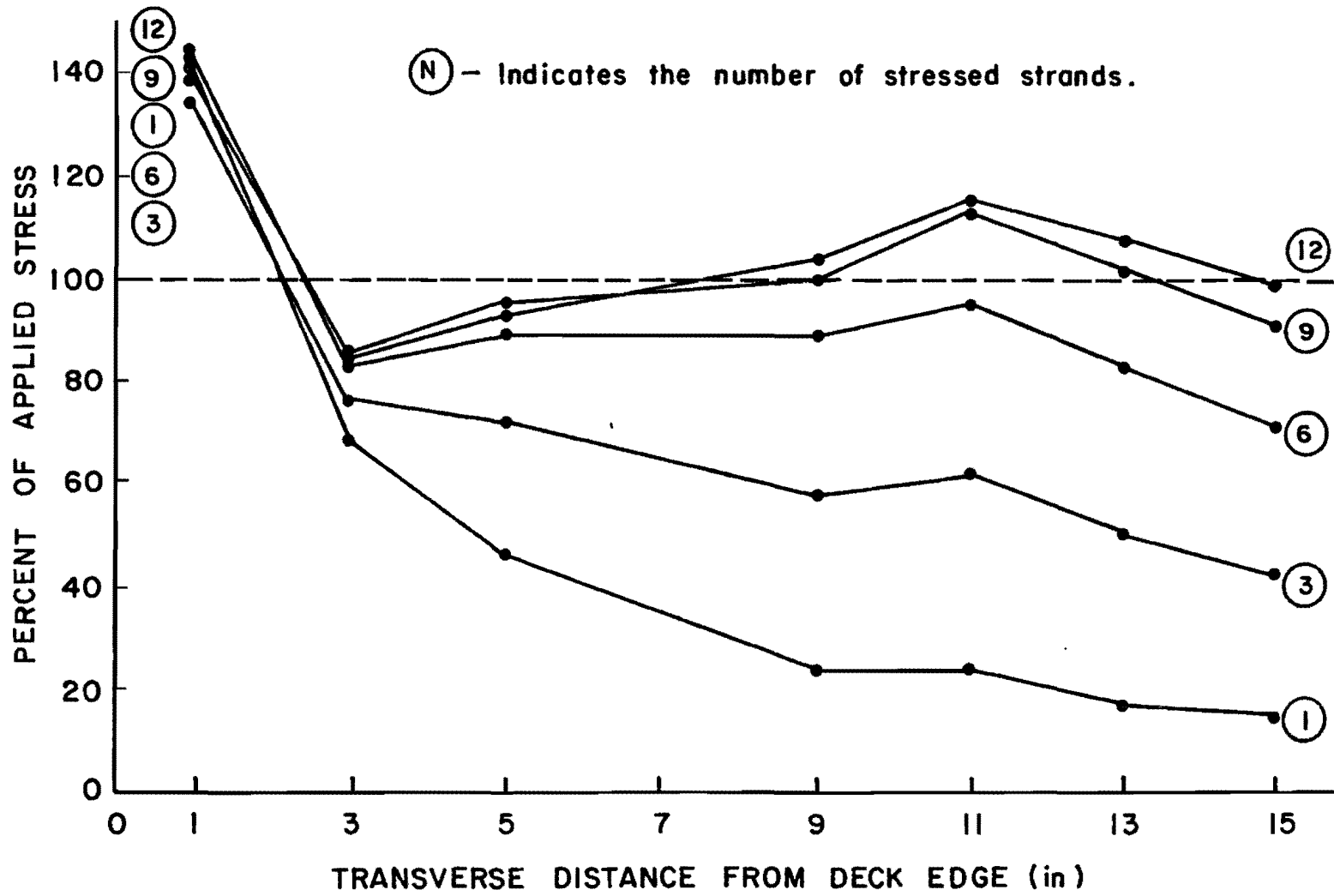


Fig. 5.38 Percent of applied stress in slab near deck edge for various number of tensioned strands

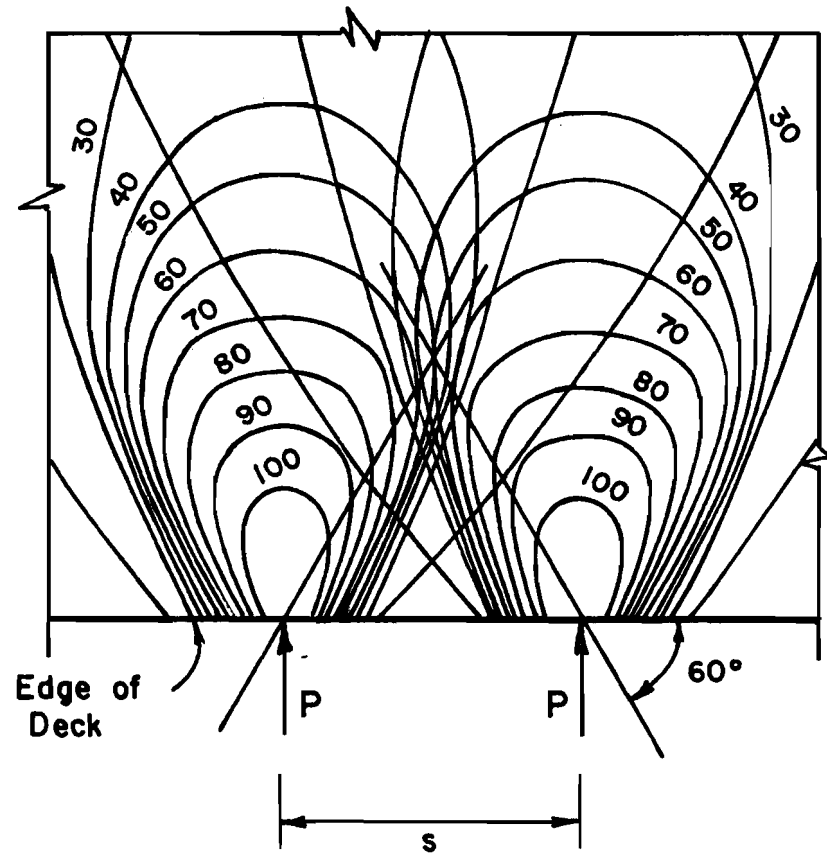


Fig. 5.39 Area of ineffective prestress between strands at edge of deck

The results of the second test discussed earlier indicate that the reductions in tendon force and stresses near the slab edge due to the tensioning of adjacent tendons are less than 5%. This loss in stress, however, is compensated for with the tensioning of strands beyond the strands adjacent to the location under consideration. Therefore, the loss of posttensioning stresses near the slab edge due to tensioning of adjacent strands need not be considered in design.

C H A P T E R 6

ANALYTICAL PARAMETRIC INVESTIGATIONS OF SLAB-GIRDER AND BOX GIRDER BRIDGES

6.1 General

The transverse strength of bridge decks, whether computed according to AASHTO design specifications, using influence surfaces of Homberg or Pucher, or other rigorous analytical methods, can be provided by either conventional or prestressed reinforcement. When transverse reinforcing bars are used, no direct stresses are introduced by the reinforcement. However, prestressed transverse reinforcement compresses the slab and introduces stresses in the slab as well as other members of the bridge. This is due to the restraining action of the webs or girders and the diaphragms on the transverse movement of the slab.

The finite element program described in Section 4.5.2 was used to study the effects of several parameters on the slab transverse stress distribution in both slab-girder bridges and box girder bridges when transverse prestressing is employed. Full results are contained in Ref. 60 and are briefly summarized in this chapter.

6.2 Slab and Girder Bridge

6.2.1 Dimensions, Material Properties, and Loading. The effects of varying each of the parameters were investigated using the prototype composite slab-girder bridge, shown in Fig. 6.1. The seven girders are standard Texas C-type. Slab thickness is 8.25 in. Standard end diaphragms and interior diaphragms placed at third points are included. Figure 6.2 and Table 6.1 give the geometry and material properties of the slab, girders and standard diaphragms.

Based on bridges similar to that of Fig. 6.1, parameter variations studied included girder stiffness, bridge length, slab thickness, straight and draped tendons, diaphragm stiffness and bridge skew.

6.2.2 Finite Element Modeling. Typical mesh configurations are shown in Fig. 6.3. The equivalent loads for the straight prestress profile are basically horizontal transverse nodal loads. For the draped prestress profile, the equivalent nodal loads are horizontal transverse nodal loads and vertical nodal loads determined from load balancing concepts.

6.2.3 Parametric Investigations. The effects of the parameters were compared in terms of the top and bottom transverse stresses in the slab at the six different critical locations on the bridge shown

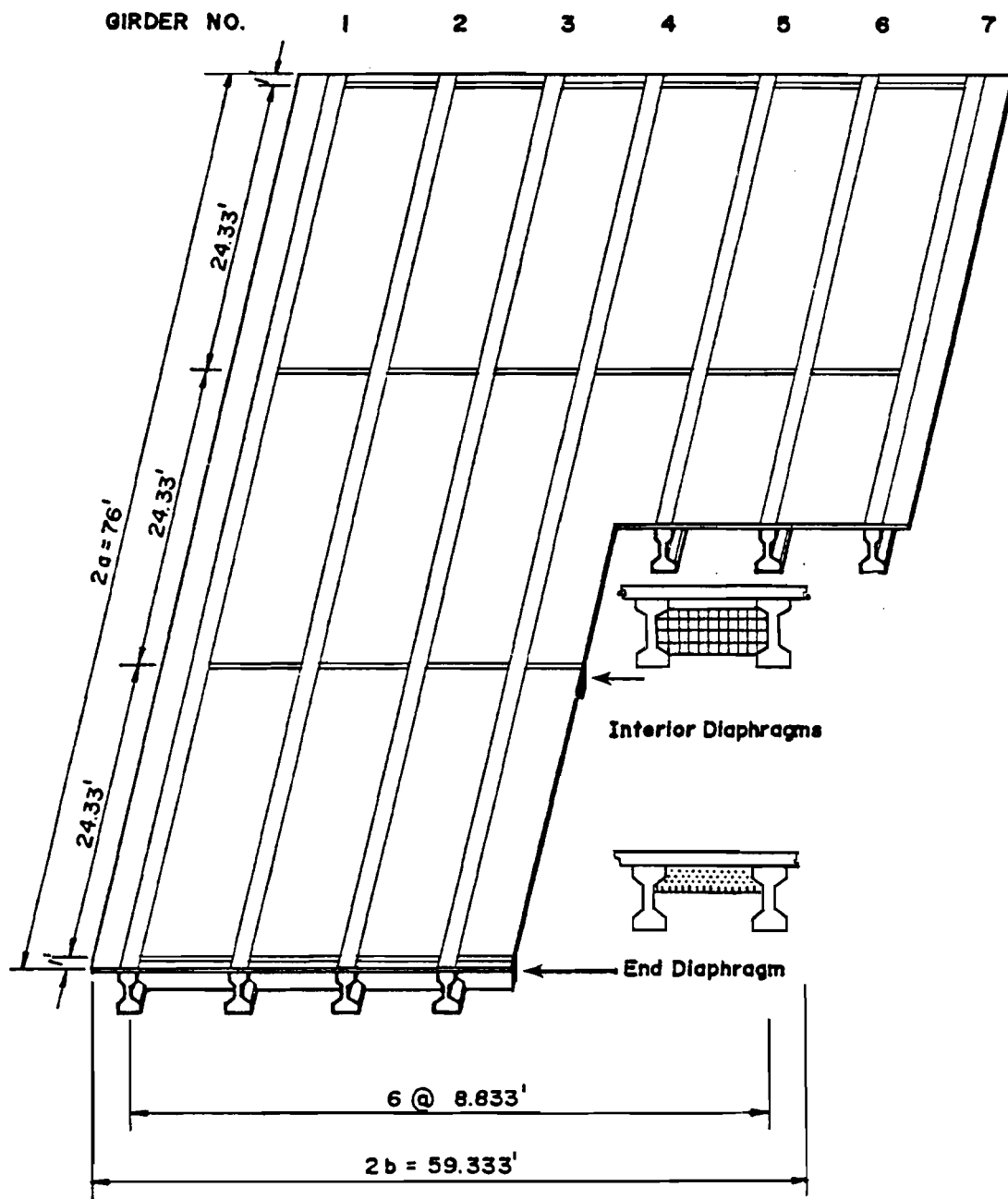
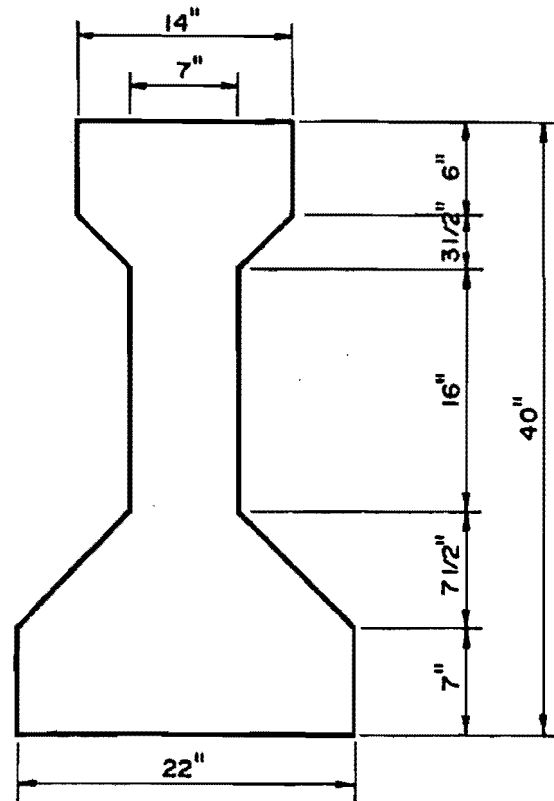
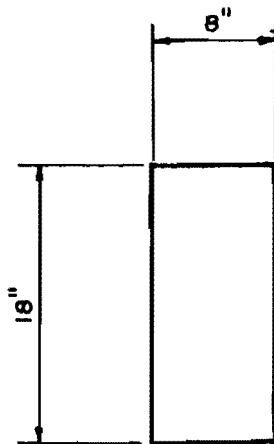


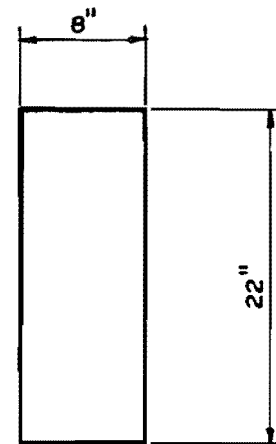
Fig. 6.1 Layout of a typical bridge



(a) Texas I - Girder Type C



(b) End Diaphragm



(c) Interior Diaphragm

Fig. 6.2 Girder and diaphragm dimensions

Table 6.1 Material Properties of Girders, Diaphragms and Slab

	Area or Thickness (in.)	Long. Moment of Inertia (in. ⁴)	Lateral Moment of Inertia	Eccentricity* (in.)	Modulus of Elasticity (ksi)	Shear Modulus of Elasticity (ksi)
Girder	A = 495	82602	8632	27.035	4460	1828
End Diaphragm	A = 144	3888	768	13.125	4460	1828
Interior Diaphragm	A = 176	8111	981	15.625	4460	1828
Slab	t _s = 8.25	--	--	--	4070	1696

*Eccentricity from the midsurface of the slab.

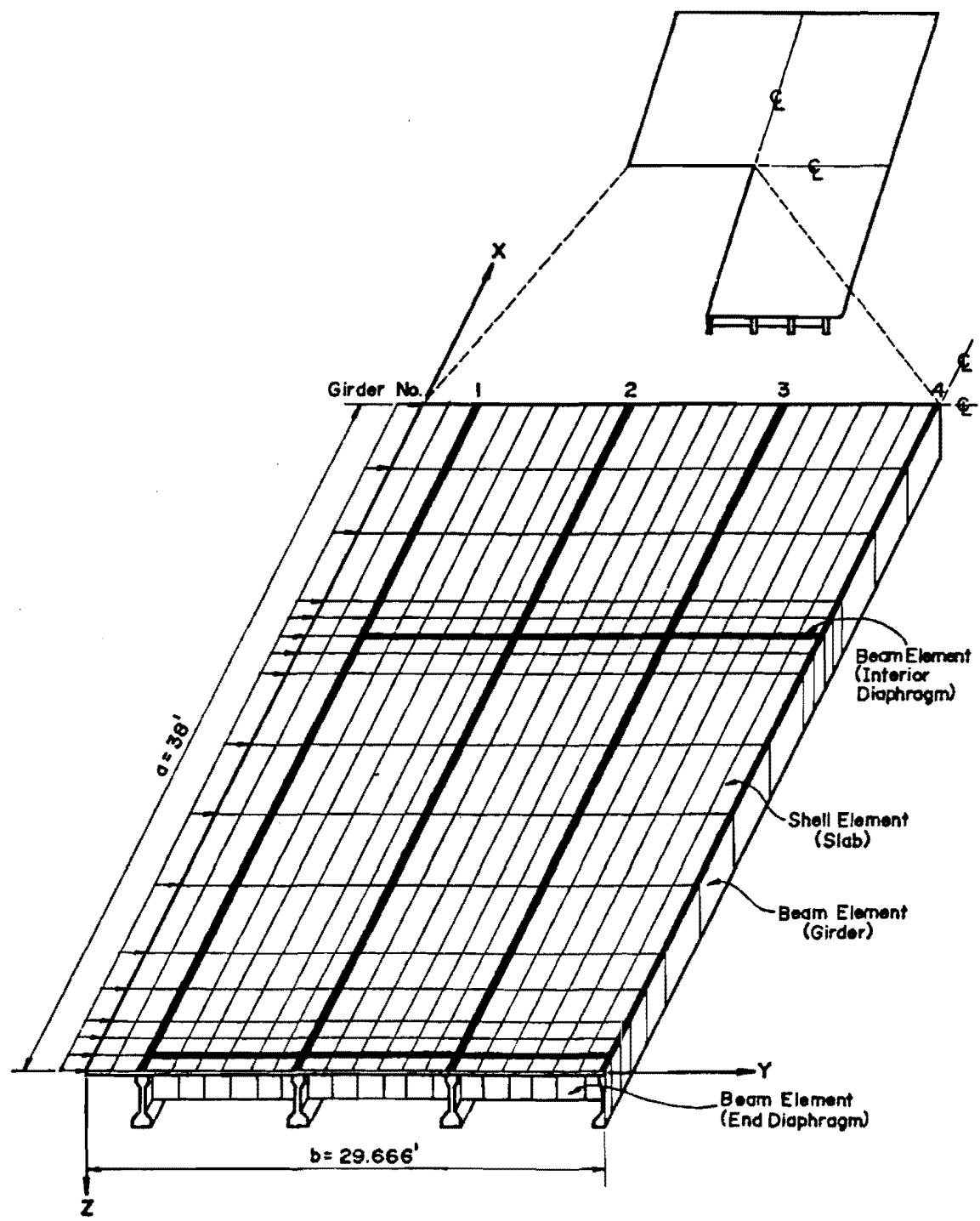


Fig. 6.3 Finite element mesh configuration

in Fig. 6.4. For simplicity the transverse stresses are displayed as contours of percentages of the unrestrained (unaffected) stresses in the transversely prestressed slab when the longitudinal girders and transverse diaphragms do not exist.

The effects of the parameters were also measured in terms of the maximum axial force in the end and interior diaphragms. If the girders or the diaphragms do not affect slab stresses, axial forces in the diaphragms would be zero. Table 6.2 gives a list of the cases considered for each parameter.

6.2.3.1 The Effects of Lateral Stiffness of Girders. In order to study the effects of the lateral stiffness of the girders alone, all the diaphragms were omitted from the analytical model. The analysis results both for straight and for draped strands showed that the transverse stress distribution was not affected at all by the lateral stiffness of the girders even when different slab thicknesses ranging from 6.00 to 8.25 in. were considered.

6.2.3.2 The Effects of Varying Diaphragm Size. The bridge of Fig. 6.1 was analyzed with three different sizes of end and interior diaphragms as shown in Table 6.2.

Typical transverse stress contours for one quarter of the slab for the end-diaphragm only and the all-diaphragm cases with straight strands and standard diaphragms are shown in Figs. 6.5 and 6.6. For the end-diaphragm only case of Fig. 6.5 the stresses in the slab are affected only near the diaphragm regions and are mostly affected in the region of the outer two diaphragms.

For the all-diaphragm case of Fig. 6.6 the effects of adding the interior diaphragms are noticed throughout the slab, increasing the top stresses and decreasing the bottom stresses in the interior-diaphragm regions.

The results of varying diaphragm size are presented in Fig. 6.7. Figure 6.7(a), (b), (c) show the effect of diaphragm size on transverse top and bottom stresses at selected points in the slab. Figure 6.7(d) shows the effect of diaphragm size on the maximum axial force taken in either end or interior diaphragms (F_D) as a ratio of the average edge prestressing per ft (F_S).

Stresses at the remote points A, B, C, and D for the end-diaphragm only case do not change as the size of the end diaphragms change, as shown in Fig. 6.7(a) and (b) but are affected by the addition of interior diaphragms. The results show that the effect of diaphragm size was more pronounced in the end-diaphragm region than in the interior-diaphragm region. As expected, Fig. 6.7(d) shows that increasing the size of the diaphragms will increase the axial force

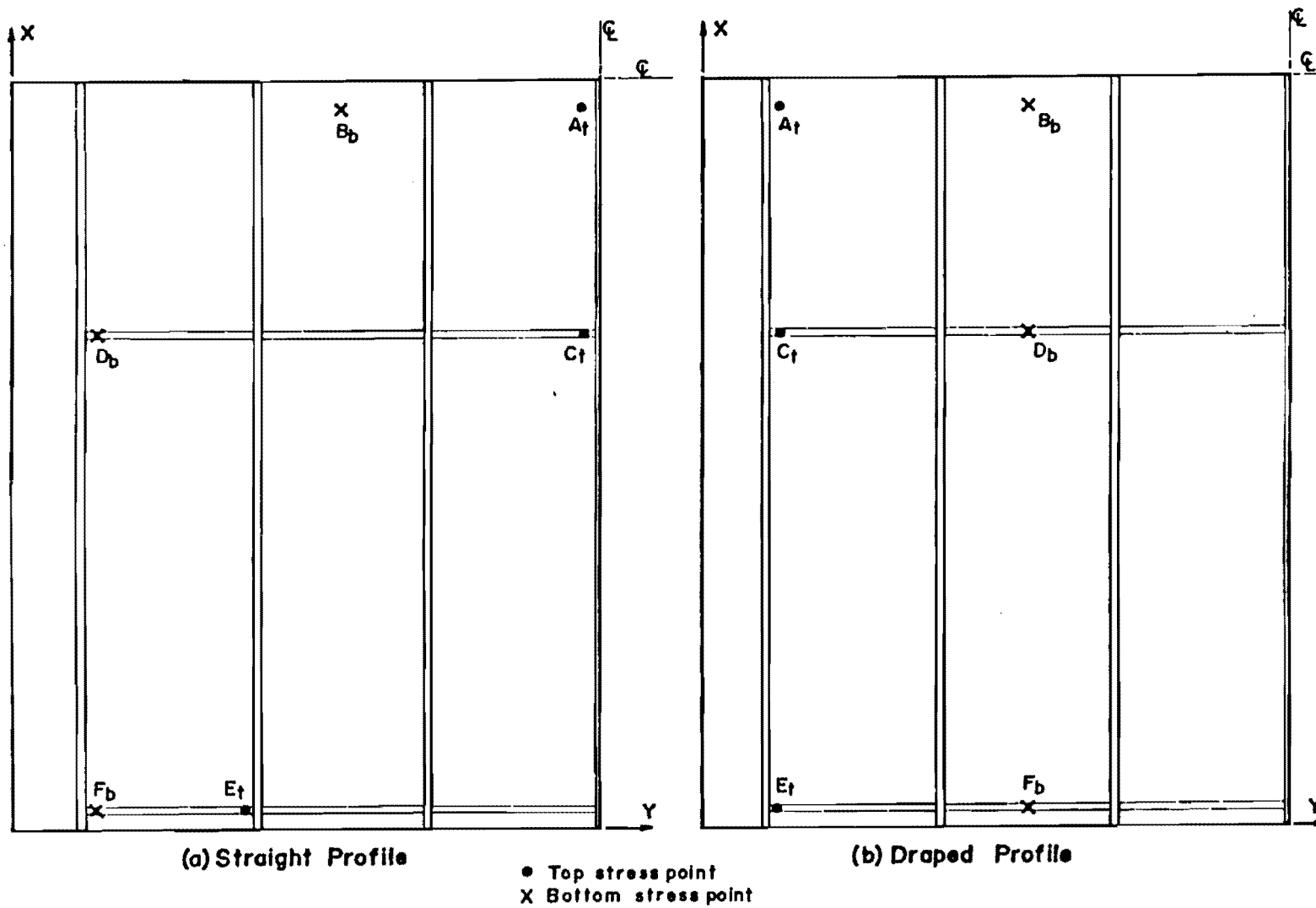


Fig. 6.4 Location of the points studied in the parametric investigation

Table 6.2 Slab-Girder Bridge
Parametric Study Cases

Parameter	Name	Diaphragm Size in. ²		Bridge Length (ft.)	Slab Thickness (in.)	Prestress Profile	Skew Angle
		End	Interior				
Diaphragm Size	SDE1	144	--	76	8.25	Straight	0 ⁰
	SDE2	264	--	76	8.25	Straight	0
	SDA3	75	75	76	8.25	Straight	0
	SDA4	144	176	76	8.25	Straight	0
	SDA5	264	264	76	8.25	Straight	0
	DDE6	144	--	76	8.25	Draped	0
	DDE7	264	--	76	8.25	Draped	0
	DDA8	144	176	76	8.25	Draped	0
	DDA9	264	264	76	8.25	Draped	0
Slab Thickness	STE1	144	--	76	6.00	Straight	0
	STE2	144	--	76	7.00	Straight	0
	STE3	144	--	76	8.25	Straight	0
	STA4	144	176	76	6.00	Straight	0
	STA5	144	176	76	7.00	Straight	0
	STA6	144	176	76	8.25	Straight	0
Bridge Length	SLE1	144	--	38	8.25	Straight	0
	SLE2	144	--	57	8.25	Straight	0
	SLE3	144	--	76	8.25	Straight	0
	SLA4	144	176	38	8.25	Straight	0
	SLA5	144	176	57	8.25	Straight	0
	SLA6	144	176	76	8.25	Straight	0
Skew Angle	SSE1	144	--	76	8.25	Straight	0 ⁰
	SSE2	144	--	76	8.25	Straight	20 ⁰
	SSE3	144	--	76	8.25	Straight	40 ⁰
	SSA4	144	176	76	8.25	Straight	0 ⁰
	SSA5	144	176	76	8.25	Straight	20 ⁰
	SSA6	144	176	76	8.25	Straight	40 ⁰

Note:

1. Cases with no diaphragms are not included.
2. Standard diaphragm area: End = 144 in.²
Interior = 176 in.²
3. Diaphragms with cross-sectional area of 264 in.² are assumed to be compositely connected to the slab.

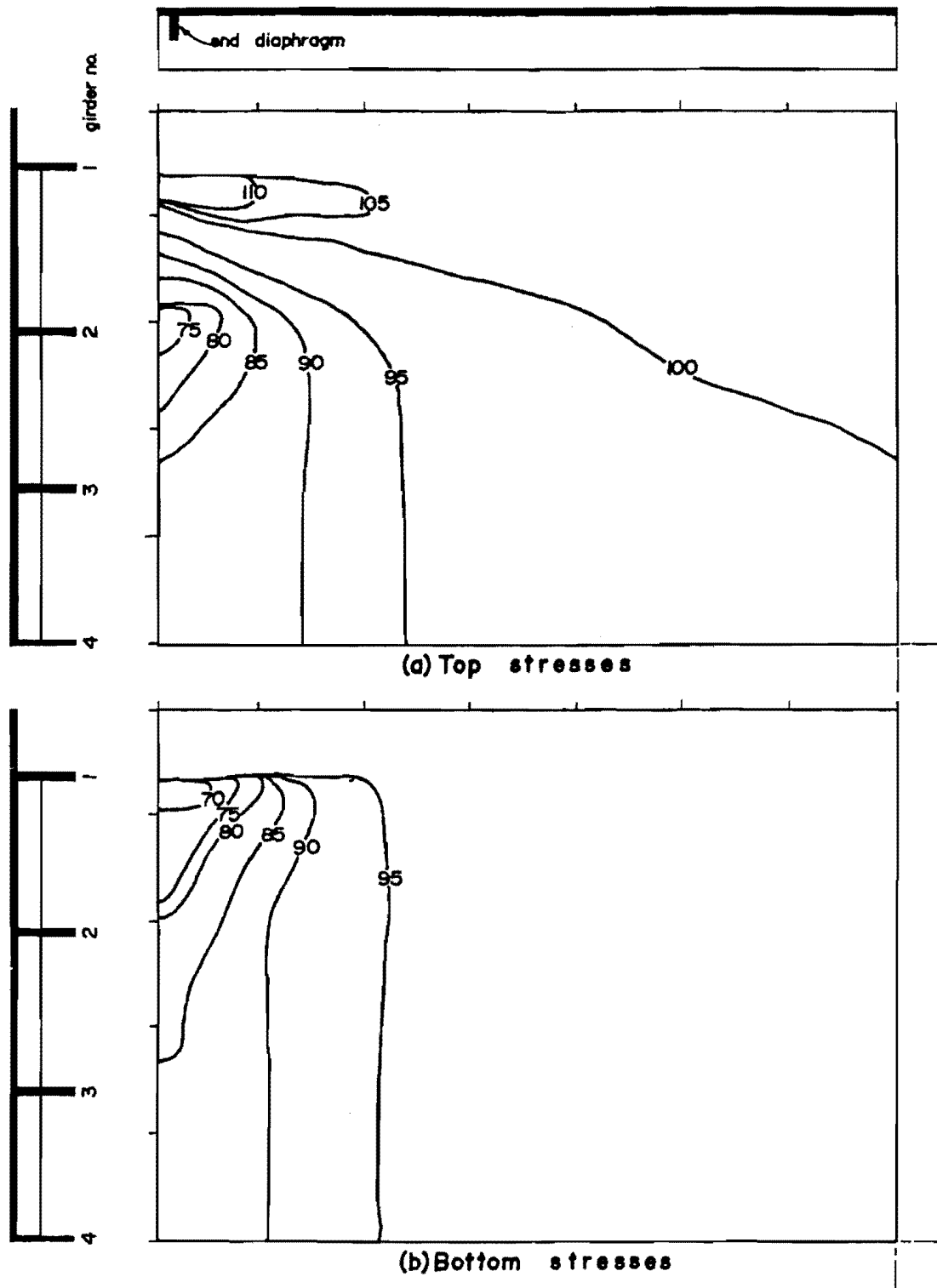


Fig. 6.5 Transverse stress distribution in deck slab, end-diaphragm case with straight strands, Case = SDE1

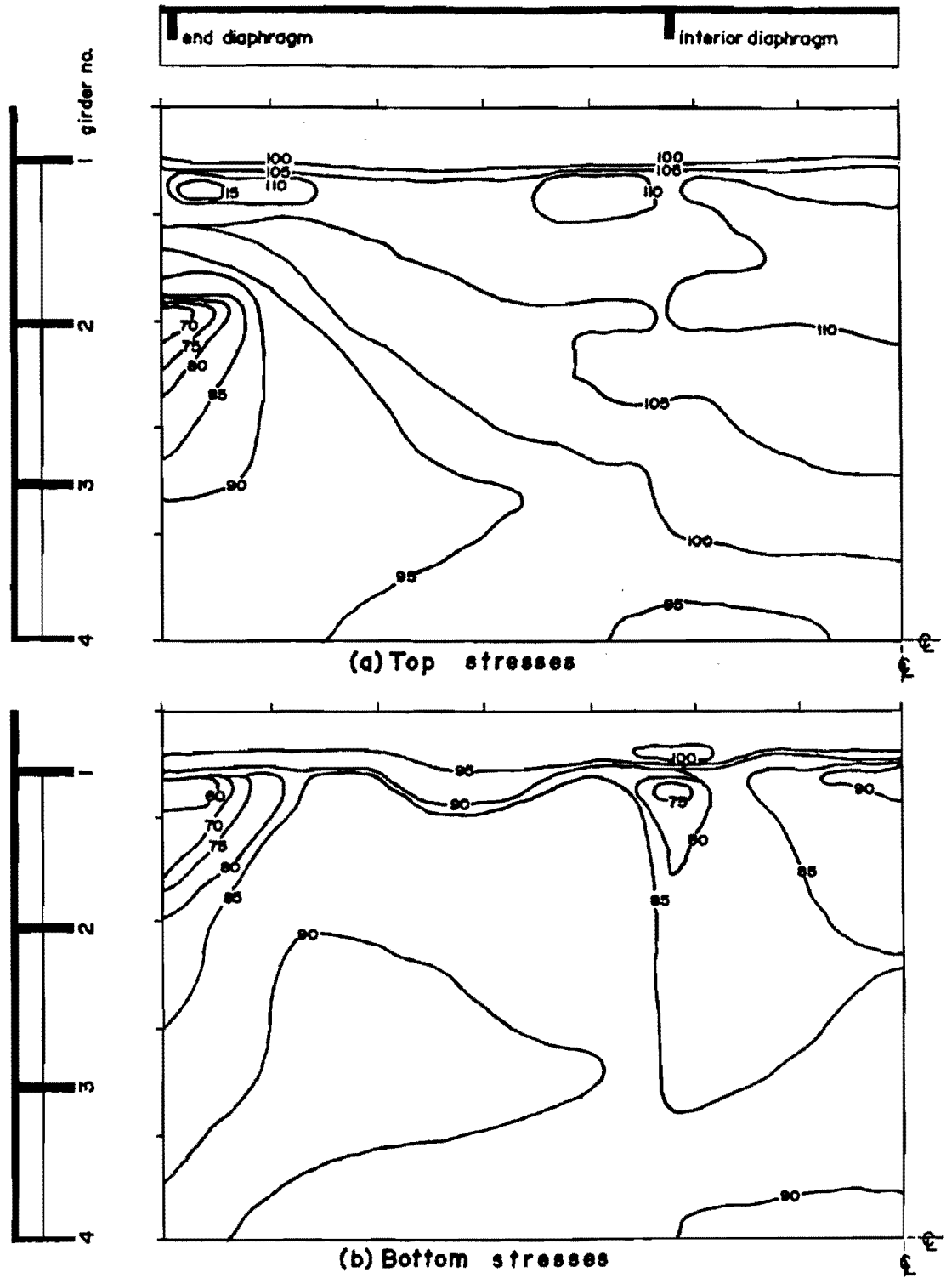


Fig. 6:6 Transverse stress distribution in deck slab, all-diaphragm case with straight strands, Case = SDA3

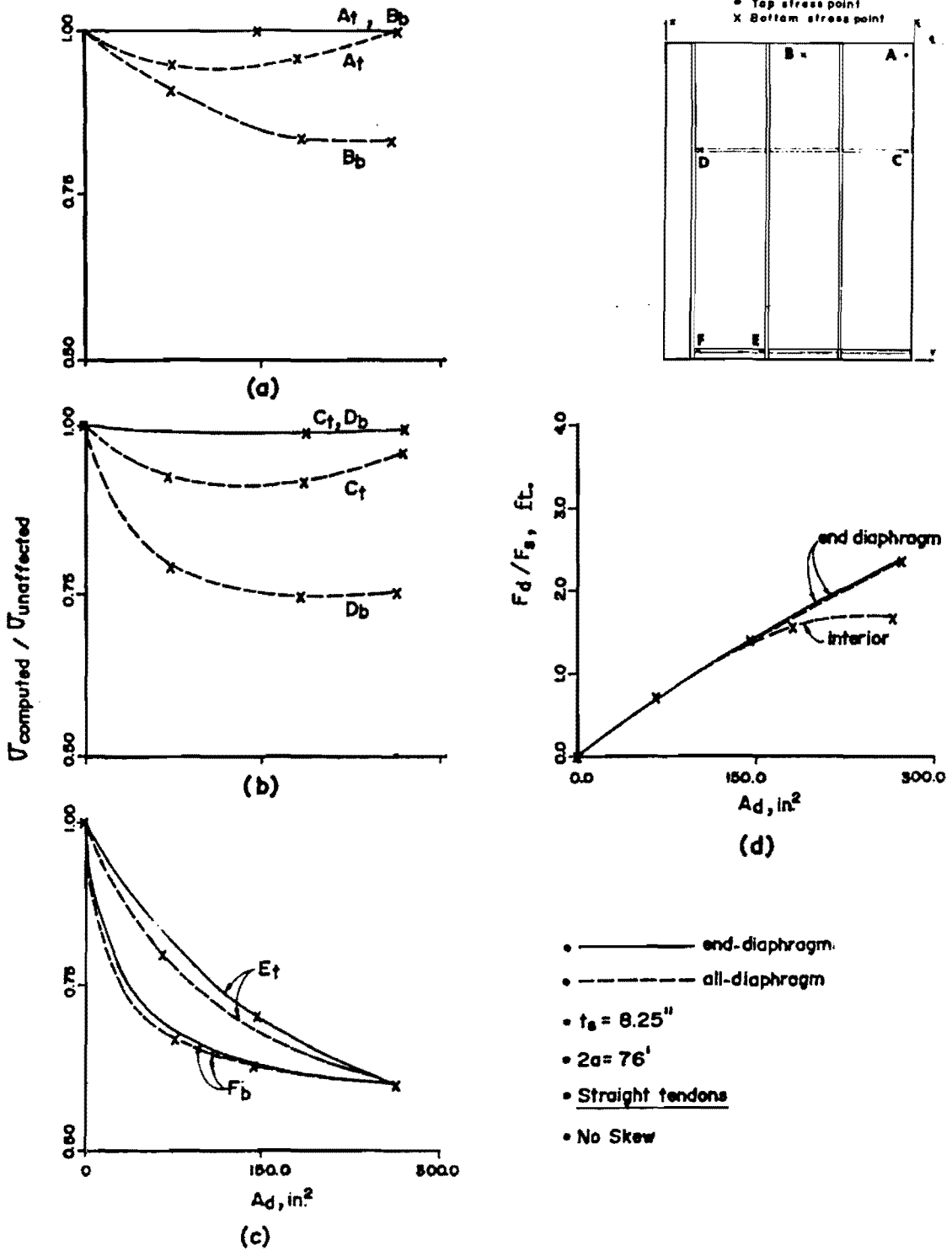


Fig. 6.7 The effect of diaphragm size on slab transverse stresses and diaphragm axial force

they attract since the stiffer diaphragm imposes more restraint on slab shortening.

The transverse stress distribution contours are even more pronounced for the end-diaphragm and the all-diaphragm cases with standard diaphragms and draped strands as shown in Figs. 6.8 and 6.9. Since draped strands produce higher compressive stresses at the highest draping points, these stresses are critical. Because of this, stress contours are only plotted for these maximum stresses. Figure 6.8 for the end diaphragm only case shows that only the diaphragm regions are affected. In contrast to the greatest variation in the slab stresses shown in Fig. 6.5 for the same case with straight strands, the variation with draped strands was practically consistent from one panel to another.

Figure 6.9 for the all-diaphragm case with draped strands shows that the addition of the interior diaphragms has resulted in a decrease in the maximum top and bottom stresses at the highest draping points in the interior-diaphragm region. The values show substantially more effect than the straight strand case.

The results of varying diaphragm size are shown in Fig. 6.10. Figure 6.10(a) and (b) show that for the end-diaphragm only case, the stresses at points A, B, C, and D are not affected by the end diaphragms. The same figures for the all-diaphragm case, show small effects at A and B but much larger effects at C and D as the interior diaphragm size increases. While the stress at F consistently decreases as the size of the end diaphragms increases, the stress at E has a minimum point and then increases at larger sizes of the end diaphragm. Both Fig. 6.7(d) and Fig. 6.10(d) show similar effect of increasing the size of the diaphragms on the maximum diaphragm axial force.

6.2.3.3 The Effects of Varying Slab Thickness. The bridge of Fig. 6.1 has been studied with practical slab thickness ranges from 6.00 in. to 8.25 in. The effects of varying slab thickness are shown in Fig. 6.11.

Slab stress and diaphragm force vary linearly with slab thickness. The effects of varying slab thickness are less pronounced than the effects of varying diaphragm size.

6.2.3.4 The Effect of Varying Span Length. Figure 6.12 shows that when the span length of the bridge shown in Fig. 6.1 is varied, that especially for the all-diaphragm case, decreasing the span length tends to increase the relative lateral stiffness of the diaphragms and girders and, consequently, increases the effects of the interior diaphragms on the transverse stresses in the slab. As is to be expected, decreasing the span length increases the restraint due to the diaphragms and thus increases the maximum axial force in them.

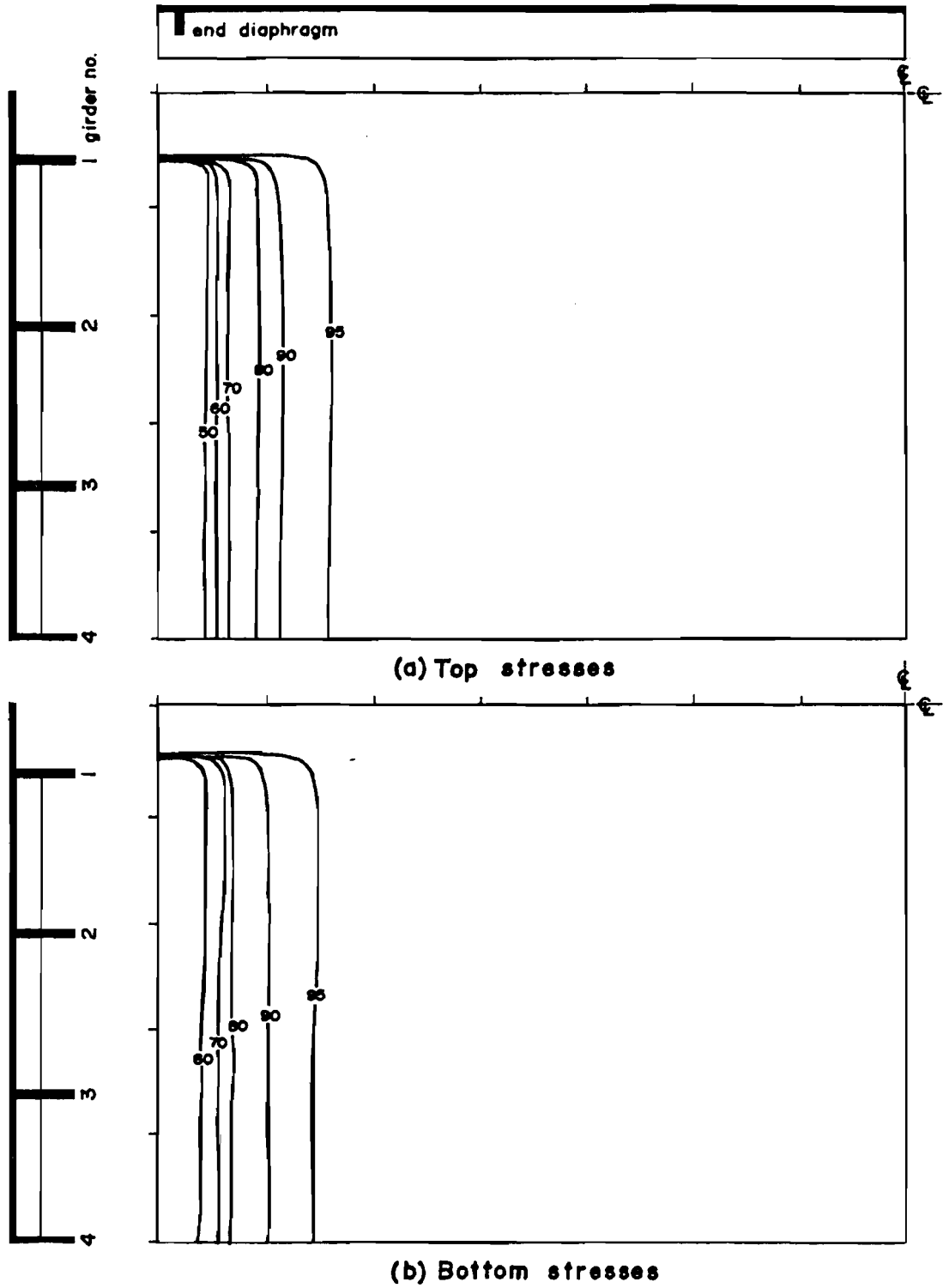


Fig. 6.8 Transverse stress distribution in deck slab, end-diaphragm case with draped strands, Case = DDE6

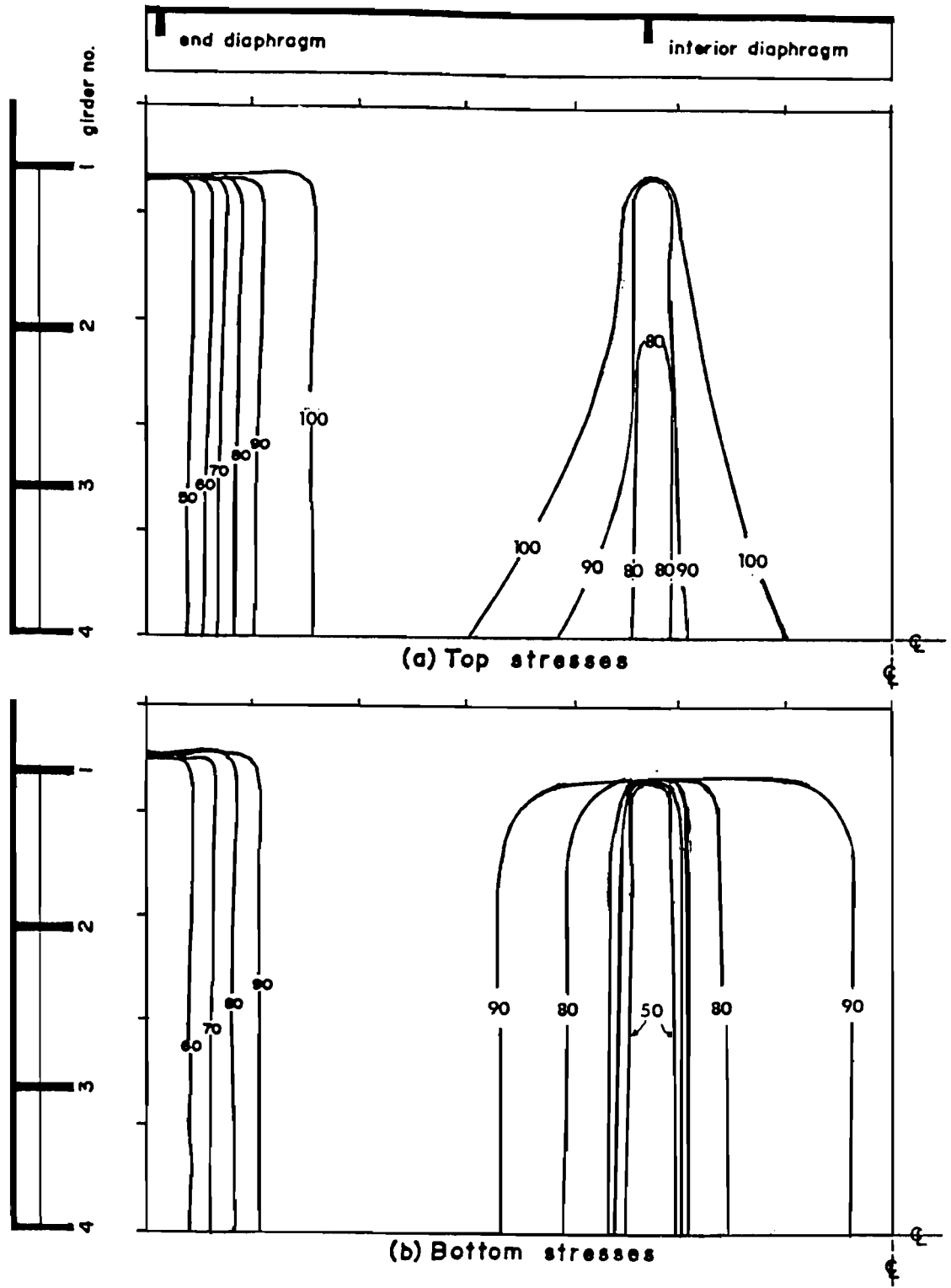


Fig. 6.9 Transverse stress distribution in deck slab, all-diaphragm case with draped strands, Case = DDA8

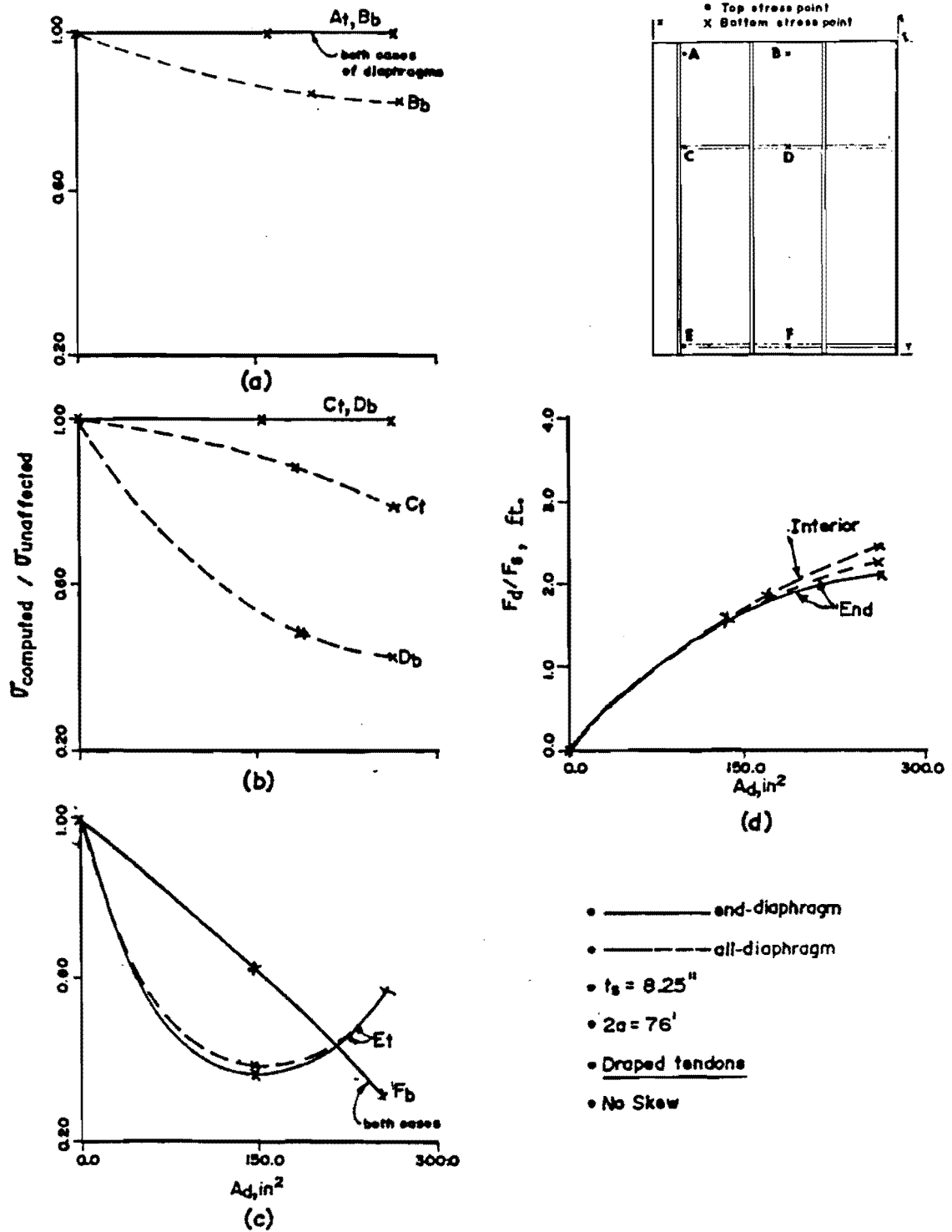


Fig. 6.10 The effect of diaphragm size on slab transverse stresses and diaphragm axial force

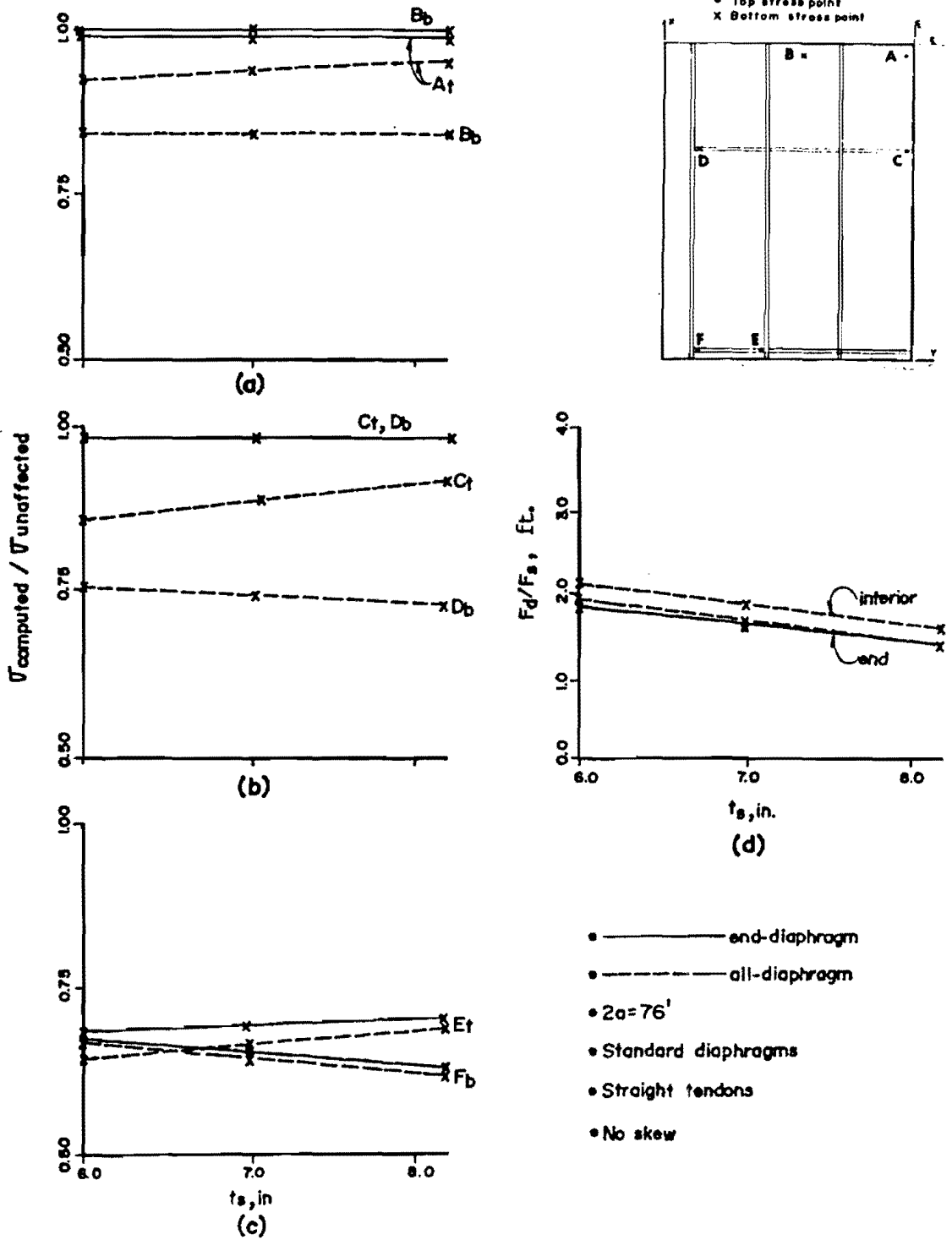


Fig. 6.11 The effect of slab thickness on slab transverse stresses and diaphragm axial force

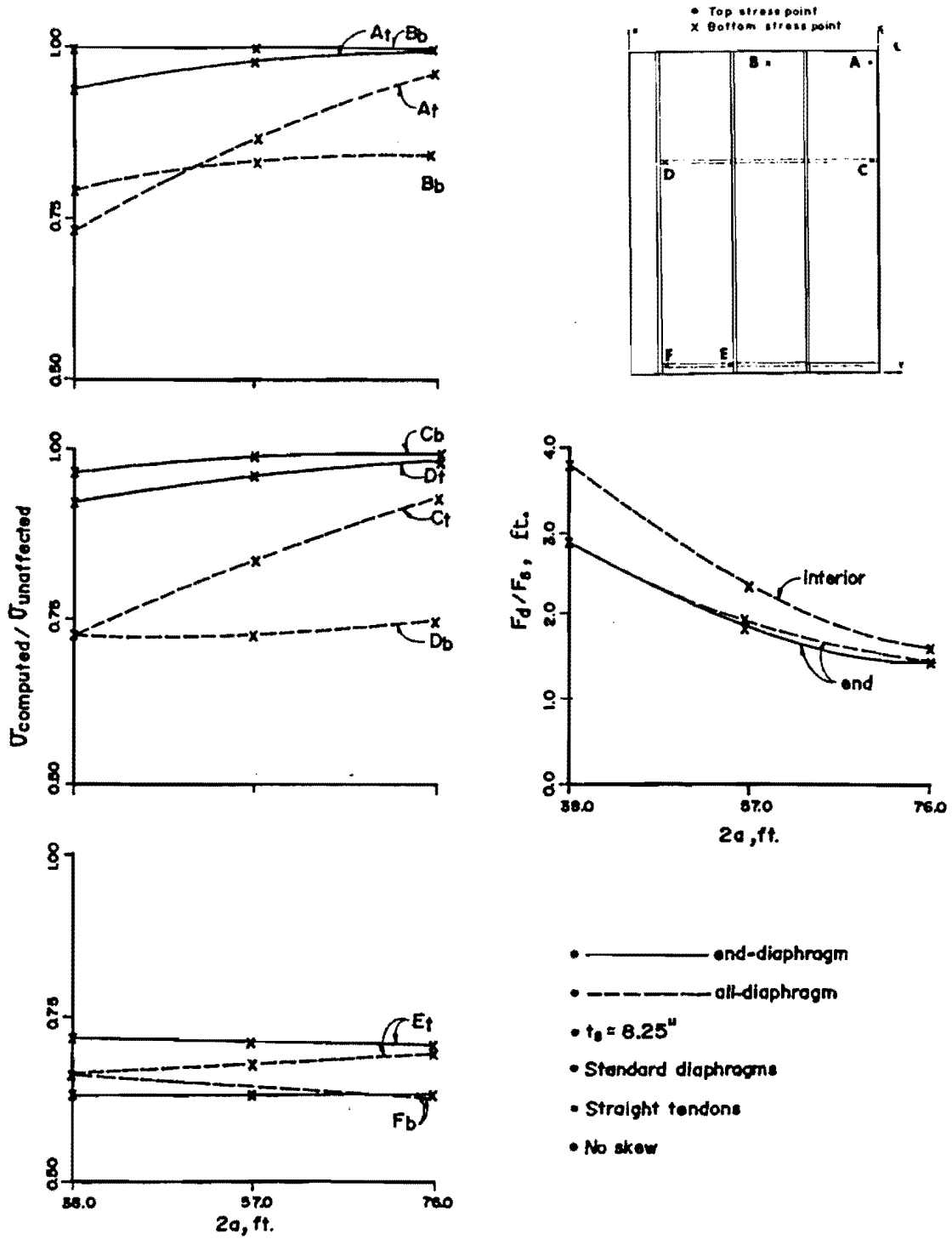


Fig. 6.12 The effect of span length on slab transverse stresses and diaphragm axial force

6.2.3.5 The Effects of Varying Bridge Skew. Since a high percentage of the bridges built are skewed, the basic bridge of Fig. 6.1 was studied with skew angles of 20 and 40 degrees. It is more favorable, from a structural point of view, to place the interior diaphragms parallel to the end diaphragms [88]; however, they are usually built perpendicular to the longitudinal girders for ease of construction as shown in Fig. 6.13. The straight transverse prestressing strands were assumed placed perpendicular to the longitudinal girders.

As a result of skewing, the symmetry of the bridge is destroyed and the complete bridge must be considered for analysis as shown for a 40-degree skewed bridge in Fig. 6.14. To simplify the mesh for the 20-degree skew, the interior diaphragms were assumed parallel to the end diaphragms. With small skew angles the structural behavior difference between the diaphragms parallel to the end or perpendicular to the girders is negligible [89].

The effects of varying skew angle on the transverse slab stresses and the diaphragm axial force is shown in Fig. 6.15. Interior slab stresses for the end-diaphragm only case do not change significantly with skew angle. For the all-diaphragm case, there is some variation at the interior points but large variations at E and F above the end diaphragms. The restraining effect of the diaphragms decreases as they become more skewed. Slab stresses at E and F return toward normal and the restraining force in the diaphragms decreases.

6.2.4 Possible Method to Account for Diaphragm Effect in Slab and Girder Bridges. The parametric study in the previous section indicates some reduction in effective prestress due to diaphragms. To counteract or compensate for this reduction, several methods are possible:

1. Applying additional transverse prestressing strands in the slab as close to the diaphragm line as possible.
2. Applying prestress force to the diaphragms themselves. By prestressing the diaphragms with a force equal to 1.4 the applied transverse force per ft of the slab, the slab and the diaphragms would have about equal shortening.
3. Inserting a thin steel plate of thickness equal to the maximum shortening in the slab, at one side of each diaphragm for construction purposes only. Prior to the application of the transverse prestressing, the plates should be removed to allow for free shortening of the slab. After the application of the transverse prestressing, the gap can be grouted.

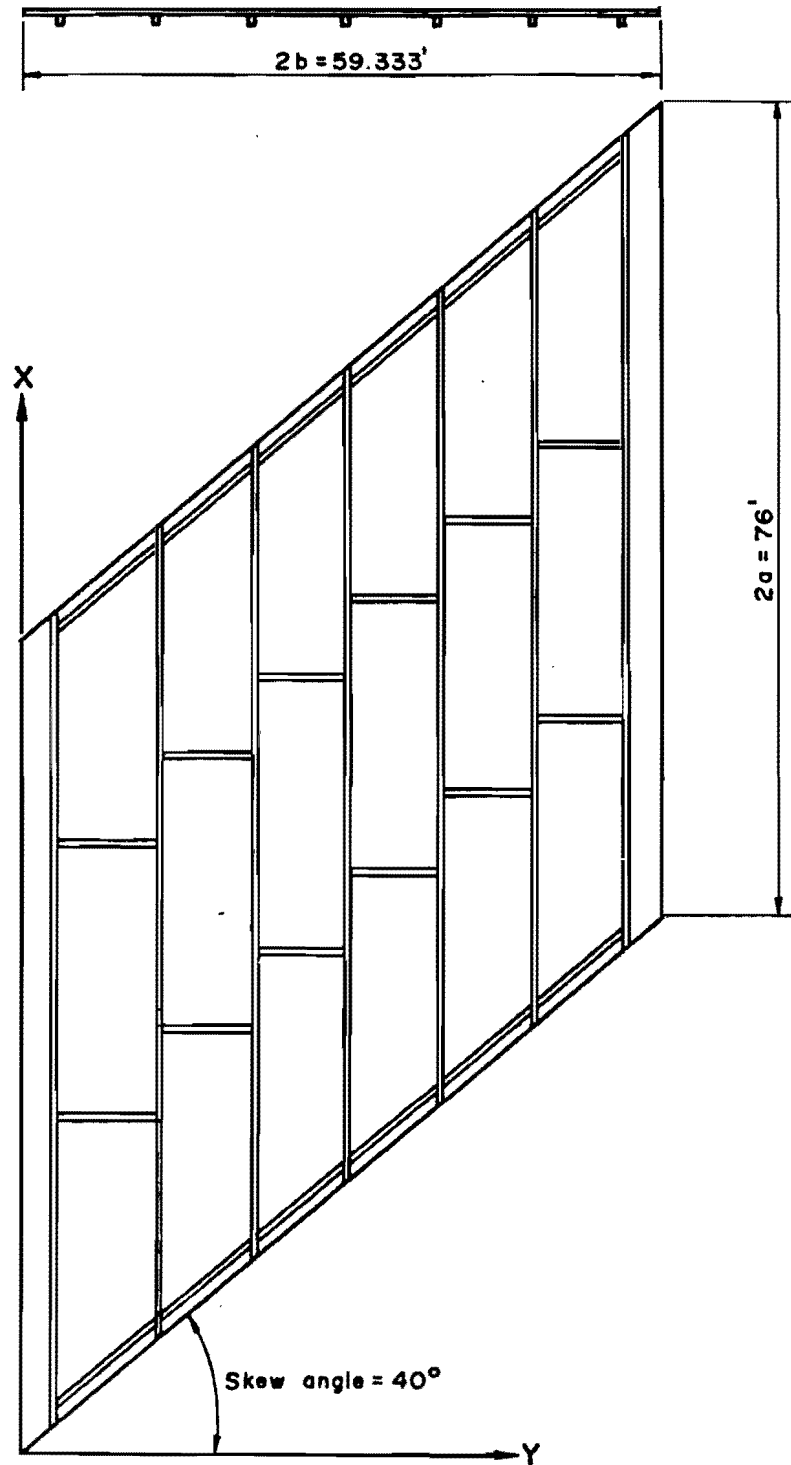


Fig. 6.13 Layout of the study bridge, 40° skew case

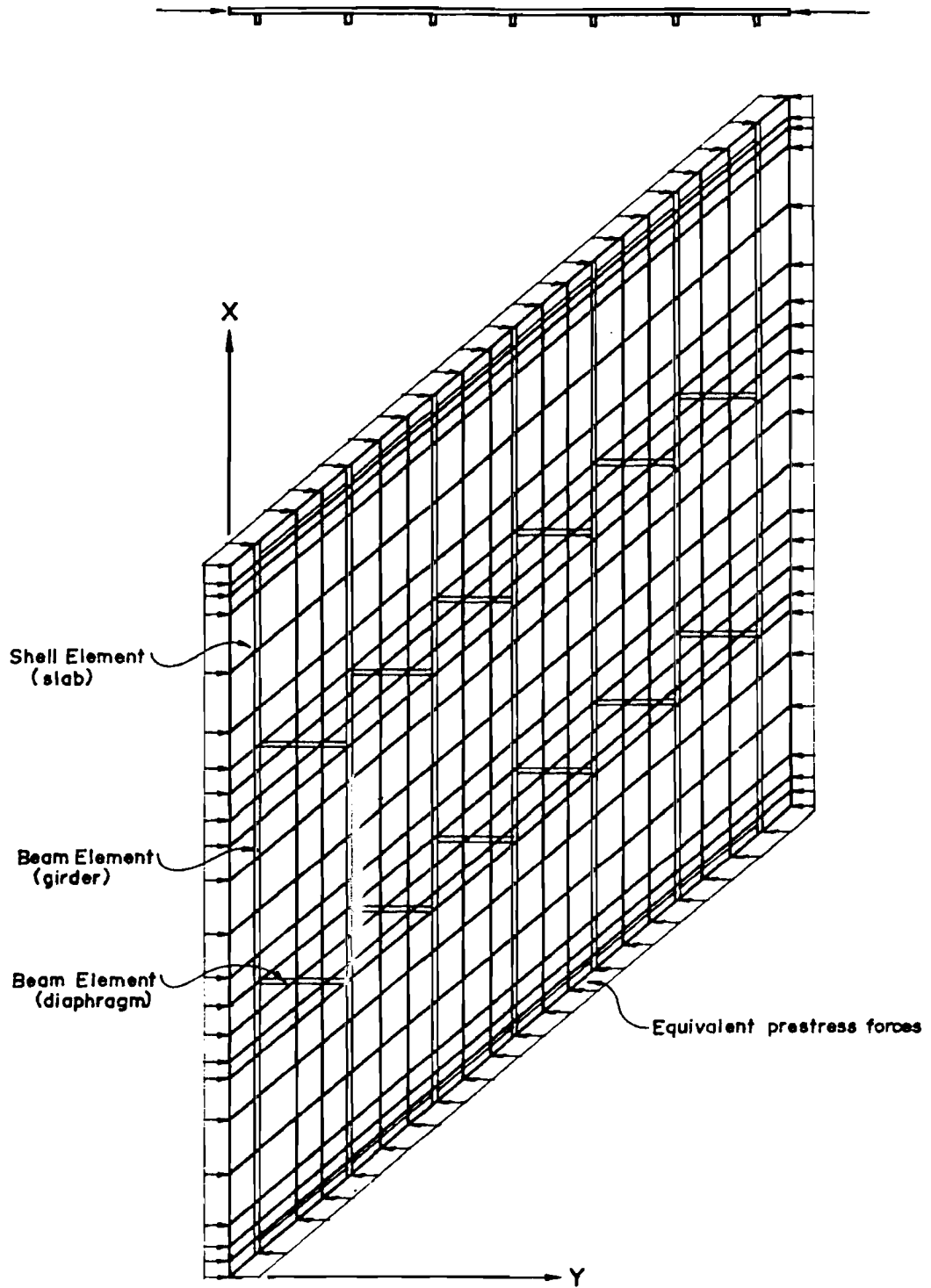


Fig. 6.14 F.E. mesh configuration of the all-diaphragm case of the study 40° skew case

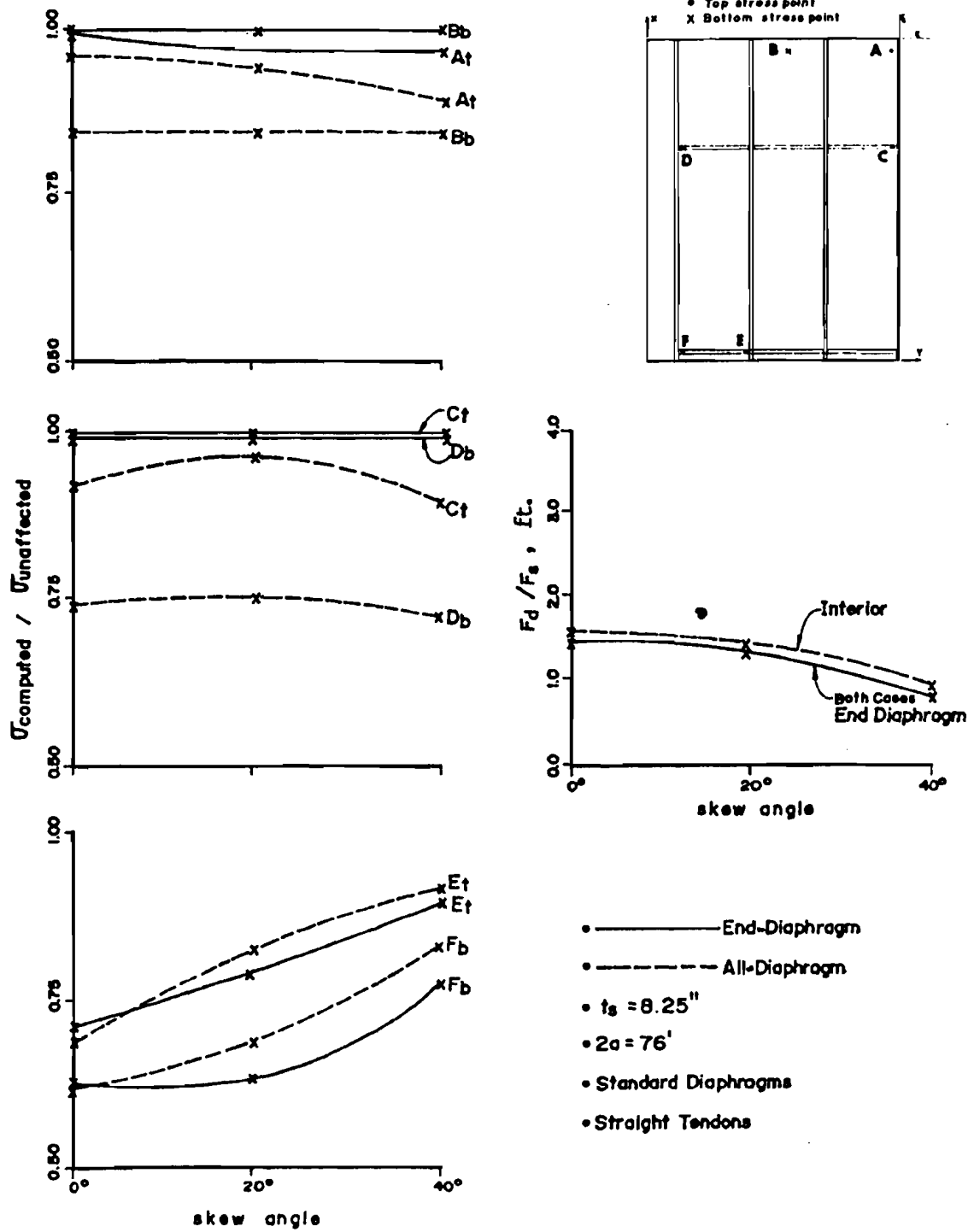


Fig. 6.15 The effect of skew angle on slab transverse stresses and diaphragm axial force

4. Omit the permanent diaphragms and use small temporary diaphragms for construction bracing which can be removed before transverse prestressing.

6.3 Box-Girder Bridges

In contrast to the open-section configuration of the slab-girder bridges treated in the previous section, box-girder bridges have closed-section configurations. In the open-section slab-girder bridges, the transverse elastic shortening of a transversely prestressed slab will definitely generate additional transverse moments and stresses that should be distributed throughout the section. Eventually, these additional moments alter the transverse stress distribution in the slab. They must be accounted for in the design of transversely prestressed box girder bridge decks.

6.3.1 Descriptions of the Bridges Studied. Based on reviews of Refs. 90 and 91, three typical sections with the same roadway width shown in Fig. 6.16 were chosen for the parametric investigations. The range of the parameters for each section used in these investigations is listed in Table 6.3.

Because intermediate interior diaphragms are not usually required in concrete box-girder bridges [90,91,92], the analysis of an interior portion of the bridge with a uniformly transversely prestressed deck is reduced to the simple case of a frame subjected to transverse loads in the top member. This is not true in the regions near the end diaphragms. As a result of this, it was decided to divide the parametric study into two parts.

The first part included the study of the effects of the top and bottom slab thicknesses, section depth, and web inclination on the transverse stress distribution in the top slab of an interior portion of the bridge using frame analysis. The results are reported in Ref. 60. They may be briefly summarized as:

1. Due to the restraining action of the webs and bottom slab on the transverse movement of the top slabs of the three sections, the smallest change in the transverse stresses in the top slab are found in the one-cell section. For straight strands, the maximum increases or decreases in the transverse stresses in the top slab are less than 10, 15, and 30% for one-, two-, and three-cell sections, respectively.
2. Draped strands produced less variation in the transverse stresses in the top slab than the straight strands.

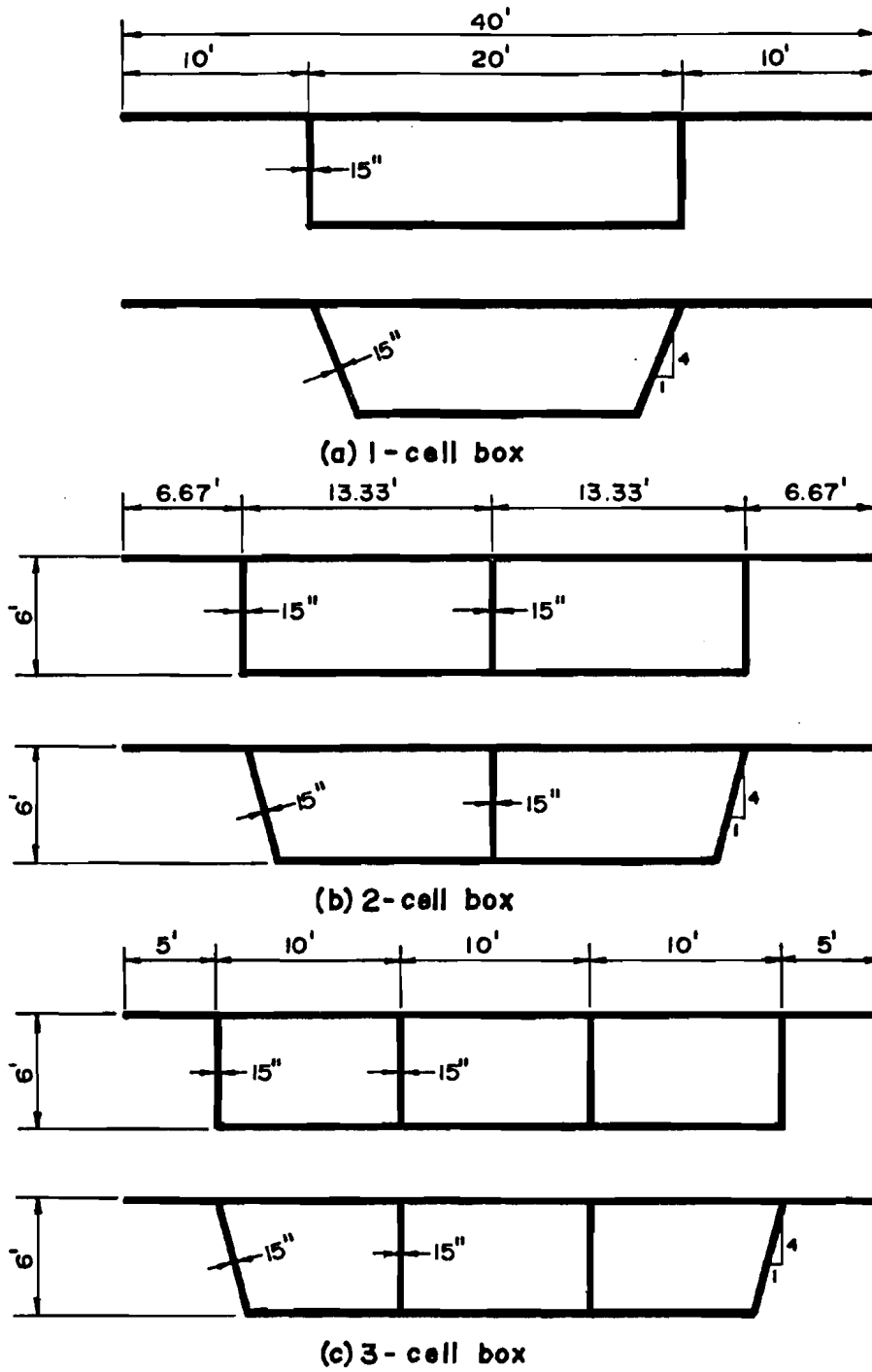


Fig. 6.16 Typical box girder bridge sections

Table 6.3 Parametric Study Cases, Part II

Section	Case	t_{s_t} , in	t_{s_b} , in	D, ft	Strand Profile	Web	Diaphragm
1-cell	1	11	12	6	Straight	Vertical	End
	2	11	12	6	Draped	Vertical	End
	3	11	12	6	Straight	Vertical	Pier, Type I
	4	11	12	6	Draped	Vertical	Pier, Type I
2-cell	1	8	12	6	Straight	Vertical	End
	2	8	12	6	Draped	Vertical	End
	3	8	12	6	Straight	Vertical	Pier, Type I
	4	8	12	6	Draped	Vertical	Pier, Type I
3-cell	1	8	12	6	Straight	Vertical	End
	2	8	12	6	Draped	Vertical	End
	3	8	12	6	Straight	Vertical	Pier, Type II
	4	8	12	6	Draped	Vertical	Pier, Type II

t_{s_t} = top slab thickness

t_{s_b} = bottom slab thickness

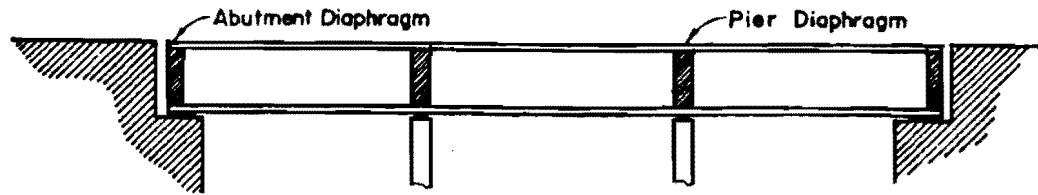
D = section depth.

3. Although the one-cell section with vertical and inclined webs had the same stress distribution in the top slab, in two- or three-cell sections, the inclined webs introduce less restraint.
4. In order to reduce the transverse moments set up in the section due to the elastic shortening of the top slab, the dimensions of the webs and bottom slab should be as small as possible.
5. The tensile stresses at the exterior bottom corners in the one-cell section are smaller than those in the two- and three-cell sections. Since the stiffness of the bottom slab in sections with inclined webs is larger than in sections with vertical webs, the tensile stresses at the bottom corners in sections with inclined webs are larger than those in sections with vertical webs. Also, tensile stresses at the bottom corners are highest near the piers because the bottom slab is thickest. The corner tensile stresses can be minimized by the use of the thinnest possible sections that are consistent with strength requirements, and with the use of vertical webs.
6. It appears that the most efficient section, from the application of transverse prestressing point of view, is the one-cell section.

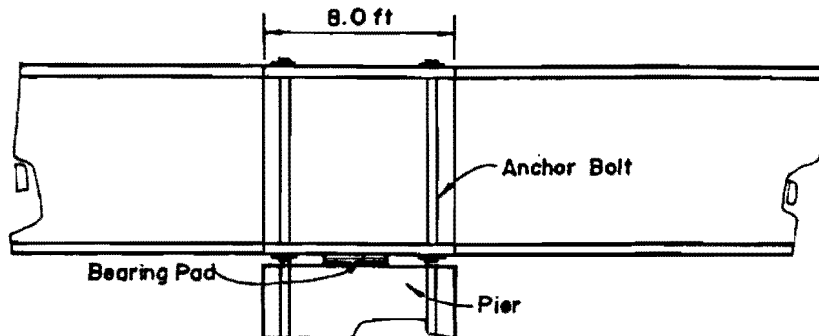
The second part included the study of the effects of the diaphragms on the transverse stress distribution in the top slab using the finite element program described in Section 4.5. The effects of three typical diaphragms, shown in Fig. 6.17, were investigated. These diaphragms represent an end (abutment) diaphragm and two commonly used types of pier diaphragms. Type I is a typical diaphragm used in one- and two-cell sections while Type II is used in three- and multi-cell sections. In studying the effects of the existence of these diaphragms on the transverse stress distribution in the top slab, only portions of the corresponding affected regions were considered for analysis as shown in Figs. 6.18 to 6.20 along with their finite element idealizations.

Based on the results of Part I, it was decided to limit the finite element model investigation to the most critical parameter values that may affect the transverse stresses in the top slab as shown in Table 6.3. It can be seen that such parameter values have emphasized thick sections.

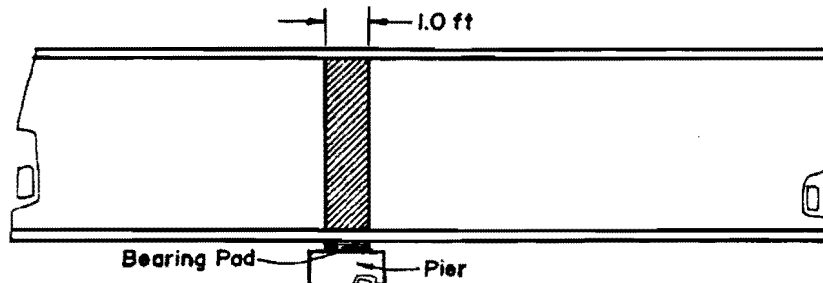
As indicated in Fig. 6.18, the Type I pier diaphragm generally used in segmental or cast-in-place one- and two-cell box-girder bridges, was not actually modeled by individual finite elements. Because such diaphragms are made relatively thick, they were assumed



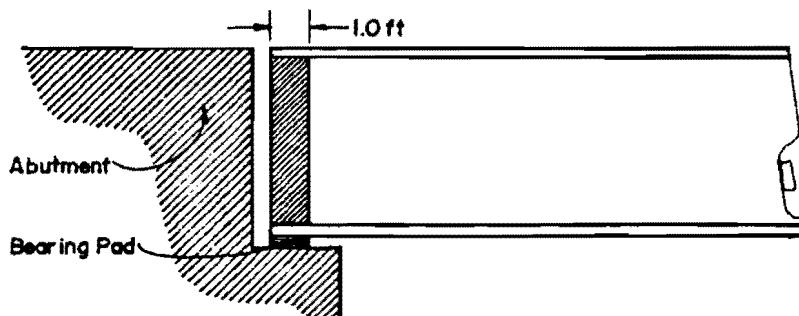
(a) Side view of continuous bridge



(b) Pier Diaphragm, Type I



(c) Pier Diaphragm, Type II



(d) End (Abutment) Diaphragm

Fig. 6.17 Typical diaphragm types and locations

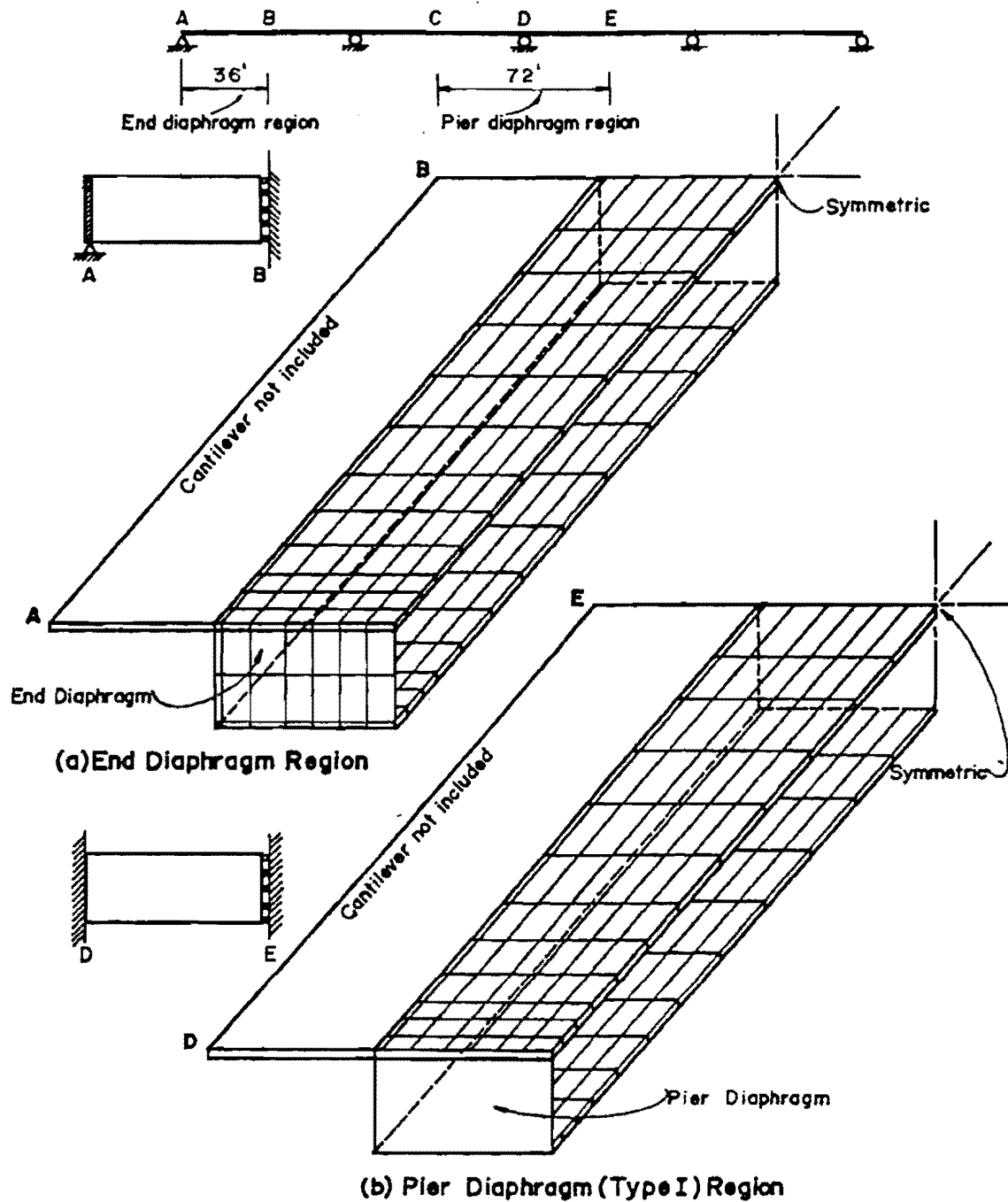


Fig. 6.18 1-cell box girder bridge: F.E. idealization of end- and pier-diaphragm regions

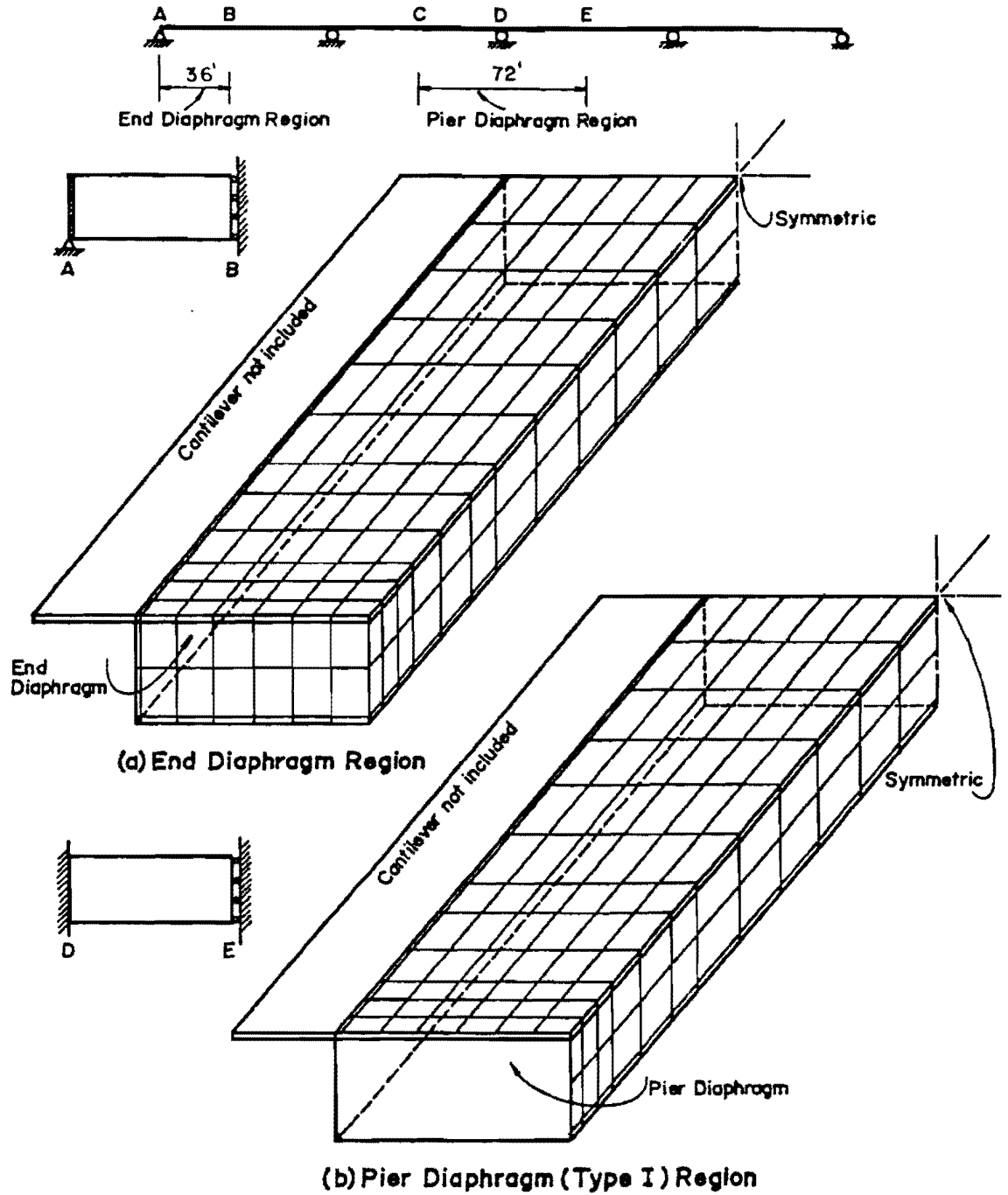


Fig. 6.19 2-cell box girder bridge: F.E. idealization of end- and pier-diaphragm regions

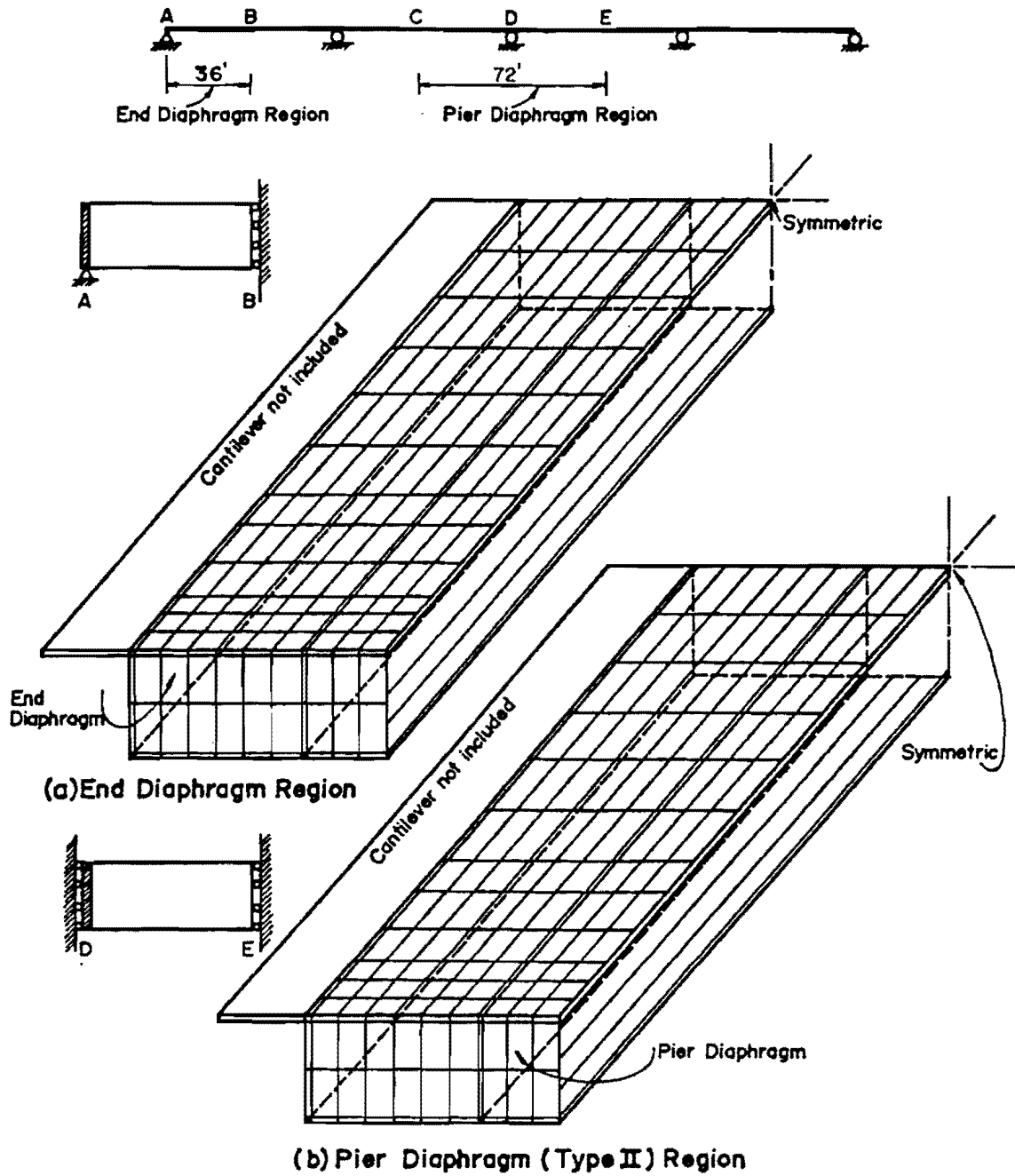


Fig. 6.20 3-cell box girder bridge: F.E. idealization of end- and pier-diaphragm regions

to be completely rigid diaphragms. In their finite element presentation, nodes at the pier diaphragm intersection were assumed to be rigidly fixed.

The finite element analysis results are only given for the transverse stress distribution in the top slab. As before, stresses are given as percentages of the nominal stresses. Stress contours for top and bottom mid surface stresses in the top slab for single-cell box girder bridges with end and pier diaphragms are shown in Figs. 6.21 to 6.23. Similar stress contours for two- and three-cell box girder bridges are shown in Figs. 6.24 to 6.27.

These figures show that the diaphragm effect on top slab transverse stresses generally follow the same trends in all three box sections. While the restraint from the end diaphragms are somewhat smaller than from the pier diaphragms, both cases cause appreciable reductions in the diaphragm vicinity. In regions adjacent to the diaphragms, top slab transverse stresses are frequently reduced as much as 45 to 90%.

When the transverse prestressing is used to provide the transverse strength of the top slab, it is certainly desirable to minimize the interaction between the diaphragms and the top slab at the time of prestressing. This is possible in segmental precast construction of box girder bridges, where transverse prestressing of the top slab is done either by pretensioning in the casting bed or by posttensioning transversely before connecting the segments together. It is more difficult in cast-in-place construction. In either case, massive transverse posttensioning of the pier and end diaphragm regions are recommended to produce better transverse compatibility.

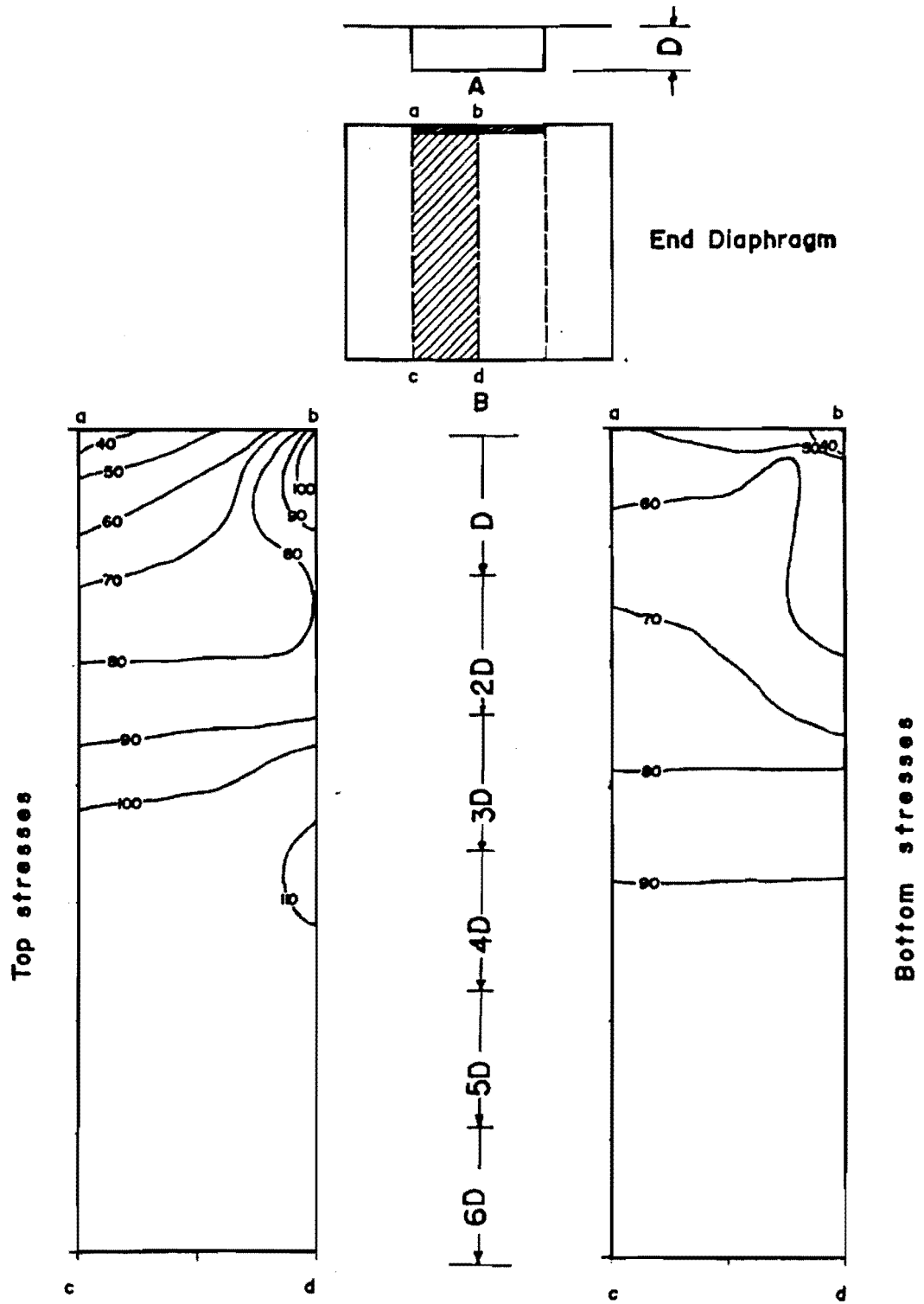


Fig. 6.21 1-cell box girder bridge: the effect of end diaphragm on top slab transverse stresses, straight strands

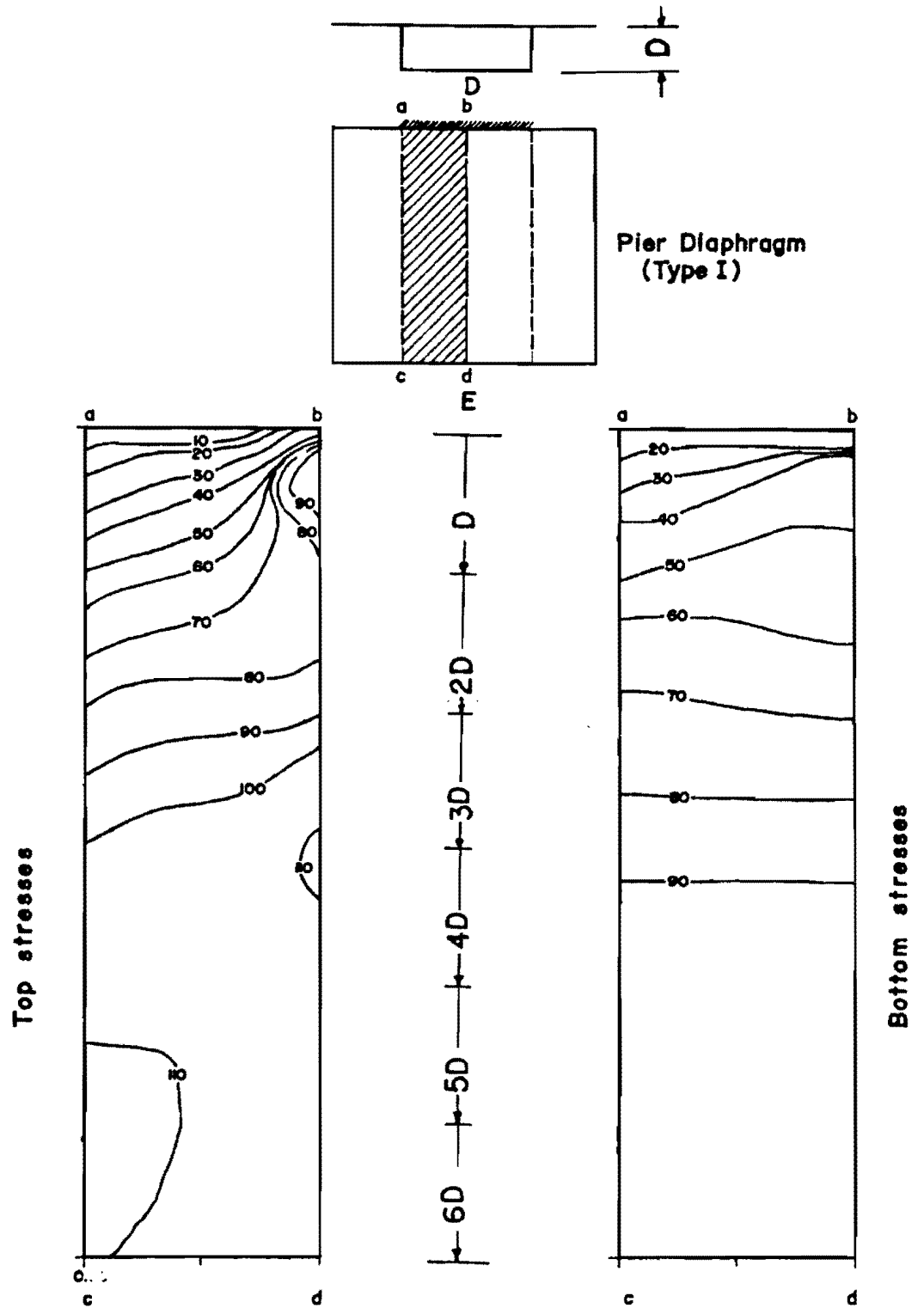


Fig. 6.22 1-cell box girder bridge: the effect of pier diaphragm on top slab transverse stresses, straight strands

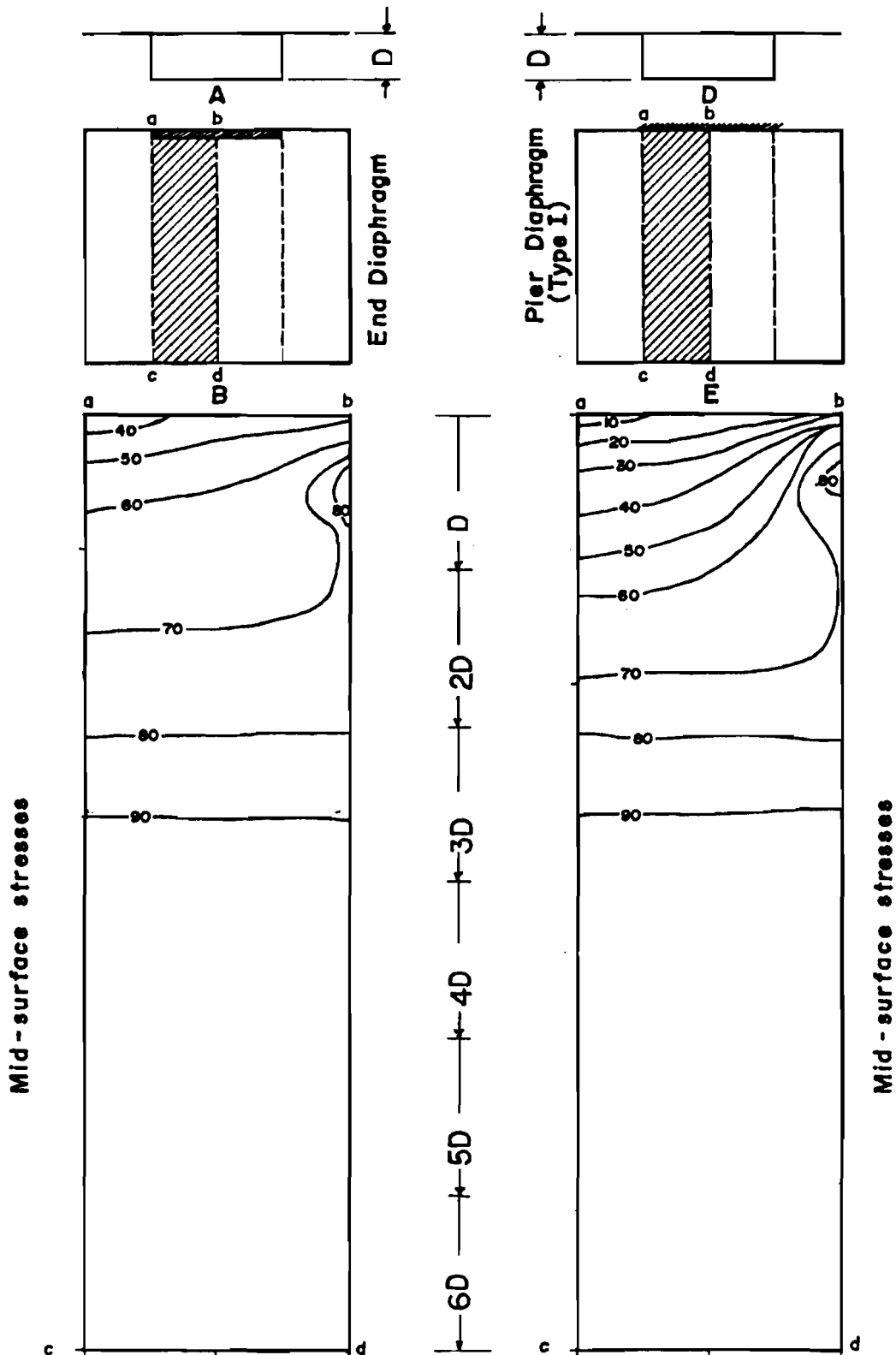


Fig. 6.23 1-cell box girder bridge: the effects of end and pier diaphragms on top slab transverse stresses, draped strands

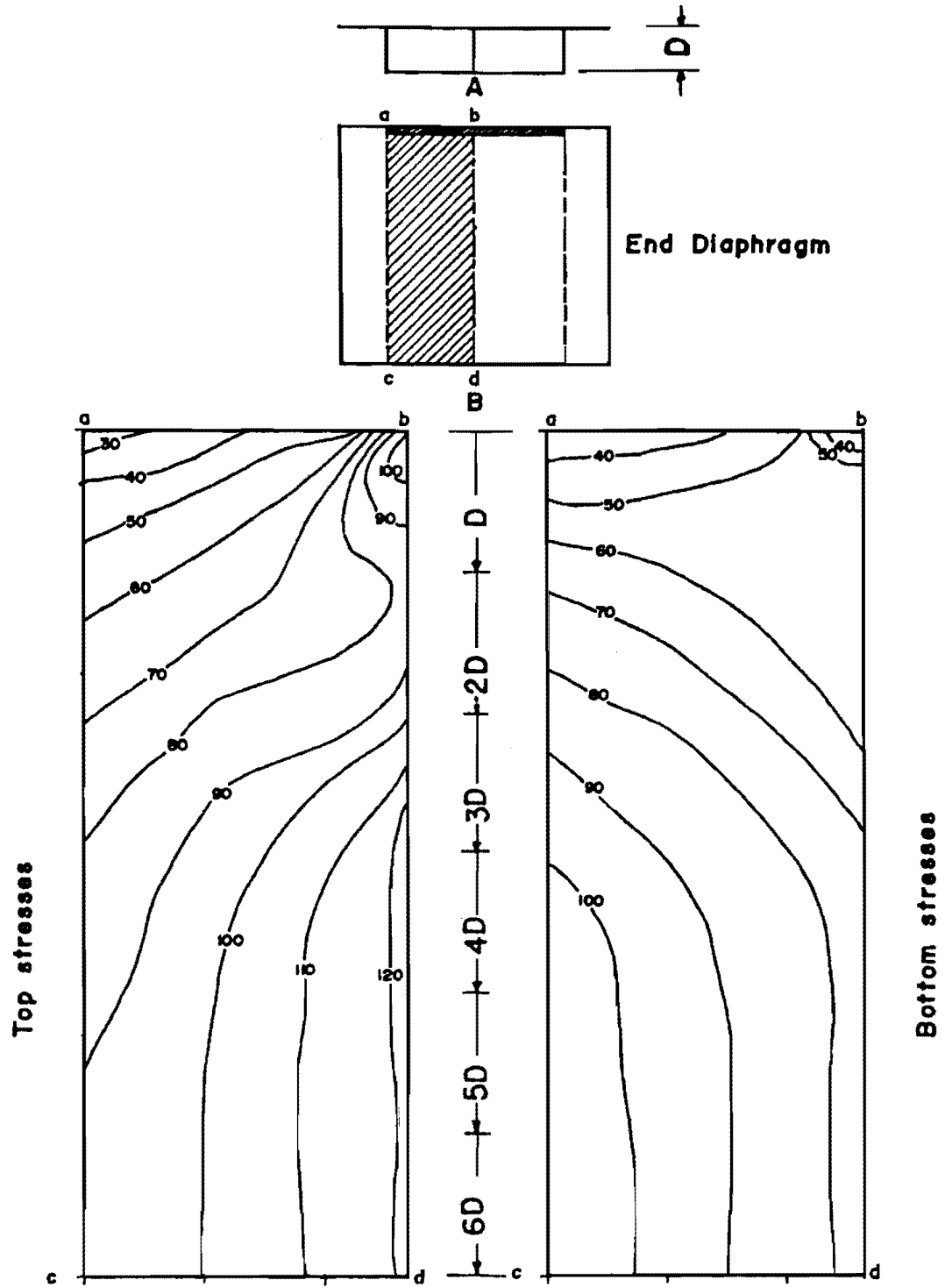


Fig. 6.24 2-cell box girder bridge: the effect of end diaphragm on top slab transverse stresses, straight strands

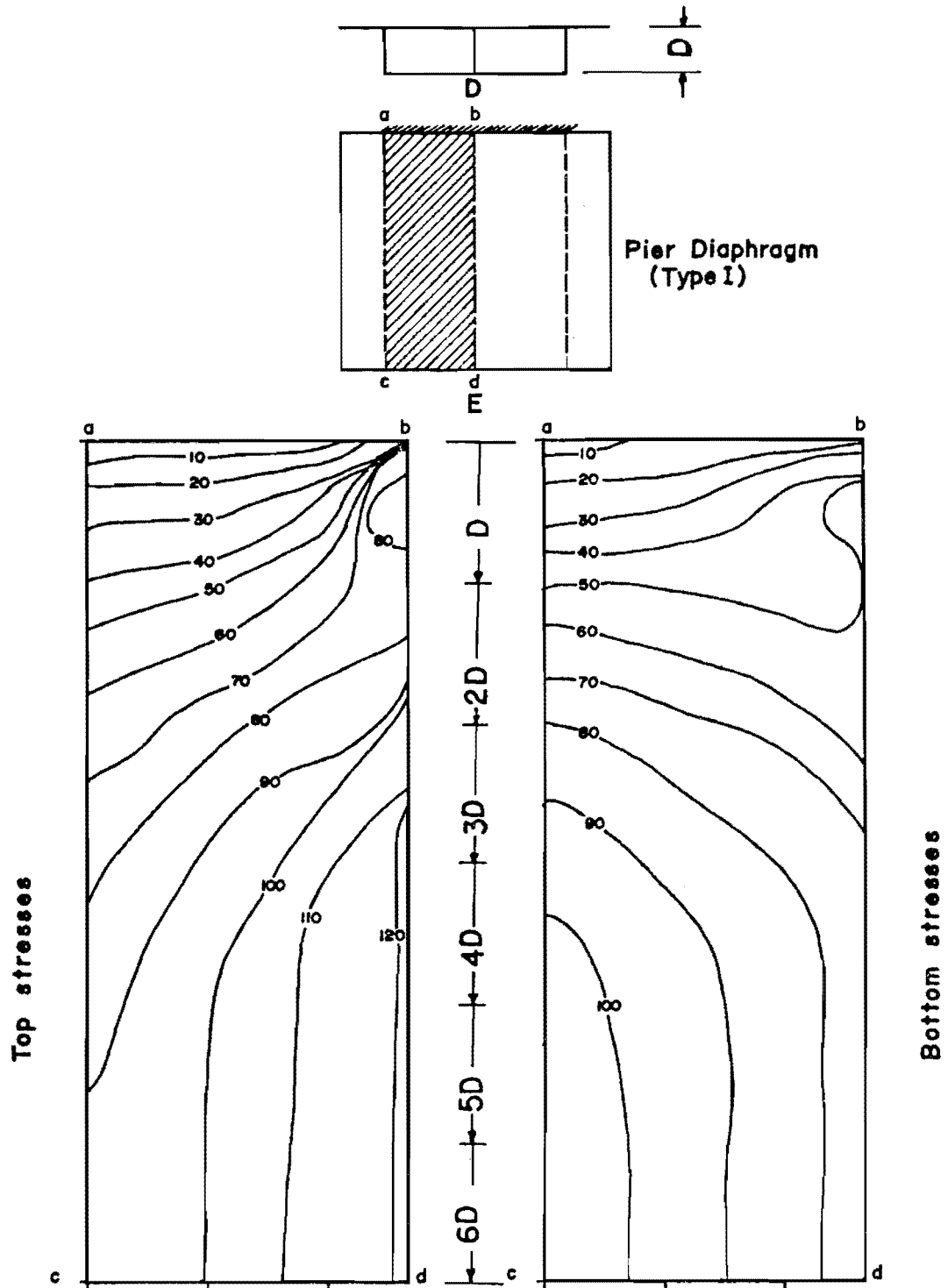


Fig. 6.25 2-cell box girder bridge: the effect of pier diaphragm on top slab transverse stresses, straight strands

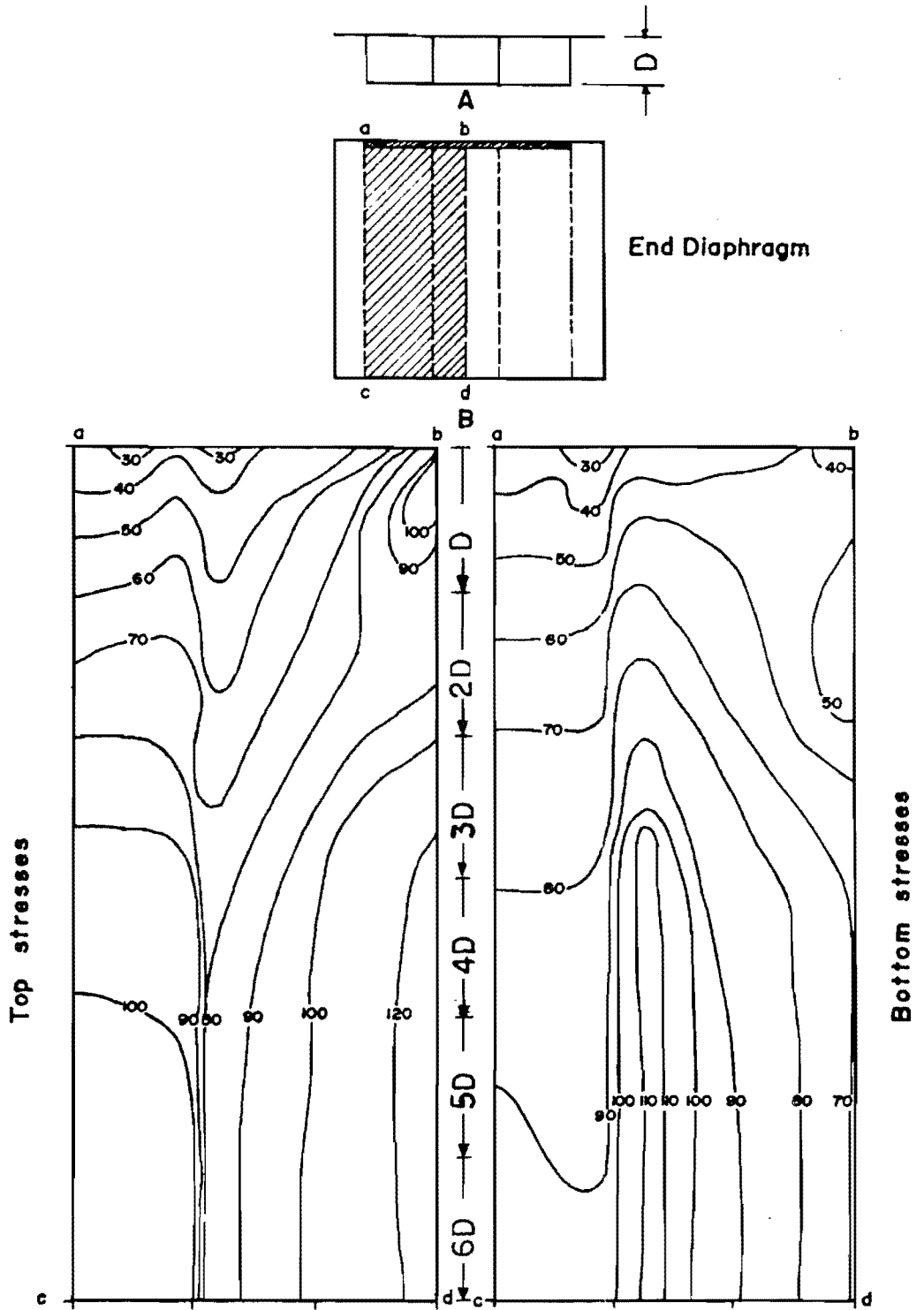


Fig. 6.26 3-cell box girder bridge: the effect of end diaphragm on top slab transverse stresses, straight strands

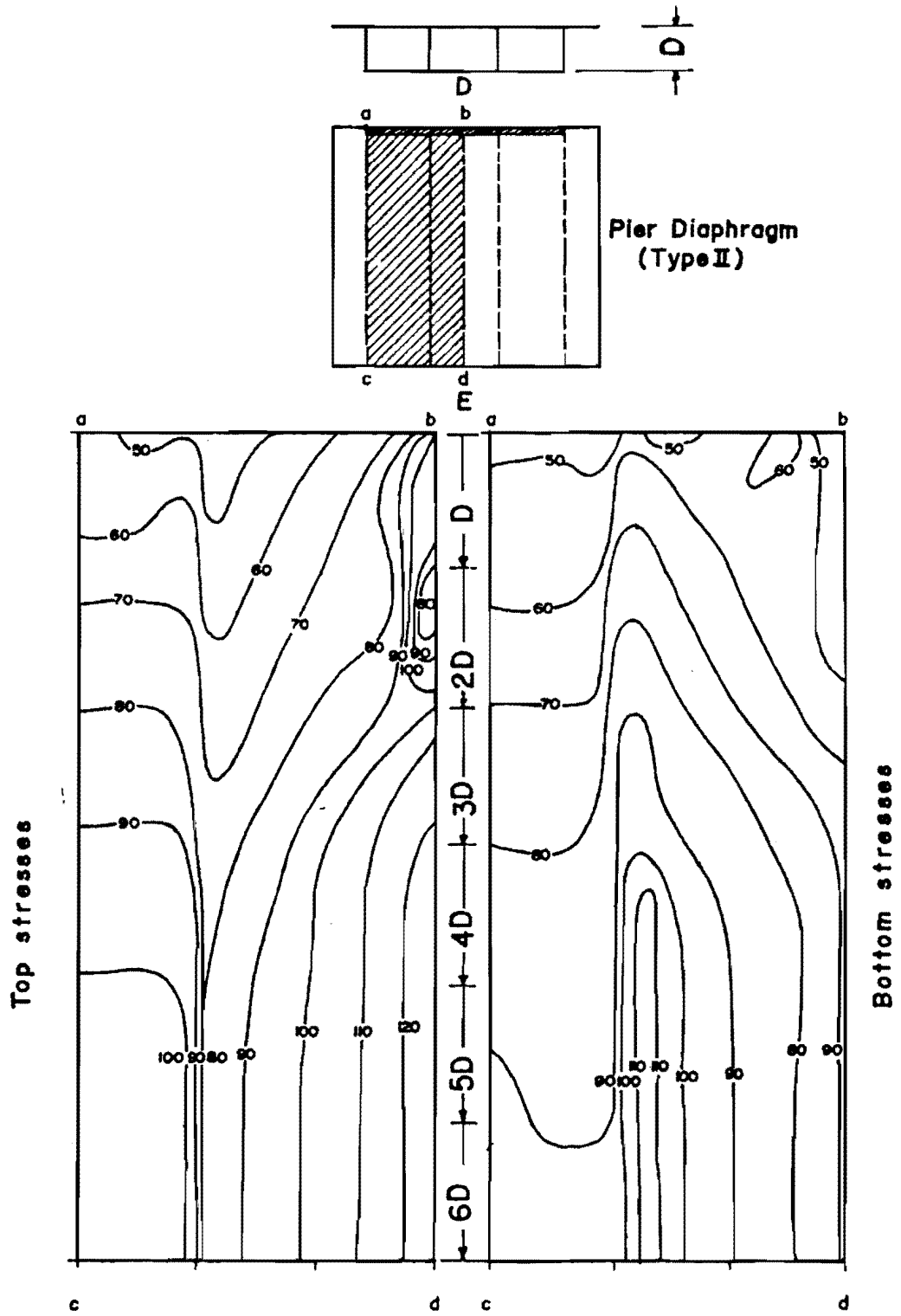


Fig. 6.27 3-cell box girder bridge: the effect of pier diaphragm on top slab transverse stresses, straight strands

C H A P T E R 7

SUMMARY, CONCLUSIONS, AND RECOMMENDATIONS

7.1 Summary

The principal objective of the overall study was to examine the concept of improving bridge deck design by the application of transverse prestressing, and to specifically examine the improvement of durability due to protection from chloride-induced corrosion. The specific objective of this report was to provide documentation of the structural analysis and behavior studies carried out in the development of recommendations for proper use of modern prestressing systems to ensure effective distribution of transverse prestress throughout deck slabs. The scope was primarily limited to bridge decks of composite slab-girder bridges; however, analytical techniques were extended to include box girder bridges. Many of the study findings are applicable to other prestressed and reinforced concrete bridge structures.

The general background of structural bridge slab theory and of transverse prestressing are summarized in Chapters 2 and 3.

To investigate the structural effects of transverse prestressing, a model bridge was constructed and tested. Effective prestress distribution as determined from the model test results was presented in Chapter 4. The structural behavior of a posttensioned slab under vertical load and the distribution of concentrated lateral edge loads as determined in the model test program are summarized in Chapter 5. Finite element analyses were also used to study the structural effects of transverse prestressing in both slab-girder and box girder bridges. The analysis findings were presented in Chapter 6.

The design implications, recommendations and examples from both the durability and structural studies of transverse prestressing will be presented in the concluding report of this series, 316-3F.

7.2 Conclusions

7.2.1 General Conclusion. The principal conclusion from this study is that the application of transverse prestressing is possible in composite slab-girder bridges with currently available technology. There is no need to build such bridges noncompositely. However, in box girder bridges, substantial lateral prestressing of the diaphragm segments will be required.

7.2.2 Specific Conclusions. The more important conclusions from all structural studies may be summarized as follows:

1. If diaphragms are omitted from a bridge at the time of transverse slab prestressing, the transverse stress distribution is essentially uniform and slab stresses equal the applied edge stress less normal friction and time losses. This implies that the lateral stiffness of girders have little effect on transverse stress distribution.
2. Diaphragms which are in place at the time of transverse prestressing significantly affect transverse stress distribution. The overall transverse prestress reduction effect of diaphragms depends on cross sectional diaphragm stiffness, interior diaphragm spacing, slab thickness, bridge skew angle, and, to some degree, strand profile.
3. To account for transverse prestress reduction effects of diaphragms, two basic approaches can be followed:
 - a. Compensate for the diaphragm effects by either using additional prestressing in the slab over diaphragm regions or by prestressing the diaphragms themselves.
 - b. Prevent the diaphragms from affecting transverse slab prestress either by removing them or not putting them in place before prestressing or by creating temporary gaps between the girders and diaphragms to allow for unrestrained elastic shortening of the slab at the time of transverse prestressing.
4. Losses in prestressing, especially posttensioning friction losses, can result in substantially less effective compression to resist cracking and must be adequately accounted for in design.
5. Jacking sequence of deck transverse posttensioning does not have a significant influence on final transverse stress distribution in typical bridge decks.
6. No significant vertical cambers or deflections should arise from transverse prestressing a bridge deck to the compression levels which are necessary to ensure a "crack-free" design.
7. A transversely prestressed deck designed in accordance with the procedures presented in Report 316-3F and the AASHTO slab live load moments, should exhibit essentially linear elastic behavior through factored load levels. If a more "exact" method is used to determine the slab live load moments, the deck should still behave elastically beyond service load levels. Failure of a transversely prestressed

deck is expected to be by punching shear at a minimum factor of safety against live load plus impact of seven. This high factor of safety suggests that excluding the effects of compressive membrane forces in the structural analysis may lead to excessively conservative deck designs.

8. Errors in prestressing tendon placement in thin slab sections can have a pronounced effect on the magnitude of extreme fiber stresses.
9. Both two- and three-dimensional elastic finite element analyses provide satisfactory predictions of transverse prestressing effects in slab-girder bridge decks.

7.3 Future Research Needs

There are several areas involving the structural application of transverse prestressing which need further study. They are:

1. Reevaluation of current AASHTO provisions which are used for calculating transverse slab moments due to vehicular loads.
2. Evaluation of the interaction effects and applicable design criteria where closely spaced multiple anchorages are used in thin slab sections.
3. Experimental verification of transverse stresses near diaphragms in box girder bridges.
4. Feedback from the construction and performance of full-scale transversely prestressed bridge decks, together with the results of further research when available, should be used to refine the design and analysis recommendations presented in this report.

REFERENCES

1. Bellitto, A., "The Civil Engineer and the Decay of America's Infrastructure," Civil Engineering, ASCE, December 1983, p. 56.
2. Federal Highway Administration. "Our Nation's Highways Selected Facts and Figures," U.S. Dept. of Transportation, Office of Highway Planning, No. HHP-414-83 (50M), 1983.
3. Tonini, D., and Dean, S., Eds., Chloride Corrosion of Steel in Concrete, American Society for Testing and Materials, STP629, 1977.
4. "Cathodic Deck Protection for Bridges Come Slowly," Engineering News Record, September 6, 1979, pp. 22-24.
5. Poston, R.W., Carrasquillo, R.L., and Breen, J.E., "Durability of Prestressed Bridge Decks", Research Report 316-1, Center for Transportation Research, The University of Texas at Austin, July 1985.
6. Blaha, B., "Idea Packed Segmental Bridge Connects the Florida Keys," Concrete Products, August 1980.
7. Tedesko, A., "Bridge Decks: Transverse Post-Tensioning and Other Successful Experiences," ACI Journal, December, 1976, pp. 665-670.
8. Cusens, A.R., and Abbasi, A.F., "The Influence of Transverse Prestress on the Strength of Prestressed Concrete Bridge Slabs," Magazine of Concrete Research, London, Vol. 15, No. 44, July 1963, pp. 107-114.
9. Ralls, M., "Stress Distribution in a Transversely Prestressed Slab-Girder Bridge Deck," unpublished Master's Thesis, The University of Texas at Austin, May 1984.
10. Stollendorf, D., "Application of Transverse Prestressing for Bridge Decks," RRC Conference, Williamsburg, Virginia, December 1979.
11. American Association of State Highway and Transportation Officials, Standard Specifications for Highway Bridges, Thirteenth Edition, 1983.
12. Poston, R.W., Phipps, A.R., Breen, J.E., and Carrasquillo, R.L., "Design Procedures for Prestressed Concrete Bridge Decks," Research Report 316-3F, Center for Transportation Research, The University of Texas at Austin, November 1985.

13. Park, R., and Gamble, W.L., Reinforced Concrete Slabs, John Wiley & Sons, New York, 1980.
14. Hillerborg, A., Strip Method of Design, Translated by Cement and Concrete Association, London, 1975.
15. Johansen, K.W., Yield Line Theory, Translated by Cement and Concrete Association, London, 1962.
16. Park, R., "The Ultimate Strength and Long-Term Behavior of Uniformly Loaded Two-Way Concrete Slabs with Partial Lateral Restraint at All Edges," Magazine of Concrete Research, Vol. 16, No. 48, September 1964, pp. 139-152.
17. Park, R., "Ultimate Strength of Rectangular Concrete Slabs Under Short-Term Uniform Loading with Edges Restrained Against Lateral Movement", Proceedings--Institute of Civil Engineering, Vol. 28, June 1964, pp. 125-130.
18. Batchelor, B. deV., Hewitt, B.E., Csagoly, P., and Holowka, M., "Investigation of the Ultimate Strength of Deck Slabs of Composite Steel/Concrete Bridges," Transportation Research Record, No. 664, 1978, pp. 162-170.
19. Post-Tensioning Institute and Prestressed Concrete Institute, Precast Segmental Box Girder Bridge Manual, 1978.
20. Rawles, R.W., "Dallas Bridge has Post-Tensioned Concrete Deck," Civil Engineering, ASCE, April 1973, pp. 74-77.
21. Litvan, G., "Evaluation and Repair of Deteriorated Garage Floors", Canadian Building Digests, National Research Council, Canada, July 1982.
22. "Salt Licks Cleveland Garage," Engineering News Record, October 7, 1982, pp. 28-29.
23. Grambling, W.L., Teng, T.P., Morris, G.R., and Sheffiels, J., "Prestressed Pavement Performance in Four States," Federal Highway Administration Report No. FHWA.RD-82/169, September 1983.
24. Jensen, V.P., "Solutions for Certain Rectangular Slabs of Continuous over Flexible Supports," Bulletin No. 303, University of Illinois Engineering Experimental Station, 1938.
25. Newmark, N.M., "A Distribution Procedure for the Analysis of Slabs Continuous over Flexible Beams" Bulletin No. 304, University of Illinois Engineering Experimental Station, 1938.

26. Newmark, N.M., "Design of I-Beam Bridges," Proceedings--ASCE, Vol. 74, No. 3, March 1948.
27. Newmark, N.M., and Siess, C.P., "Research on Highway Bridge Floors at the University of Illinois, 1936-1954," Reprint Series No. 52, University of Illinois Engineering Experimental Station, 1955.
28. Westergaard, H.M., "Computation of Stresses in Bridge Slabs Due to Wheel Loads," Public Roads, March 1930, pp. 1-23.
29. Csagoly, P., Holowka, M., and Dorton, R., "The True Behavior of Thin Concrete Bridge Slabs," Transportation Research Record, No. 664, 1978, pp. 171-174.
30. Ministry of Transportation and Communications, Ontario Highway Bridge Design Code, Ontario, Canada, 1983.
31. Moll, E.L., and Drysdale, R.G., "Investigation of Transverse Stressing of Concrete Bridge Decks," Paper No. IBC-84-31, International Bridge Conference, Sponsored by Engineers' Society of Western Pennsylvania, Pittsburgh, Pennsylvania, 1984.
32. Aoki, Y., and Seki, H., "Shearing Strength and Cracking in Two-Way Slabs Subjected to Concentrated Load," Cracking, Deflection, and Ultimate Load of Concrete Slab Systems, Special Publication 30, American Concrete Institute, 1971.
33. Beal, D., "Strength of Concrete Bridge Decks," Research Report 89, New York State Department of Transportation, July 1981.
34. Brotchie, J.F., and Holley, M.H., "Membrane Action in Slabs," Cracking, Deflection, and Ultimate Load of Concrete Slab Systems, Special Publication 30, American Concrete Institute, 1971.
35. Burns, N.H., and Klingner, R.E., "Behavior of Concrete Bridge Decks on Steel Beams--Verification of the Ontario Bridge Deck Design (With and Without Panels)," Progress Report, Project 350, Ferguson Structural Engineering Laboratory, The University of Texas at Austin, September 1984.
36. Park, R., "The Lateral Stiffness and Strength Required to Insure Membrane Action at the Ultimate Load of a Reinforced Concrete Slab-and-Beam Floor," Magazine of Concrete Research, Vol. 17, No. 50, March 1965, pp. 29-38.
37. Sanders, W.W., and Elleby, H.A., "Distribution of Wheel Loads on Highway Bridges," National Cooperative Highway Research Program Report 83, 1970.

38. Taylor, R., and Hayes, B., "Some Tests on the Effect of Edge Restraint on Punching Shear in Reinforced Concrete Slabs," Magazine of Concrete Research, Vol. 17, No. 50, March 1965, pp. 39-44.
39. Van Horn, D.A., "Final Report--Research Project on Development and Refinement of Load Distribution Provisions for Prestressed Concrete Beam-Slab Bridges," Fritz Engineering Lab Report No. 387.5, Lehigh University, November 1980.
40. Colorado State Division of Highways, Drawings for Interstate 70 Through Glenwood Canyon, Project I 70-2 (88), Sheet Nos. 31-36, 1980.
41. Pucher, A., Einflussfelder Elastischer Platten, (Influence Surfaces of Elastic Plates), Springer-Verlag, New York, 1964. (In German and English).
42. Homberg, H., Fahrbahnplatten mit veraenderlicher Dicke (Decks with Variable Thickness), Volumes I and II, Springer-Verlag, New York, 1968. (In German).
43. Colorado State Division of Highways, Staff Bridge Design Memo Nos. 601.2-1 and 601.2-2, 1981.
44. "Contractor Saves \$220,000 on Bridges," Engineering News Record, January 8, 1976, pp. 22-23.
45. Figg, E.C., "Segmental Bridge Design in the Florida Keys," Concrete International, August 1980, pp. 17-22.
46. Poston, R.W. "Improving Durability of Bridge Decks by Transverse Prestressing," Ph.D. Dissertation, The University of Texas at Austin, December 1984.
47. Ballinger, C., Podolny, W., and Abrahams, M., "A Report on the Design and Construction of Segmental Prestressed Concrete Bridges in Western Europe--1977," Federal Highway Administration, Report No. FHWA-RD-78-44, June 1978.
48. Csagoly, P., Holowka, M., Campbell, T., Meades, P., Green, R., and McNeice, G., "Cracking of Voided Posttensioned Concrete Bridge Decks; The Macowan Bridge Test; Prototype for Voided Posttensioned Concrete Bridge Decks; Model Studies for Voided Posttensioned Concrete Slab Bridges; Finite Element Computer Program for Analysis of Plates with Bending and In-Plane Stresses," Roads and Transportation Association of Canada, Reports No. RR193, 194, 195, 196, 1975.

49. IABSE, "Bridges of the Tauern Highway in the Leiser Valley," IABSE Structures, C-12/80, pp. 22-23.
50. IABSE, "Le Pont du Cucloz sur la N12, St.-Legier/VD," IABSE Structures, C-7/79, 1979, pp. 50-51.
51. IABSE, "Le Pont sur le Rhin a Neuwied (RFA)," IABSE Structures, C-3/78, 1978, pp. 12-13.
52. IABSE, "Le Viaduc d'Epandes sur la N1/VD," IABSE Structures, C-7/79, pp. 52-53.
53. IABSE, "Pumicestone Road Overpass (Australia)," IABSE Structures, C-1/77, pp. 4-5.
54. IABSE, "Reconstruction of Vienna's Reichsbrucke 'Johann Nestroy' Project," IABSE Structures, C-12/80, 1980, pp. 34-35.
55. IABSE, "Standard Motorway Bridges, Zealand, Denmark," IABSE Structures, C-1/77, 1977, pp. 8-9.
56. IABSE, "Viaduct of Lake Gruyere/FR," IABSE Structures, C-7/79, 1979, pp. 40-41.
57. ENR, "Prestressing Gets a Chance," Engineering News Record, October 27, 1983, p. 38.
58. Berger, R. H, and Solldorf, D.W., "Application of Transverse Prestressing for Bridge Decks," Federal Highway Administration Report No. FHWA-RD-80-074, April 1980.
59. Gutzwiller, M.J., Lee, R.H., and Scholer, C.F., "Precast, Prestressed Concrete for Bridge Decks," Highway Research Board, No. 116, 1970.
60. Almstafa, R.A., "The Analysis of Transverse Prestressing Effects in Bridge Decks," Ph.D. Dissertation, The University of Texas at Austin, December 1983.
61. Mora Abarca, R., "Design and Construction of a Direct Model for the Study of Transverse Prestressing of Bridge Decks," unpublished Master's Report, The University of Texas at Austin, May 1983.
62. PCI, PCI Design Handbook, Prestressed Concrete Institute, Second Edition, 1978.
63. Phipps, A.R., "The Design of Transversely Prestressed Bridge Decks," unpublished Master's Thesis, The University of Texas at Austin, May 1985.

64. Libby, J., Modern Prestressed Concrete, Second Edition, Van Nostrand Reinhold, New York, 1977.
65. Lin, T., and Burns, N., Design of Prestressed Concrete Structures, Third Edition, John Wiley & Sons, New York, 1981.
66. State of Florida Department of Transportation, Memorandum from Tom Alberdie to Wayne Henneberger, August 1981.
67. Moore, D., Klodt, D., and Hensen, R., "Protection of Steel in Prestressed Concrete Bridges," National Cooperative Highway Research Program Report 90, 1970.
68. Etienne, C., Binnekamp, D, Copier, W., Hendrickx, R., and Smith, C., "Corrosion Protection of Unbonded Tendons," HERON, Vol. 26, No. 3, 1981.
69. Dorton, R., "The Conestogo River Bridge Design and Testing," Canadian Structural Engineering Conference, 1976.
70. Timoshenko, S., and Goodier, J., Theory of Elasticity, Third Edition, McGraw-Hill, New York, 1970.
71. Newmark, N., and Siess, C., "Moments in I-Beam Bridges," Bulletin No. 336, University of Illinois Engineering Experimental Station, 1942.
72. Sengupta, S., and Breen, J., "The Effect of Diaphragms in Prestressed Concrete Girder and Slab Bridges," Research Report 158-1F, Center for Highway Research, The University of Texas at Austin, October 1973.
73. Stone, W., and Breen, J., "Analysis of Post-Tensioned Girder Anchorage Zones," Center for Transportation Research, The University of Texas at Austin, No. CTR-3-5-77-208-1, June 1981.
74. Stone, W., and Breen, J., "Design of Post-Tensioned Girder Anchorage Zones," Center for Transportation Research, The University of Texas at Austin, No. CTR-3-5-77-208-3F, June 1981.
75. Stone, W., Paes-Filho, W., and Breen, J., "Behavior of Post-Tensioned Girder Anchorage Zones," Center for Transportation Research, The University of Texas at Austin, No. CTR-3-5-77-208-2, April 1981.
76. FIP, "Tentative Recommendations for Corrosion Protection of Unbonded Tendons," PCI Journal, January/February 1983.
77. Schupack, M., "Protecting Post-Tensioning Tendons in Concrete Structures," Civil Engineering, ASCE, December 1982, pp. 43-45.

78. Post-Tensioning Institute, "Specification for Unbonded Single Strand Tendons," Ad-Hoc Committee for Unbonded Single Strand Tendons, October 1984.
79. Overman, T., "Flexural Fatigue Behavior of Pretensioned Concrete Girders," unpublished Master's Thesis, The University of Texas at Austin, December 1984.
80. American Concrete Institute, Building Code Requirements for Reinforced Concrete (ACI 31-83), American Concrete Institute, 1983.
81. Meyer, C. A., "Analysis and Design of Curved Box Girder Bridges, SESM-70-22, Department of Civil Engineering, University of California, Berkeley, December 1970.
82. Mehra, M., "Finite Element Analysis of Skew Composite Girder Bridges," SESM-67-28, Department of Civil Engineering, University of California, Berkeley, November 1967.
83. Willam, K. J., and Scordelis, A. C., "Analysis of Orthotropic Folded Plates with Eccentric Stiffeners," SESM-70-2, Department of Civil Engineering, University of California, Berkeley, February 1970.
84. Texas State Department of Highways and Public Transportation, Standard Specification for Construction of Highways, Streets, and Bridges, September 1982.
85. Morley, L.S.D., Skew Plates and Structures, The Macmillan Company, New York, 1963.
86. Kabir, A. F., and Scordelis, A. C., "Computer Program for Curved Bridge on Flexible Bents," SESM-74-10, Department of Civil Engineering, University of California, Berkeley, September 1974.
87. Post-Tensioning Institute, Post-Tensioned Box Girder Bridge Manual, 1978.
88. Libby, J. R., and Perkins, N. D., Highway Bridge Superstructures, Granville Publishing Co., San Diego, Ca., 1976.
89. Newmark, N. M., "Design of I-Beam Bridges," Transactions ASCE, Volume 114, Paper No. 2381, 1949.
90. Feasibility of Standard Sections for Segmental Prestressed Concrete Box Girder Bridges, Federal Highway Administration, Draft Report, November 1981.

91. Sisodiya, R. G., Ghali, A., and Cheung, Y. K., "Diaphragms in Single- and Double-Cell Box Girder Bridges with Varying Angle of Skew," American Concrete Institute Journal, July 1972.
92. Swann, R. A., "A Feature Survey of Concrete Box Spine-Beam Bridges," Technical Report 42.469, Cement and Concrete Association, London, June 1972.

APPENDIX A

**DESIGN CALCULATIONS FOR TRANSVERSELY PRESTRESSED DECK
OF LABORATORY BRIDGE MODEL**

A. 1 Slab Span (AASHTO 1.3.2(A))

$$\begin{aligned}
 S &= \text{girder spacing} - \text{half flange width} \\
 &= 8.83 - 14/12 \\
 &= 8.25 \text{ ft}
 \end{aligned}$$

A. 2 Impact Factor (AASHTO 1.2.12(C))

$$\begin{aligned}
 I &= 50/(125 + S) \leq 0.30 \\
 &= 50/(125 + 8.25) \\
 &= 0.30
 \end{aligned}$$

A. 3 Design MomentsA. 3.1 Dead Load

$$\begin{aligned}
 M_{DL} &= (0.105)(8.25)^2/10 \\
 &= 0.71 \text{ k-ft/ft}
 \end{aligned}$$

A. 3.2 Live Load (AASHTO 1.2.5(C) and 1.3.2(C))

$$\begin{aligned}
 M_{LL+I} &= 1.3 (0.8) P (S + 2)/32 \\
 &= 1.3 (0.8) (16) (8.25 + 2)/32 \\
 &= 5.33 \text{ k-ft/ft}
 \end{aligned}$$

A. 3.3 Total

$$\begin{aligned}
 M_{TL} &= M_{DL} + M_{LL} \\
 &= 0.71 + 5.33 \\
 &= 6.04 \text{ k-ft/ft}
 \end{aligned}$$

A. 4 Service Load Stresses

$$A = 12(8.25) = 99 \text{ in.}^2/\text{per ft width of slab}$$

$$S_{\text{gross}} = I/C \text{ (ignoring steel)}$$

$$= 12(8.25)^2/6$$

$$= 136 \text{ in.}^3/\text{per ft width of slab}$$

$$f_c = \pm 0.533 \text{ ksi}$$

A. 5 Prestressing

A. 5.1 Straight Tendon Profile

A. 5.1.1 Accounting for Friction Losses

$$f_c = 0.9 P/A$$

$$f_c/0.9 = P/A$$

$$\pm 0.537/0.9 = \pm 0.592 \text{ ksi}$$

A . 5.1.2 Required Prestressing for Service Loads

$$0 = -P_T/99 - P_T (1.875/136) - P_B(1.875)/136 \\ + 0.592$$

$$0.140 = -P_T/99 + P_T (1.875/36) - P_B/99 - (P_B(1.875))/136 \\ + 0.592$$

$$P_T = 28.3 \text{ kips}$$

$$P_B = 23.2 \text{ kips}$$

Assuming effective prestress force $P_e = 22.95 \text{ kips}$

$$\text{Bottom tendon spacing} = 22.95/23.2$$

$$= 0.99 \text{ ft}$$

$$= 11-7/8 \text{ in.}$$

$$\text{Top tendon spacing} = 22.94/28.3$$

$$= 0.81 \text{ ft}$$

$$= 9-3/4 \text{ in.}$$

Check for compression stresses $< 0.4 f'_c$ OK

A. 5.2 Draped and Straight Tendon Profile

A. 5.2.1 Accounting for Friction Losses

$$f_c = 0.80 P/A$$

$$f_c/0.80 = P/A$$

$$\pm 0.533/0.8 = \pm 0.666 \text{ ksi}$$

A. 5.2.2 Required Prestressing for Service Loads

$$0 = -P_T/99 - (P_T(1.875))/136 - P_B/99 + (P_B(1.875))/136 \\ + 0.666$$

$$\text{But, } P_B = P_T/3$$

$$P_T = 29.1 \text{ kips}$$

$$\text{Tendon spacing} = 22.95/29.1$$

$$= 0.79 \text{ ft}$$

$$= 9-1/2 \text{ in.}$$

For a given repeating section, there is one straight tendon top and bottom, and two draping tendons.

Check for compression stresses $< 0.4 f_c$ OK

A. 6 Bonded Reinforcement (ACI 318-83 18.9.2)

$$\begin{aligned} A_s &= 0.004 A \\ &= 0.004(8.25/2)(12) \\ &= 0.20 \text{ in.}^2/\text{per ft width of slab} \end{aligned}$$

Using #4 bar:

$$\begin{aligned} S &= 0.20/0.20 \\ &= 1 \text{ ft} \\ &= 12 \text{ in.} \end{aligned}$$

The #4 bars are required top and bottom of slab in the transverse direction

A. 7 Shrinkage and Temperature Reinforcement (AASHTO 1.5.12)

$$1.8 \text{ in.}^2/\text{per ft width of slab}$$

For #4 bar:

$$\begin{aligned} S &= 0.20/0.125 \\ &= 1.6 \text{ ft} \\ &= 19.2 \text{ in.} > 18 \text{ in.} \end{aligned}$$

Use at least #4 bar at 18 in. in both transverse and longitudinal directions on both and top and bottom of slab.

A. 8 Check for Ultimate Moment (AASHTO 1.6.9(A))

A. 8.1 Straight Tendon Profile

$$\begin{aligned} M_u &= \phi A_s F_{su} d (1 - 0.6 \rho f_{su}/f_c) \\ \phi &= 0.95 \text{ (for cast-in-place posttensioned concrete)} \\ A_s &= 0.153 (12/11.875) \\ &= 0.155 \text{ in.}^2/\text{per ft} \end{aligned}$$

$$\begin{aligned}
 f_{su} &= f_{se} + 15000 \\
 &= 150,000 + 15000 \\
 &= 165,000 \text{ psi} \\
 &= 165 \text{ ksi}
 \end{aligned}$$

$$\begin{aligned}
 M_u &= (0.95)(0.155)(165)(6)(1 - 0.6(0.0022(165)/5)) \\
 &= 140 \text{ in.-k/ft} \\
 &= 11.6 \text{ k-ft/ft}
 \end{aligned}$$

Factored Moment (AASHTO 1.2.22)

$$\begin{aligned}
 M_{uf} &= 1.3(0.71) + 2.17(5.33) \\
 &= 12.5 \text{ k-ft/ft}
 \end{aligned}$$

11.6 < 12.14 (but bonded nonprestressed reinforcement provides enough additional strength to satisfy requirement)

A. 8.2 Straight and Draped Tendon Profile

$$\begin{aligned}
 A_s &= 0.153 (12/9.65) \\
 &= 0.193 \text{ in.}^2/\text{ft}
 \end{aligned}$$

$$\begin{aligned}
 M_u &= (0.95)(0.193)(165)(6)(1 - 0.6(0.0027(165)/5)) \\
 &= 172 \text{ in.-k/ft} \\
 &= 14.3 \text{ k-ft/ft}
 \end{aligned}$$

$$M_{uf} = 12.5 \text{ k-ft/ft}$$

$$14.3 > 12.5 \quad \text{OK}$$

Minimum Moment (Moment Reversal)

$$\begin{aligned}
 A_s &= 0.153(12/28.5) \\
 &= 0.064 \text{ in.}^2/\text{ft}
 \end{aligned}$$

$$\begin{aligned}
 M_u &= (0.95)(0.064)(165)(6)(1 - 0.6(0.0009(165)/5)) \\
 &= 59.1 \text{ in.-k/ft} \\
 &= 4.9 \text{ k-ft/ft}
 \end{aligned}$$

$$\text{Minimum Moment} = M_{uf}/2 = 6.2$$

$$4.9 < 6.2 \quad \text{No good}$$

Including Bond Reinforcement

$$A_s = 0.20 \text{ in.}^2/\text{ft}$$

$$M_u \leq \phi A_s f_y [0.9d]$$

$$= 0.90 (0.20)(60)(0.9(6))$$

$$= 58.3 \text{ in.-k/ft}$$

$$= 4.9 \text{ k-ft/ft}$$

$$M_{uTOT} = 4.9 + 4.9$$

$$= 9.8 \text{ k-ft/ft}$$

$$9.8 > 6.2 \quad \text{OK}$$

- A. 9 Check Maximum and Minimum Steel Percentages
(AASHTO 1.6.10(A) and 1.6.10(B))

OK by inspection